A Thesis submitted for the degree of Doctor of Philosophy

Modulating the Heat-Shock Response : A Potential Therapy for Lysosomal Storage Disorders

James Gray
St. Cross College, Oxford

Michelmas Term 2014

Department of Pharmacology
University of Oxford

Acknowledgements

I would like to thank my supervisor, Professor Frances Platt for her quiet encouragement and immense help with the theoretical and practical issues throughout this project. I am also grateful for the support of my sponsors, Orphazyme ApS. In particular, Dr Thomas Kirkegaarde for his endless enthusiasm and knowledge of all things HSP70, and Dr Signe Jorgensen for her patience and problem-solving. I would also like to mention Dr Ian Williams, who mentored me through the early stages of this project, taught me everything I know about IHC, and encouraged me to follow a PhD, and Dr Kerri-Lee Wallom, and Dr David Priestman for all their knowledge and hard work on the Sandhoff and Fabry models.

This project has also been helped immensely, by various people. Within our laboratory, particular thanks go to Dave "Dr. Dolittle" Smith, for all the endless work on behaviourals, looking after all my mice, and my sanity in general. Also to Jennifer Atkins, for all her work with the CatWalk progam optimisation, and endless answering of my questions & report writing. Lauren Morris has been instrumental in providing genotyping of mice and a general sense of humour within the lab. Allie Colaco, has also kindly read through my thesis, provided excellent input and also been a great person to work with, especially on the sphingosine assays. Paul Fineran for his classic jokes, being my thesis buddy and providing me with important deadline reminders throughout my time here (not to mention supplying the milk!). I'd like to thank Dr Raluca Nicoli, for being the only person here in the early hours of thesis writing, and saving my sanity! I would also like to mention Danielle Taylor te-Vruchte for her help with the LysoTracker assay.

Most importantly, I would like to thank my partner, Sarah, for her unwavering support and belief throughout my studies.

Abstract

Lysosomal storage disorders (LSDs) comprise a broad disease group of inherited metabolic disorders, the majority of which are associated with CNS pathology, significant disability and reductions in life expectancy. LSDs are caused by mutations in genes encoding proteins critical for the correct functioning of lysosomal homeostasis. The disruption of lysosomal homeostasis results in the abnormal accumulation of lysosomal content, initiating intracellular pathological events, including calcium dysregulation and lysosomal membrane permeablisation (LMP) affecting cell function and inducing cellular death mechanisms. These pathological events are particularly damaging within the CNS, due to its limited capacity for regeneration. Despite intensive scientific research into these disorders, and an increased understanding of the pathological events underlying these diseases, effective treatments are still lacking for most LSDs. Several therapeutic approaches have been investigated in the last 30 years, including enzyme replacement therapy, bone marrow transplantation, substrate reduction therapy, chemical chaperones and gene therapy. However, the CNS pathology in many of the LSDs remains unaddressed due to the restricted ability of many therapeutic agents to cross the blood-brain barrier.

The heat-shock response (HSR) is an emerging element involved in the pathogenesis of a variety of disorders. The HSR is a physiological response to a wide range of cellular stresses. It functions to protect the cell from the aggregation of misfolded proteins and LMP. Of the HSR, several key players are integral to mounting a heat shock response, these include the heat-shock factor 1 (HSF-1) and HSP70.

In this thesis, we provide proof-of-principle for the use of recombinant HSP70, and the small molecule up-regulator of the HSR, arimoclomol in treatment of a range of LSDs. We show that HSP70 is able to access the CNS, and increase the degradative capacity of lysosomal hydrolases. This provides differential behavioural, biochemical and survival effects in LSD models

of Niemann-Pick type C, Sandhoff and Fabry disease. Additional studies using the HSF-1 up-regulator arimoclomol, show a complex dose-response between the different models, possibly reflecting essential differences in the calcium dysregulation between these disease states.

Abbreviations

ADA	anti-drug antibody
ANOVA	analysis of variance
ASM	acid sphingomyelinase
BSA	bovine serum albumin
BMP	bis-(mono)acylglycerophosphate
CLEAR	coordinated lysosomal expression and regulation genes
CNPase	2',3'-Cyclic-nucleotide 3'-phosphodiesterase
CNS	central nervous system
DAPI	4',6-diamidino-2-phenylindole
ER	endoplasmic reticulum
ERAD	endoplasmic reticulum associated degradation
ESCRT	endosomal sorting complex required for transport
ELISA	enzyme-linked immunosorbent assay
FCS	fetal calf serum
FACS	flow assisted cell sorting
GalA	α-galactosidase A
GM2-AP	GM2 activator proteins
GSL	glycosphingolipids
HexA/B/S	A/B/S isozymes of the β-hexosaminidase enzyme
HPLC	high-performance liquid chromatography
HSF	heat-shock factor
HSP70, 90	heat-shock protein 70, 90 etc
HSR	heat-shock response

LE	late endosome
LIMP1	lysosomal integral membrane protein 1
LSD	lysosomal storage disorder
Ly	lysosome
LYNUS	lysosomal nutrient sensing machinery
M6P	mannose-6-phosphate
MBP	myelin basic protein
MEFL	molecular equivalents of fluorescent labeling
MPR	mannose-6-phosphate receptor
mTOR	mammalian target of Rapamycin
mTORC	mammalian target of Rapamycin complex
MVB	multivesicular bodies
NPC	Niemann-Pick type C disease
NPC1/2	Niemann-Pick type C proteins 1/2
OPA	o-pthaldehyde
PBS	phosphate buffered saline
PFA	paraformaldehyde
SAPs	sphingolipid activator proteins
SERCA	sarcoplasmic/endoplasmic reticulum calcium ATPase
TFEB	transcription factor EB
V-ATPase	vacuolar type proton ATPase

Contents

Acknowledgements i

Abstract ii

Abbreviations iv

1 Introduction 1
- 1.1 Lysosomal Storage Disorders . . . 1
  - 1.1.1 Lysosomal Structure and Function . . . 1
  - 1.1.2 Lysosomal Formation and Maturation . . . 1
  - 1.1.3 Lysosomal Enzymes . . . 3
  - 1.1.4 Lysosomal Membrane Permeablisation . . . 8
- 1.2 Lysosomal Storage Disorders . . . 9
  - 1.2.1 Functional Consequences of Mutation . . . 9
  - 1.2.2 GM2 Gangliosidosis . . . 11
  - 1.2.3 Fabry disease . . . 13
- 1.3 Niemann-Pick type C Disease . . . 14
  - 1.3.1 NPC: Pathologies . . . 15
- 1.4 Current Therapies for Lysosomal Storage Disorders . . . 18
  - 1.4.1 Enzyme Replacement Therapy . . . 18
  - 1.4.2 Gene Therapy . . . 18
  - 1.4.3 Chemical Chaperones . . . 19
  - 1.4.4 Substrate Reduction Therapy . . . 20
  - 1.4.5 Cyclodextrin . . . 21
  - 1.4.6 Histone De-acetylase Inhibitors . . . 22
- 1.5 The Heat Shock Response . . . 22
  - 1.5.1 Induction of Heat Shock Response . . . 23
  - 1.5.2 The Roles of HSP70 . . . 25
  - 1.5.3 HSP70 and Lysosomes . . . 28
- 1.6 Aims . . . 30

2 Materials & Methods 31
- 2.1 Mouse Models . . . 31
- 2.2 Compounds . . . 31
- 2.3 Tissue Processing . . . 31
  - 2.3.1 Biochemistry . . . 32
  - 2.3.2 Western Blotting . . . 32
  - 2.3.3 Immunofluorescence . . . 32
- 2.4 Immunofluorescent Staining Protocols . . . 33
- 2.5 Protein Quantification . . . 34

2.6 Quantification of GSLs . . . 35
2.7 Quantification of Cholesterol and Cholesteryl ester. . . . 35
2.7.1 Method Development: Cholesterol Extraction . . . 36
2.8 Quantification of Sphingosine: Comparison of Existing Protocols . . . 37
2.8.1 Method 1 : Merrill *et al* 1998 [1] . . . 37
2.8.2 Method 2 : Fryst *et al* 2001 [2] . . . 38
2.8.3 Method 3 : Schuchman *et al* 2010 [3] . . . 39
2.9 Lysosomal Volume Assay . . . 41
2.9.1 Mononuclear Cell Preparation . . . 41
2.9.2 LysoTracker Assay . . . 42
2.10 Behavioural Analysis . . . 42
2.10.1 Tremor . . . 42
2.10.2 Manual Rearing . . . 43
2.10.3 Activity Monitor Logger . . . 43
2.10.4 SHIRPA testing . . . 43
2.10.5 Gait Analysis . . . 43
2.11 Anti-Drug Antibody Assay . . . 44
2.11.1 Treatment . . . 44
2.11.2 Collection of Blood . . . 44
2.11.3 Anti-Drug Antibody ELISA . . . 44
2.12 Data Collection . . . 45
2.13 Statistical Analysis . . . 45
2.13.1 Biochemical Analysis . . . 45
2.13.2 Lysosomal volume assay . . . 46
2.13.3 Behavioural Analysis . . . 46
2.13.4 Immunohistochemical Analysis . . . 46
2.13.5 Anti-Drug Antibody Comparison . . . 46

3 In Vivo Effects of rhHSP70 Treatment in Niemann-Pick Type C Disease 47
3.1 Introduction . . . 47
3.2 Hypothesis . . . 48
3.3 Materials & Methods . . . 49
3.3.1 Mice . . . 49
3.3.2 Treatment . . . 49
3.4 Results . . . 49
3.4.1 Bioavailability of rhHSP70^{his} . . . 49
3.4.2 CNS localisation of rhHSP70^{his} . . . 50
3.4.3 Growth Curves . . . 53
3.4.4 Rearing . . . 53
3.4.5 Tremor . . . 63
3.4.6 Gait Analysis . . . 67
3.4.7 SHIRPA Testing . . . 70
3.4.8 Biochemical Findings . . . 72
3.4.9 Lysosomal Volume . . . 79
3.4.10 CNS Pathologies . . . 79
3.4.11 Antibody Response . . . 87
3.5 Discussion . . . 87

4 In Vivo Use of Non-His Tagged rhHSP70 **95**
4.1 Introduction . . . 95
4.2 Hypothesis . . . 95
4.3 Materials & Methods . . . 95
4.3.1 rhHSP70$^{\text{non-his}}$ . . . 95
4.3.2 Treatment . . . 95
4.3.3 Anti-Drug Antibody Comparison . . . 96
4.4 Results . . . 96
4.4.1 Growth Curves . . . 96
4.4.2 Manual Rearing . . . 96
4.4.3 SHIRPA Testing . . . 96
4.4.4 Glycosphingolipid Quantification . . . 99
4.4.5 Sphingosine Quantification . . . 99
4.4.6 Lysosomal Volume . . . 99
4.4.7 Antibody response following rhHSP70$^{\text{non-his}}$ administration . . . 102
4.5 Discussion . . . 105

5 Arimoclomol: Upregulator of the Heat-Shock Response as a Therapeutic for NPC Disease **106**
5.1 Introduction . . . 106
5.2 Hypothesis . . . 108
5.3 Materials & Methods . . . 108
5.3.1 Mice . . . 108
5.3.2 Taste Aversion Test . . . 108
5.3.3 Treatment . . . 108
5.4 Gait Analysis . . . 109
5.5 Results . . . 109
5.5.1 Taste Aversion Test . . . 109
5.5.2 Weights . . . 109
5.5.3 Survival . . . 110
5.5.4 Behavioural Data . . . 111
5.5.5 Biochemistry Data . . . 115
5.5.6 Dose Response : Manual Rearing . . . 119
5.5.7 Dose Response : Gait Analysis . . . 119
5.6 Discussion . . . 126

6 Arimoclomol & HSP70: Effects on Fabry and Sandhoff Disease **132**
6.1 Sandhoff Disease . . . 132
6.1.1 Introduction . . . 132
6.1.2 Materials & Methods . . . 134
6.1.3 Results . . . 135
6.1.4 Lysosomal Volume Assay . . . 141
6.2 Discussion . . . 141
6.3 Arimoclomol & HSP70: Effects on Fabry Disease . . . 145
6.3.1 Introduction . . . 145
6.3.2 Materials & Methods . . . 146
6.3.3 Results . . . 147
6.4 Discussion . . . 148

7 Discussion **151**
7.1 Lysosomal Storage Disorders 151
7.2 Heat-Shock Therapies 152
7.3 Heat-Shock Therapies: Effects of HSP70 153
7.4 Heat-Shock Therapies: Effects of Arimoclomol 156
7.5 Current Therapies 158
7.6 Future Directions 159

List of Figures

1.1 Introduction : Sphingolipid degradation pathways 7

2.1 Effects of rhHSP70^{his} treatment *in vivo* : Cholesterol methods, effects of glass extraction 36
2.2 Sphingosine methods development : Fryst *et al* 39
2.3 Sphingosine methods development : The method of Schuchman *et al* Optimisation 40
2.4 Sphingosine methods development : Schuchman *et al* recovery 41

3.1 Effects of rhHSP70^{his} treatment *in vivo* : Biodistribution. 50
3.2 Effects of rhHSP70^{his} treatment *in vivo* : Localisation, whole brain 3 days 51
3.3 Effects of rhHSP70^{his} treatment *in vivo* : Localisation, whole brain 7 days 52
3.4 Effects of rhHSP70^{his} treatment *in vivo* : Localisation, cerebellum 54
3.5 Effects of rhHSP70^{his} treatment *in vivo* : Localisation, cerebellum 55
3.6 Effects of rhHSP70^{his} treatment *in vivo* : Localisation, cortex 56
3.7 Effects of rhHSP70^{his} treatment *in vivo* : Localisation, caudate putamen 57
3.8 Effects of rhHSP70^{his} treatment *in vivo* : Growth curves 58
3.9 Effects of rhHSP70^{his} treatment *in vivo* : Manual rearing 60
3.10 Effects of rhHSP70^{his} treatment *in vivo* : Manual rearing 61
3.11 Effects of rhHSP70^{his} treatment *in vivo* : Automated rearing 62
3.12 Effects of rhHSP70^{his} treatment *in vivo* : Automated rearing 64
3.13 Effects of rhHSP70^{his} treatment *in vivo* : Automated rearing 65
3.14 Effects of rhHSP70^{his} treatment *in vivo* : Tremor 66
3.15 Effects of rhHSP70^{his} treatment *in vivo* : Catwalk, speed and cadence 68
3.16 Effects of rhHSP70^{his} treatment *in vivo* : CatWalk, step and duty cycles 69
3.17 Effects of rhHSP70^{his} treatment *in vivo* : CatWalk, max signal intensity 70
3.18 Effects of rhHSP70^{his} treatment *in vivo* : SHIRPA tests 71
3.19 Effects of rhHSP70^{his} treatment *in vivo* : Peripheral total GSL accumulation . . 72
3.20 Effects of rhHSP70^{his} treatment *in vivo* : Peripheral individual GSL accumulation 73
3.21 Effects of rhHSP70^{his} treatment *in vivo* : Forebrain GSL accumulation 75
3.22 Effects of rhHSP70^{his} treatment *in vivo* : Cerebellar GSL accumulation 76
3.23 Effects of rhHSP70^{his} treatment *in vivo* : Forebrain sphingosine accumulation *in vivo* 77
3.24 Effects of rhHSP70^{his} treatment *in vivo* : Lysosomal hydrolase binding assay . . 78
3.25 Effects of rhHSP70^{his} treatment *in vivo* : Peripheral free cholesterol 79
3.26 Effects of rhHSP70^{his} treatment *in vivo* : Lysosomal volume 80
3.27 Effects of rhHSP70^{his} treatment *in vivo* : Purkinje cell counts 81
3.28 Effects of rhHSP70^{his} treatment *in vivo* : Microglial counts 83
3.29 Effects of rhHSP70^{his} treatment *in vivo* : Cerebellar white matter area 84
3.30 Effects of rhHSP70^{his} treatment *in vivo* : Cerebellar MBP expression 85
3.31 Effects of rhHSP70^{his} treatment *in vivo* : Forebrain MBP expression 86

3.32 Effects of rhHSP70^{his} treatment *in vivo* : Antibody response 87

4.1 Effects of rhHSP70$^{non\text{-}his}$ treatment *in vivo* : Growth curves 97
4.2 Effects of rhHSP70$^{non\text{-}his}$ treatment *in vivo* : Manual rearing 98
4.3 Effects of rhHSP70$^{non\text{-}his}$ treatment *in vivo* : SHIRPA tests 100
4.4 Effects of rhHSP70$^{non\text{-}his}$ treatment *in vivo* : Forebrain GSL accumulation 101
4.5 Effects of rhHSP70$^{non\text{-}his}$ treatment *in vivo* : Sphingosine accumulation 102
4.6 Effects of rhHSP70$^{non\text{-}his}$ treatment *in vivo* : Lysosomal compartment volume . . 103
4.7 Effects of rhHSP70$^{non\text{-}his}$ treatment *in vivo* : Antibody response 104

5.1 Arimoclomol, effects in NPC disease : Structure of arimocomol 106
5.2 Arimoclomol, effects in NPC disease : Drug consumption 110
5.3 Arimoclomol, effects in NPC disease : Growth curves 111
5.4 Arimoclomol, effects in NPC disease : Survival 112
5.5 Arimoclomol, effects in NPC disease : Manual rearing 113
5.6 Arimoclomol, effects in NPC disease : Tremor 114
5.7 Arimoclomol, effects in NPC disease : Cholesterol accumulation 115
5.8 Arimoclomol, effects in NPC disease : Liver GSL accumulation 117
5.9 Arimoclomol, effects in NPC disease : Cerebellar GSL accumulation 118
5.10 Arimoclomol, effects in NPC disease : Forebrain GSL accumulation 120
5.11 Arimoclomol, effects in NPC disease : Dosing effects, manual rearing scores . . . 121
5.12 Arimoclomol, effects in NPC disease : CatWalk average speeds 122
5.13 Arimoclomol, effects in NPC disease : CatWalk cadence 123
5.14 Arimoclomol, effects in NPC disease : CatWalk stand time 124
5.15 Arimoclomol, effects in NPC disease : CatWalk, initial and terminal dual stance 125
5.16 Arimoclomol, effects in NPC disease : CatWalk, step sequences and support . . . 127

6.1 Heat Shock Therapy in Sandhoff Disease : Growth curves 136
6.2 Heat Shock Therapy in Sandhoff Disease : Survival 137
6.3 Heat Shock Therapy in Sandhoff Disease : Manual rearing 138
6.4 Heat Shock Therapy in Sandhoff Disease : Bar-crossing 139
6.5 Heat Shock Therapy in Sandhoff Disease : CNS GSL accumulation 140
6.6 Heat Shock Therapy in Sandhoff Disease : Liver GSL accumulation 142
6.7 Heat Shock Therapy in Sandhoff Disease : Lysosomal volume 143
6.8 Heat Shock Therapy in Fabry Disease : Gb3 accumulation following rmHsp70 treatment 147
6.9 Heat Shock Therapy in Fabry Disease : Gb3 accumulation following Arimoclomol Treatment 148

List of Tables

1.1 Introduction: Lysosomal storage disorders, their causes, substrates and pathologies 10
1.2 Introduction : Conditional knock-outs of NPC1 in neuronal cell lineages. 17

2.1 Effects of rhHSP70^{his} treatment *in vivo* : Primary antibodies for immunofluorescence 33
2.2 Effects of rhHSP70^{his} treatment *in vivo* : Secondary antibodies for immunofluorescence 33

3.1 Effects of rhHSP70^{his} treatment *in vivo* : Catwalk inclusion numbers 67

5.1 Arimoclomol, effects in NPC disease : Manual side rearing n and p values 112
5.2 Arimoclomol, effects in NPC disease : Manual centre rearing n and p values . . . 114
5.3 Arimoclomol, effects in NPC disease : Tremor n and p values 114
5.4 Arimoclomol, effects in NPC disease : Dosing effects, manual rearing n and p values 119
5.5 Arimoclomol, effects in NPC disease : Catwalk inclusion numbers 122

7.1 Discussion: HSP70 results summary 155
7.2 Discussion: Arimoclomol results summary 156

1 Introduction

1.1 Lysosomal Storage Disorders

1.1.1 Lysosomal Structure and Function

Lysosomes were first described by Christian de Duve [4] as distinct acidic compartments, which contained specific classes of enzymes with optimal activities at acidic pH. Lysosomes are catabolic organelles, which are rich in protons, calcium, functionally distinct acid hydrolases, proteases, and a variety of cofactors [5]. The abundance of these elements have led to the long held belief that lysosomes function simply as the waste disposal/recycling centre of the cell. Whilst lysosomes are responsible for the degradation of a wide variety of macromolecules, extensive study of these organelles has revealed a highly dynamic biological system [5]. Lysosomes have emerged as key nutrient sensing organelles [6] with roles in calcium signalling [7] which are integral to the correct functioning of many aspects of cellular function [5].

1.1.2 Lysosomal Formation and Maturation

Lysosomes are not a distinct organelle, but rather are constantly reformed by a process of maturation of newly formed endosomes and autophagosomes by their fusion with exisiting endosomes and lysosomes, thus merging lysosomal content and pH with luminal cargo [5]. In the early stage of endosome formation, endocytosis of extracellular material is the main form of cargo trafficking [8]. The best characterised form of endocytosis arises from the formation of clathrin coated pits at the plasma membrane along with the clustering of various cell surface receptors, such as the mannose-6-phosphate receptor (MPR), the transferrin receptor and the low-density lipoprotein receptor, through the interction of their cytoplasmic tail sorting motifs [9, 10]. This is followed

by the subsequent invaginating and budding off of the membrane to form a sealed double membrane bound vesicle with the previously extracellular components on the luminal side. At this point, these endosomes are often called sorting endosomes, and as the name suggests, the various components of endosomal contents are either returned to the plasma membrane, trafficked to the endocytic recycling compartment (ERC) or retained in the endosome [8].

Alongside endocytosis, lysosomes also receive material through two other pathways; via the *trans*-Golgi network (TGN) [11], or through autophagy of macromolecules and cellular organelles [12, 13]. Newly synthesised lysosome-bound proteins including the vacuolar- type proton ATPase (V-ATPase), acidic hydrolases and degradative proteases such as the cathepsins, are glycosylated in the ER, before the sugars are phosphorylated in the *cis*-Golgi to mannose-6-phosphate (M6P) residues [14]. These M6P tagged enzymes are recognised by the MPR, and subsequently packed into clathrin coated vesicles [15]. These vesicles are then delivered to endosomes, whereby the drop in luminal pH causes the receptor to dissociate from its substrate and the free receptor is returned to the ER [11, 15].

Following the initial sorting of contents, endosomes experience a drop in pH as they mature, both by fusing with existing endosomes and through the actions of V-ATPase [16]. From this point, there are several theories as to how material from early endosomes arrives in lysosomes. One theory is that there is a gradual maturation process, whereby the endosomes keep maturing and fusing with existing lysosomes until they gradually acquire the properties of lysosomes [17, 18]. Another theory is that lysosomes recieve their cargo through the vesicular transport of endosomal contents termed endocytic carrier vesicles [18]. Recent evidence suggests that lysosomes and late endosomes are distinct organelles, which may undergo transient "kissing" events to transfer material, as well as whole-organelle fusion events, after which the lysosome reforms [19, 20]. At a practical level, the identification and differentiation of early endosomes, late endosomes and lysosomes is a rather grey area. Early endosomes can be differentiated from late endosomes and lysosomes as they contain several housekeeping markers such as the transferrin receptor, as well as having a higher pH [21]. As endosomes mature, they begin to develop vesicular bodies within the endosome, this has led to the term multivesicular bodies (MVB). These are probably developed by sequential budding and pinching off of endosomal membranes,

controlled by the endosomal sorting complex required for transport (ESCRT) proteins I-III [22]. Differentiating between late endosomes and lysosomes is more problematic, as they are equally acidic and present very similar markers, as would be expected if one is simply a gradual extension of the other. Lysosomes do, however contain much higher levels of the anionic phospholipid, bis(monoacylglycero)-phosphate (BMP) in the internal and limiting membranes [23] as well as expressing no MPR.

Lysosomal biogenesis has been shown to be closely regulated in response to lysosomal signals by the actions of mammalian target of Rapamycin (mTOR) and transcription factor EB (TFEB) [6]. mTOR is located within the mTOR complex 1 (mTORC1) bound to the lysosomal surface through interactions with both V-ATPase and a proposed lysosomal Na^+ channel, composed of the two-pore channels (TPC) 1 and 2 [24, 25]. The binding of mTORC1 in this conformation activates the complex at the lysosomal surface [26]. In addition to several co-factors (including Ragulator, RagA/B and RagC/D), this has been termed the lysosomal nutrient sensing (LYNUS) machinery [27].

TFEB interacts with Rag proteins A-D within mTORC1 at the lysosome cytoplasmic surface, and is phosphorylated by mTORC1 [28, 29], keeping it bound to the LYNUS machinery. Inhibition of lysosomal function releases this complex and results in dephosphorylation of TFEB [24]. This induces nuclear translocation of TFEB [30, 29, 31, 32]. In the nucleus, TFEB binds promotors of Coordinated Lysosomal Expression and Regulation (CLEAR) genes involved in lysosomal biogenesis, inducing both more production of TFEB and driving the biogenesis of lysosomes [33, 29].

1.1.3 Lysosomal Enzymes

The lysosome contains several distinct hydrolases, which are responsible for the degradation of all major classes of macromolecule targetted through the LE/Ly system. These include approximately 50 acid lipases, which are typically responsible for the degradation of complex lipids, recycled from the cell membranes, into their constituent components [34]. In addition, lysosomes contain several adaptor proteins which serve to enhance the binding of hydrolases to their substrates [34]. The sphinglipid activator proteins (SAPs), GM2 activator protein (GM2-

AP) and the saposins, are vital to the function of acid hydrolases *in vivo*. There are several storage disorders which arise from dysfunction of these cofactors, the phenotype of which is similar to that caused by a lesion to the hydrolase(s) which the SAP assists [34, 35, 36, 37, 38]. The saposins are formed from the cleavage of prosaposin by proteases in the lysosome, to form saposins A-D [39]. Prosaposin deficiency leads to a neonatal fatal disorder whereby cells accumulate large amounts of many sphingolipids [34]. This highlights the vital role that SAPs play in the sphingolipid degradative pathway.

To protect the cell from the degradative contents of these organelles, the lysosome is bound by a double leaflet membrane. The outer membrane consists of much the same material as the plasma membrane, whereas the inner lysosomal (limiting) membrane is made up of highly *N*-glycosylated membrane proteins known as the glycocalxy [40, 41]. The sugar-rich heads of these proteins protude into the lysosomal lumen, protecting the lipids in the membrane leaflet from degradation by the hydrolases, and the cell itself from the digestive capacity of the lysosomal contents.

As lipids within the limiting membrane are protected from degradation, lipid substrates are transferred to intraluminal vesicles by ESCRT proteins by tubular formation and budding, followed by scission [42]. These platforms within lysosomes are proposed to be the site at which the main degradation of substrates occurs [43]. The drop in luminal pH, caused by fusion of LE/Ly, alongside the actions of the V-ATPase, occurs concurrently with an increase in the lysosomal concentration of the anionic phospholipid, BMP [44], which, even at low pH retains its negative charge [45]. BMP is predominantly located in the intra-luminal vesicles seen within LE/Ly, and may account for up to 70% of the lipid content of intra-luminal vesicles [46], despite only accounting for <1% of total lipid in most cells and tissues [47, 48]. As proteins within acidic environments become positively charged [48], BMP with its negative charge serves to facilitate insertion of SAPs and hydrolases into the intra-luminal vesicle membrane. BMP has been shown to be vital for the catabolism of various substrates including GM2 *in vitro*, and the addition of BMP to liposomes has been shown to increase activity of hexosaminidase A by 100 fold [48]. This is a property inherent to anionic lipids in general, as the addition of PI, PA have similar effects [49, 50].

Alongside the decrease in luminal pH, levels of cholesterol which are initially high, decrease as the lysosome matures. Although the exact mechanism remains unclear, two proteins are heavily involved in this process NPC1 [51] and NPC2 [52]. NPC2 is a soluble endosomal cholesterol transporter which most likely removes cholesterol from the intra-luminal vesicle and delivers it to the limiting membrane [53, 54]. At this point it is believed that NPC1 is involved in effluxing the molecule from within the lysosome whereby it is returned to the ER and Golgi [55]. It has been proposed that the removal of cholesterol from intra-lysosmal membranes decreases the lateral packing of the membranes, increasing fluidity and allowing the access of degradative machinery [56, 57].

Within the periphery, cholesterol is predominantly acquired either by *de novo* synthesis, or from dietary uptake, and is predominantly circulated bound to the low density lipoprotein, LDL [58]. From this point, circulating cholesterol can be acquired by cells, which then process the molecule at the ER into esterfied cholesterol through the actions of acyl-CoA cholesterol acyltransferase (ACAT) [59]. LDL associated cholesterol circulating in the periphery is excluded by blood brain barrier, possibly through the action of endothelial ATP-binding cassette A1 (ABCA1) [60] and as such, cholesterol synthesis in the CNS after birth is restricted to local *de novo* synthesis [61]. This synthesis is predominantly carried out by oligodendrocytes and astrocytes, although some evidence does exist for neuronal cholesterol production, particularly in immature neurons [62]. The cholesterol produced by astrocytes has been shown *in vitro* to be effluxed by the ABC1 cholesterol effluxer and transferred to neurons bound to ApoE [63]. The uptake of cholesterol bound to ApoE is probably mediated by the various lipoprotein receptors including the LDL receptor and LRP1 [61]. LRP1 is a promiscuous receptor with over forty ligands, binding of which results in endoytosis of the ligand and eventual lysosomal delivery [64]. LRP1 is strongly expressed expressed in the CNS, and particularly by neurons [65, 66, 67], including the Purkinje cells of the cerebellum [67]. Although CNS cholesterol synthesis is relatively high in the immature CNS, this production falls as the CNS matures, and ultimately, most CNS cholesterol is recycled [68]. Cytochrome P46 (CYP46) expressed in neurons converts cholesterol to 24S-dehydrocholesterol which can be either taken up by neighbouring astrocytes, or due to its altered membrane properties is favourably expelled across the blood brain barrier

[68].

Another major lipid class degraded in the lysosome are the sphingolipids, comprising sphingomyelin and glycosphingolipids (GSLs). Sphingomyelin is degraded by neutral sphingomyelinase at the plasma membrane [69], or by acid sphingomyelinase within the lysosome to form ceramide and phosphocholine [70]. Sphingomyelin has also been shown to strongly bind cholesterol [71] and further increases the lateral packing and rigidity of membranes [57]. The ability of NPC2 to extract cholesterol from membranes has also been shown to be inhibited by sphingomyelin *in vitro* and the conversion of sphingmyelin to ceramide has been shown to increase the cholesterol removal capability of NPC2 [72]. Additionally, increases in lysosomal sphingomyelin are associated with increased susceptibility of lysosomal membrane permeablisation (LMP), which will be discussed later in this section.

GSLs are degraded by the actions of lysosomal hydrolases, working in concert with SAPs. This occurs in a step-wise fashion by removal of the monosacharrides which project into the lysosomal lumen. The removal of sugars occurs at the non-reducing end sequentially, with each the removal of each sugar revealing a less complex GSL [34]. Degradation pathways for some of the sphingolipids and the enzymes and SAPs responsible for each step are shown in **Figure 1.1**. Loss of function of the relevant hydrolase, or its corresponding SAP results in accumulation of the target lipids(s).

The degradation of sphingolipids results in the generation of ceramide, a lipid which in itself has many biological properties. Ceramide, and its phosphorylated form, ceramide-1-phosphate, has been implicated in a wide variety of biological cascades, including apoptosis [73] and cell growth arrest [74, 75]. Ceramide has also been shown to have far less affinity to cholesterol than sphingomyelin, and that the conversion of sphingomyelin to ceramide by ASM increases the fluidity of intraluminal membranes along with cholesterol efflux [76].

The final step in the degradative cascade of sphingolipids is the catabolism of ceramide into sphingosine by acid ceramidase [77] and under specific conditions, the reverse reaction [78]. Sphingosine can subsequently be converted to the potent signalling molecule sphingosine-1-phosphate (S1P) by the sphingosine kinase isozymes [79], or recycled via the salvage pathway into GSLs [80].

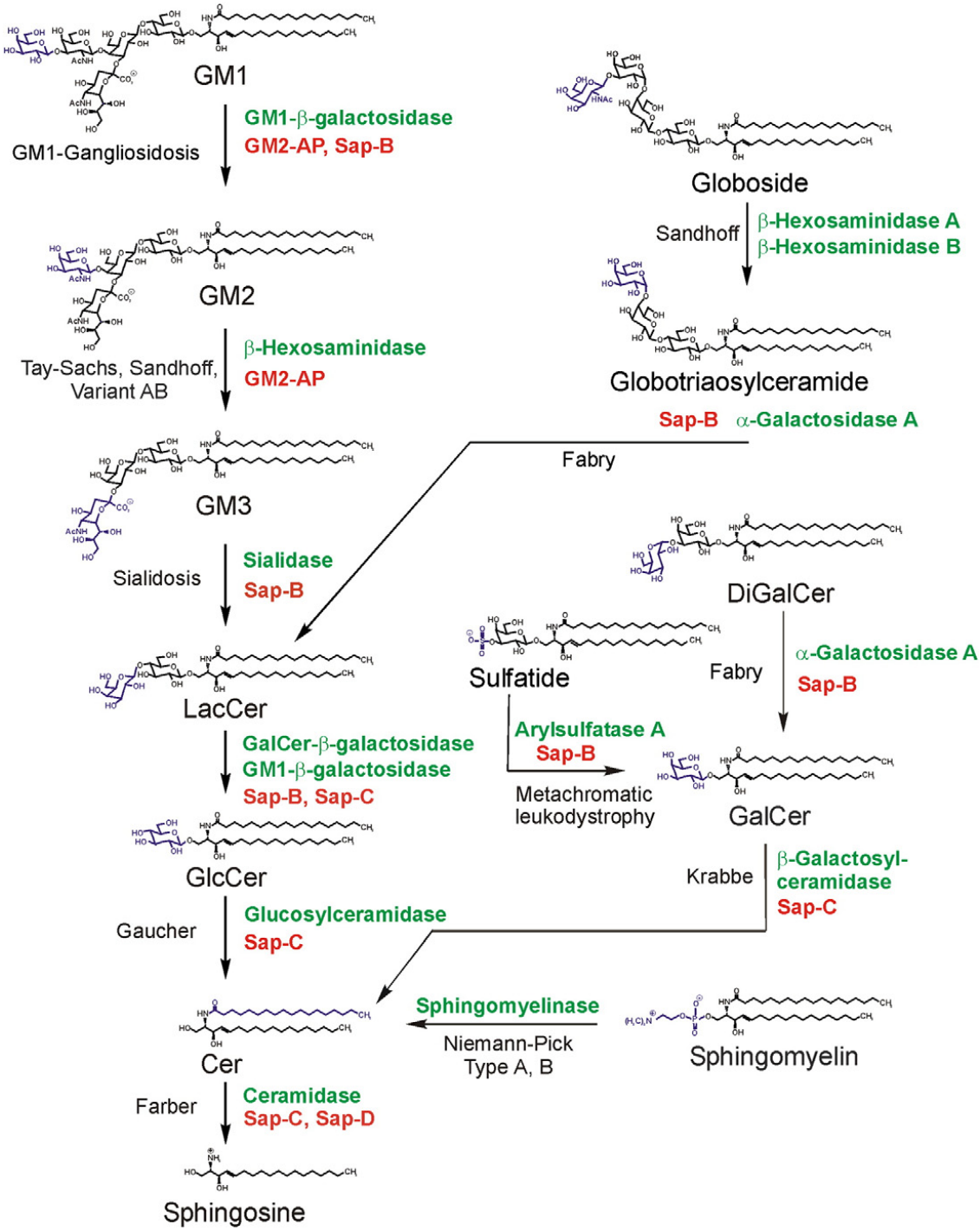


Figure 1.1: Sphingolipid degradation and sphingolipidoses. The names of individual inherited diseases are indicated. Degrading enzymes are given in green, activator proteins required for the respective degradation step *in vivo* in red. Variant AB, variant AB of GM2 gangliosidosis. Figure originally from[34]

.

S1P has many biological functions including promoting cell migration of immune cells [81, 82] and during development of multiple systems including the CNS [83, 84, 85] and vasculature [86, 87]. Sphingosine itself has been shown to inhibit PKC, at pH values where the amine group is protonated [88]. PKC itself is responsible for phosphorylating and thereby activating ASM [89, 90]. Calcium release by the sarcoplasmic reticulum has also been shown to be inhibited by sphingosine [91], as has the filling of lysosomal calcium stores [7]. Due to its free amine group, sphingosine is positively charged in the lysosome (pKa 6.7-8.4) [92]. This positive charge gives sphingosine detergent properties, and probably accounts for its potent cytotoxic properties at high concentrations [92]. As it is positively charged, it may not freely cross the limiting membrane, and it needs to be effluxed by an, as yet unidentified, transporter [93]. The lysosomal trans-membrane protein NPC1 has been proposed to be a possible effluxer of sphingosine, given its homology to the bacterial resistance-nodulation-division (RND) permease family [94].

1.1.4 Lysosomal Membrane Permeablisation

The lysosome also contains several proteases which operate best at lysosomal pH. Among these are the lysosomal protease family of cathepsins. Despite operating optimally at pH4-5, cathepsins can still function at neutral pH but with decreased stability and/or altered specificity [95]. The cathepsins have been shown to have specific functions in various processes including antigen presentation, epidermal homeostasis, prohormone processing, maintenance of the central nervous system in mice and angiogenesis [96]. The release of cathepsins from the lysosome has also been shown to be an important trigger for apoptosis [96, 97, 98], as well as a non-classical mechanism of programmed cell death [99, 98, 100]. Lysosomal membrane permeablisation (LMP) can be triggered by a variety of stressors such as H_2O_2 [101], L-leucyl-L-leucine methyl ester [102], sphingosine [92, 90, 89], the lysosomotropic antibiotics norfloxacin and ciprofloxacin [103], and the absence of HSP70 [104]. The degree of lysosomal permeablisation has been suggested to determine whether the cell undergoes apoptosis or non-classical programmed cell death [92]. An example of this is the exogenous addition of sphingosine, which at low concentrations causes apoptosis, and high concentrations causes rapid necrosis [90, 89]. In the first instance this has been shown to be mediated by cathepsins which activate the caspase pathways, as the apoptosis

can be inhibited by cathepsin inhibitors [92].

1.2 Lysosomal Storage Disorders

Lysosomal storage disorders (LSDs) arise from deficiencies in the function, translation, localisation and trafficking of lysosomal proteins, resulting in the accumulation of primary and secondary degradative material [93]. That most LSDs are associated with severe neurological symptoms alongside varied phenotypical presentation underscores both the vital role that lysosomes play in a broad range of physiological processes **(Table 1.1)**, and the susceptibility of this system to disruption.

The loss of hydrolase activity in several LSDs where the primary lesion is in a gene encoding for a lysosomal hydrolase results in decreased ability for the cell to degrade accumulating substrates. It is estimated that residual activities of lysosomal hydrolases above 10% are sufficient to prevent the accumulation of most lipid substrates, although this varies between hydrolases, probably due to the different rates of lipid turnover [105, 106]. Deficiencies below 15% normal activity of glucosylceramidase are sufficient to cause a rapid accumulation in glucosylceramide in Gaucher patient fibroblasts [107]. LSDs of particular relevance to this thesis will be discussed in more detail later in this chapter.

1.2.1 Functional Consequences of Mutation

Different mutations, depending on their location and magnitude within the encoding gene, can have varying consequences on the sebsequent fate and function of the protein. Mutations in or around the active site, can give rise to altered specificity and activity of enzymes. Mutations which affect the binding of M6P to the lysosomal protein, or in the case of ML-II, a defective capacity to generate M6P tags, results in the mistargetting of proteins to extra-lysosomal locations.

Sometimes mutations encode proteins which have normal activity, but are processed abnormally through the proteasomal system, in a process called endoplasmic reticulum associated degradation (ERAD). The functional consequence is that significant or complete reductions in the levels of proteins expressed by the cell prevents normal protein function. The processing and

Deficiency Class	**Disease**	**Protein**	**Accumulating Substrate**	**Organ(s) Affected**
Lysosomal Enzyme	Fabry	α-galactosidase A	Gb3	Kidney, Heart, DRG
	Sandhoff	β-hexosaminidase A/B	GM2, GA2	Liver, Spleen CNS
	Tay-Sach	β-hexosaminidase A	GM2, GA2	CNS
	Multiple Sulfatase Deficiency	Sulfatase-modifying factor 1	sulfated GAGs	Spleen/Liver, Bone
Lysosomal Membrane Protein	Niemann Pick type C1	NPC1	Multiple	Liver, Spleen, CNS
	Cystinosis	Cystinosin	Cystine	Kidney, Eye
	Mucolipidosis IV	Mucolipin I	Multiple	Eye
Lysosomal Soluble Protein	Niemann Pick type C2	NPC2	Multiple	Liver, Spleen CNS
	GM2-gangliosidosis, v. AB	GM2-AP	GM2, GA2	Liver, CNS
Extra-Lysosomal Proteins	Mucolipidosis-II	N-acteyl glucosamine phosphoryl transferase	Multiple	Liver, Spleen, Heart, Skeletal, CNS

Table 1.1: Table showing common and rare LSDs. As enzyme specifificities, substrates and affected organs vary between species, this refers only to human versions of the diseases.

ERAD of missense mutations may contribute to the heterogeneity underlying LSD symptoms, for example in Gaucher disease [108]. The processes determining the refolding of proteins, and their degradation is discussed at greater length in **section 1.5**.

1.2.2 GM2 Gangliosidosis

The GM2 gangliosidoses are thus named due to characteristic accumulation of GM2 and, variably GA2 in the periphery and/or CNS of affected individuals [109]. These diseases are chatacterised by a high degree of disability and significant reductions in life expectancy [110, 111]. The causes of these deficiencies arise from mutations in the *HEXA*, *HEXB*, and *GM2A* genes, encoding the α and β subunits of the lysosomal hydrolase β-hexosaminidase and the GM2 sphingolipid activator protein, GM2-AP respectively. Mutations in *HEXA* give rise to Tay-Sachs disease, which results in the accumulation of GM2 [112, 113] whilst mutations in *HEXB* give rise to Sandhoff disease [114], resulting in the accumulation of GM2 and GA2. Due to the required activty of GM2-AP for the isozymes of β-hexosaminidase, mutations in the *GM2A* gene gives rise to a variant classified as AB, reflecting its shared phenotype with both diseases. As detailed previously, variations in the residual activity of both isozymes of β-hexosaminidase gives rise to a significant degree of variability in the severity and age of onset of these disorders, the disorders are subsequently classified into infantile, juvenile and adult-onset [105, 106].

Tay-Sachs Disease

Tay-Sachs disease is characterised by the loss of function of the α- subunit of the β - hexosaminidase enzyme, resulting in the loss of function of the isozymes HexA ($\alpha\beta$) and HexS ($\alpha\alpha$). Although the function of HexS has been regarded as physiologically irrelevant in human disease loss of function of HexA results in the accumulation of the storage lipid GM2 [115, 116]. Infantile Tay-Sachs patients suffer from mental and motor dysfunction from 1 year, accompanied by macrocephaly, and the development of seizures, deafness, blindness and spasticity, with early death typically in the third year of life [111]. Juvenile Tay-Sachs symptoms typically begin later, with dementia, ataxia, speech loss, seizures and a vegetative state occuring before the 10th year, and death occurs soon after [117]. Late-onset patients develop symptoms of cerebellar-ataxia,

dementia, speech abnormalities with a high degree of variablity and is a very heterogenous disease group. Infantile Tay-Sachs patients accumulate significant levels of GM2 during the course of disease, and by the time of death, GM2 and GA2 accumulations in the CNS, have been reported of 300 and 20-fold, respectively [118].

Sandhoff Disease

Sandhoff disease is caused by mutations in the *HEXB* gene which encodes the β subunits of the β hexosaminidase isozymes HexA ($\alpha\beta$) and HexB ($\beta\beta$). This results in an inability to degrade the GSLs GM2, GA2, and Gb4. The clinical features of infantile Sandhoff disease are remarkably similar to those observed in infantile Tay-Sachs disease, but with the addition of significant non-neuronal disease burden which is absent in Tay-Sachs disease. This peripheral presentation includes enlargement of the spleen and liver and skeletal abnormalites [111, 119]. Accumulation in the CNS of GM2 and GA2 occurs in infantile Sandhoff disease patients, and increases can be as high as 300 and 100 -fold respectively, this occurs in conjunction with an apparent decrease of the major brain GSLs, GD1a, GD1b and GT1b. In peripheral organs, the accumulation of Gb4 is also increased in the spleen and liver [111, 120, 118, 121, 122, 123]. There is also a concurrent accumulation of secondary storage lipids, which are not normal degradative substrates for the HexA and HexB isozymes, including GD2, GD1a, and lyso-GM2 [111, 119].

Sandhoff disease A/B Variant : GM2 Activator Protein Deficiency

Sandhoff disease variant A/B is caused by the loss of the GM2-AP, which has shown essential roles in the presentation of GM2 and related lipids from the lysosomal membranes to HexA [48]. Loss of function of this protein causes accumulations of lipids in a profile similar to Tay-Sachs disease, but patients have normal enzymatic degradative function of both HexA and B towards an artifical substrate, but not towards GM2 itself [124].

Patients typically present with a clinical presentation very similar to infantile Tay-Sachs disease, with death usually occuring by the 4th year [111].

Pathologies of the GM2 Gangliosidoses

The pathology of the 3 variants of the GM2 pathologies in the CNS is remarkably similar in humans, but varies within the variants depending on the severity of the deficiency in enzyme activity [111, 121, 125]. Infantile onset patients brains show severe atrophy, and an increase in ventricular volume [111]. Neurons in the GM2 gangliosidosis brain display abnormal morphology, including meganeurite outgrowth, dendritic atrophy, and this degeneration of neurons is accompanied by marked gliosis [111]. The brain regions most severely affected in the GM2 gangliosidosis, are the hippocampus, cortex, brain stem, spinal cord and the cerebellar granule cells [111]. There is a pronounced loss of white matter in Sandhoff disease accompanied by decreases in the myelin lipids sulfatide and galactosylceramide (GalCer) [111], which is less prominent in the other two variants [120]. The storage of lipids is reflected in the appearance of MVBs within the cytoplasm, which are positive for periodic-acid Schiff staining, indicating the presecence of sugar residues [111].

The precise role that the storage of lipids and β-hexosaminidase deficiency play in the pathology of the GM2-gangliosidoses is unclear, but shared accumulation of GM2 within the CNS between the three variants likely contributes to the observed phenotype.

1.2.3 Fabry disease

Fabry disease arises from the loss of function of the lysosomal hydrolase α-galactosidase A (GalA) [126]. Loss of function of this enzyme results in the accumulation of lipids containing terminal α-galactosyl sugar moieties within the LE/Ly system. As the gene responsible, *GALA* is located at Xq22 [127], the disease is both more prevalent, and more severe in males than females, although the distribution cannot be considered to be X-linked recessive [128]. Male hemizygotes ($GALA^{-/0}$) present with classical symptoms of corneal opacity, peripheral neuropathic pain, intolerance to heat [129, 130]. Later in life, progressive kidney disease, cardiac symptoms and cerebrovascular disease develop [129]. Kidney disease often results in kidney failure, requiring treatment by dialysis and organ transplantation [131]. Hemizygote males suffer from a reduced life expectancy, with early death in the 4th and 5th decades, typically from kidney failure and cardiac complications [128]. Affected females display a remarkable heterogeneity of symptom

presentation, with many heterozygotes being either asymptomatic or having sporadic symptom presentation. The symptoms reported in heterozygotes include neuropathic pain, reduced kidney function and failure, hypertrophic caridac myopathy, although symptom presentation is not predictable[128], most likely due to random X-inactivation in affected females [132]. A retrospective study of hemizygotes for the *GALA* gave an incidence of 1:117,000 live births, and extrapolation to heterozygotes as high as 1:57,000 live births [133]. The heterogenous symptom presentation and late-onset of disease often lead to misdiagnosis, and it is suspected that the true figure of incidence could be much higher. Studies examining incidences of *GALA* mutations and GalA deficiencies put the incidence at 1:4000 in the general population [134, 135]. GalA deficiency results in lysosomal accumulation of neutral lipids with galactosyl moeities at the terminal α linkage. The main accumulating lipid in Fabry disease is Gb3. Gb3 accumulation is detected in the endo- and parathelial cells of of the vasculature, in the the endothelial cells of the kidney [136] and within ganglion cells of the autonomic nervous system [137], correlating closely with the affected organs. Some sporadic neuronal involvement has also been observed in the CNS, typically in select populations of neurons in the spinal cord and mid- and hind-brain structures [138].

1.3 Niemann-Pick type C Disease

Niemann-Pick type C disease (NPC) is an autosomal recessive genetic disorder arising from mutations in the genes *NPC1* [139] or *NPC2* [140], encoding proteins of the same name. Dysfunction of either of these two proteins results in a clinically indistinguishable disease phenotype characterised by progressive ataxia, tremor, learning difficulties, dementia and premature death [141]. NPC1 is a 13 trans-membrane spanning protein which contains a leucine zipper, a sterol-sensing motif and is localised to the LE/Ly compartment [139]. Mutations in *NPC1* account for 95% of cases NPC disease, the other 5% of cases occur as a result of mutations in the *NPC2* gene [142, 143, 144]. There are over 130, mostly missense mutations in the *NPC1* protein [145], which result in a broad clinical presentation in terms of age of onset and severity of disease presentation and progression [144]. Mutations in *NPC1* occur throughout the gene, but are particularly localised in a portion encoding a cysteine rich domain of the protein between residues 927 and

958 [145]. The most common mutation occuring in humans, $NPC1^{I1061T}$ has been shown to result in a protein which is subjected to endoplasmic reticulam associated degradation (ERAD) [146].

A spontaneous mutant mouse model known as the Npc^{nih} mouse (herein referred to as *Npc1*$^{-/-}$) results from insertion of 824bp of non-coding DNA into the *Npc1* gene, resulting in a truncated protein with only 2 of its 13 transmembrane-domains. The *Npc1*$^{-/-}$ mouse has an aggressive disease course similar to the infantile-onset form of the human disease. Mice develop tremor and ataxia at around 6 weeks of age and die at 11 weeks [147]. At the cellular level, a variety of lipids are stored in late endosomes/lysosomes (LE/Ly) [148] including cholesterol, bis(monoacylglycero)phosphate (BMP), sphingomyelin (SM) [149], fatty acids [150], glycosphingolipids (GSLs), and sphingosine (SphO) [151].

NPC displays a profound block in endocytic transport which has previously been shown to be mediated through a sphingosine-dependant lysosomal calcium deficiency [7]. This trafficking deficiency can be induced by the exogenous addition of sphingosine, or by addition of the class II amphiphile U18666A to wildtype cells. Impaired lysosomal calcium release is presumed to occur through severely impaired filling of lysosomal calcium stores as shown by abrogated calcium release from lysosomal stores in NPC1 deficient cells following treatment with either Gly-Phe β-naphthylamide (GPN) or Bafilomycin A1 [7]. Chelation of lysosomal calcium using high-affinity Rhodamine-Dextran was also sufficient to induce an NPC phenotype in control cells [7].

1.3.1 NPC: Pathologies

Neuronal pathology in NPC is characterised by the accumulation of lipids within LE/Lys, axonal blebbing, neuronal degeneration, in particular the progressive and patterned loss of cerebellar Purkinje cells in a rostro-caudal fashion beginning at lobule I and progressing through to lobule IX [152, 147]. Interestingly, zebrin–II^{+} (including lobules XI and X) Purkinje cells are resistant to cell death, with the majority of these Purkinje cells surviving until death of the animal [152]. The reason behind the particular susceptibilty of zebrin–II^{-} Purkinje cells is unclear, but various disease states including global cerebral ischaemia [153] and the lysosomal storage disorder, Niemann Pick type A (NPA) [154] also result in the preferential loss of zebrin–II^{-}

Purkinje cells, suggesting that their function or physiology conveys vulnerability to stress.

Inflammation of the CNS is an early event in NPC, and reactive astrocytosis has been identified in several regions of the CNS, including the thalamic nuclei, hippocampus, substantia nigra, cortex and cerebellum as early as 2 weeks [155, 156]. Transgenic rescue studies of astrocytes restored with functional NPC1 [157], and conditional knockouts under the GFAP promoter did not show any significant effects on neuronal pathology [158]. However, a recent study showing that the anti-inflammatory ibuprofen gave moderate improvements in the lifespans of *Npc1*$^{-/-}$ mice [159], and an *in vivo* transgenic rescue of *Npc1*$^{-/-}$ mice expressing *Npc1* in astrocytes showed phenotypic rescue [160]. These data provides some evidence of a role for inflammation in the pathology of NPC, but not a causative one.

NPC shares many pathological features with NPA, which is a genetic disorder resulting from deficiency of acid sphingomyelinase (ASM) [161] a lysosomal enzyme which catalyses the catabolism of sphingomyelin into ceramide and phosphocholine [162]. Loss of function of ASM results in the accumulation of sphingomyelin and cholesterol within LE/Lys, which is associated with a decrease in lysosomal stability to photo-oxidation induced damage [163]. NPA patients and the corresponding *ASM* knockout mice share a very similar pattern of cerebellar neuronal loss to that observed in the *Npc1*$^{-/-}$ mouse, in particular the progressive and patterned loss of cerebellar Purkinje cells [154]. The accumulation of sphingomyelin in NPC has been shown to be caused in part by a secondary defect in the half-life and activity of ASM [164, 165] but not the localisation of the protein [166]. Correction of the secondary ASM deficiency has been shown to correct cholesterol storage in human NPC patient fibroblasts [167], which is probably due to the very high affinity between these two lipids.

Conversely to the gross increase in neuronal lipid levels, decreases in the levels of galactosyl ceramide, cholesterol and phospholipids were observed in the white matter of confirmed sufferers of NPC [168]. Both cholesterol and galactosyl ceramide are heavily represented in the lipids of the myelin sheath, suggesting decreased myelination in patients. Recent studies using MRI have also observed significant alterations of the white matter consistent with reduced myelin content [169]. Studies on the *Npc1*$^{-/-}$ mouse showed that the development of myelin is stunted, with the development and extension of myelin basic protein (MBP)$^{+}$ oligodendrocytes being significantly

delayed both at 21 days and 54 days within both the cerebellum and the forebrain [170].

Promoter	**Cell Lineage**	**Cell Loss**	**Myelination**	**Symptoms**	**Life Span**
Pcp-2[171]	Purkinje cell	6 weeks, PC	Normal	Tremor, Ataxia	>20 weeks
Syn1[172]	All Neuronal	6 weeks, PC	Impaired	Tremor, Ataxia	13 weeks
CNP[172]	All Glial	23 weeks, PC	Delayed	Delayed Tremor, Ataxia	>23 weeks

Table 1.2: Introduction : Conditional knock-outs of NPC1 in neuronal cell lineages.

Studies of the effects of NPC1 deficiency in several cell types of the CNS have helped to elucidate the role of NPC1 in neuronal pathology (see **Table 1.2**). Conditional *Cre* recombinase knockouts of *Npc1* in Purkinje cells under the control of the *Pcp-2* promotor ($Npc1^{flox/-}$;*Pcp2*-Cre^{+}) showed that whilst Purkinje cell death is responsible for some of the physical manifestations in NPC disease, in particular the development of ataxia and tremor, the mice did not display weight loss and none of the mice died prematurely, although the mice were only followed for 20 weeks [171]. Furthermore, it is also apparent that the Purkinje cell death is an autonomous event [171], rather than the result of inflammation or dysfunctional support by other neuronal and non-neuronal populations. Cre-mediated deletion of *Npc1* in global neuronal cell populations using the *Syn1* promotor ($Npc1^{flox/-}$;*Syn1*-Cre^{+}) results in a hypomyelination phenotype indistinguisable from global deletion of the NPC1 protein, whereas Cre-mediated deletion of *Npc1* in glial cell populations using the *CNP* promotor ($Npc1^{flox/-}$;*CNP*-Cre^{+}) resulted in delayed myelination that recovered to levels comparable to controls by P54 [172]. Whilst the neuron specific knockouts displayed a typically aggressive disease course, they did live slightly longer than the global null mutants. Additionally, and perhaps surprisingly, the glial specific knockouts did display a delayed onset of tremor with the loss of significant numbers of Purkinje cells at 23 weeks [172]. These data suggest that whilst the majority of symptoms are associated with neuronal pathology, particularly the loss of Purkinje cells, the loss of NPC1 in other cells of the CNS is sufficient to exacerbate the course of NPC disease.

1.4 Current Therapies for Lysosomal Storage Disorders

1.4.1 Enzyme Replacement Therapy

Where the cause of an LSD is the loss of function of a lysosomal hydrolase, two therapies, enzyme replacement therapy (ERT) and bone marrow transplantation (BMT) have been shown to be of clinical benefit. ERT relies on the infusion of recombinant enzymes, and BMT relies on transplanted bone marrow from non-affected indivivuals synthesising and delivering enzyme via circulating cells. Only lysosomal hydrolases with a Mannose/M6P tag are delivered to the endosomal system, as circulating enzymes need to endocytosed by the mannose/insulin-like growth factor (IGF) II receptor to reach the endocytic system. As such, initial attempts at ERT failed, mainly due to the fact that enzymes prepared lacked the relevant tag [173].

Direct replacement of missing enzyme function by either ERT or BMT has worked particularly well at correcting the peripheral storage in several LSDs. Type 1, non-neuronopathic Gaucher disease is one particularly successful story of ERT, and early intervention with glucocerebrosidase is sufficient to prevent the occurence of physical disease [174, 175, 176]. Galactosidase A ERT has also been applied to Fabry disease with reasonable success [177, 178], using two commercial preparations (Fabrazyme and Replagal). ERT has also been trialled in several other peripheral storage disorders where there is minimal CNS involvement with reasonable success [179, 180].

Unfortunately, availability of systemic enzymes in the CNS is low or non-existent meaning that the neurological disease component goes almost completely untreated [181, 182]. However, preclinical studies of BMT in Sandhoff disease have shown that there is some CNS protection offered by BMT, presumably through secretion of lysosomal hydrolases through bone-marrow derived glial cells [183, 184]. However, additional issues of graft rejection and graft-versus host disease mean that this therapy has major drawbacks [185].

1.4.2 Gene Therapy

Gene therapy (GT) is an experimental therapy which holds great promise for the treatment of inherited disease. Current GT approaches involve using viral constructs to stably transfect cells with functioning copies of mutated genes, such that normal protein function is restored. As the majority of LSDs are autosomal recessive, and as such, cells only require one functioning

copy, allied with the low level of protein function required, they are an attractive target for GT [186]. Typically, the stable transfer of genes is sporadic and localised to injection sites within the CNS [187]. As such, to acheive a viable treatment, transfected cells must be able to secrete the therapeutic protein, thereby "cross-correcting" adjacent cells [188]. However, for this to be an option, the target protein must be soluble. Therefore, cross correction for membrane bound proteins (e.g. NPC1) is not an option [187].

Another major barrier to successful GT, is the fact that, like ERT and BMT, to correct the CNS the viral constructs must cross the blood brain barrier [187]. Additionally, as most neuronal populations are post-mitotic, viral constructs muct be able to stably transfect non-mitotic cells [187]. Despite these issues, proof of concept studies in several disorders have shown efficacy in treating LSDs, when initiated at an early phase. Adenoviral delivery of the *HexB* gene in cats has shown promise in the treatment of Sandhoff disease [189], as has work focussed on mucopolysaccharidosis (MPS) VII (β-glucuronidase deficiency), and viral delivery systems have shown great efficacy in mouse models of this disease, reducing CNS storage, delaying symtpom onset and increasing survival following neonatal intracranial injection [190, 191, 181]. However the viral gene expression decreases rapidly following treatment [192, 193].

While viral induced expression of recombinant proteins is an attractive therapeutic target for the future, the issues of reliable gene expression, and the low availability in the CNS without direct intrathecal injection, remain problematic for the development of successful gene therapy [194]. Additionally, immune responses of virally transfected cells are only beginning to be understood and the silencing of transfected gene products also remains an issue [195, 196, 194].

1.4.3 Chemical Chaperones

Mutated enzymes are often misfolded, and as such are degraded by ERAD. Chemcial chaperone therapy seeks to use chemical inhibitors of the enzyme, to allow them to more readily undertake their functional shape, allowing them to escape the ER and reach their functional destination [197]. In the case of lysosomal hydrolases, this is the lysosome. At this point, the chemical chaperone is released by the drop in pH, and the enzyme is then ready to perform its normal function. Fibroblasts from Fabry disease patients carrying the missense mutation $GALA^{\mathrm{Q279E}}$

were shown to have defective activity due to ERAD of the misfolded protein [198]. Treatment of these fibroblasts, and other fibroblasts carrying missense mutations, with galactose, stabilised the mutant protein and allowed delivery to lysosomes where it functioned normally [199]. Further studies using the inhibitor, 1-deoxygalactonojirimycin (DGJ) on both Fabry and Gaucher fibroblasts carrying point mutations showed further efficacy [200, 201]. The use of chemical chaperones has shown efficacy in preclinical trials in Gaucher disease [202, 203] and Fabry disease [204], and several clinical trials are currently underway.

1.4.4 Substrate Reduction Therapy

Substrate reduction therapy (SRT) is a mode of therapy whereby reducing the substrates of a defective/missing enzyme(s) partially corrects the imbalance between impaired catabolism and metabolism [205]. One SRT which has been extensively tested in various LSDs is *N*-butyldeoxynojirimycin (*N*B-DNJ), also known as miglustat, a imino-sugar which is a GSL biosynthesis inhibitor [206]. Miglustat inhibits the ceramide glucosyltransferase-catalyzed biosynthesis of glucosyl-ceramide (GlcCer), resulting in reduced synthesis of all GlcCer derived GSL species [206]. Initial *in vivo* studies of the effects of SRT using miglustat has shown benefits in several LSDs including Sandhoff disease [207] and Tay-Sach disease [208]. Miglustat is also licensed as a treatment for type-1 Gauche disease, having shown efficacy in human patients [209].

Miglustat is also the only currently licensed treatment for NPC, having shown efficacy in a randomised controlled study [210]. In NPC, treatment with miglustat results in decreases in GSL storage in brain and peripheral tissues and delays the onset of symptoms and increases patient survival [210]. In the *Npc1*$^{-/-}$ mouse model, treatment with miglustat at P21 delays the loss of Purkinje cells, along with the associated onset of physical manifestations and significantly increases the lifespan of the mice [159, 211]. A study of miglustat on cats with a naturally occuring mutation in *NPC1* have also shown significant clinical benefits on the progression of the disease, including GSL accumulation, and a decreased rate of Purkinje cell death [212].

Miglustat treatment does not correct peripheral cholesterol storage in NPC [212, 211], whilst levels of glucosylceramide [211] in the brain are increased following treatment, probably due to off-target inhibition of the non-lysosomal glucosylceramidase, Gba2. Studies in our laboratory

have also shown that the effects of miglustat do not affect the hypomyelination phenotype in NPC (unpublished data, Boland, B). However, a small study using magnetic resonance spectroscopy in NPC patients on long-term miglustat treatment, did find evidence of normalisation of white matter, although the study size and lack of baseline controls in the study do pose limitations [213].

1.4.5 Cyclodextrin

A serendipitous discovery of the effects of 2-hydroxypropyl-β-cyclodextrin (CD) in NPC disease was made when *Npc1*$^{-/-}$ mice, given the hormone allopregnenalone dissolved in CD, showed a remarkable improvement in cholesterol sequestration in LE/Lys, and improvements in the lifespan and behavioural defects associated with NPC disease [214]. Further studies of CD administration found that early intervention with just CD in neonatal *Npc1*$^{-/-}$ mice significantly improved lifespan both as a single injection [215, 216], and as a chronic treatment [217, 218]. It was shown that treatment with cyclodextrin reduced cholesterol synthesis in the liver [216], and improved the excretion of cholesterol in the bile of *Npc1*$^{-/-}$ mice [218].

Cholesterol synthesis in the liver of *Npc1*$^{-/-}$ mice is significantly raised compared to *Npc1*$^{+/+}$ mice, due to the sequestration of cholesterol within the LE/Ly system. The sequestration of cholesterol prevents its esterification by ACAT, located at the ER [59]. This probably drives the production of cholesterol through the lack of inhibition from the cholesterol sensing proteins SREBP, and SCAP [219]. Treatment with CD reduces the amount of free cholesterol in the liver of *Npc1*$^{-/-}$ to wildtype levels, and increases the levels of cholesterol ester 3-fold [218]. The majority of work has focused on CDs cholesterol depleting properties. However, the mechanism of CD effects in NPC disease is unclear for several reasons. Firstly, whilst CD cannot cross the blood-brain barrier [220], treatment with CD slows Purkinje cell loss significantly, and improves the hypomyelination phenotype [216]. It is also unlikely that changes in peripheral cholesterol levels are affecting the neuorlogical phenotype as cholesterol in the brain is synthesised at an almost completely local level, mainly within oligodendroglial cells [221, 222], but also neurons themselves [223]. As such, the brain receives almost no peripherally-derived cholesterol.

Whilst the effects of CD have been hypothesised to be mediated mainly through its effects

on cholesterol, it has been shown that CD induces calcium-dependant lysosomal exocytosis [224]. In support of these findings, circulating B-cells from patients treated with CD show marked elevations in GSLs and lysosomal volume, suggesting that exocytosed material is being endocytosised by scanvenging cells [225].

1.4.6 Histone De-acetylase Inhibitors

Histone deacetlyses (HDAC) and histone acetyl transferases (HAT) function in synchrony to remodel the chromatin and regulate gene transcription [226]. HDAC levels have been shown to be dysregulated in fibroblasts of patients suffering from NPC disease [227]. Recent studies have shown therapeutic potential of inhibitors of HDAC (HDACi) in treating NPC. Treatment of *NPC1*$^{\mathrm{I1061T}}$ mutant fibroblasts (the most common mutation of NPC) with HDACi has been shown to rescue the NPC phenotype [228]. Whilst it has been speculated that this is achieved by enabling the proper post-translational glycosylation of the NPC1 protein rescuing it from ERAD [229], due to the broad effects of these drugs, the true mechanism will be difficult to elucidate. In addition to the obvious role of HDACi in rescuing improperly processed NPC1 proteins, it is possible that secondary enzyme deficits in NPC, such as the mislocalisation of ASM may also be mediated through a HDAC dependant mechanism.

The potential mechanisms of action of HDACi, are broad due to the multiple downstream effects of the target proteins, however, the proposed mechanism of rescue from ERAD, and subsequently proper processing of misfolded proteins is a therapeutic possibility shared with HSP70, a molecular chaperone with broad effects on cellular physiology. This will be discussed further in the following section.

1.5 The Heat Shock Response

The heat shock response (HSR) is the cellular response to environmental, pathophysiological, and physiological stressors which include the eponymous heat shock [230] alongside oxidative stress, nutrient deprivation, protein misfolding and aggregation [231] and ER stress [232]. Induction of the HSR results in a wide array of cellular responses, including the activitation and upregulation of molecular chaperones such as the heat shock proteins (HSPs), [230] sorting and folding of

new and damaged proteins [231], the targetting of mis-folded and denatured proteins to the ubiquitin/proteasomal system (UPS) [233] alongside other cellular processes for the maintenance of proper proteostasis.

1.5.1 Induction of Heat Shock Response

The induction of the HSR is tightly regulated at a transcriptional level [234]. Heat shock factors control transcription through binding to the heat shock element (HSE) which consists of inverted repeats of 3 or more 5'-nGAAn-3' repeats [235]. Vertebrates have 4 HSFs, of which HSF1 appears the most functionally important to mounting a HSR. For example, *hsf1*$^{-/-}$ mice [236] and fibroblasts [237] are unable to mount a HSR to a variety of stressors. Knock-outs of *hsf*s*2-4* can mount a HSR, although the repetoire of proteins induced is characteristically different in each case [238, 239, 240]. This suggests that the other HSFs are responsible more for the modulation of the HSR rather than its induction [238].

HSF1 is constitutively expressed in most tissues although the expression varies both between tissues and at different developmental stages. HSF1 is highly expressed in the rat kidney at postnatal days 2-10, but declines rapidly afterwards, and conversely is expressed at low levels in the cerebellum, brainstem and cerebrum from postnatal day 2, but increases in expression until adulthood, where it declines to a steady state [241]. In the mouse, significant differences in HSF1 mRNA were observed at 6 weeks of age, with the testis and ovaries displaying by far the highest levels, whereas the liver, kidney, heart and lung had still very strong mRNA levels [242]. Surprisingly, in this study the brain had very little HSF1 mRNA [242].

HSF1 is normally resident both within the cell nucleus and the cytoplasm [243, 244, 245]. Although it is shuttled between the nucleus and the cytoplasm, it is mainly concentrated within the nucleus in its inactive, monomeric form [246, 247]. Under conditions of stress, HSF1 trimerises thereby gaining DNA-binding function, undergoes nuclear localisation, and gains extensive post-translational modifications, including phosphorylation [248]. The HSE binding ability of HSF1 increases by several orders of magnitude following trimerisation [249].

Trimerisation of HSF1 is stressor dependant, and several proposed mechanisms exist for the regulation of this acivation step. A common feature of all cellular stressors to which a HSR is

generated is the production of unfolded/denatured proteins and the subsequent binding of HSPs to assist in protein refolding, or targetting for degradation [250]. It has been hypothesised that HSP90, found abundantly in most cell types under normal conditions, may regulate the activity of HSF1 by holding HSF1 in its non-active state [251, 252, 253]. HSP90 binds HSF1 under normal conditions, but upon association with unfolded proteins the binding of HSF1 is greatly reduced [254, 255]. This is supported by the finding that pharmacological inhibition of HSP90 can increase HSF1 trimerisation [256]. Suppression of HSF1 is diminished upon heatshock, and HSF1 monomers are available to trimerise and become activated. In addition to HSP90 holding HSF1 in an inactive conformation, HSP70 and HSP40 may inhibit the *trans*-activating function of HSF1 [257]. HSP90 also inhibits the HSF1 coactivator Daxx, which has been shown to be a potent upregulator of trimeric HSF1 activity [258]. Together these provide compelling evidence for the regulation of the HSR by both the proteostatic environment of the cell, and through the gene products of the HSR itself.

HSF1 has been shown to trimerise and bind the *hsp70* promotor within seconds of exposure to heat stress and levels of HSF1 bound to the promotor become saturated within minutes of initiation of the response [259]. The kinetics suggest it is unlikely that the interaction of HSP90 with unfolded protein and subsequent release of HSF1 is the only mechanism regulating HSF1 activation. Indeed, addition of a ribonucleoprotein complex comprising a translation elongation factor, (eEF1A) and heat-shock RNA-1, (HSRNA-1) is sufficient to induce the HSR, whilst additon of RNAi against HSRNA-1 attenuates the HSR [260]. It is hypothesised that heat-induced conformational changes in the RNA make-up of these molecules may serve as a 'RNA thermometer' to regulate the induction of the HSR [261]. Another mechanism proposed to initiate the HSR is the altering of fluidics of specific membrane regions. The fluidity of a membrane is dependant on several factors, mainly; the lipid composition, the presence of membrane proteins, and the temperature of the membrane [262]. The altering of membrane lipid composition is sufficent to sensitise a cell to heat-shock [263], and multiple cell types increase the fluidity of membranes under conditions of chilling through the conversion of saturated fatty-acids to unsaturated fatty acids [264] through the induction of desaturase genes [265]. Conversely, hyperthermia results in an increase of membrane fluidity, as does exposure to alcohol or a

number of psychotropic drugs and anaesthetics [262]. Increases in the fluidics of membranes are sufficient to induce a heat-shock response in the absence of misfolded proteins, through either the generation of lipid signalling molecules such as cholesterol glucoside [266] and sphingosine-1 phosphate [267, 268], or via effects on lipid rafts [269]. Modulation of membrane fluidics results in the downstream activation of HSF-1 and induction of the HSR [270].

Whilst these mechanisms are vital for the trimerisation, and subsequent DNA-binding capacity, of HSF1, this is insufficient to induce an adequate HSR, further posttranslational modifications of HSF1 are required for it to gain the required *trans*-activating properties for transcription of the HSPs [271, 272, 273]. Phosphorylation of HSF1 occurs concurrently to trimerisation upon activation of the protein and occurs signifcantly on serine residues [274], with a small number of phosphorylation sites upon threonine residues [275, 276, 277, 278]. Mutagenesis studies of the phosphorylation sites show that, whilst most of the phosphorylation sites are not required for *trans*-activation of *hsp* genes, (indeed, several of the sites are inhibitory to HSF1 *trans*-activatory activity [279]), phosphorylation of S326 and S230 increase *trans*-activation of the *hsp* genes [280, 258].

S326 enhances the interaction between HSF1 and the constitutively expressed coactivator Daxx [258], increasing both basal and heat-induced HSP70 expression. Serine-alanine substitution, or deletion of the residue ameliorated these effects [258]. S230 was identified as being a target for Calmodulin Kinase II (CaMKII). Inhibition of CaMKII activity reduces HSF1 phosphorylation at S230, and subsequent *trans*-activation, resulting in a much reduced HSR [280].

1.5.2 The Roles of HSP70

Molecular chaperones are often defined as being any protein which interacts, stabilises or allows another unfolded protein to acquire a functionally active conformation without being present in its final state [281]. Molecular chaperones serve several key proteostatic functions, including the folding of newly synthesised or misfolded proteins and the targetting of unfolded proteins to the proteasome [282]. Under normal conditions, molecular chaperones function to maintain proteins in their functional state, and to aid in the folding, and degradation of newly synthesised proteins from the ER. In the diseased state, molecular chaperones function to inhibit protein aggregate

formation through the induction of autophagy [282]. The inducible molecular chaperones are collectively known as the heat shock proteins (HSPs) and are grouped into families according to their molecular weights. These families are HSP40, HSP60, HSP70, HSP90, HSP100 and the small HSPs. Three families intrinsic for a normal HSR (and consequently, the most well studied) are HSP70, HSP90 and to some extent HSP60 [231]. These proteins are heavily involved in *de novo* protein folding and refolding following stress. Due to the complexity of the multi-domain structure and function of eukaryotic proteins, they are particularly susceptible to changes in their functional state [283]. Conformational changes to protein structure often results in hydrophobic regions being exposed to the intracellular milleau [231]. Proteins with exposed hydrophobic regions, are energetically inclined to form protein aggregates, fibrils and plaques which are highly toxic *in vitro* and *in vivo*, a process common across many degenerative states [284]. To prevent the formation of toxic aggregates, mis-folded proteins are bound by molecular chaperone machinery within the ER, which inhibit the undesired protein conformations, increasing the probability of a favourable conformation being reached [231].

HSP70 binds to exposed hydrophobic regions of misfolded proteins in an ATP dependant reaction. When bound to ATP, HSP70 is in an 'open' conformation, whereby it readily accepts non-native proteins delivered by HSP40 cofactors. The hydrolysis of ATP to ADP by HSP40 allows HSP70 to hold the protein in a stable conformation, preventing the aggregation of these exposed regions, and thus allowing proper folding of the protein. The protein, once stabilised, is released via recycling of the ADP to ATP by nucleotide exchange factors (NEFs) [285, 286]. The cycling of ATP is regulated by several co-factors; HSP70-interacting protein (HIP) retains the HSP70 in its ADP bound (closed) state, increasing the amount of re-folding time, whereas the protein, bcl-2 associated anathogene-1 (BAG-1), and the C-Terminus of HSP70 binding protein (CHIP), both have inhibitory effects [287, 288]. Whilst many proteins are folded by binding and release from HSP70, (many larger protein require several interactions) proteins which are unable to find their native state are transferred to the small HSPs (chaperonins) [289]. These proteins enclose the non-native protein in a cylindrical "cage" [290, 291, 292] allowing for restructuring of the steric environment for more favourable refolding conditions [293, 294, 289].

HSP70 is bound to HSP90 through the tetratricopeptide repeat (TPR) domain containing

protein, HOP [295]. The TPR domains allow the docking of HOP to HSP90, binding it to HSP70 and allowing the fast and direct transfer of substrate between the two [296]. HSP90 functions as a dimer, with the two subunits bound by their C-terminal domains, leaving two N-terminal domains free to interect with ATP [285]. Denatured proteins probably bind the two dimers at the middle section of non-ATP associated HSP90 (apo-HSP90) [285]. Binding of ATP, along with the substrate, causes a conformational change which locks the substrate in position, allowing the protein to adjust to its new conformation. The small co-chaperone specific for ATP-bound HSP90, p23, stabilises this conformation [297]. ATPase activity of the N-terminal domains of HSP90 hydrolyse the ATP returning the chaperone to its starting conformation, releasing the protein [298, 299].

Proteins which cannot be refolded in this manner, are targetted for degradation via either the proteasome [300] or the aggressome [301]. The initial step towards either fate occurs through the attachment of ubiquitin to lysine residues on the protein [302, 303]. CHIP, which has E3 ubiquitin ligase activity, associates with HSP90 through its TPR domain and ubiquitinates target proteins [287], whereas BAG-1 which binds HSP70, also associates with the proteasome [288]. Thus the systems of protein refolding and degradation are functionally and physically linked by the HSR. Given HSP70's pivotal role within the protein degradation pathways, modulation of the heat shock response has the potential to modulate ERAD of misfolded proteins in NPC disease, such as the $NPC1^{I1061T}$ mutation. Treatment of mutant fibroblasts carrying missense mutations of the *NPC1* gene with the proteasome inhibitor MG132 showed restoration of NPC1 levels, and an improvement in cholesterol trafficking [304]. Recent *in vitro* work has shown that CHIP was responsible for ubiquitinating the $NPC1^{I1061T}$ protein at the ER, resulting in significant downregulation of the mutated protein [305]. Adenoviral Hsp70 overexpression, or the use of the chemical chaperone geronylgeronyl acetone (GGA) was able to rescue the ERAD degradation of the mutated protein [305]. The constitutively expressed heat shock protein, heat-shock cognate 70 (Hsc70) has also been shown to perform a similar function to Hsp70 [306]. In cell lines expressing a mutant form of the cystic-fibrosis transmembrane conductance receptor (CFTRΔF508), the CHIP-Hsc70 complex was shown to target CFTRΔF508 by ubiquitination to degradation through the proteasome [306]. Inhibition of CHIPs interaction

with Hsc70 through targeted mutation of its TPR domain, and inhibiton of E3 ligase activity both blocked ERAD, and allowed normal targeting of CFTRΔF508 to the plasma membrane [306]. Thus, the coordinated actions of the heat-shock machinery are involved in the aberrant degradation of immature and mutant proteins at the ER.

Whilst the HSR is a commonly preserved cellular mechanism, neuronal expression and induction of HSPs displays marked regional variation. Many neurons, including motor neurons, do not appear to upregulate HSP70 in response to stress [307], whereas other neuronal populations, such as cerebellar Purkinje cells, alongside oligodendrocytes and glia show significant induction upon stress [308]. In an *in vitro* neuroblastoma cell model, differentiated neurons have a diminished capacity to produce HSP70 following heat shock, whereas glial cell expression does not decrease [309]. Furthermore, it appears that there is significant transfer of glial derived HSP70 to neurons in this model [309]. This raises the possibility that glial-neuron transfer of HSP70 is an important response to neuronal stress.

1.5.3 HSP70 and Lysosomes

In addition to the role of HSP70 as a molecular chaperone, various lines of evidence point to HSP70 playing an important role in protecting cells from lysosomal membrane permeablisation (LMP). Depletion of HSP70 enhances susceptibility of cells to LMP [310] and the exogenous addition of HSP70 provides protection of against LMP [311, 312]. Additionally in the field of cancer-cell survival, the translocation of HSP70 from its cytosolic locale to the endo-lysosomal compartment, provides a membrane protective function against LMP [310]. LMP has been shown to be a mechanism of cell death in several LSDs, including NPC [163, 313, 314, 315].

Within the LE/Ly system, HSP70 has been shown to increase the activity of ASM in NPA fibroblasts [163]. This decreased the levels of sphingomyelin and decreased the susceptibility of the cells to LMP [163]. The activity of HSP70 was dependant on its interaction with BMP. Inhibiting this reaction, either using the mutant $HSP70^{W90F}$ or by binding BMP with antibody blocks this association [163]. As most lysosomal hydrolases are dependant on an association with BMP [48], this shows a potential role of HSP70 in lysosomal hydrolase function.

HSP70 has been shown to be a target for endocytosis by the membrane protein LRP1 [316],

which has is highly expressed in both hepatocytes and neurons, but is also expressed in some level on most cell types, including on capillary epithelial cells, glia, oligodendrocytes and astrocytes of the CNS [317], where it has been proposed to play a role in the uptake of CNS cholesterol through endocytosis of ApoE [318]. Binding of targets to LRP1 causes rapid endocytosis, and delivery of contents to lysosomes [319]. Intracellularly, LRP1 has also been implicated in several signalling events within neurons, having over 100 intracellular interacting proteins. Synthetic agonists of the LRP1 receptor have been shown to activate TrkA in a Src family kinase dependant manner [320], stimulating axonal growth *in vitro* and following CNS injury *in vivo* [321]. The cytoplasmic tail of LRP1 has a pair of NPXY microdomain motifs which have been shown to be phosphorylated upon binding of extracellular ligands. When prepared synthetically, and used to probe brain lysates, the distal $NPXY^{4507}$ motif has been shown to have several binding partners including PLC-γ, PI3K, Shp-1, Shp-2, Src, and Fyn [322] whilst the proximal $NPXY^{4473}$ motif most likely confers specificity.

1.6 Aims

The aims of this thesis are threefold;

1. To establish whether the use of exogenously added HSP70 shows therapeutic benefits on the progression of Niemann-Pick type C disease.

2. To establish whether a small molecule upregulator of the heat-shock response, arimoclomol, can provide therapeutic benefits in Niemann-Pick type C disease.

3. To see whether the heat-shock response can be of a wider benefit to other lysosomal storage disorders.

2 Materials & Methods

2.1 Mouse Models

BALB/c-Nctr-*Npc1*$^{m1N/J}$ (Jackson laboratory, Charles River, UK) mice (termed *Npc1*$^{-/-}$mice) were maintained by heterozygote brother/sister matings, and genotyped as previously described [206].

The Sandhoff (*Hexb*$^{-/-}$) disease mouse model was provided by Dr Richard Proia (NIH). Mice were maintained by heterozygote brother/sister matings and recently fully backcrossed to C57B/6 background.

The Fabry mouse model (kindly provided to us by Asok Kulkarni, NIH) was generated by targeted disruption of the emphGALA gene in C57BL/6 mice[323]. Hemizygous α-Gal A males (*Gala*$^{-/0}$) were bred with homozygouse females (*Gala*$^{-/-}$).

Mice were group housed in ventilated cages with irradiated food and bedding and autoclaved water available *ad libitum*. All animal studies were approved by the UK Home Office for the conduct of regulated procedures under licence (Animal Scientific Procedures Act, 1986).

2.2 Compounds

rhHSP70$^{\text{his}}$, rhHSP70$^{\text{non-his}}$ and arimoclomol were supplied by *Orphazyme ApS*.

2.3 Tissue Processing

Several methods of euthanasia for tissue collection are unsuitable due to damage to the brain structures or the prevention of proper perfusion (e.g. cervical dislocation, decapitation). Although the option to use sodium pentobarbital was available, the effects on lipids in the use of

terminal anaesthetics is unclear, and we therefore used rising concentrations of CO_2 to kill the mice before confirming death by exsanguination followed by perfusion.

2.3.1 Biochemistry

Mice were killed by asphyxiation in rising concentrations of CO_2, exsanguinated by making an incision in the right atrium, and perfusing through the left cardiac ventricle with ice-cold phosphate-buffered saline (PBS). Organs were removed and stored at -80 ℃ until needed. Organs were homogenised in soft tissue homogenisation tubes (Precellys) with ice-cold PBS using the Precellys 24-dual homogeniser (Precellys) at 2x 6000Hz over 13 seconds. Homogenates were then aliquoted and frozen at -80 ℃.

2.3.2 Western Blotting

Homogenates generated above were mixed with equal volumes of 2x Lysis buffer to give final concentrations of 1% IGEPAL-CA 630, 0.5% Sodium deoxycholate, 0.1% SDS and 1% protease inhibitor cocktail (Sigma, P-8340). Homogenates were aliquoted and frozen at -80 ℃.

2.3.3 Immunofluorescence

Npc1$^{-/-}$ mice were treated with 3mg/kg rhHSP70^{his} (n=6) or with PBS as control (n=6) as i.p. injections 3x weekly. Mice were killed at 54 days by asphyxiation in rising concentrations of CO_2, exsanguinated by severing the right atrium, and perfused through the left cardiac ventricle with ice-cold 4% paraformaldehyde (PFA) in PBS. For rhHSP70^{his} localisation studies, 3 week old *Npc1*$^{-/-}$ and 3 week old *Npc1*$^{+/+}$ mice were injected with a single dose of 3mg/kg rhHSP70^{his} and killed either 3 or 7 days after injection as described above. Brains were removed and left overnight in 4% PFA at 4 ℃ before transferring to a 30% sucrose solution until the brains sank. Cryo-protected brains were mounted onto chucks in a cryostat, embedded in ice, and left for 10 minutes on the rapid freezing shelf at -30 ℃ until frozen solid. The mounted brains were then transferred to the cutting face, and left for another 30 minutes at -12 ℃. Brains were then sectioned para-sagittally at 30μm and resulting serial sections collected into 6 individual pots. Sections were stored at -20 ℃ in a glycerol/ethylene glycol storage solution until staining.

2.4 Immunofluorescent Staining Protocols

Prior to staining, sections stored at -20 ℃ were left for 30 minutes at room temperature and were then washed three times in PBS. Sections were incubated in wells overnight at 4 ℃ with primary antibodies made up in PBS with 0.5% Triton X100 and 2% normal goat serum. Primary antibodies are listed in **Table 2.1**.

Antigen	**Host Species**	**Concentration**	**Supplier**	**Cat. No**
Anti-Calbindin	mMouse	1:3000	Swant	300
	pRabbit	1:1500		CB38
Anti-MBP	mMouse	1:2500	Cambridge Bioscience	SMI-99P-100
Anti-CD68	pRat	1:1000		OASA05377

Table 2.1: Effects of rhHSP70^{his} treatment *in vivo* : Primary antibodies for immunofluorescence

Host Species	**Reactivity**	**Fluorophore**	**Concentration**	**Supplier**	**Cat. No**
Goat	Mouse	488	1:2000	Thermo Fisher	35502
	Rabbit	488			35552
	Mouse	594			35510
	Rabbit	594			35560
Donkey	Rat	488	1:500		A-21209

Table 2.2: Effects of rhHSP70^{his} treatment *in vivo* : Secondary antibodies for immunofluorescence

Secondary antibodies were made up in PBS with 0.5% Triton X100 and 2% normal goat serum and were incubated for 2 hours at room temperature. Secondary antibodies are listed in **Table 2.2**. Filipin staining (Sigma, Cat. F4767) was performed using a 50μg/ml solution in PBS 0.25% Triton X100 and 2% BSA. Sections were left for 30 minutes at room temperature. Cholera toxin B subunit directly conjugated to Alexa-Fluor488 (Invitrogen, Cat. C-34775) used at 1:500 in PBS with 0.5% Triton X100 and 2% BSA. Sections were incubated overnight at 4 ℃. All washing steps were performed three times in PBS with 0.5% Triton X100 unless otherwise stated. Stained sections were mounted onto Superfrost slides and allowed to air dry overnight protected from light and dust before mounting in Mowiol. Images were collected using a Zeiss fluorescent microscope and Zeiss AxioVision camera and software.

For CD68 counts, images of lobules IV and VI (early and late degenerating lobules respectively) were obtained at 10x magnification. Individual images were photostitched together by eye using

Photoshop CS 5.1 (Adobe software), to form a complete image of the lobule, and counts of the total number of $CD68^+$ cells present in each image obtained. To account for differences arising from different lobular area, the entire outline of the lobule was drawn around using ImageJ software (Version 1.46r; NIH, USA), and the total numbers of $CD68^+$ normalised by this area. Counts of Purkinje cells ($calbindin^+$) were performed under the microscope at 20x magnification, whereby all Purkinje cells within the Purkinje cell layer were counted sequentially for each lobule (sulci $\rightarrow$ sulci). Images of the entire cerebellum were obtained at 2.5x magnification and were then photostitched as described above. To account for different cerebellar size, the Purkinje cell numbers were normalised against the length of the Purkinje cell layer, as measured by drawing the length of the Purkinje cell layer for each lobule using ImageJ software (Version 1.46r; NIH, USA).

To quantify the area of myelin, individual images of lobules stained with Cholera toxin B subunit directly conjugated to Alexa-Fluor488 and counterstained with calbindin and DAPI, were collected at 10x magnification, and photostitched together by eye using Photoshop CS 5.1 (Adobe software). To assess the area of myelin in the sections, the white matter was drawn around using ImageJ software, and then normalised against the total lobular area, as described above.

All images and counts were collected from vermal cerebellar sections which contained complete lobules I-X. At least 5 sections were counted per animal for each experiment.

2.5 Protein Quantification

Protein was quantified as previously described [324] using a commercial bicinchoninic acid (BCA) assay kit (Sigma, Cat. BCA-1). Briefly, homogenized samples and a protein standard were diluted in ddH_2O. A mixture of bicinchoninic acid and copper (II) sulphate was then added. The reaction is then left for 30 minutes at 37 ℃. Plates were analysed using a FLUOStar Optima plate reader (BMG Labtech, Ortenburg, Germany) and absorbance measured at 560±10nm.

2.6 Quantification of GSLs

Glycosphingolipid analysis was performed as described previously [325] with minor adjustments. Briefly, homogenates were adjusted to 0.5mg/ml protein and 0.5ml was extracted in 4 volumes 1:2 chloroform/methanol overnight. Total GSLs were recovered using SepPakTM C18 columns, eluted with chloroform/methanol and the samples were dried under nitrogen. To release the glycan moiety, samples were resuspended in 50mM sodium acetate pH5.5 with 1mg/ml sodium taurodeoxycholate and incubated at 37 ℃ overnight with ceramide glycanase. Samples were then labelled with 0.21M 2-anthranilic acid (2-AA) at 80 ℃ in the presence of 0.72M cyanoborohydride. Derivatized oligosaccharides were purified on Spe-ed Amide-2 columns (Applied Separations, Allentown, PA). Normal phase-HPLC (NP-HPLC) was carried out on a Waters 2695 separations module with a Waters 2475 fluorescence detector (Waters Corporation, Hertfordshire, UK). A TSK-amide 80 NP-HPLC column (4.6 ± 250 mm, Tosoh Biosciences, Sigma-Aldrich, UK) was used for the separation and maintained at 30 ℃ using a Waters column heater. The solvents and gradient conditions were as previously described [325]. The peak area per femtomole of GSL-derived oligosaccharide present was determined and used to quantify the concentration of GSLs in the tissue samples as described previously [325].

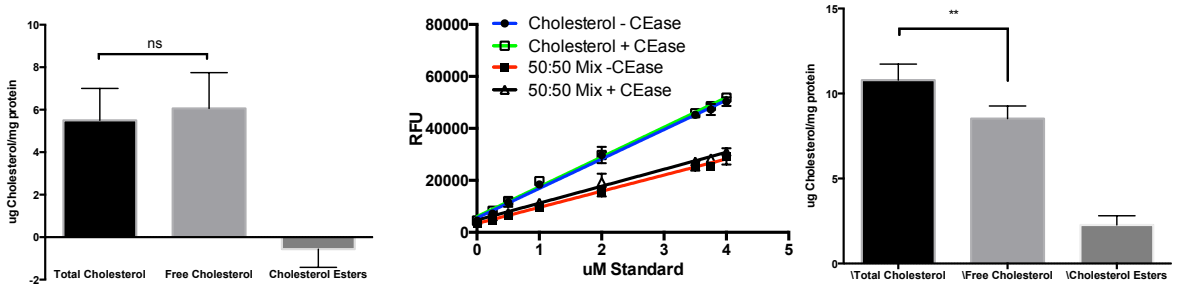
2.7 Quantification of Cholesterol and Cholesteryl ester.

Free cholesterol content was assessed using the Amplex Red cholesterol assay kit as described previously [31]. Briefly, extracted samples were resuspended in 1x reaction buffer (supplied) at a concentration equivalent to 0.5mg/ml protein. 50μl of sample was loaded into a 96 well plate in triplicate alongside a cholesterol reference standard (0μg-20μg). For the reaction to measure free cholesterol, an equal volume of 1x reaction buffer containing 150μM Amplex Red, 1 U/ml HRP, and 1 U/ml cholesterol oxidase was added to the wells. To measure the total cholesterol content, the same buffer was supplemented with 0.1U/ml cholesterol esterase. The plate was then incubated for 30 minutes at 37 ℃. Fluorescence was analysed using a FLUOStar Optima plate reader (BMG Labtech, Ortenburg, Germany) excitation 560±10nm, emission 590±10nm. Values for cholesterol ester content were calculated by subtracting the free cholesterol value from

the total cholesterol value.

2.7.1 Method Development: Cholesterol Extraction

Cholesterol was extracted using a modified Folche extraction method [30]. Briefly, samples were adjusted to 0.5mg/ml protein content in ddH_2O and extracted in twenty volumes of 2:1 chloroform/methanol for 2 hours at room temperature. Following extraction, 4 volumes of methanol were added and samples centrifuged to remove insoluble material. To the retained supernatant, chloroform and water were added to achieve a final ratio of 8:4:3 chloroform/methanol/water. Following vortexing and centrifugation, the upper phase was removed by pipetting and the lower phase washed three times with theoretical upper phase, composed of 3:48:47 chloroform/methanol/water. Washed lower phase containing cholesterol was dried under nitrogen, before being redissolved in 100µl of sample buffer.



(a) (b) (c)

Figure 2.1: *Extraction of cholesterol in glass significantly improves recovery of cholesterol and cholesterol esters* a) Extraction of cerebellar cholesterol in plastic showed no significant differences between total and free cholesterol, resulting in a cholesterol ester value of < 0. n=24 b) Cholesterol ester standards were undetectable following extraction in plastic. n=3/data point c) Extraction of cerebellar cholesterol in glass improved cholesterol recovery and resulted in significant differences between total and free cholesterol. n=24. *CEase*, cholesterol esterase, *50:50 Mix*, equal proportions of cholesterol and cholesterol oleate standards giving equivalent concentration to 4µM cholesterol. Data was analysed with a students two tailed t-test. **, p=0.01

When using plastic, we found much lower recovery of cholesterol and total cholesterol than had been published using other methods [326], and the kit was also unable to detect any cholesterol esters in the sample **(Figure 2.1a)**. To examine this further, standards of either cholesterol or a 50:50 mixture of cholesterol and cholesterol oleate were dried down and extracted in 1x reaction

buffer before being assayed as described for both free and total cholesterol **(figure 2.1b)**. As we saw with the samples, the kit reliably detected the free cholesterol, regardless of whether the mixture did or did not contain cholesterol esterase. However, the 50:50 mixture only saw a marginal increase in fluorescence when incubated with cholesterol esterase compared to the the mixture without cholesterol esterase. This was not due to inactivity of the esterase, as other commercial available enzymes did not work any better (data not shown), whilst FBS when used without extraction gave total cholesterol readings 6x higher than free cholesterol (data not shown, L. Ingemann, personal communication). Importantly when using plastic, it was clear there was material adhering to the sides of the tubes which was insoluble in the reaction buffer required for the correct activity of the kit, even after extensive incubation, sonication and heating to temperatures of 50 ℃. As there was a possibility that this material was dried cholesterol/cholesterol ester, we tested whether using borosilicate glass alleviated this problem. Extraction in glass followed by sonication gave 29% greater recovery of cholesterol than the same method in plastic **(Figure 2.1 c)**. Furthermore, extraction in glass also allowed for the detection of a significant proportion of cholesterol esters, which were undetectable when using plastic.

2.8 Quantification of Sphingosine: Comparison of Existing Protocols

Several methods exist for the extraction of sphingosine from tissues. Several older methods [1, 2] rely on solid-phase extraction steps with elutions in aqueous phases which are time consuming to perform. More recent protocols published disregard the column steps and instead rely on extraction with aqueous detergents, but carry the risk of contamination with other lipids. To determine the quickest and most efficent extraction method available we compared several pubished methods.

2.8.1 Method 1 : Merrill et al 1998 [1]

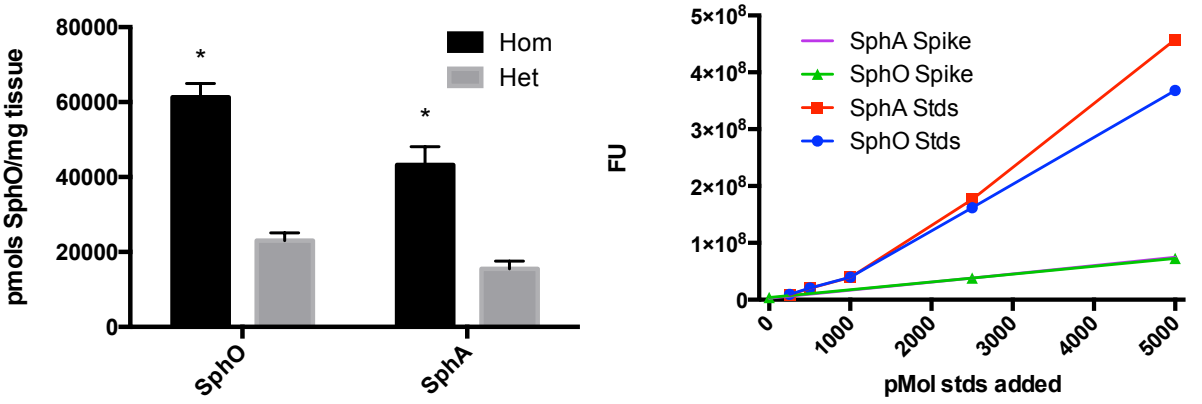
Samples were homogenised in 4 volumes of PBS, and then extracted in 15 volumes of 1:2 chloroform:methanol, followed by vortexing and mixing. 10 volumes each of chloroform and water were added and the phases seperated by centrifugation at $1700g$ for 10 minutes. The upper

phase was discarded and the organic phase dried under nitrogen. Extracts were resuspended in 1ml 0.1M potassium hydroxide in methanol and heated to 37 ℃ for 1 hour. 1ml of chloroform and water were then added and the organic phase was recovered before washing three times. The final organic solvent was then washed with water three times and dried under nitrogen.

2.8.2 Method 2 : Fryst et al 2001 [2]

To assess this method, 25mg of liver tissue from *Npc1*$^{-/-}$ or $^{+/-}$ mice was homogenised in 40 volumes of 1:1 chloroform:methanol with or without the addition of 400pmol sphingosine and sphinganine standards, followed by sonication in a water bath for 5 minutes. Samples were then spun at 1700g for 10 minutes to remove debris and the supernatant transferred to a new tube, and dried under nitrogen. 100µl of 0.1M potassium hydroxide in methanol was then added, followed by vortexing, and sonication, and the samples incubated at 37 ℃ for 2 hours to allow hydrolysis of esterified acyl chains. The samples were then cooled to room temperature, dried under nitrogen, before being resuspended in 2 ml of chloroform- methanol (2:1; v/v). To obtain a phase split, 500µl water was then added, and samples were vortexed, followed by centrifugation at 1,700g for 5 min to obtain a clear separation of the two phases. The organic phase was recovered and washed three times with water. The washed organic phase was dried down in a speed vac and resuspended in 500µl of 1:1 methanol-water containing 0.1% glacial acetic acid. C18-E solid-phase extraction columns (100 mg/ml) (Supelco) were initially wetted with 200µl of methanol, followed by equilibration with 1 ml of 1:1 methanol-water containing 0.1% glacial acetic acid. Samples were applied to the equilibrated C18-E column, followed by a wash with 1 ml of 1:1 methanol-water containing 0.1% glacial acetic acid. A second wash of the column was performed by the addition of 500µl of methanol. Sphingoid bases were eluted from the column with 500µl methanol-20 mM ammonium acetate (9:1; v/v) and dried down under nitrogen. Dried lipids were labelled with OPA as described previously.

The method allowed us to distinguish significant differences between *Npc1*$^{-/-}$ and $^{+/-}$ levels of sphingosine and sphinganine accumulation **(Figure 2.2a)**. However, the spiking of samples with standards showed that the recovery of sphingosine was only approximately 10% of the sam-



(a) (b)

Figure 2.2: *Extraction of sphingosine using Fryst* et al *method gave good distinction between het and hom, but poor recovery* a) liver extracts from 9 week old *Npc1*$^{-/-}$ (hom) n=3 and Npc$^{+/-}$ (het) mice, n=3 showed significant differences in both sphingosine (SphO) and sphinganine (SphA) accumulation. p=0.0008 and 0.006 respectively. Data was analysed using multiple students two-tailed t-test, with Bonferroni-Sidak corrections for multiple comparisons b) Samples spiked with increasing amounts of sphingosine and sphinganine standards showed poor recovery rates of approximately 20%

ple loaded **(Figure 2.2b)**. Additionally, the method was very time consuming, taking about 3 days from start to finish, with the solid phase extraction being exceptionally labour intensive, and having to dry large volumes of aqueous material, which takes a long time.

2.8.3 Method 3 : Schuchman et al 2010 [3]

To evaluate the effects of centrifugation and the presence of IGEPAL CA-630 on sphingosine and sphinganine recovery, 1.5g of 9 week old *Npc1*$^{-/-}$ livers was homogenised with 1.5ml of homogenisation buffer with or without 0.2% IGEPAL CA-630 and the homogenate then split into 12 tubes of 100µl each. Homogenised tissue was then centrifuged at a variety of speeds to remove cellular debris, and 25µl of supernatant was then mixed with 150µl 1:2 chloroform:methanol. 10µl 3M sodium hydroxide was then added followed by vortexing, and 60 minutes incubation with rotation. Following alkaline hydrolysis, a further 100µl chloroform was then added to the mixture followed by intensive vortexing before centrifugation at 13000g for 2 minutes. The bottom organic layer was collected and dried under nitrogen before labelling with OPA reagent

as described above.

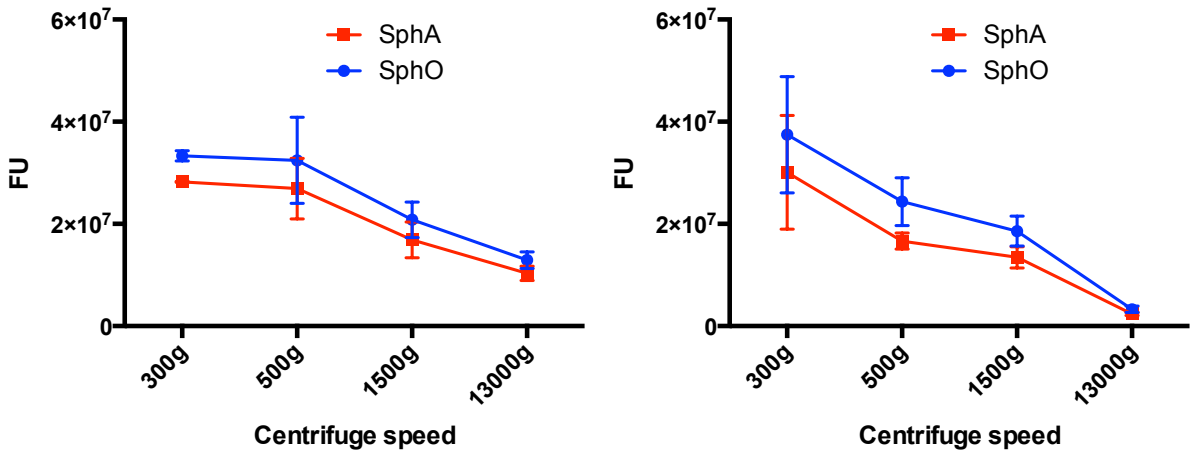
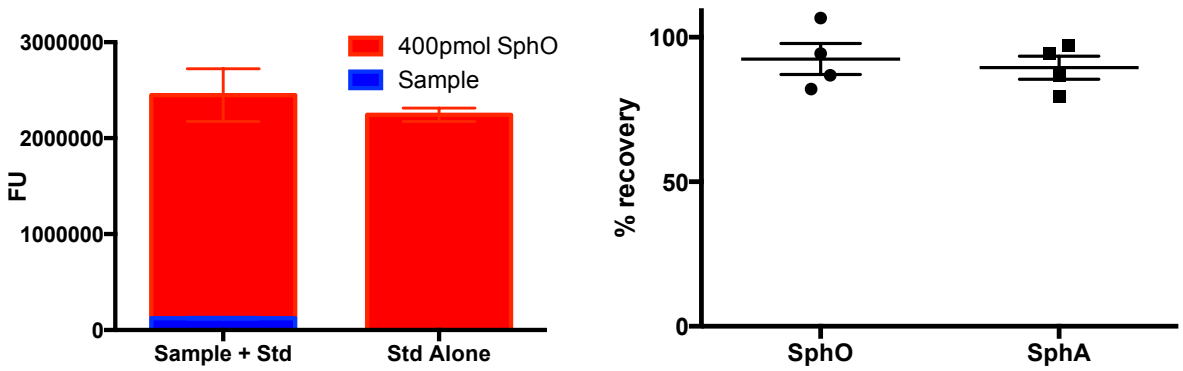


Figure 2.3: *Effects of IGEPAL and spin speed on sphingosine and sphinanine recovery* liver extracts from 9 week old *Npc1*$^{-/-}$ in the presence a) or absence b) of 0.2% IGEPAL CA-630 n=3/data point. 300g spin speed in the prescence of IGEPAL gave the greatest recovery with the least variation.

Centrifugation speeds of 300g gave the best recovery in both IGEPAL and water homogenised tissue, most likely due to the higher speed spins removing too much of the subcellular contents **(Figure 2.3)**. Samples which were not spun were unusable due to the prescence of broad, non specific peaks (data not shown). The inclusion of 0.2% IGEPAL CA-630 in the homogenisation buffer gave the most reliable data **(Figure 2.3a)**.

To test the recovery of sphingosine, we extracted the lipids as from homogenates of 9 week old *Npc1*$^{-/-}$ mouse livers with or without 400pmol sphingosine standards. Standards were added to the extraction buffer and then extracted as described above. Unextracted sphingosine and sphinganine standards were dried down without any extraction. Samples and standards were then processed as previously described. The values obtained from the sample alone were subtracted from the values from the samples with standards **(Figure 2.4a)**. This value was then compared against the unextracted standard values to calculate the percentage recovery. The recoveries were 92% and 89% for sphingosine and sphinganine respectively and the coefficient of variation was 11.6% and 8.8%. All subsequent sphingosine analysis was performed using this method with the inclusion of IGEPAL in the homogenisation buffer and a 60 minute sodium



(a) (b)

Figure 2.4: *The method of Schuchman* et al *gave consistently good recovery of both sphingosine and sphinganine standards.* a) graph showing total fluorescent values of sphingosine from liver samples spiked with 400pmol sphingosine, compared to unextracted sphingosine. b) graph showing the % recovery rates of sphingosine (92%) and sphinganine (88%) using this method.

hydroxide incubation.

2.9 Lysosomal Volume Assay

2.9.1 Mononuclear Cell Preparation

Spleens from *Npc1*$^{+/+}$, and 3mg/kg rhHSP70^{his} treated and untreated *Npc1*$^{-/-}$ 7 week old mice were obtained, following PBS perfusion as described above. The spleens were squeezed between glass slides and washed in 10ml cold PBS to extract the detached cells. Cell suspension was centrifuged at 800g for 5 minutes and the cell pellet retained. 5ml of red cell lysis buffer (Qiagen) was then added and the samples were vortexed thoroughly before incubating for 5 minutes at room temperature. The cell suspension was then filtered through a cell strainer which was then washed with 10ml of cold PBS. The sample was then centrifuged again and the cell pellet resuspended in 1ml FCS with 10% (v/v) DMSO. The prepared mononuclear cells were then stored in a liquid phase nitrogen cell bank until all samples had been collected.

2.9.2 LysoTracker Assay

Mononuclear cells (1x 10^6) were incubated with PE-conjugated mouse anti-human CD19 antibody (clone LT19; Abcam) in PBS for 30 minutes on ice in the dark. The reaction was stopped with 100µl 10% BSA in PBS, and cells were spun for 5 minutes at $800g$, then either resuspended in 0.5 ml FACS buffer (0.1% BSA, 0.02M NaN_3 in PBS) or stained with 1 ml of 200 nM LysoTracker-green DND-26 (Invitrogen) in PBS for 10 minutes in the dark at room temperature. Cells were centrifuged for 5 minutes at $800g$, resuspended in 0.5 ml FACS buffer, and kept on ice for a maximum of 1 hour prior to flow cytometric analysis (BD Biosciences FACSCanto II). The cytometer was calibrated using Cytometer Setup and Tracking beads (BD), and compensation was performed using cells stained with LysoTracker and anti-mouse CompBeads (BD) stained with PE antibody using FACSDiva software (BD). Samples were acquired with gating on singlets (FSC-H versus FSC-A) and CD19+ events. CD19+ gate was calculated from the unstained controls. In total, 50,000 singlet events and 10,000 singlet gate CD19+ events were collected. The mean fluorescence of the CD19+ events was calculated using FACSDiva^{TM} software (BD). MEFL was calculated using 8-peak Rainbow calibration beads (BD) using the fluorescein equivalent values provided by the manufacturer.

2.10 Behavioural Analysis

Behavioural tests were performed weekly. Mice were allowed to acclimatize to the testing room for 30 minutes before behavioural testing was started.

2.10.1 Tremor

Tremor was measured with a commercial tremor monitor (San Diego Instruments) according to the manufacturer's instructions. The tremor monitor was housed on an anti-vibration table and the mice were monitored for 256s. The tremor monitor was connected to a computer via a National Instruments PCI card and the output (amplitude/time) was analysed (fast Fourier transform) using LabView software, to give a measurement of power at each frequency (0-64 Hz).

2.10.2 Manual Rearing

Mice were placed in a large open field cage box for 5 minutes. A side rear was recorded when mice reared on hind legs using the side of the cage as support. A centre rear was recorded when mice reared on hind legs un-aided. Rearings that were uncontrolled/the mouse fell over were discounted. As rearing data in the later stages of disease progression loses normal distribution, data was normalised using a [Log+1] transformation, and data analysis performed using these values.

2.10.3 Activity Monitor Logger

As above, mice were placed in an open field for 5 minutes. Activity was recorded using the AMLogger with activity monitor software AM1053 (Linton Instrumentation, England).

2.10.4 SHIRPA testing

SHIRPA testing was designed as a wide spanning and comprehensive assessment for the phenotypic characterisation of genetic mutants [327]. We used a subset of the assessments, based on observed and recognised NPC phenotypes. Mice were placed in an open field and observed for 5 minutes. During this time, they were scored on the following criteria; Palpebral (eye lid) closure, pilo erection (abnormally raised coat hair), pelvic elevation, tail elevation, skin colour, spontaneous activity, respiratory rate, tremor and gait. Scores were determined using the standardised scale [327]. Scoring was performed blind to treatment. *Npc1*$^{+/+}$ were included as comparators only.

2.10.5 Gait Analysis

Gait analysis was performed using the Catwalk XT 9.1 system (Noldus). Mice were filmed walking five times across a backlit stage at weekly intervals. The camera gain was set to 14.05 and the intensity was set to 0.12, and a 100% maximum speed variation of each run. These were chosen based upon optimal settings for print collection of 9 week old mice, and these results were able to reliably detect differences between wildtype and *Npc1*$^{-/-}$ mice between 5 and and 10 weeks of age.

For analysis, the .cwz backup file was opened in CatWalk 10.5 and steps were classified (RF, LF, etc.) using the auto-classify function. Unlabelled steps were then labelled manually and all runs were checked through visually. Right and left paws were averaged to Front and Hind paws due to negligible variation across sides. Of the 5 runs collected, the 3 runs with the lowest speed variation were utilised for analysis. We used data segmentation profile settings of 12-45cm/s speed range, 8 minimal step inclusion and 60% maximum variation, which we had previously determined to be optimal for the NPC mouse model.

2.11 Anti-Drug Antibody Assay

2.11.1 Treatment

Npc1$^{-/-}$ mice were generated as described above. *Npc1*$^{-/-}$ mice (3 males, 3 females per group) were treated with 0.3, 1 and 5mg/kg rhHSP70^{his} 3x per week, i.p. for 1, 2, 3 and 4 weeks.

To compare the anti-drug antibody development of both rhHSP70^{his} and rhHSP70$^{non\text{-}his}$, *Npc1*$^{-/-}$ and *Npc1*$^{+/+}$ mice (2 males, 3 females per group) were treated with 3mg/kg rhHSP70^{his} or rhHSP70$^{non\text{-}his}$, or with PBS alone, as indicated, 3x per week, i.p. for 4 weeks.

2.11.2 Collection of Blood

Mice were terminally anaesthetised with 600mg/kg bodyweight sodium pentobarbital. Blood was obtained by cardiac puncture, and collected in uncoated vials, incubated at RT for 2 hours and centrifuged (1000*g*, 10 min at RT) to obtain serum. The serum was frozen in three aliquots on dry ice and stored at -80°C until analysis.

2.11.3 Anti-Drug Antibody ELISA

For ELISA analysis of ADA, 10µL serum was diluted in sample buffer (50 mM Tris + 0.14 M NaCl + 1% BSA, 0.05% Tween 20).

A standard curve was prepared using anti-Hsp70 antibody raised in mouse (Assays Design, 1 mg/ml; Cat no. C92F3A-5) at a concentration of 0-500ng/ml in sample buffer.

Plates were coated with 50µL diluted antigen (10µg/ml, in 0.05 M sodium-bicarbonate, pH

9.6) in NUNC Maxisorp 96-well plates, and incubated overnight at 4℃. Plates were washed 3 times in ELISA washing buffer (50 mM Tris + 0.14 M NaCl + 0.05% Tween 20). Plates were blocked with 200µL blocking buffer (50 mM Tris + 0.14 M NaCl + 1% BSA, pH 8,0) incubation 30 min at 25℃. Plates washed 3 times in wash buffer, before incubating with standards or the serum generated above for 60mins at 25℃. Plates were again washed 3 times in wash buffer.

50µL HRP-conjugated anti-mouse IgG (Bethyl Laboratories) diluted 75000 fold in sample buffer was added per well and incubated 60 min at 25℃. Plate was then washed 3 times in ELISA wash buffer 50µL TMB one Ready-to-use substrate (Kem-En-Tec diagnostic (Cat no. 4380H Lot no. 91204)) was added and plates were incubated in dark until blue color develops. Reaction stopped by adding 50µL 1M HCl. Absorbance measured at 450±nm, using FLUOStar Optima plate reader (BMG Labtech, Ortenburg, Germany).

2.12 Data Collection

Data was plotted in Excel for Mac 2011 (version 14.2.5; Microsoft, USA).

2.13 Statistical Analysis

All statistical tests and transformations were performed using PRISM software v6.0e (Graphpad software inc)

2.13.1 Biochemical Analysis

Individual GSL species were analysed using multiple students *t*-tests with Holm-Sidak corrections for multiple comparisons, comparing untreated groups to treatment.

Total GSLs, free cholesterol and sphingosine data were analysed using either one or two-tailed Students *t*-tests (where appropriate), comparing untreated groups to treatment.

Wildtype groups were not included in statistical analysis.

2.13.2 Lysosomal volume assay

Lysosomal volume MEFLs were analysed using two-tailed Students *t*-tests, comparing *Npc1*$^{-/-}$ group to treatment.

Npc1$^{+/+}$ groups were not included in statistical analysis.

2.13.3 Behavioural Analysis

Outliers were identified using the ROUT analysis tool with Q=1%.

Data sets were analysed for normal distribution using the D'Agostino & Pearson omnibus normality test. Data sets where one or more groups showed non-normal distribution were transformed using Y=[LogY+1] transformation and reassessed for normality using the D'Agostino & Pearson omnibus normality test.

Normally distributed data were then analysed using either two-way ANOVA for data gathered over time, or one-way ANOVA for single timepoints. The tests and transformations applied are listed below each figure. Wildtype groups were not included in statistical analysis.

2.13.4 Immunohistochemical Analysis

Counts of Purkinje cells and glial cells were analysed using multiple students *t*-tests with Holm-Sidak corrections for multiple comparisons, comparing *Npc1*$^{-/-}$ group to treatment. Measurements of myelin were analysed using a two-tailed Student's *t*-test.

2.13.5 Anti-Drug Antibody Comparison

Data were compared using one-way ANOVA comparing all groups, with Dunnett's corrections for multiple comparisons.

3 In Vivo Effects of rhHSP70 Treatment in Niemann-Pick Type C Disease

3.1 Introduction

NPC is an autosomal recessive genetic disorder arising from mutations in the genes *NPC1* [139] or *NPC2* [140] which encode proteins of the same name. Dysfunction of either of these two proteins results in a clinically indistinguishable disease phenotype characterised by progressive ataxia, tremor, learning difficulties, dementia and eventually death at an early age [141]. The only therapy available for NPC disease is miglustsat, which shows some delay of disease progression in patients [210]. Cyclodextrin is currently under examination, but there are significant issues, particularly wirth regards its low CNS penetration [220].

The *Npc1*$^{-/-}$ mouse has an aggressive disease course similar to the infantile onset form of the human disease, with mice developing tremor and ataxia at around 6 weeks of age before death at 11 weeks [147]. Cells exhibit a block in the endocytic pathway resulting in the accumulation of a variety of lipids including cholesterol, glycosphingolipids (GSLs), bis-(monoacylglycero)phosphate (BMP), sphingomyelin and sphingosine in late endosomes/lysosomes (LE/Lys) [148, 149, 150, 151]. The block in the endocytic pathway is caused by reduced calcium release from lysosomal stores, this prevents lysosomal fusion events and limits flux of lipids through the LE/Lys [7].

Neuronal pathology in NPC1 disease is characterised by accumulation of lipids within lysosomes, axonal blebbing, neuronal degeneration in particular the loss of cerebellar Purkinje cells and widespread inflammation [139, 156]. The development of ataxia and associated tremor has been shown to be a result of the progressive and patterned loss of Purkinje cells [171]. The development of myelin in the *Npc1*$^{-/-}$ mouse brain is stunted with the development and exten-

sion of MBP^+ oligodendrocytes being significantly delayed both at 21 days and 54 days within both the cerebellum and the forebrain. This has been shown to correspond to an increase in $CNPase^+$ immature oligodendrocytes whilst $O4^+$ cell numbers (representing total numbers of oligodendrocytes) remain stable [170].

Given the severity of Niemann-Pick type C disease, and the limited treatments available, new therapies are urgently needed. New therapeutics targeting unexplored disease pathways are of great interest. HSP70 is a highly conserved 72kDa chaperone protein, with many roles in normal cell function, including proteostasis and ERAD [231]. HSP70 has also been implicated in cancer cell survival by inhibiting lysosomal membrane permeablization [310]. Exogenously administered HSP70 is endocytosed and co-localises with lysosomal and endosomal markers such as LIMP1 and acridine orange [163]. The addition of recombinant human HSP70 (rhHSP70) to NPA fibroblasts, reduces sphingomyelin content and increases resistance to lysosomal disruption [163]. Due to the shared ASM deficiency between NPA and NPC, alongside similarities of neuronal pathology, treatment of *Npc1*$^{-/-}$ mice with HSP70 may provide therapeutic benefit, either by protecting cells against lysosomal membrane disruption by the increased activity of ASM, or through a broader effect on other lysosomal hydrolases.

A pilot study of a single dose (3mg/kg) of rhHSP70 has previously shown significant reductions of GSL storage in the CNS and periphery, alongside reduced liver and kidney cholesterol storage, at 7 weeks. These effects were lost at 9 weeks of age, as were behavioural improvements in rearing ability and appearance of the mice.

In this section, we further evaluated the effects of rhHSP70 treatment in the *Npc1*$^{-/-}$ mouse model. A variety of outcomes, including behavioural performance and appearance were assessed on a range of doses, using a his tagged protein ($rhHSP70^{his}$). Furthermore, intensive evaluation of the effects of the optimal range of dosing was performed to better understand the effects on neuronal pathology, and the accumulation of lipid substrates in the various organs of the mouse.

3.2 Hypothesis

Treatment with $rhHSP70^{his}$ will improve behavioural deficits and reduce the accumulation of lipids in brain and peripheral tissues in *Npc1*$^{-/-}$ mice.

3.3 Materials & Methods

3.3.1 Mice

Npc1$^{-/-}$ mice were group housed in ventilated cages with irradiated food and bedding and autoclaved water available *ad libitum*. Wildtype mice (*Npc1*$^{+/+}$) were generated from the same litters as the *Npc1*$^{-/-}$ mice. All animal studies were approved by the UK Home Office for the conduct of regulated procedures under licence (Animal scientific Procedures Act, 1986).

3.3.2 Treatment

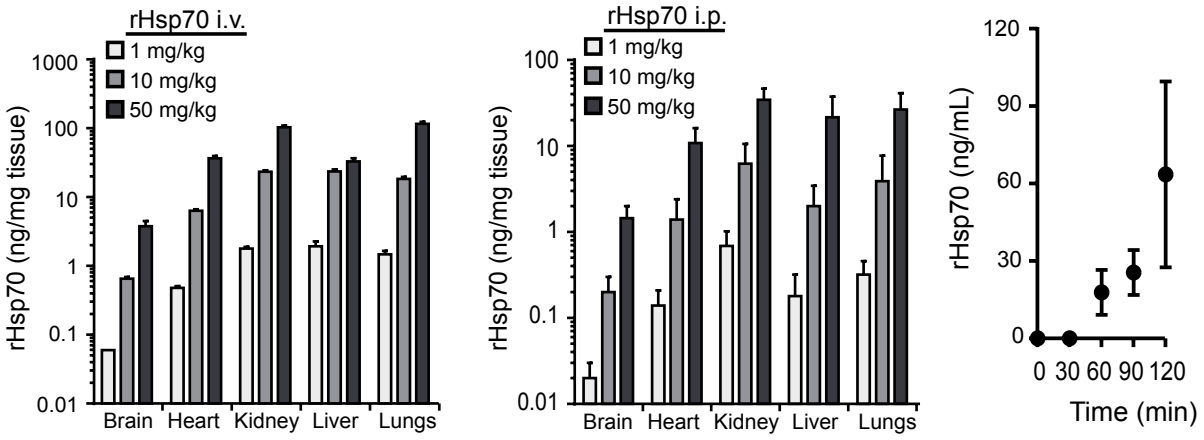
3 week old *Npc1*$^{-/-}$ mice were treated with rhHSP70^{his} at either 3mg/kg (n=12), 1.5mg/kg (n=12) and 1mg/kg (n=11) of body weight or with PBS alone (n=12). Mice were injected 3 times per week i.p..Wildtype BALB/c mice (*Npc1*$^{+/+}$) were used as baseline controls (n=11). Mice were either killed at 54 days of age (7 week) or at 68 days (9 week).

All other methods were performed as described in **Chapter 2**.

3.4 Results

3.4.1 Bioavailability of rhHSP70^{his}

To assess the bioavailability of rhHSP70^{his}, Analysis of the organ distribution of rhHSP70^{his} after both i.v. and i.p. administration of single, increasing doses of rhHSP70^{his} showed essentially similar dose-dependent profiles **(Figure 3.1 a)**. Importantly, both routes of administration showed that rhHSP70^{his} not only efficiently distributed to all the peripheral organs but penetrated the blood-brain barrier **(Figure 3.1 a,b)**. This distribution pattern, including the potential CNS uptake of rhHSP70^{his}, fits well with the described ubiquitous expression of the proposed receptor systems for HSP70 and particularly the CNS transcytotic capacities of one of the main receptors for HSP70, the low density lipoprotein receptor-related protein 1 receptor (LRP1) [316, 328].



(a) (b)

Figure 3.1: Bioavailability of rhHSP70^{his}. a) Intra-peritoneal (i.p.) and Intra-venous (i.v.) administration of rhHSP70^{his} shows dose dependant tissue distribution to peripheral organs and CNS after 60 minutes n=3/dose.b) rhHSP70^{his} concentration in the striatum of freely moving rats shows detectable rhHSP70^{his} 60 minutes after 10mg/kg i.p. injection. Experiments performed by A. Begley. This data was provided courtesy of Orphazyme ApS

.

3.4.2 CNS localisation of rhHSP70^{his}

To assess what specific regions of the brain rhHSP70^{his} localised to, we injected 3 week old *Npc1*$^{-/-}$ mice with a single dose of 3mg/kg rhHSP70^{his} and culled them after either 3 or 7 days. The sections were stained with an antibody against a 6x his tag and counterstained with antibody against calbindin. Cell nuclei were labelled with DAPI. At 3 days post injection rhHSP70^{his} reactivity was observed throughout the forebrain, although the intensity varied by region. The highest levels of immunoreactivity were observed in the spinal cord, brainstem, cerebral cortex, cerebellum and olfactory bulb **(Figure 3.2)**. Very little immunoreactivity was detected within the striatum **(Figure 3.2)**. 7 days post injection, immunoreactivity was significantly diminished in all regions although immunoreactivity was still detectable in the CA1 region of the hippocampus **(Figure 3.3)**.

At 3 days post injection, rhHSP70^{his} displayed predominantly nuclear localisation. Although rhHSP70^{his} was detected in most brain regions, differential uptake was apparent between different cell types. In the cerebellum, rhHSP70^{his} immunofluorescence was predominantly located in the Purkinje cell layer, and in the deep cerebellar nuclear region of the cerebellum **(Figure**



Figure 3.2: *rhHSP70^{his} immunofluoresence is detected in multiple regions of the forebrain.* Whole forebrain sagittal section showing immunoreactivity of rhHSP70^{his} 3 days post injection, regions showing strongest immunoreactivity were; the brainstem, the cerebral cortex, hippocampus, inferior collicus, cerebellum, midbrain regions and the olfactory bulb.

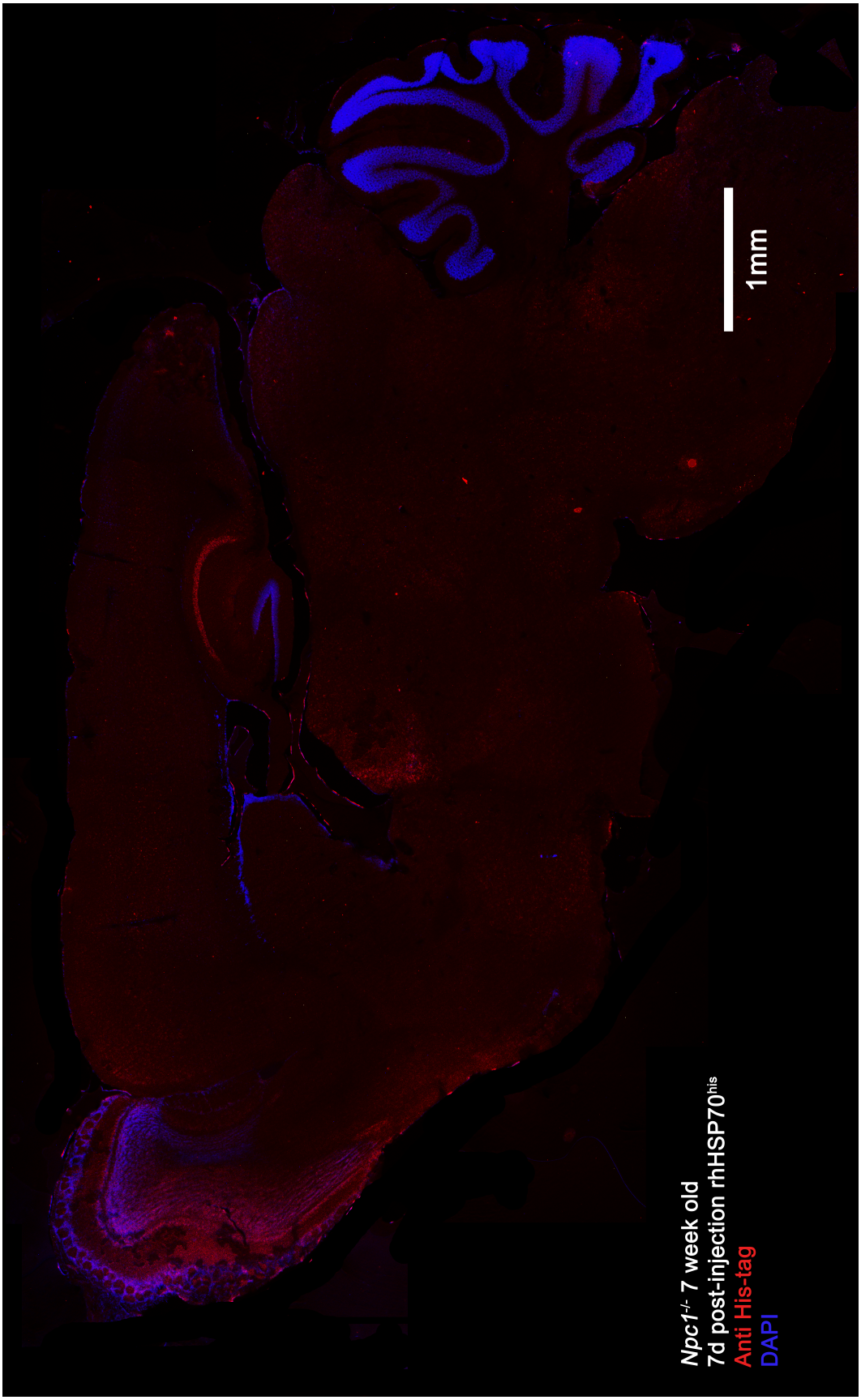


Figure 3.3: *rhHSP70^{his} is diminished in most regions of the forebrain 7 days following injection.* 7 days post-injection, rhHSP70^{his} displays diminished reactivity, however it is still strongly detectable in the CA1 region of the hippocampus.

3.4). The majority of the immunoreactivity appeared to be localised to the cell body in both Purkinje cells **(Figure 3.5 a)** and the deep cerebellar nuclear region **(Figure 3.5 b)**, where it appeared mainly in the cell nucleus.

In the cortex, 3 days post-injection, rhHSP70^{his} reactivity was predominantly localised to layer V **(Figure 3.6)**. At 7 days post-injection, immunoreactivity in the cortex was undetectable (data not shown).

Not all areas displayed uptake of the protein. At 3 days post injection, the caudate putamen was remarkably empty of immunoreactivity, except for a few intensely positive cells **(Figure 3.7a)**. At 7 days post injection, the numbers of rhHSP70^{his+} cells was greatly increased, although the brightness of cells was diminished **(Figure 3.7b)**. This suggests that the protein had been redistributed between cells.

3.4.3 Growth Curves

Untreated *Npc1*$^{-/-}$ mice show a characteristically stunted growth curve compared to *Npc1*$^{+/+}$ control, whereby they gain weight more slowly than *Npc1*$^{+/+}$ mice and then begin to lose weight at around 7 weeks of age, culminating in their death around 10 weeks of age. Treatment with 3mg/kg rhHSP70^{his} did not affect the growth kinetics of *Npc1*$^{-/-}$ mice **(Figure 3.8)**, suggesting that it is well tolerated in the mice.

3.4.4 Rearing

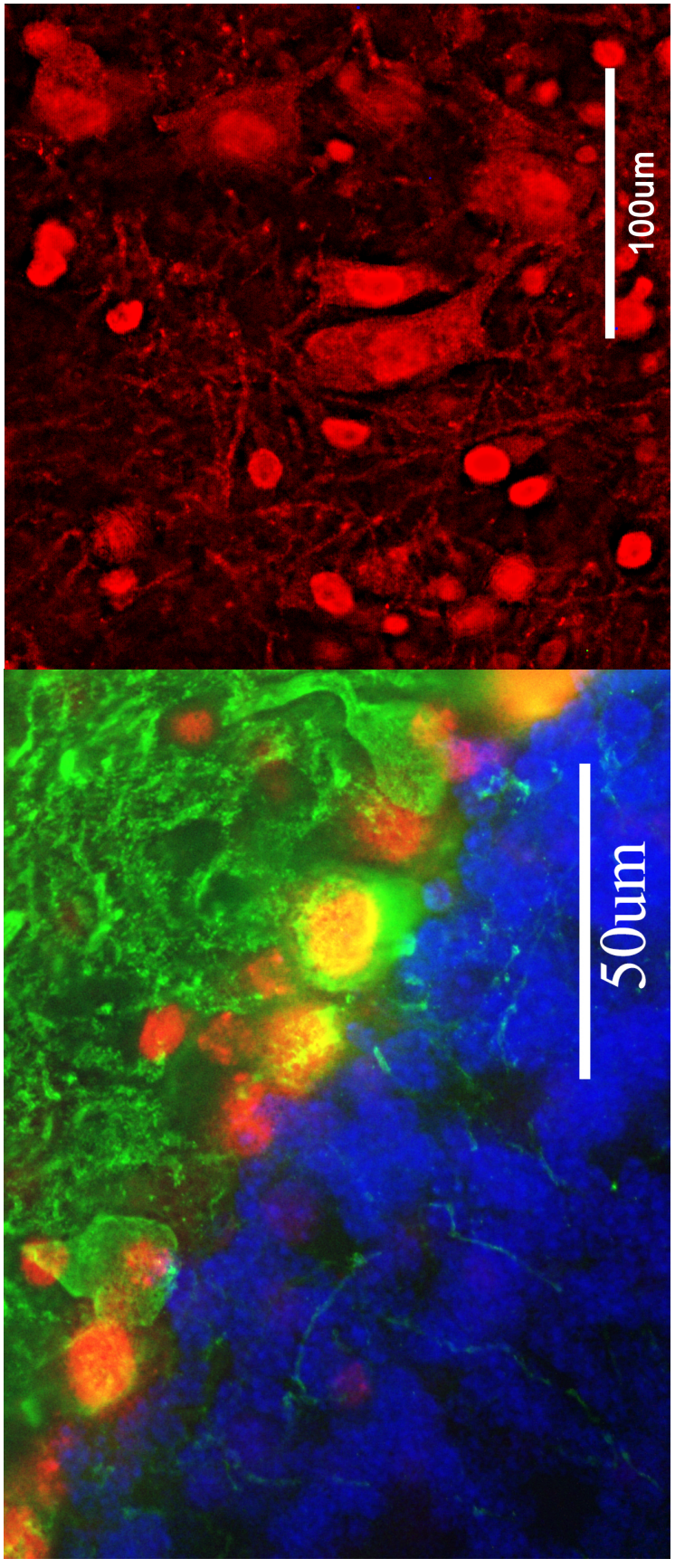
The loss of rearing behaviour is associated with disease progression in NPC [159]. Rearings performed using the side of the cage as a support (termed 'side rearing') require less coordination than rearing in the centre of the open field, in which the animal is required to balance itself. Typically, centre rearing ability declines much more rapidly than side rearing ability, as it requires a greater degree of coordination and balance from the animal.

Manual Rearing Measurements

Treatment of *Npc1*$^{-/-}$ mice with 3mg/kg rhHSP70^{his} showed small but non-significant improvements in side rearing compared to untreated *Npc1*$^{-/-}$, when analysed either as 4 - 7 week averages



Figure 3.4: *In the cerebellum, rhHSP70^{his} localises to the Purkinje cell layer and deep nuclear region 3 days following single injection* Whole cerebellar midline section showing strong immunoreactivity of rhHSP70^{his} in the Purkinje cell layer and deep nuclear region.



(b) (a)

Figure 3.5: *In the cerebellum, rhHSP70^{his} localises to the Purkinje cell layer and deep nucleii, 3 days following single injection* a) image of lobule X of the cerebellum showing immunoreactivity of rhHSP70^{his} (red) in the Purkinje cell layer (calbindin, green). Counterstained with DAPI. b) Deep cerebellar nucleii show his-tag immunoreactivity (red).

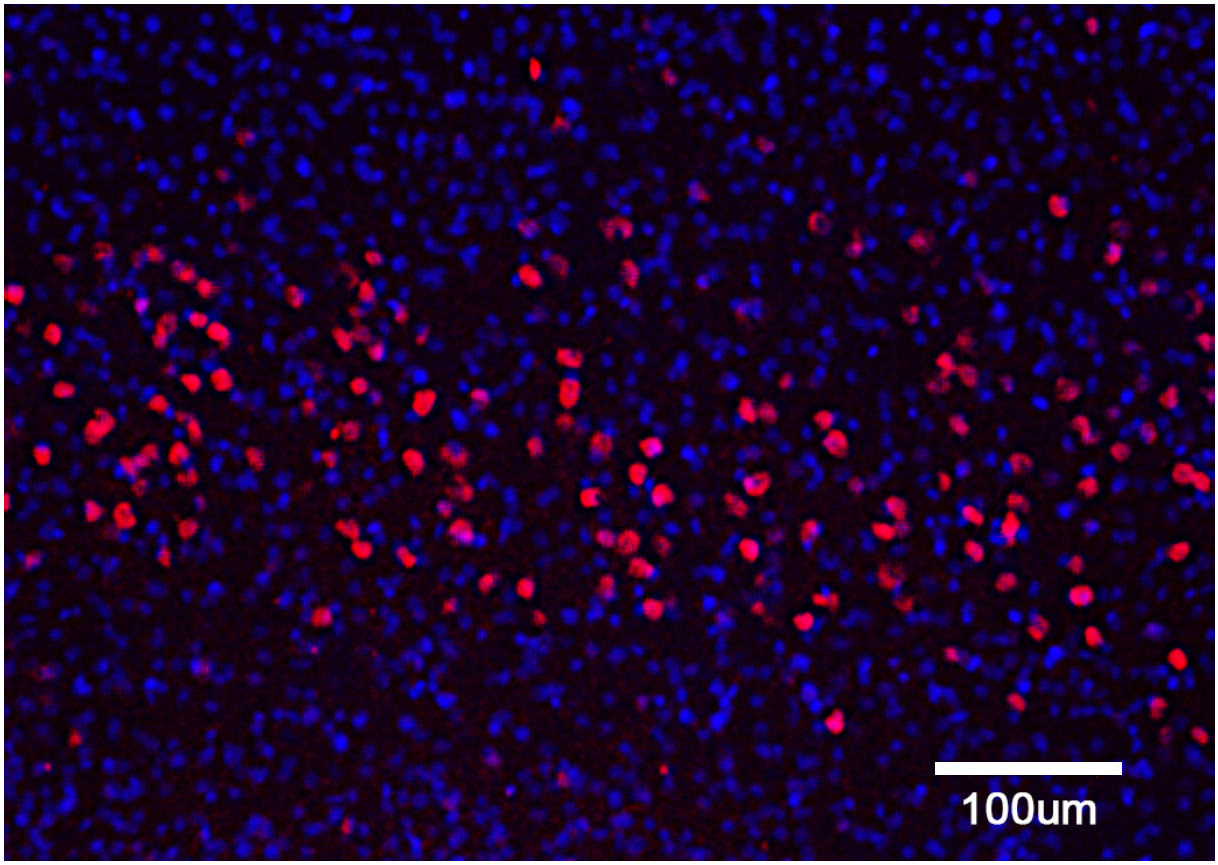


Figure 3.6: *In the cortex, rhHSP70^{his} staining is predominantly within layer V, 3 days following single injection* image of the cerebral cortex layer V stained with anti-His tag (red) and DAPI (blue) showing immunoreactivity 3 days following injection of rhHSP70$^{\text{his}}$

.

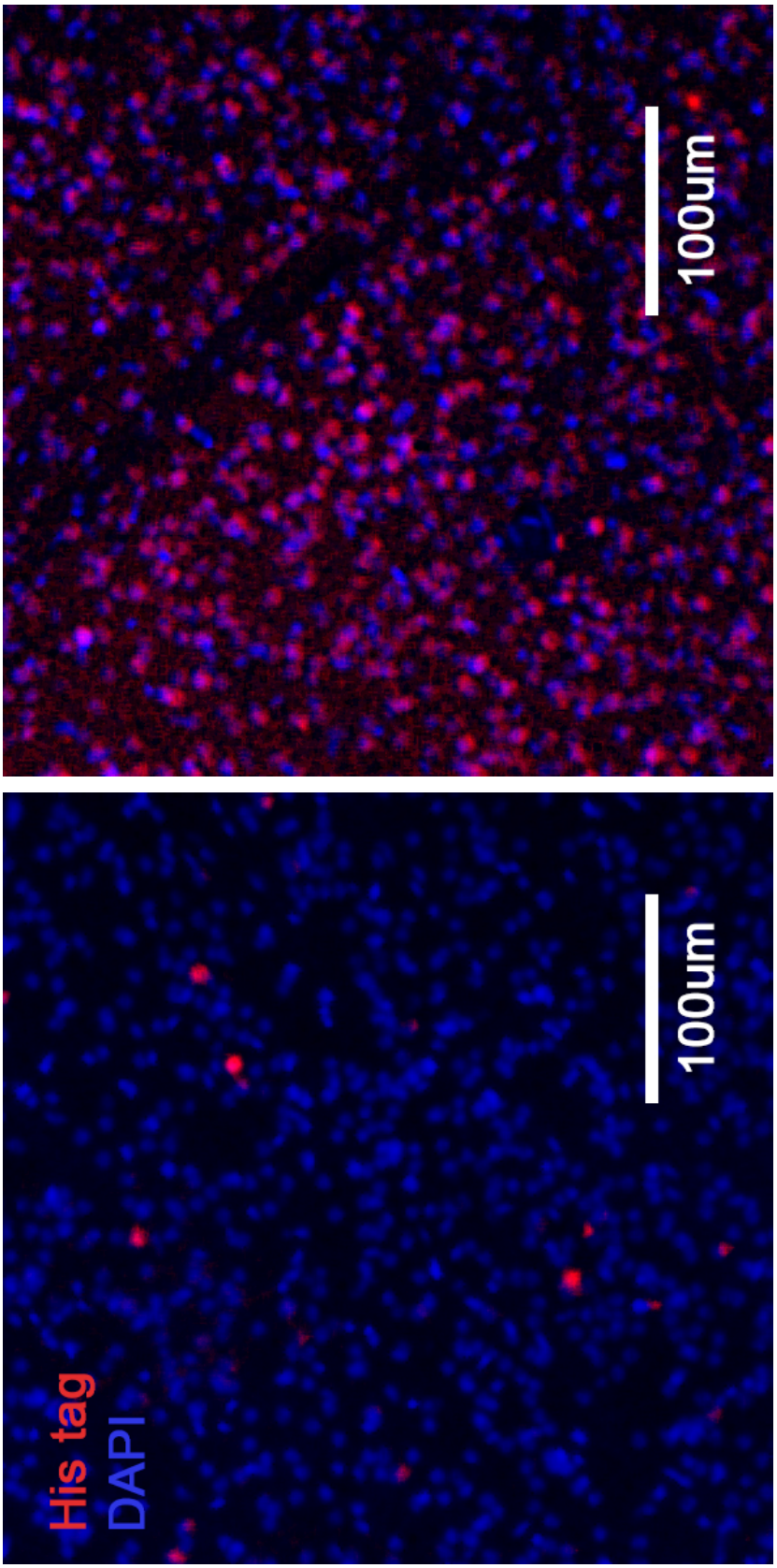
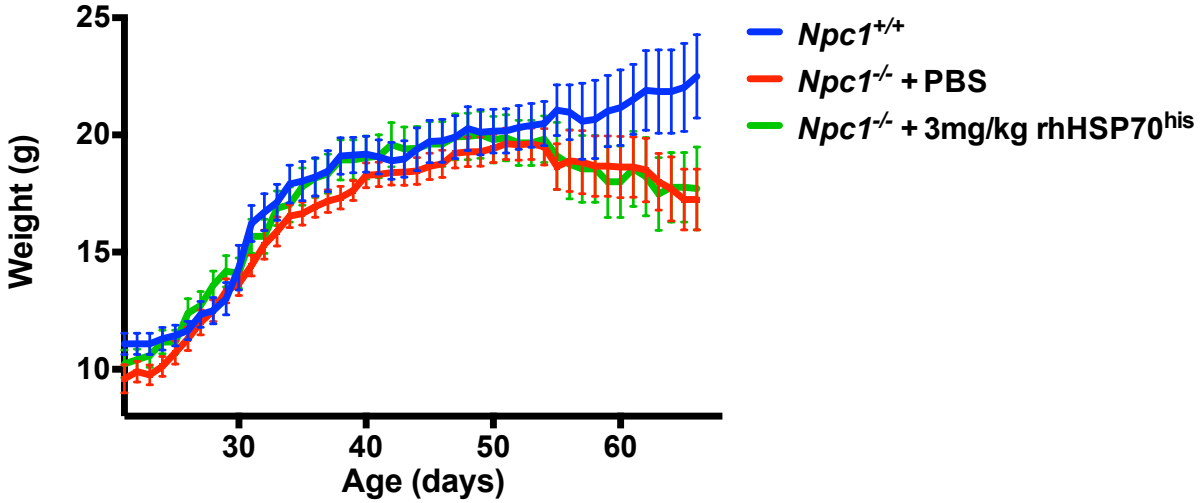
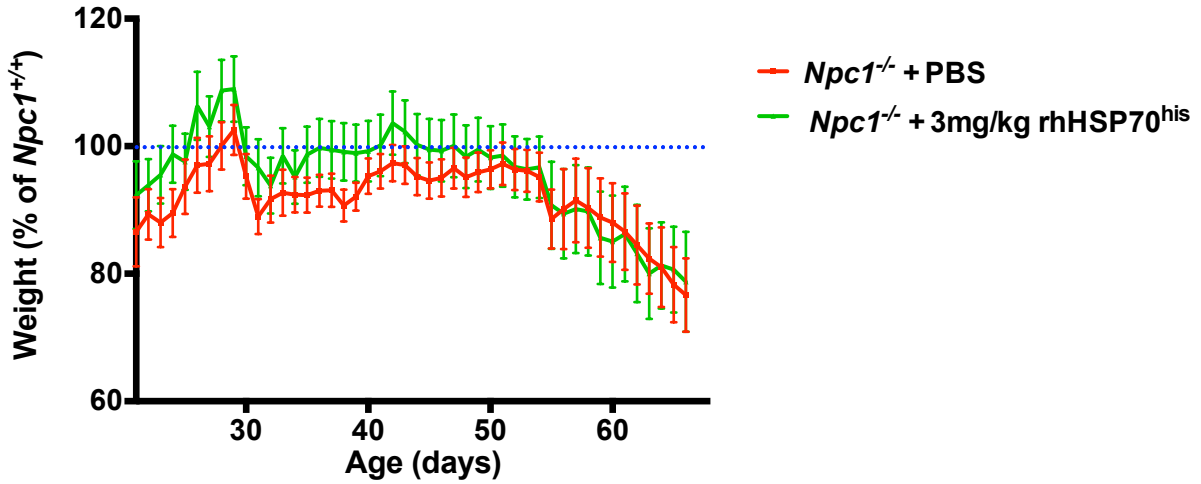


Figure 3.7: *In the caudate putamen, rhHSP70^{his} was detectable in very few, scattered cells. 7 days following injection, rhHSP70^{his} reactivity was widespread.* a) 3 days following injection, few cells in the caudate putamen were rhHSP70^{his+} (red) b) by 7 days post-injection, rhHSP70^{his} immunoreactivity was widespread.



(a)



(b)

Figure 3.8: *rhHSP70^{his} treatment does not affect growth curves in* Npc1$^{-/-}$ *mice* Growth curves showing a) absolute body weights and b) as a percentage of *Npc1*$^{+/+}$.

(Figure 3.9a) or as weekly scores **(Figure 3.9b)** up to 7 weeks compared to untreated *Npc1*$^{-/-}$ controls when measured manually, although these improvements did not reach statistical significance. Centre-rearing showed an improvement at 8 weeks following treatment with 3mg/kg rhHSP70^{his}, compared to untreated *Npc1*$^{-/-}$ controls **(Figure 3.10b)**, although the average early centre rearing score was not changed **(Figure 3.10a)**. *Npc1*$^{-/-}$ mice treated with1.5mg/kg rhHSP70^{his} showed significant improvements in side rearing behaviour at weeks 5, 6 and 8 **(Figure 3.9b)**, and significant improvements in average centre-rearing scores of weeks 4-7 **(Figure 3.10a)** as well as significant improvements in weekly centre rearing scores at weeks 5 and 6 **(Figure 3.10b)**. *Npc1*$^{-/-}$ mice treated with 0.3mg/kg rhHSP70^{his} did not display improvements in either side or centre rearing behaviour.

Automated Rearing Measurements

AMlogger measurements of the improvements in the numbers of side rears showed a dose dependant improvement in side rearing behaviour. *Npc1*$^{-/-}$ mice treated with 3mg/kg rhHSP70^{his} showed significant improvements at 4 weeks compared to untreated *Npc1*$^{-/-}$ mice **(Figure 3.11a)** but this improvement lost significance at later timepoints. Mice treated with 1.5 mg/kg rhHSP70^{his} did not show significance at any time point compared to untreated *Npc1*$^{-/-}$ mice, although the scores were consistently raised. Centre rearing **(Figure 3.11b)** showed no significant improvements at any timepoint compared to untreated *Npc1*$^{-/-}$ mice, although again it was raised at the early timepoints following 3mg/kg treatment with rhHSP70^{his}. *Npc1*$^{-/-}$ mice treated with 1.5mg/kg rhHSP70^{his} had consistently elevated rearing scores compared to untreated *Npc1*$^{-/-}$ mice, but again, the improvement did not reach significance. Treatment of *Npc1*$^{-/-}$ mice with 0.3mg/kg rhHSP70^{his} gave scores indistinguishable from untreated *Npc1*$^{-/-}$ mice.

The amount of time spent rearing **(Figure 3.12a)** was significantly increased in the 3mg/kg rhHSP70^{his} treated mice at 4 weeks and in the 1.5mg/kg rhHSP70^{his} treated *Npc1*$^{-/-}$ mice at weeks 5 and 7, when compared to untreated *Npc1*$^{-/-}$ mice. Again, these improvements were lost by 9 weeks of age. Surprisingly, the average rear duration was significantly raised in the 0.3mg/kg

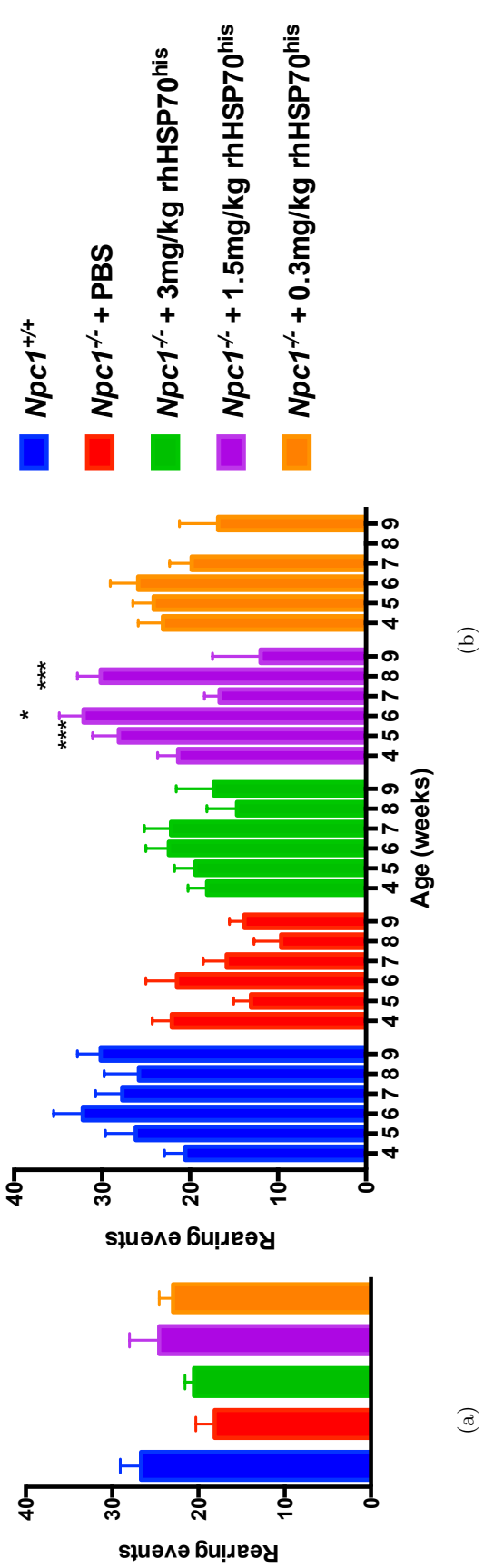


Figure 3.9: *Treatment with rhHSP70^{his} shows early improvement in manual scores of side rearing compared to untreated* Npc1$^{-/-}$ *mice.* a) Side rearing averages of 4-7 week rearing scores. b) weekly scores in side rearing. *Npc1*$^{+/+}$, n= 11, 11, 11, 6, 6., *Npc1*$^{-/-}$ +PBS, n= 12, 12, 12, 6, 6., 3mg/kg rhHSP70^{his} treated *Npc1*$^{-/-}$ n= 12, 12, 12, 6, 6., 1.5mg/kg rhHSP70^{his} treated *Npc1*$^{-/-}$ n= 8, 8, 8, 6, 6., 0.3mg/kg rhHSP70^{his} treated *Npc1*$^{-/-}$ n= 12, 12, 12, 0, 6 for weeks 4, 5, 6, 7, 8 and 9 respectively. p= *<0.05, **<0.01, ***<0.001. Data were analysed using a one-way ANOVA with Dunnett's multiple comparison test (graph a), and a two-way ANOVA with Dunnetts multiple comparison test (graphs b)

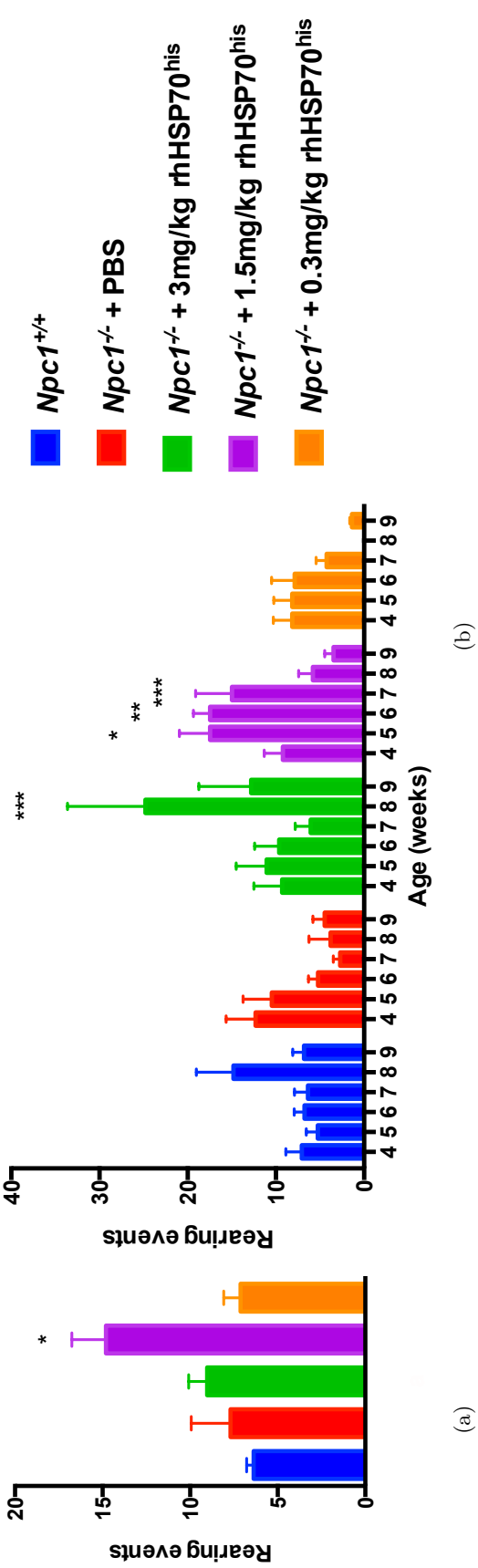


Figure 3.10: *Treatment with rhHSP70^{his} shows improvement in manual scores of centre rearing compared to untreated* Npc1$^{-/-}$ *mice.* a) Centre rearing averages of weeks 4 - 7. b) weekly centre rearing scores. *Npc1*$^{+/+}$, n= 11, 11, 11, 6, 6., *Npc1*$^{-/-}$ +PBS, n= 12, 12, 12, 6, 6., 3mg/kg rhHSP70^{his} treated *Npc1*$^{-/-}$ n= 12, 12, 12, 6, 6., 1.5mg/kg rhHSP70^{his} treated *Npc1*$^{-/-}$ n= 8, 8, 8, 6, 6., 0.3mg/kg rhHSP70^{his} treated *Npc1*$^{-/-}$ n= 12, 12, 12, 0, 6 for weeks 4, 5, 6, 7, 8 and 9 respectively. p= *<0.05, **<0.01, ***<0.001. Data were analysed using a one-way ANOVA with Dunnett's multiple comparison test (graph a), and a two-way ANOVA with Dunnetts multiple comparison test (graph b)

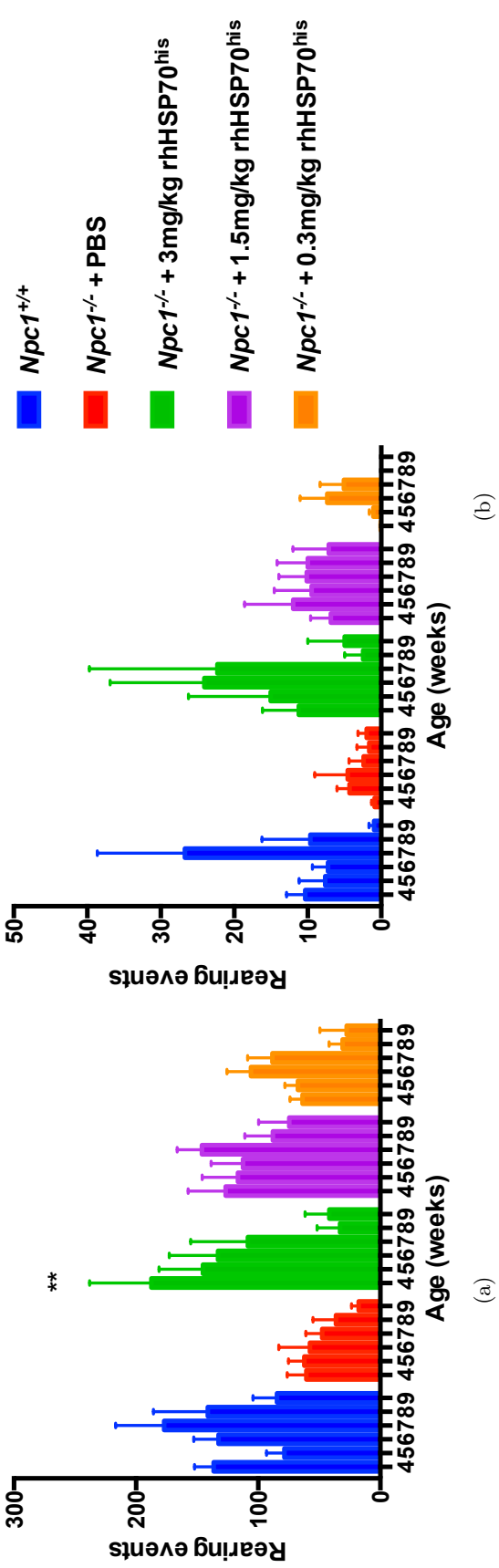


Figure 3.11: *Treatment with rhHSP70^{his} shows dose-dependant early improvement in side and centre rearing ability of* Npc1$^{-/-}$ *mice when measured by AMLogger.* Side rearing scores a) were significantly improved at 4 weeks, and remained elevated (ns) until 8 weeks of age following treatment with 3mg/kg rhHSP70^{his}, compared to unreated *Npc1*$^{-/-}$ mice. Similarly centre rearing scores b) showed consistent increases (ns) compared to untreated *Npc1*$^{-/-}$ mice following treatment with 3mg/kg rhHSP70^{his}. In both measurements, positive effects declined with duration of treatment. *Npc1*$^{+/+}$, n= 11, 11, 11, 6, 6., *Npc1*$^{-/-}$ + PBS, n= 12, 12, 12, 6, 6., 3mg/kg rhHSP70^{his} treated *Npc1*$^{-/-}$ n= 12, 12, 12, 6, 6., 1.5mg/kg rhHSP70^{his} treated *Npc1*$^{-/-}$ n= 8, 8, 8, 6, 6., 0.3mg/kg rhHSP70^{his} treated *Npc1*$^{-/-}$ n= 12, 12, 12, 6, 6 for weeks 4, 5, 6, 7, 8 and 9 respectively. p= *<0.05, **<0.01. Data were analysed using two-way ANOVAs with Dunnett's multiple comparison test.

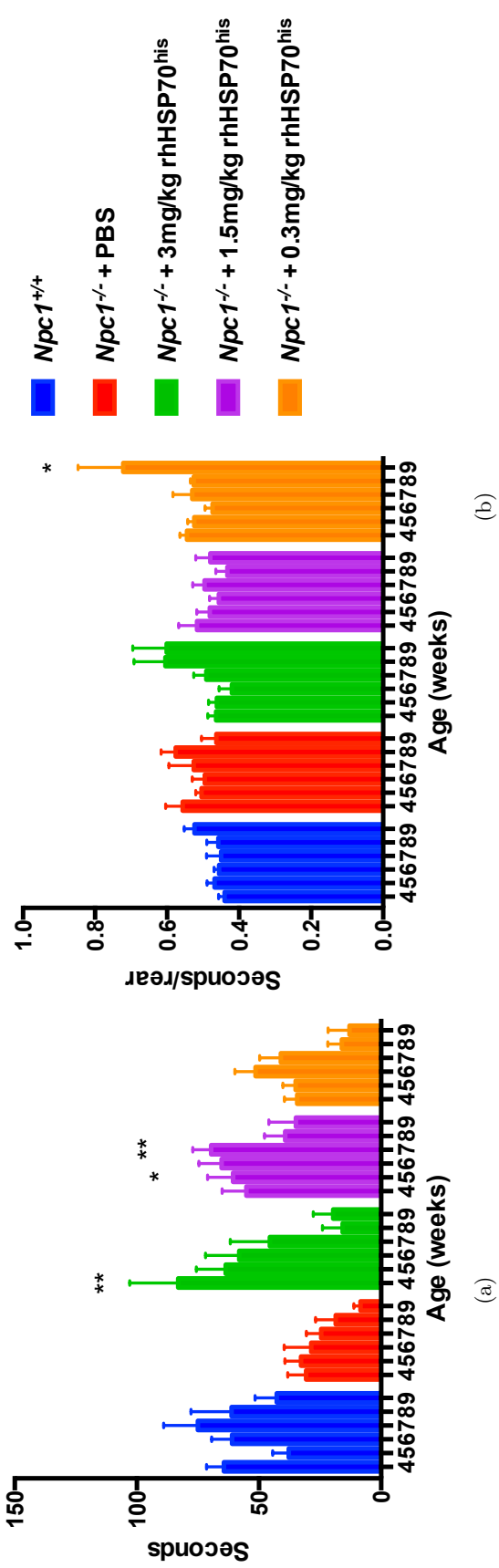
rhHSP70^{his} treated *Npc1*$^{-/-}$ mice at the 9 week timepoint, compared to untreated *Npc1*$^{-/-}$ mice **(Figure 3.12b)**. This suggests, that although at the later timepoints, the 0.3mg/kg rhHSP70^{his} treated *Npc1*$^{-/-}$ mice were not rearing more, they were however able to sustain their rearings significantly better than the untreated *Npc1*$^{-/-}$ mice.

These data suggest that mice treated with 3mg/kg and 1.5mg/kg rhHSP70^{his}, show early improvements in their rearing ability. Indeed, if the weekly rearing scores for each mouse over the period of 4-7 weeks are averaged, the 3mg/kg rhHSP70^{his} treated *Npc1*$^{-/-}$ mice showed significant improvements in both side rearing **(Figure 3.13 a)**, centre rearing **(Figure 3.13 b)** and the amount of time spent rearing **(Figure 3.13 c)**, resulting in scores comparable to *Npc1*$^{+/+}$ mice. *Npc1*$^{-/-}$ mice treated with 1.5mg/kg rhHSP70^{his} also showed smaller, but significant improvements in side rearing **(Figure 3.13 a)** and total rearing time **(Figure 3.13 c)**, compared to untreated *Npc1*$^{-/-}$ controls. As before, 0.3mg/kg rhHSP70^{his} treated *Npc1*$^{-/-}$ mice showed no improvement.

3.4.5 Tremor

The development of high frequency tremor is associated with disease progression in *Npc1*$^{-/-}$ mice [159]. Tremor is typically associated with the loss of Purkinje cells of the cerebellum, and the first signs of tremor begin to appear at 6 weeks of age, corresponding to initiation of Purkinje cell death. To assess whether we were impacting the development of tremor, we placed the mice in a tremor monitor for 5 minutes and recorded the rate and frequency at which the mice tremor at. An example histogram showing 7 week tremor frequencies for *Npc1*$^{+/+}$, untreated *Npc1*$^{-/-}$, and 3mg/kg rhHSP70^{his} treated *Npc1*$^{-/-}$ mice, is shown in **Figure 3.14a**.

Low frequency tremor (11Hz) is associated with disease progression, however it is subject to large variations, as normal behaviour such as grooming, will be recorded by the tremor monitor in the low frequency range. For this reason, it is not commonly used to assess disease progression in the *Npc1*$^{-/-}$ disease model. However, large increases in low frequency tremor had previously been observed following treatment with 3mg/kg rhHSP70^{his} in the pilot study, which we hypothesised, could be due to increased normal behaviour of the treated mice. This large increase was not recapitulated during this study **(Figure 3.14b)**, although 11Hz tremor in the



(a) (b)

Figure 3.12: *Treatment with rhHSP70^{his} shows dose-dependant early improvement in rearing ability of* Npc1$^{-/-}$ *mice when measured by AMLogger.* The total time spent rearing a) showed significant increases at 4 weeks following treatment of *Npc1*$^{-/-}$ with 3mg/kg rhHSP70^{his} compared to untreated *Npc1*$^{-/-}$ mice, and remained again consistently elevated up to 7 weeks. 1.5mg/kg rhHSP70^{his} treated *Npc1*$^{-/-}$ mice showed significant improvements at 5 and 7 weeks of age compared to untreated *Npc1*$^{-/-}$ mice. Rearing duration b), calculated as the average seconds per rear, showed a surprising improvement in the 0.3mg/kg rhHSP70^{his} treated *Npc1*$^{-/-}$ mice at 9 weeks compared to untreated *Npc1*$^{-/-}$ mice, suggesting that the treated mice were better able to maintain their balance whilst rearing, whereas the untreated mice started losing the ability to mainatin their rearings.
Npc1$^{+/+}$, n= 11, 11, 11, 6, 6., *Npc1*$^{-/-}$ + PBS, n= 12, 12, 12, 6, 6., 3mg/kg rhHSP70^{his} treated *Npc1*$^{-/-}$ n= 12, 12, 12, 6, 6., 1.5mg/kg rhHSP70^{his} treated *Npc1*$^{-/-}$ n= 8, 8, 8, 6, 6., 0.3mg/kg rhHSP70^{his} treated *Npc1*$^{-/-}$ n= 12, 12, 12, 6, 6 for weeks 4, 5, 6, 7, 8 and 9 respectively. p= *<0.05, **<0.01. Data were analysed using two-way ANOVAs with Dunnett's multiple comparison test.

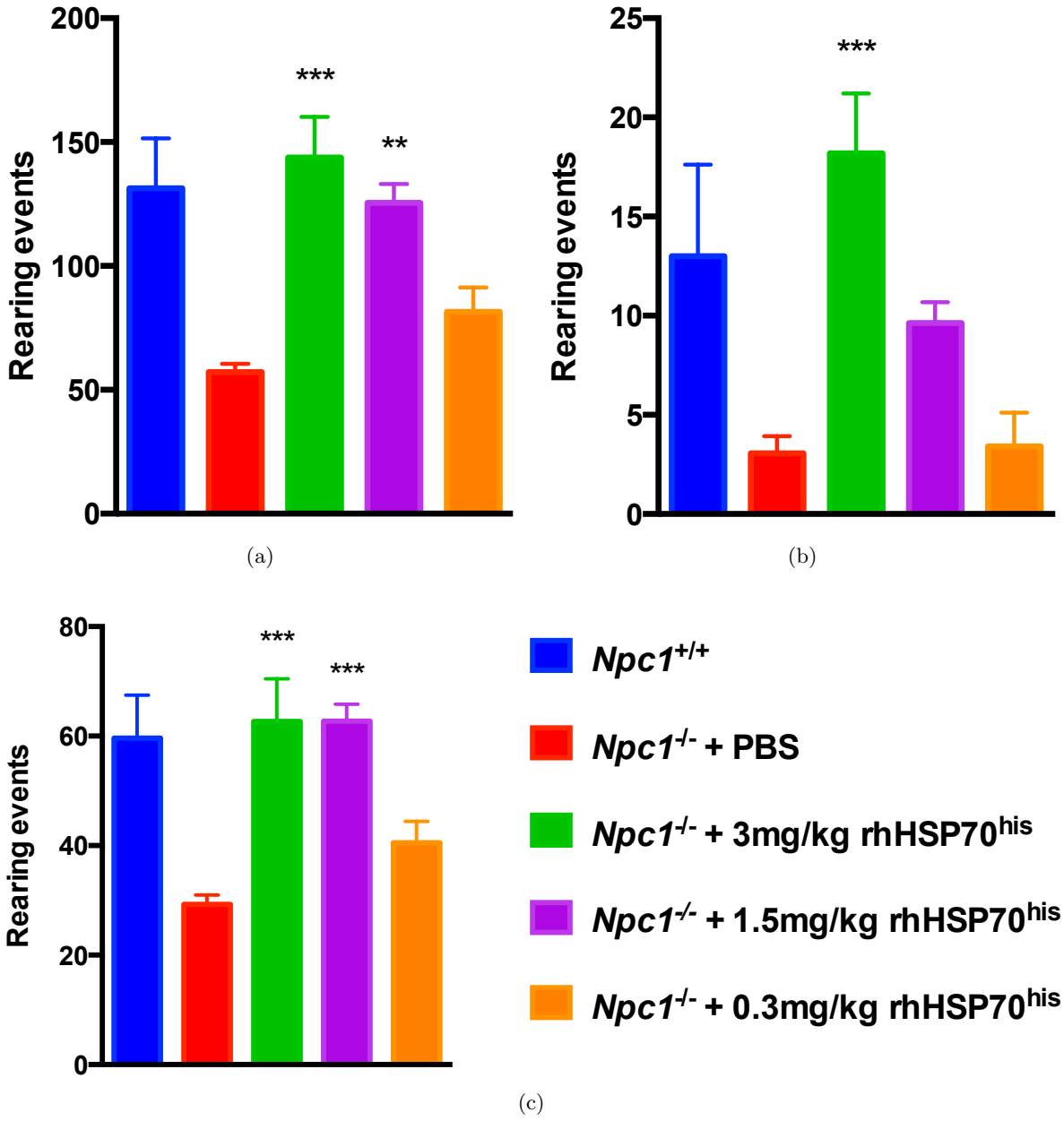
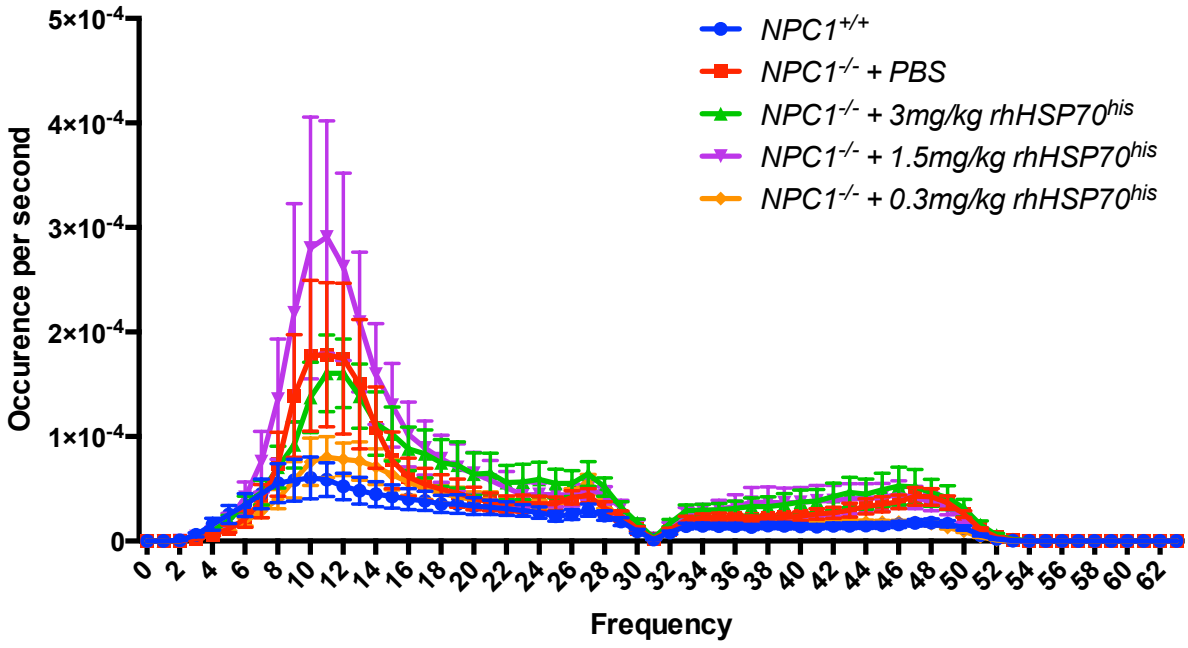
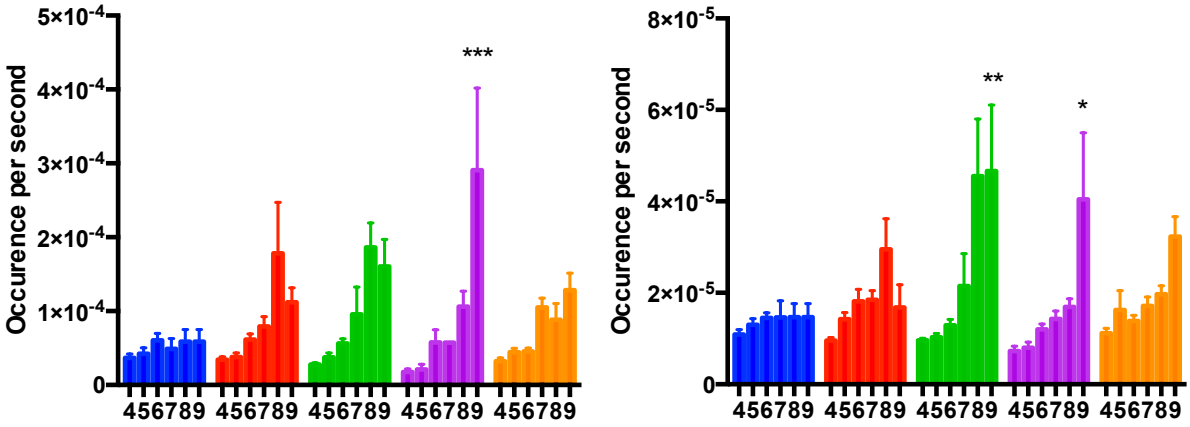


Figure 3.13: *Treatment with rhHSP70^{his} shows dose-dependant improvements in rearing ability of* Npc1$^{-/-}$ *mice at 4 - 7 weeks.* The average rearing scores for early weeks (4 - 7) show signifcant differences in side rearing a), centre rearing b) and time spent rearing c) following treatment with 3mg/kg rhHSP70^{his} compared to untreated *Npc1*$^{-/-}$ mice, 1.5mg/kg rhHSP70^{his} showed similar improvements in side rearing and rearing time compared to untreated *Npc1*$^{-/-}$ mice. 0.3mg/kg rhHSP70^{his} treatment was unchanged. *Npc1*$^{+/+}$, n= 11., *Npc1*$^{-/-}$ + PBS, n= 12., 3mg/kg rhHSP70^{his} treated *Npc1*$^{-/-}$ n= 12, 1.5mg/kg rhHSP70^{his} treated *Npc1*$^{-/-}$ n= 8, 0.3mg/kg rhHSP70^{his} treated *Npc1*$^{-/-}$ n= 12. p= **<0.01, ***<0.001. Data were analysed using a one-way ANOVA with Dunnett's multiple comparison test. Error bars are SEM.



(a)



(b) (c)

Figure 3.14: *Automated tremor values show significant increases following treatment with 1.5mg/kg and 3mg/kg rhHSP70^{his}.* a) Example traces of *Npc1*$^{+/+}$, untreated and 3mg/kg, 1.5mg/kg and 0.3mg/kg rhHSP70^{his} treated *Npc1*$^{-/-}$ mice at 7 weeks of age b) occurence of 11Hz tremor over time c) occurence of 43Hz tremor over time. *Npc1*$^{+/+}$, n= 11, 11, 11, 6, 6., *Npc1*$^{-/-}$ + PBS, n= 12, 12, 12, 6, 6., 3mg/kg rhHSP70^{his} treated *Npc1*$^{-/-}$ n= 12, 12, 12, 6, 6., 1.5mg/kg rhHSP70^{his} treated *Npc1*$^{-/-}$ n= 8, 8, 8, 6, 6., 0.3mg/kg rhHSP70^{his} treated *Npc1*$^{-/-}$ n= 12, 12, 12, 6, 6 for weeks 4, 5, 6, 7, 8 and 9 respectively. p= *<0.05, **<0.01. Data was analysed using two-way ANOVAs with Dunnett's multiple comparison test. Error bars are SEM

	Week 5		Week 6		Week 7	
	no. Mice	no. Runs	no. Mice	no. Runs	no. Mice	no. Runs
Npc1$^{+/+}$	6	17	6	16	6	14
Npc1$^{-/-}$	6	16	6	17	6	18
3mg/kg rHSP70^{his}	6	18	6	17	6	18

Table 3.1: Table showing numbers of mice and trials which met the inclusion criteria for each group at each time point.

1.5mg/kg rhHSP70^{his} group did increase at 9 weeks.

Mice treated with both 1.5mg/kg and 3mg/kg rhHSP70^{his} showed an increase in characteristic high frequency tremor (43Hz) at 9 weeks of age compared to untreated *Npc1*$^{-/-}$ mice **(Figure 3.14c)**. However, the tremor of untreated *Npc1*$^{-/-}$ mice was not significantly different to *Npc1*$^{+/+}$ controls at 9 weeks, which is unusual as the tremor of *Npc1*$^{-/-}$ mice increases until the animal dies. Normally a large increase, particularly of high frequency tremor would be expected at 9 weeks of age in untreated *Npc1*$^{-/-}$ mice.

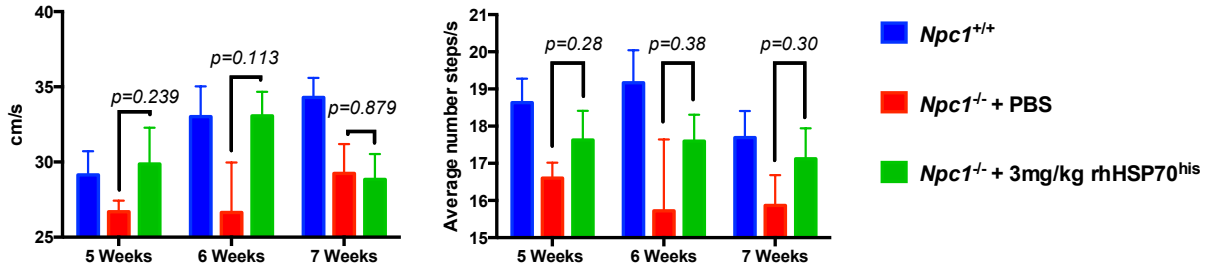
The following analyses focussed on 3mg/kg rhHSP70^{his} treatment, as this showed the most promising behavioural effects.

3.4.6 Gait Analysis

The CatWalk gait analysis equipment and software measures over 100 parameters of gait, and is a highly sensitive tool for gait analysis, having shown usefulness in several disease models. However, recent work has shown that all of the dynamic, and most of the non-dynamic measurements are highly dependant on speed variations, even in wildtype mice [329]. We applied data segmentation profiles to minimise the variations in speed between the mice, described in more detail in **Chapter 2**. Based on these settings, the numbers of mice and runs per week which were utilised for the gait analysis are shown in **Table ??**.

Average speed between untreated *Npc1*$^{-/-}$ and 3mg/kg rhHSP70^{his} treated *Npc1*$^{-/-}$ mice was comparable at all timepoints, and within the 9.25cm/s range specified as significantly affecting parameters, although some differences were observed following treatment **(Figure 3.15a)**. At 6 weeks, 3mg/kg rhHSP70^{his} treated *Npc1*$^{-/-}$ mice showed similar speed to *Npc1*$^{+/+}$ mice, whereas untreated *Npc1*$^{-/-}$ mice began to slow down , although these differences were not significant **(Figure 3.15a)**. Cadence, which is the number of steps per second, has been shown to be

modified in a model of striatal lesion in rats [330]. Cadence showed consistent improvements following treatment with 3mg/kg rhHSP70^{his}, although this did not reach significance at any timepoint **(Figure 3.15b)**.

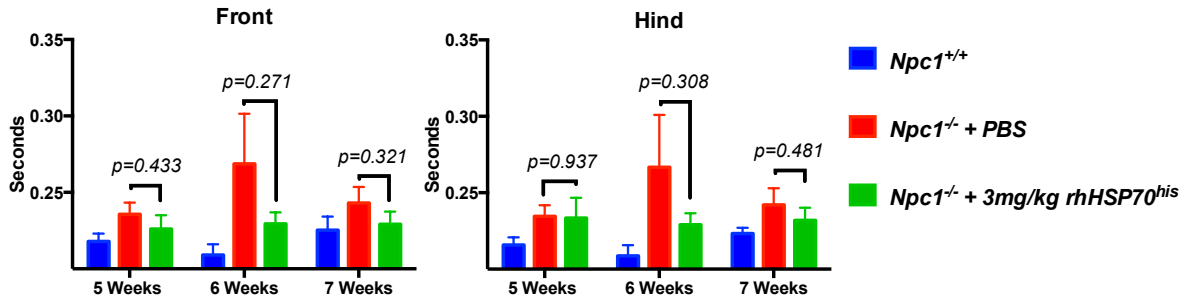


(a) (b)

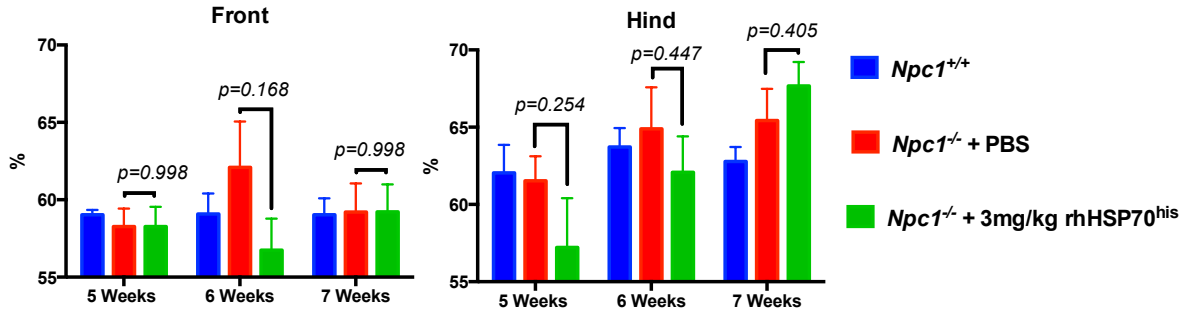
Figure 3.15: *Treatment with rhHSP70^{his} shows trends towards improvement of both speed and cadence* Treatment with rhHSP70^{his} shows small improvements in a) speed and b) cadence compared to *Npc1*$^{-/-}$ mice. *Npc1*$^{+/+}$, n= 6, 6, 5. *Npc1*$^{-/-}$ + PBS, n= 6, 6, 6., 3mg/kg rhHSP70^{his} treated *Npc1*$^{-/-}$ n= 6, 6, 6., for weeks 5, 6 & 7 respectively. Data were analysed using multiple two-tailed students t-tests, with Holm-Sidak corrections for multiple comparisons. Error bars are SEM.

Step cycle and duty cycle are dynamic paw measurements which have both been shown to be strong indicators of treatment efficacy in a rat model of Parkinson's disease [331]. Step cycle is the time between consecutive placements of the same paw, and significantly increases with disease progression in untreated *Npc1*$^{-/-}$ compared to *Npc1*$^{+/+}$. Treatment with 3mg/kg rhHSP70^{his} shows the greatest reductions at 6 weeks, although this was non-significant **(Figure 3.16a)**. These differences decreased at 7 weeks of age. Duty cycle is the percentage of the step cycle which the mouse spends standing, and as such is another dynamic measurement of the speed of paw placement. Duty cycle also significantly increases with disease progression in untreated *Npc1*$^{-/-}$ compared to *Npc1*$^{+/+}$. At 6 weeks front paw duty cycle showed some improvements, although these improvements were not consistent amongst timepoints and at the later timepoint appeared to increase in the hind paws of the 3mg/kg rhHSP70^{his} treated mice **(Figure 3.16b)**.

Max contact AT (%) provides a measurement of the % of the paw stand time that the maximum print area is achieved. This has been shown to be altered in rats which have undergone spinal cord injury, and correlated significantly with injury severity [332]. *Npc1*$^{-/-}$ mice showed



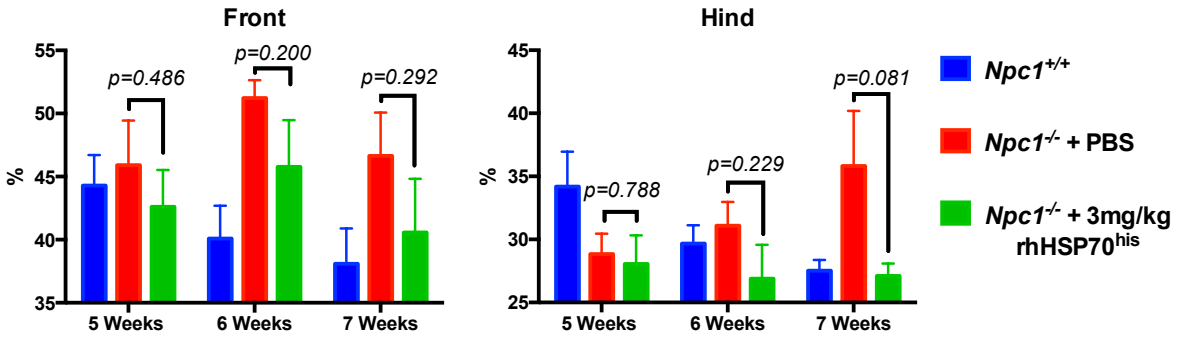
(a)



(b)

Figure 3.16: *Treatment with rhHSP70^{his} shows trends towards improvements in both step cycle and duty cycle* Treatment with rhHSP70$^{\text{his}}$ shows small, non-significant improvements in a) step cycle but not b) duty cycle compared to *Npc1*$^{-/-}$ mice. *Npc1*$^{+/+}$, n= 6, 6, 5. *Npc1*$^{-/-}$ + PBS, n= 6, 6, 6., 3mg/kg rhHSP70$^{\text{his}}$ treated *Npc1*$^{-/-}$ n= 6, 6, 6., for weeks 5, 6 & 7 respectively. Data was analysed using multiple two-tailed students t-tests, with Holm-Sidak corrections for multiple comparisons. Error bars are SEM.

decreases in max conact AT, particularly in the hind paws. This showed some correction following treatment with rhHSP70^{his} treatment, although again, this did not reach significance **(Figure 3.17)**.



(a)

Figure 3.17: *Treatment with rhHSP70^{his} shows trend towards improvement in both Front and Hind paw contact* Treatment with rhHSP70^{his} shows consistent improvements (non-significant) at 6 and 7 weeks in maximum signal intensity of paw placement compared to *Npc1$^{-/-}$* mice, partiularly for the hind paws. *Npc1$^{+/+}$*, n= 6, 6, 5. *Npc1$^{-/-}$* + PBS, n= 6, 6, 6., 3mg/kg rhHSP70^{his} treated *Npc1$^{-/-}$* n= 6, 6, 6., for weeks 5, 6 & 7 respectively Data was analysed using multiple two-tailed students t-tests, with Holm-Sidak corrections for multiple comparisons. Error bars are SEM.

3.4.7 SHIRPA Testing

NPC mice display a range of phenotypes as disease progresses, such as tail dragging, dragging of pelvis on the floor, poor coat condition (piloerection), partial eyelid (palpebral) closure, fast and shallow respiratory rate, and decreased spontaneous activity. Mice were scored using the SHIRPA assessment criterion for these areas. Treatment with 3mg/kg rhHSP70^{his} showed consistent improvements in several parameters assessed **(Figure 3.18)**. Of particular note, palpebral closure, which results in a squinting phenotype in untreated *Npc1$^{-/-}$* mice, was greatly improved following treatment, with all mice a 7 weeks showing no phenotype. The coat condition of the treated mice was also greatly improved, with the treated animals displaying a normal coat indistinguishable from *Npc1$^{+/+}$* mice.

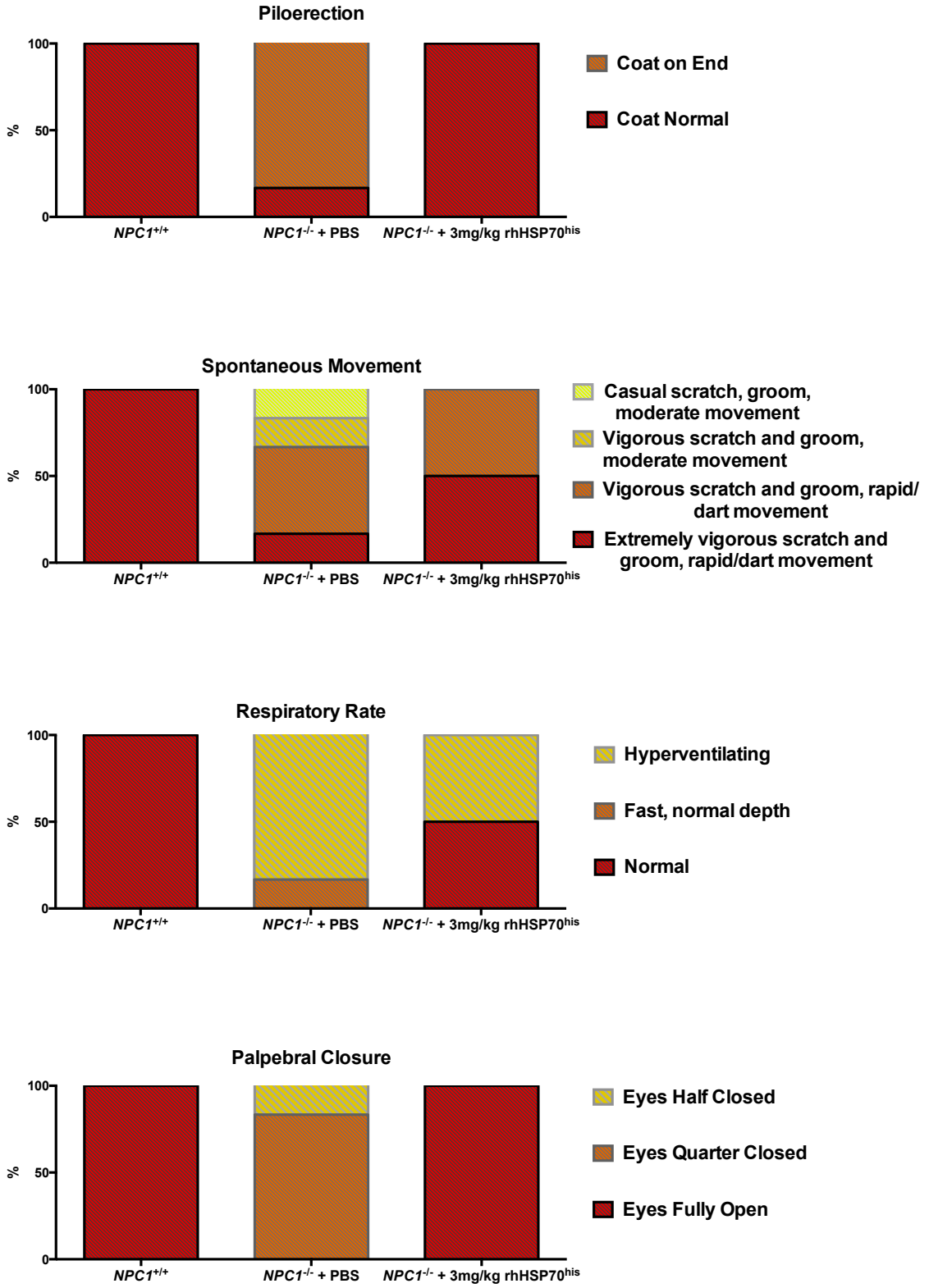


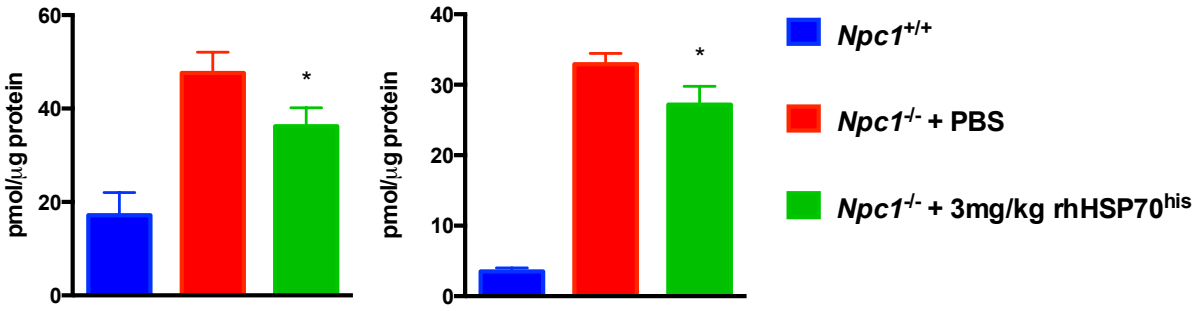
Figure 3.18: *rhHSP70^{his} treatment improves several phenotypes as assessed by SHIRPA testing* SHIRPA testing was performed on 7 week old *Npc1*$^{+/+}$, untreated *Npc1*$^{-/-}$, and 3mg/kg rhHSP70$^{\text{his}}$ treated mice. Treated mice showed consistent improvements in several areas, in particular, palpebral closure and piloerection were most improved. n=6/group

3.4.8 Biochemical Findings

The accumulation of a variety of lipids, including unesterified cholesterol, GSLs, sphingomyelin, sphingosine and BMP is one of the hallmarks of NPC disease [149, 148, 151]. Peripheral storage of GSLs, unesterified cholesterol, sphingosine and sphingomyelin increases with disease progression, whilst storage of GSLs in the central nervous system correlates with increased neurodegeneration and the associated behavioural changes observed in the *Npc1*$^{-/-}$ mouse model [93]. To assess whether treatment with rhHSP70^{his} affected the accumulation of these lipids, we used a variety of techniques to quantify cholesterol, sphingosine and GSL accumulation in tissues.

Glycosphingolipid Quantification

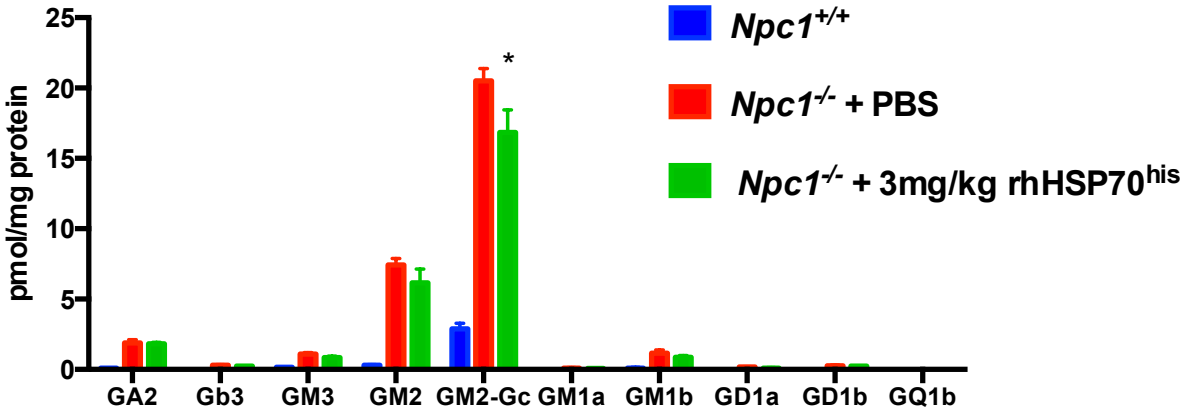
Glycosphingolipid (GSL) accumulation was evaluated in liver, kidney, forebrain and cerebellum following treatment with 3mg/kg rhHSP70^{his}. In kidney, a 33% reduction in total GSL accumulation was observed at 7 weeks (p=0.042) **(Figure 3.19a)** and in liver, a signifcant reduction of 20% following treatment with 3mg/kg rhHSP70^{his} was detected (p=0.001) **(Figure 3.19b)**. The major lipid species accumulating in liver, GM2-Gc was significantly reduced by 20% (p<0.001) following treatment **(Figure 3.4.8a)** as was the major accumulating species in kidney, Gb3 (40%, p=0.002) **(Figure 3.4.8b)**.



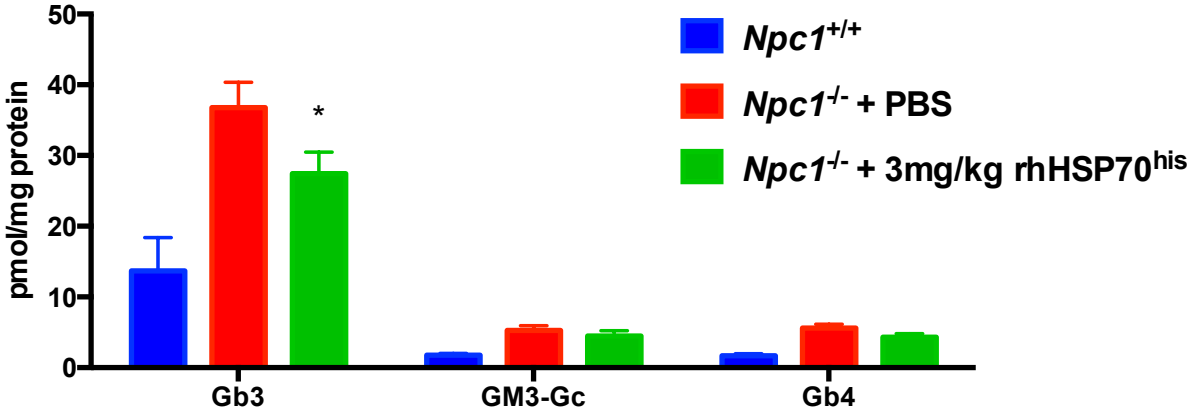
(a) (b)

Figure 3.19: *Treatment with rhHSP70^{his} reduces peripheral GSL accumulation.* Treatment with rhHSP70^{his} shows reductions in GSL storage in a) Kidney b) Liver compared to untreated *Npc1*$^{-/-}$ mice. *Npc1*$^{+/+}$, n= 5., *Npc1*$^{-/-}$ + PBS, n= 5., 3mg/kg rhHSP70^{his} treated *Npc1*$^{-/-}$ n= 6. . p= *<0.05. Data was analysed using a one-tailed students t-test. Error bars are SEM.

The forebrain of 7 week untreated *Npc1*$^{-/-}$ mice, showed large accumulations GSLs compared



(a)



(b)

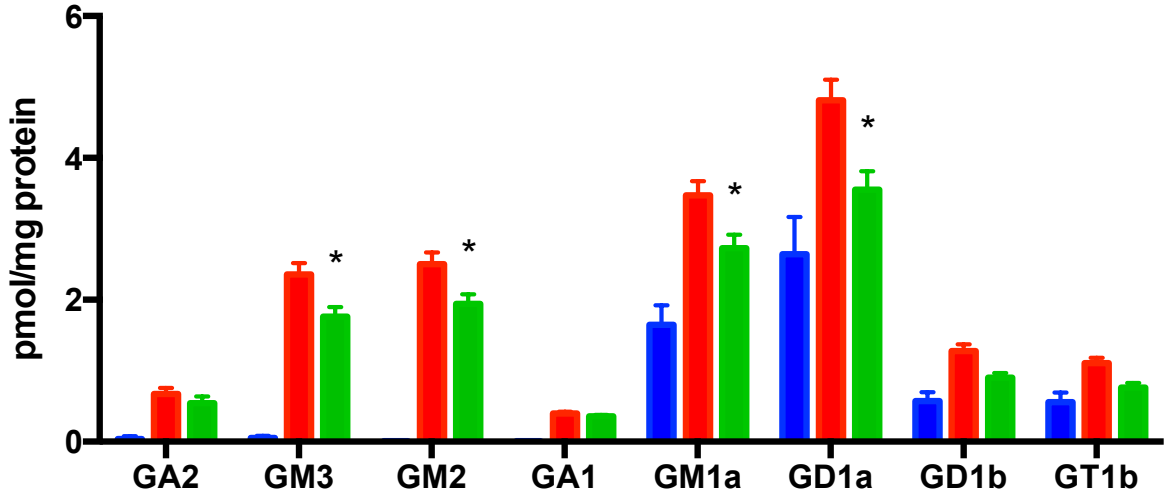
Figure 3.20: *Major accumulating GSL species are preferentially degraded following treatment with rhHSP70^{his}.* Treatment with rhHSP70$^{\text{his}}$ shows reductions of major accumulating lipid species in liver a) where GM2-Gc shows greatest reductions in accumulation compared to untreated *Npc1*$^{-/-}$ mice. In kidney b), Gb3 shows the greatest level of reduction compared to untreated *Npc1*$^{-/-}$ mice. *Npc1*$^{+/+}$, n= 5., *Npc1*$^{-/-}$ + PBS, n= 5., 3mg/kg rhHSP70$^{\text{his}}$ treated *Npc1*$^{-/-}$ n= 6. . p= *<0.05. Data was analysed using multiple students t-tests, with Holm-Sidak corrections for multiple comparisons. Error bars are SEM.

to *Npc1*$^{+/+}$ mice. Administration of rhHSP70^{his} significantly reduced the cerebral accumulation of GM3 (25%, p=0.00618), GM2 (22%, p=0.00985), GM1a (40%, p=0.0008), GD1a (58%, p<0.0001). The following GSLs were also reduced, but failed to reach significance; GA2 (20%, p=0.547), GA1 (10%, p=0.851), GD1b (53%, p=0.0792), GT1b (63%, p=0.105) **(Figure 3.4.8a)**. Treatment with 3mg/kg rhHSP70^{his} resulted in a 41% reduction (emphp=0.0076) in total forebrain GSLs **(Figure 3.4.8b)**.

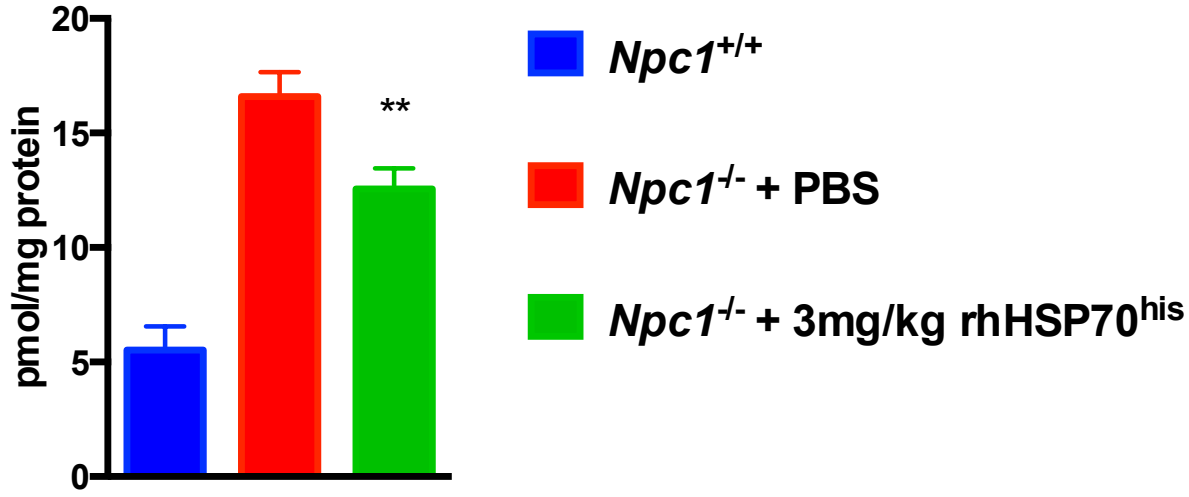
The cerebellum of 7 week untreated *Npc1*$^{-/-}$ mice showed significant accumulations of several GSL species compared to *Npc1*$^{+/+}$ mice. Treatment of *Npc1*$^{-/-}$ mice with 3mg/kg rhHSP70^{his} caused non-significant reductions in several accumulating species. The largest changes observed in individual cerebellar GSL species were in GD1a (42% p=0.197), GM1a (29% p=0.196), GM1b (23% p=0.848) and GM2 (21% p=0.168). Small changes were observed in GD1b (5% p=0.932), GM3 (11% p=0.710), GT1b (11% p=0.849), whereas GA1 (-3% p=0.940), GA2 (-4% p=0.847) were slightly increased. It is interesting to note that in both the forebrains and cerebellum of these mice that the asialo-GSL species GA1, and GA2 show the least reduction following treatment with rhHSP70^{his}. The total levels of GSLs in the cerebellum were unchanged following treatment with 3mg/kg rhHSP70^{his} **(Figure 3.4.8b)**.

Sphingosine Measurements

Sphingosine is the degradative endpoint in sphingolipid catabolism **(see Figure 1.1)**, and has been shown previously to be the earliest accumulating lipid detectable following the addition of U18666A, a class II amphiphile which induces NPC disease [7] and the addition of sphingosine *in vitro* has been shown to induce an NPC phenotype in healthy cells. To assess whether rhHSP70^{his} was affecting the accumulation of sphingosine, we extracted sphingosine from forebrain homogenates using a method previously described [3], and modified as described in the materials and methods. Sphingosine accumulation in both untreated *Npc1*$^{-/-}$ and 3mg/kg rhHSP70^{his} treated *Npc1*$^{-/-}$ forebrains were raised when compared to *Npc1*$^{+/+}$ mice. Whilst rhHSP70^{his} treated mice showed a greater accumulation (59%) when compared to untreated controls, this did not reach significance (p=0.2593) **(Figure 3.23)**.

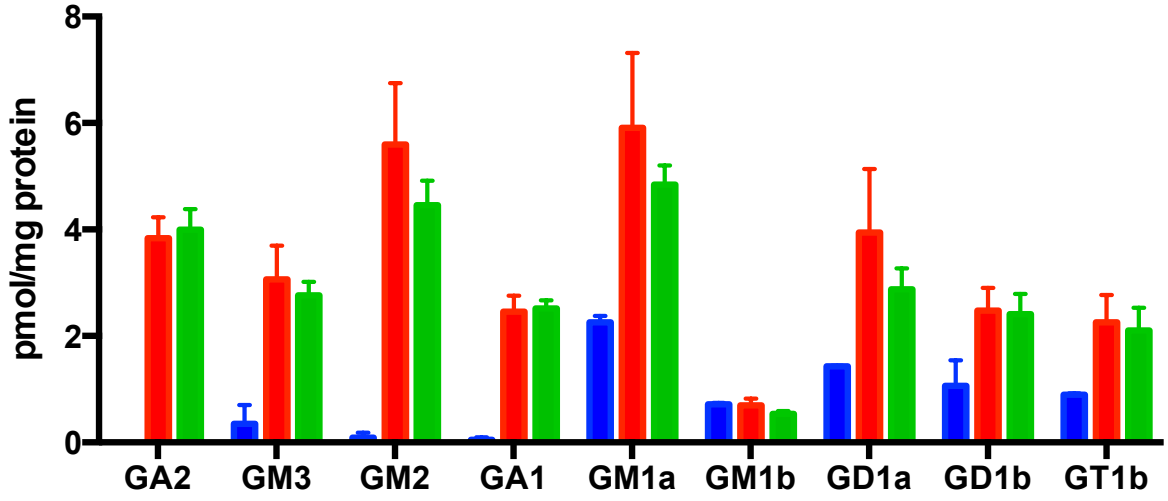


(a)

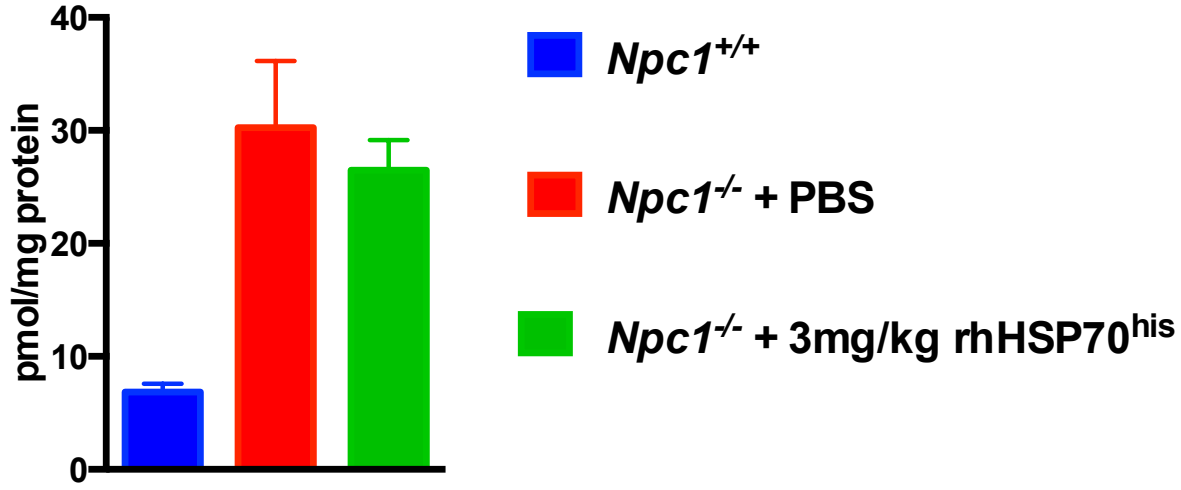


(b)

Figure 3.21: *Forebrain accumulation of GSLs is reduced by rhHSP70^{his} treatment.* Treatment with rhHSP70$^{\text{his}}$ shows reductions in total GSL species in forebrain compared to untreated *Npc1*$^{-/-}$ mice a). Graph showing the individual GSL species detected in forebrain, b). *Npc1*$^{+/+}$, n= 5., *Npc1*$^{-/-}$ + PBS, n= 5., 3mg/kg rhHSP70$^{\text{his}}$ treated *Npc1*$^{-/-}$ n= 6. p= *<0.05,. **<0.01. Data was analysed using multiple students t-tests, with Holm-Sidak corrections for multiple comparisons. Error bars are SEM.



(a)



(b)

Figure 3.22: *Cerebellar accumulation of GSLs is not reduced by rhHSP70^{his} treatment.* a) Treatment with rhHSP70^{his} shows no reduction in total GSL species in cerebellum compared to untreated *Npc1*$^{-/-}$ mice. b) Graph showing the individual GSL species detected in cerebellum. Note that the major accumulating GSL species, GM2, GM1a and GD1a show the largest reductions compared to untreated *Npc1*$^{-/-}$ mice. *Npc1*$^{+/+}$, n= 5., *Npc1*$^{-/-}$ + PBS, n= 5., 3mg/kg rhHSP70^{his} treated *Npc1*$^{-/-}$ n= 6. Data was analysed using multiple students t-tests, with Holm-Sidak corrections for multiple comparisons. Error bars are SEM.

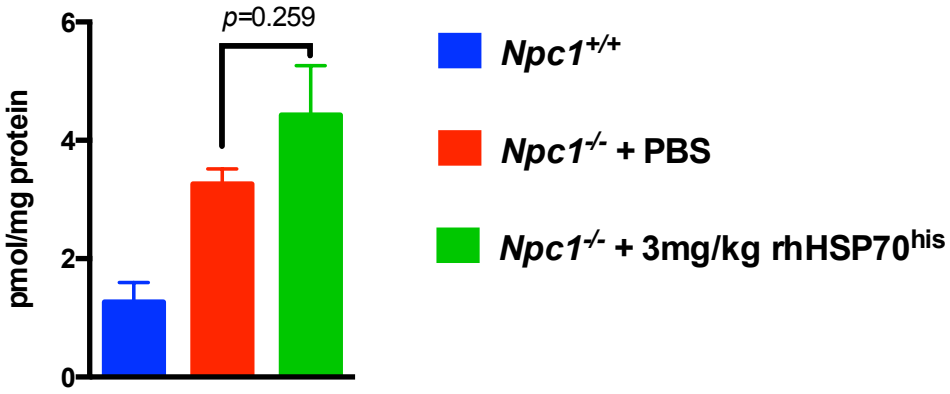
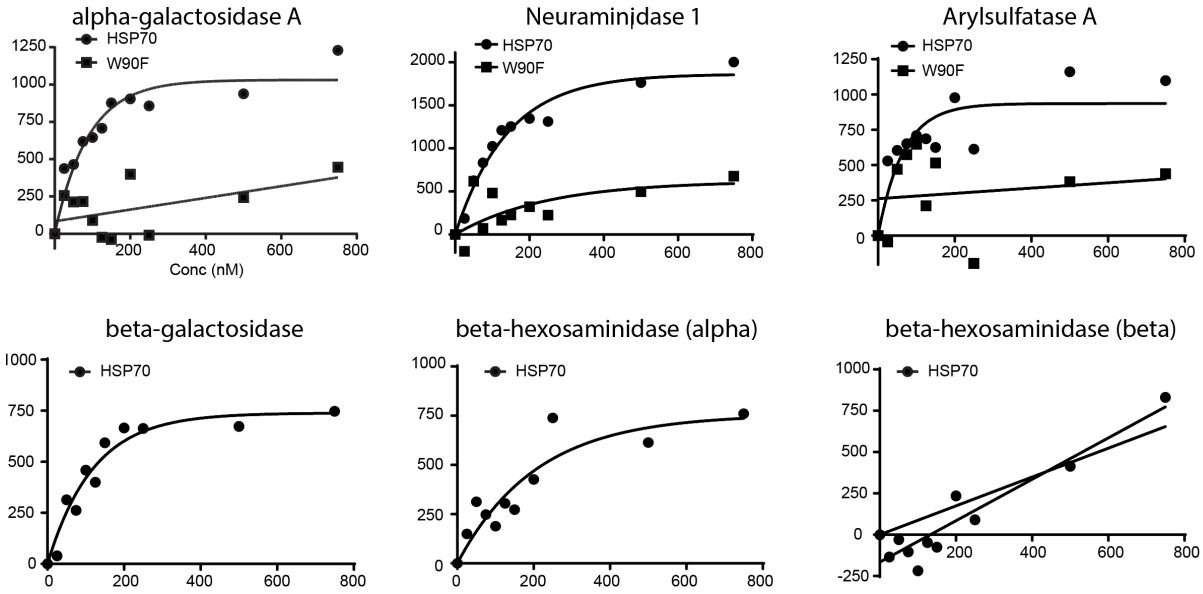


Figure 3.23: *Sphingosine accumulation indicates increase following treatment with rhHSP70^{his}.* Treatment with rhHSP70^{his} increased the levels of sphingosine present in the forebrains of treated *Npc1*$^{-/-}$ mice when compared to untreated *Npc1*$^{-/-}$ mice. Both were significantly increased when compared to *Npc1*$^{+/+}$ controls, however, the increase following 3mg/kg rhHSP70^{his} treatment did not reach significance. n= *Npc1*$^{+/+}$ 4, untreated *Npc1*$^{-/-}$ 6, 3mg/kg rhHSP70^{his} treated *Npc1*$^{-/-}$, 5. Error bars show SEM. Data was analysed using a two-tailed students t-test.

Lysosomal Hydrolase Binding Assay

HSP70 has previously been shown to increase the activity of acid sphingomyelinase (ASM) *in vitro* through increasing the association between ASM and the lysosomal phospholipid *bis*-(monoacylglycero)phosphate (BMP) [163]. As BMP is required for optimal activity of multiple hydrolases [48], HSP70 may be exerting its effects through a similar mechanism. To assess whether rhHSP70 increases the binding of lysosomal hydrolases to BMP, an assay was set-up to measure the rate of binding of fluorescently labelled hydrolases to lipid covered beads. AF488 tagged hydrolases lose fluorescence when in contact with BMP, and as such a quenching of fluorescence is observed when binding is increased. The following fluorescently tagged hydrolases (α-galactosidase A, β-galactosidase, Neuraminidase 1 , Arylsulfatase A, β-hexosaminidase α-subunit, β-hexosaminidase β-subunit) were incubated with increasing concentrations of either rhHSP70 or rhHSP70^{W90F} mutant (where indicated), which displays reduced binding to BMP. Interestingly, all of the lysosomal hydrolases excluding βHexβ exhibited a non-linear association of rhHSP70. Of the enzymes where the rhHSP70^{W90F} mutant was tested (α-galactosidase A, Arylsulfatase A Neuraminidase 1) this binding association was attenuated **(Figure 3.24)**. These data provide strong evidence that rhHSP70^{his} is exerting its effects on GSL degradation through

facilitating the binding of lysosomal hydrolases to BMP, in a similar fashion described to its association with ASM [163].



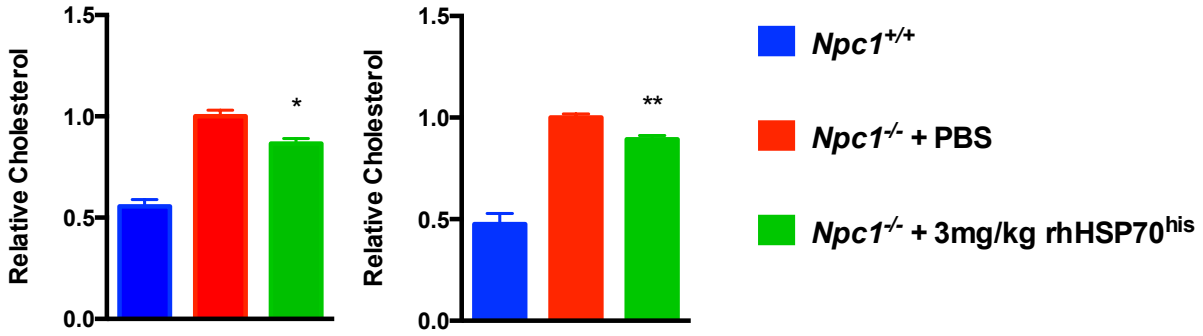
(a)

Figure 3.24: *HSP70 facilitates BMP binding of lysosomal hydrolases* in vitro. Fluorescently labelled sphingolipid-catabolic enzymes (α-galactosidase A, β-galactosidase, Neuraminidase 1, Arylsulfatase A, β-hexosaminidase α-subunit, and β-hexosaminidase β-subunit) were incubated with increasing amounts of rHSP70 (x-axis), and BMP-lipid coated beads. Fluorescence quenching (ΔFU, y axis) was calculated as the change from fluorescence with un-coated beads. Data points and association curves (non-linear regression, assuming one-phase association) are depicted on the graphs and show a clear facilitation of binding of all enzymes except β-hexosaminidase β-subunit. For α-galactosidase A, Neuraminidase 1 and Neuraminidase 1 the effect of mutant HSP70 (W90F) lacking the capacity to interact with BMP was also analysed. The W90F mutant shows a very reduced capacity to facilitate binding. Experiments were performed by Alexander Klein & Christoph Arenz, Humbolt University, Berlin. Data was supplied courtesy of Orphazyme ApS.

Cholesterol Quantification

As free cholesterol accumulation in peripheral organs is a hallmark of NPC disease, we extracted cholesterol using a modified Folche extraction **(section 2.7.1)** and measured free cholesterol content of liver and kidney homogenates using a commercially available kit. At 7 weeks we found that treatment of *Npc1*$^{-/-}$ mice with rhHSP70$^{\text{his}}$ significantly reduced the accumulation of free cholesterol in kidney **(Figure 3.25a)**, and in liver **(Figure 3.25b)** compared to untreated

Npc1$^{-/-}$ mice.



(a) (b)

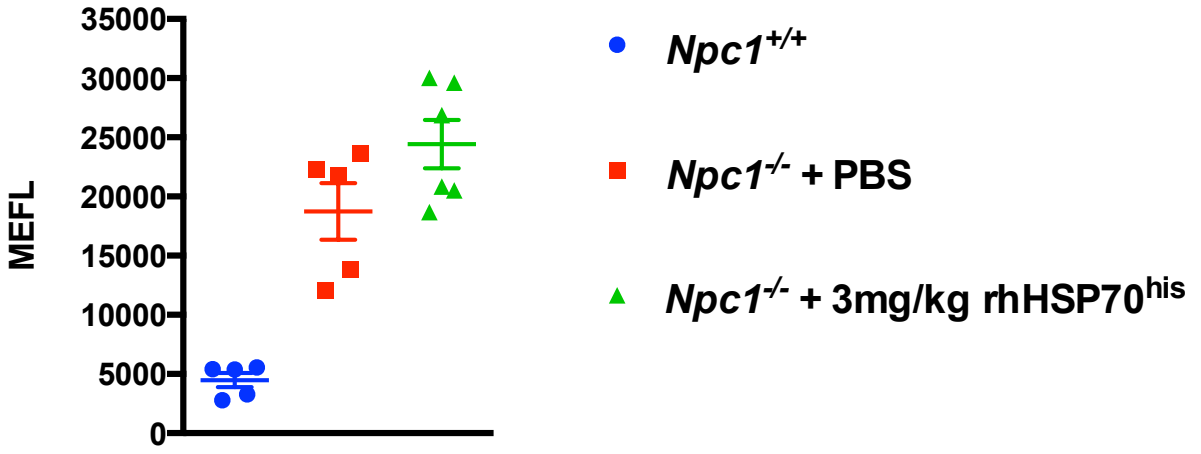
Figure 3.25: *Free cholesterol accumulation is reduced following rhHSP70^{his} treatment.* Treatment with rhHSP70^{his} significantly reduces free cholesterol accumulation compared to untreated *Npc1*$^{-/-}$ in a) kidney and b) liver. Values are the results of 3 seperate experiments. n= *Npc1*$^{+/+}$ 6, untreated *Npc1*$^{-/-}$ 6, 3mg/kg rhHSP70^{his} treated *Npc1*$^{-/-}$, 5. p= *<0.05. Data were analysed using a one-tailed students t-test. Error bars are SEM.

3.4.9 Lysosomal Volume

Due to the profound endocytic block in NPC, patients and the *Npc1*$^{-/-}$ mouse model exhibit increased volume of the acidic compartment. To assess whether the CNS and peripheral decreases in GSL and cholesterol accumulation correlate with a decrease in LysoTracker staining, we assessed acidic compartment volume of CD19^{+} splenic B-cells from 7 week old treated and untreated *Npc1*$^{-/-}$ mice, alongside *Npc1*$^{+/+}$ comparators. Although both were significantly raised when compared to *Npc1*$^{+/+}$ volumes, treated mice showed slightly (31%), although non-significantly (p=0.105) raised LysoTracker staining when compared to untreated *Npc1*$^{-/-}$ mice.

3.4.10 CNS Pathologies

To assess the impact of treatment with rhHSP70^{his} on the neurological phenotype of NPC, we utilized immunofluorescent staining of 7 week old treated and untreated *Npc1*$^{-/-}$ brain sections to assess the impact on Purkinje cell loss, neuroinflammation and myelination, alongside the storage of various lipids.



(a)

Figure 3.26: *Treatment with rhHSP70^{his} does not significantly increase lysosomal compartment volume.* a) Average MEFL values show small but non-significant differences between untreated *Npc1*$^{-/-}$ and *Npc1*$^{-/-}$ mice treated with 3mg/kg rhHSP70^{his}. Treatment with rhHSP70^{his} resulted in small but non-significant increases in MEFL values of LysoTracker stained CD19+ cells. n= *Npc1*$^{+/+}$ 5, untreated *Npc1*$^{-/-}$ 5, 3mg/kg rhHSP70^{his} treated *Npc1*$^{-/-}$, p= 0.0508 between untreated and 3mg/kg treated mice.

Purkinje Cell Loss

The Purkinje cells of the cerebellum are highly susceptible to degeneration in NPC disease and typically display axonal pathology, which is detectable from 2 weeks characterised by the appearance of large inclusions which cause the axons to swell [152, 147]. Mice treated with 3mg/kg rhHSP70^{his} showed typical axonal swellings, present on most axons which is comparable to the phenotype of untreated *Npc1*$^{-/-}$ mice.

To assess whether Purkinje cell loss was affected by treatment with rhHSP70^{his}, we counted Purkinje cell numbers in cerebellar midline sections **(Figure 3.27)**. Purkinje cell numbers were lower in all lobules, although these differences were not significant (LI, 12%, p=0.699., LII, 16%, p=0.194., LIII, 34%, p=0.134., LIV, 26%, p=0.0703., LV, 33%, p=0.0367 LVI, 26%, p=0.0791., LVII, 11%, p=0.501 LVIII, 17%, p=0.0226., LIX, 13%, p=0.121., LX, 11%, p=0.0337). It is also of interest to not that the "non-degenerating" lobules IX and X, also display relatively high rates of cell loss. Whilst this may be correct, it is possible that this may be an artifact of increased cerebellar volume, as this potentially could decrease the Purkinje cell density.

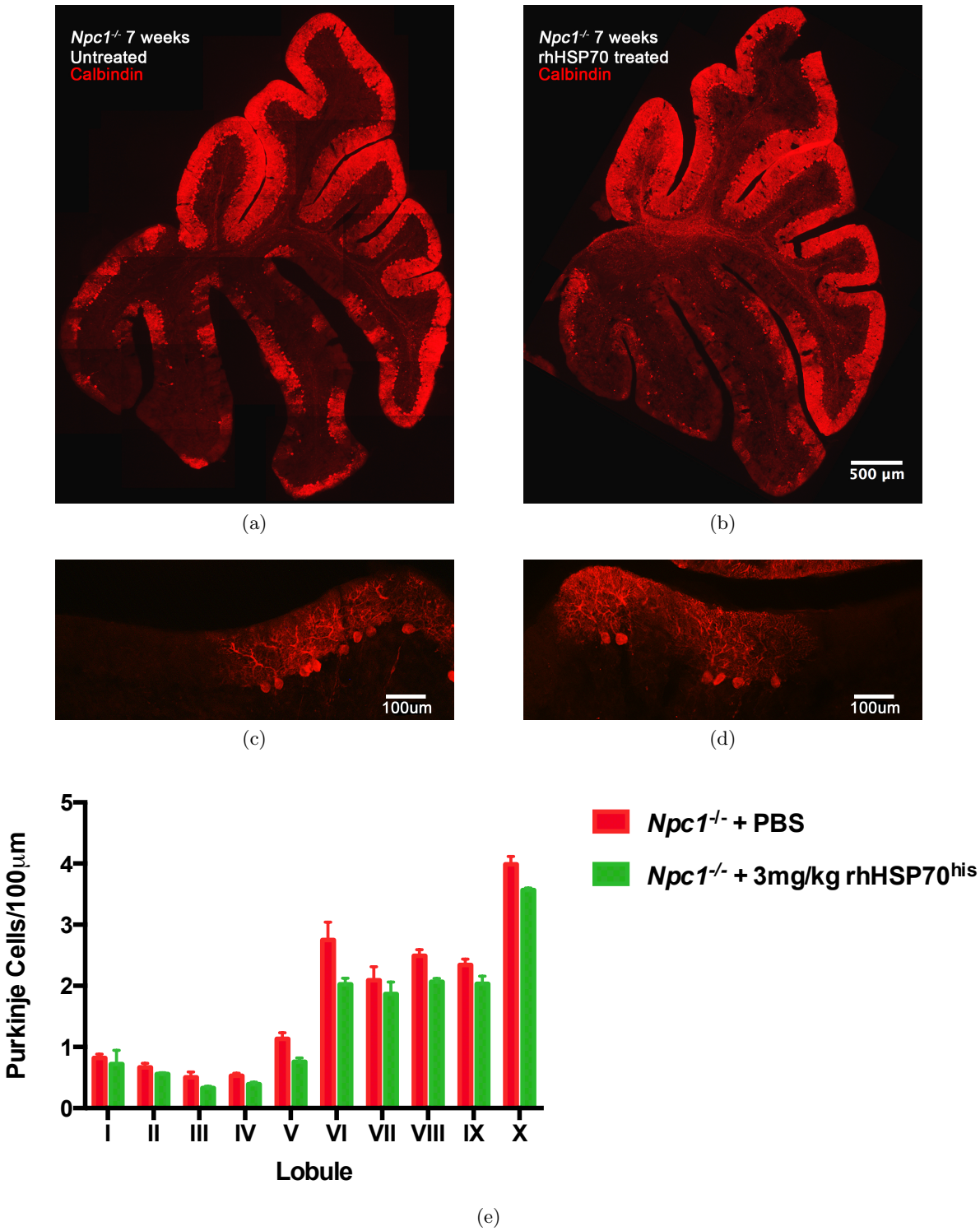


Figure 3.27: *Treatment of* Npc1$^{-/-}$ *mice with rhHSP70^{his} does not prevent Purkinje cell loss.* Representative images of cerebellar sections stained with antibodies against calbindin (red) from a) untreated *Npc1$^{-/-}$* mice and b) 3mg/kg rhHSP70^{his} treated *Npc1$^{-/-}$* mice. Images of Purkinje cell layer in lobule IV of c) untreated, and d) 3mg/kg rhHSP70^{his} treated *Npc1$^{-/-}$* mice. e) Counts of surviving Purkinje cells between untreated *Npc1$^{-/-}$* and *Npc1$^{-/-}$* mice treated with 3mg/kg rhHSP70^{his}. Treatment with 3mg/kg rhHSP70^{his} resulted in small but non-significant increases in Purkinje cell loss when compared to untreated *Npc1$^{-/-}$* controls. *n*, untreated *Npc1$^{-/-}$* = 3, 3mg/kg rhHSP70^{his} treated *Npc1$^{-/-}$* = 3. 5 cerebellar midline sections were counted per animal. Purkinje cell numbers were normalised against Purkinje cell layer length. Data was analysed using multiple two-tailed students t-tests with Holm-Sidak corrections for multiple comparisons. Error bars are SEM.

Neuorinflammation

We used CD68, a marker of microglia, to assess the degree of inflammation in the cerebellum. Most of the $CD68^+$ cells in degenerating regions displayed enlarged round morphology and stained strongly for cholesterol when assessed by filipin staining, suggesting that these microglia were actively involved in phagocytosis of degenerating Purkinje cells **(Figure 3.28a, b)**. We counted $CD68^+$ cells in lobules IV and VI, (early and late degenerating, respectively). We found similar numbers of $CD68^+$ microglia in both 3mg/kg $rhHSP70^{his}$ treated and untreated *Npc1*$^{-/-}$ mice at 7 weeks of age (LIV, p=0.8949., LVI, p=0.218 respectively), indicating a broadly similar inflammatory status between the treatments **(Figure 3.28c)**.

Myelination

To assess the level of myelination in *Npc1*$^{-/-}$ cerebellum, we stained untreated **(Figure 3.29a)** ,and treated **(Figure 3.29b)** *Npc1*$^{-/-}$ midline cerebellar sections for myelin basic protein (MBP) and counterstained with calbindin. Measurements were made of the white matter area, and normalised against the total lobular area. Mice treated with 3mg/kg $rhHSP70^{his}$ showed increased thickness of the white matter in the cerebellum at 7weeks (58%, p=0.0434) **(Figure 3.29c)**.

To assess the effects on myelination further, western blots of cerebellar homogenates were prepared and probed for MBP, and CNPase, a marker of developing oligodendrocytes, normalised against β-actin expression **(Figure 3.30a)**. A non-significant decrease (12%, p=0.195) was observed in the expression of CNPase, but a significant difference was observed in the expression of MBP (49%, p=0.0372) **(Figure 3.30b)**. This suggests that treatment with $rhHSP70^{his}$ improves the myelination status of the NPC mice.

As the forebrain has a more severe hypomyelination phenotpye than the cerebellum, we also performed western blots of the expression of MBP and CNPase in this region **(Figure 3.31a)**. Unlike the cerebellum, MBP expression did not appear to be changed in the forebrain (p=0.654) **(Figure 3.31b)**.

Treatment with $rhHSP70^{his}$ improves the myelination status of the cerebellum, as observed by both western blotting for MBP expression and immunohistochemistry, although this effect does not extend to the forebrain, where the gross myelination status of the mice remains unchanged.

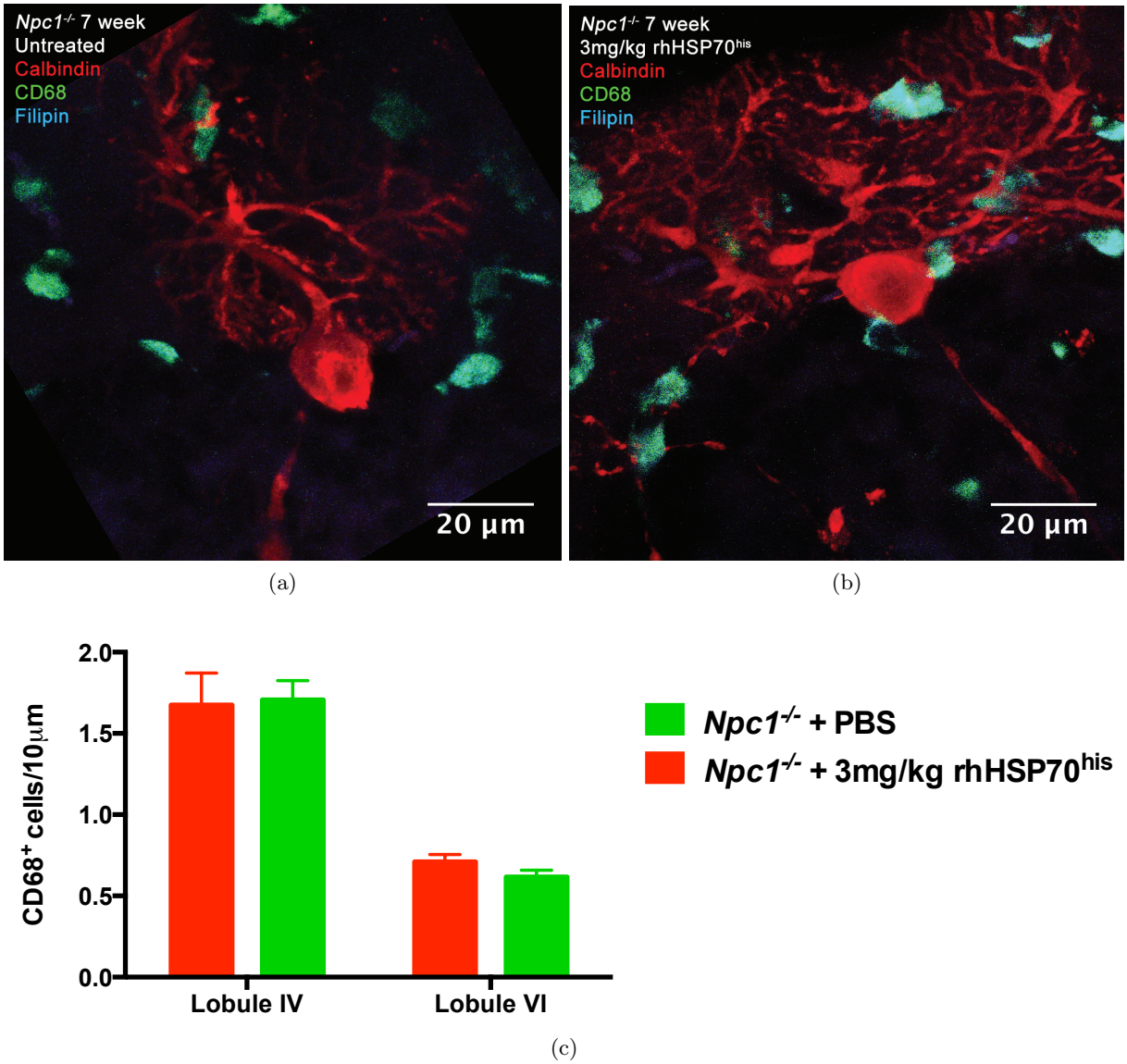
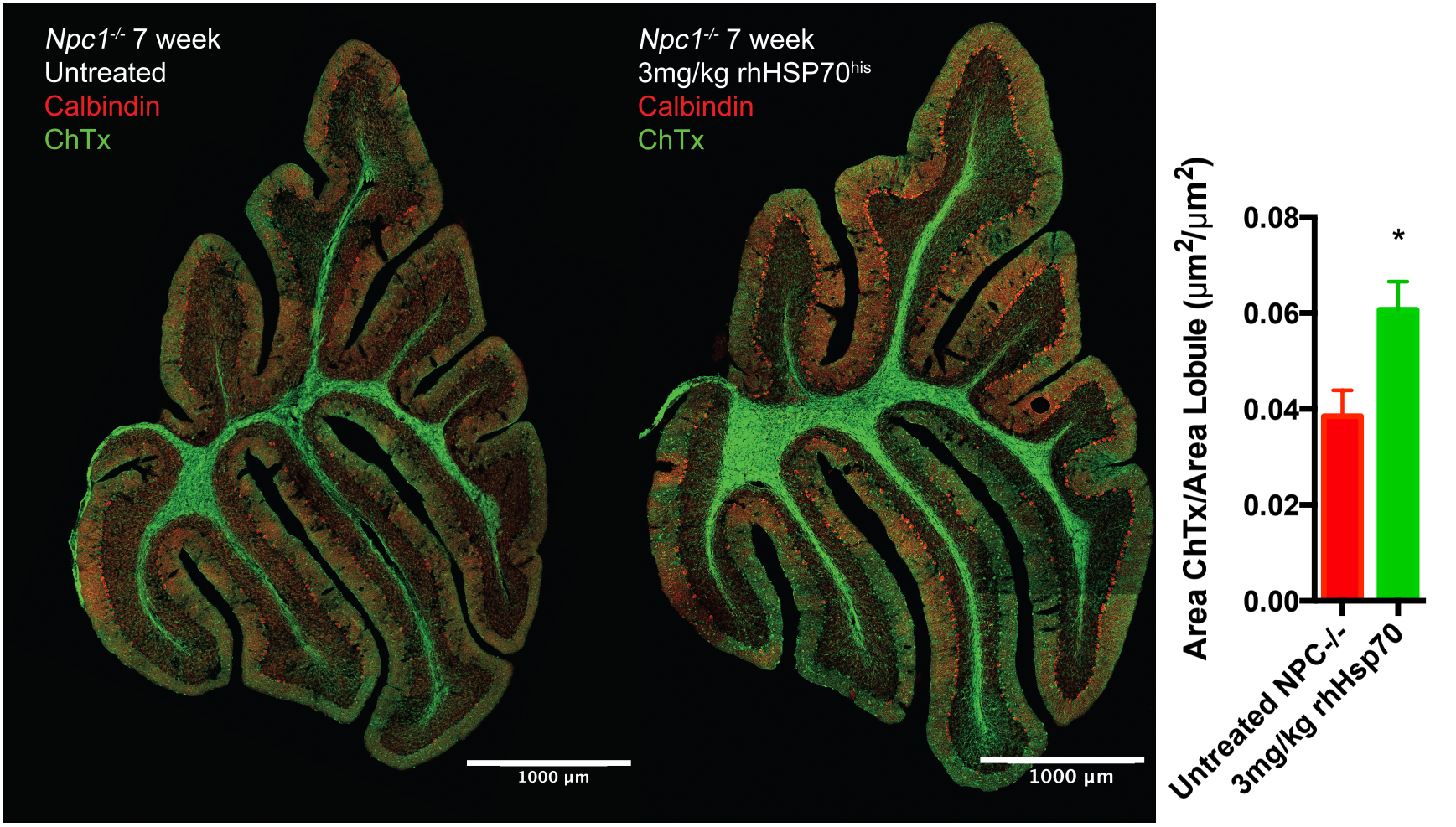
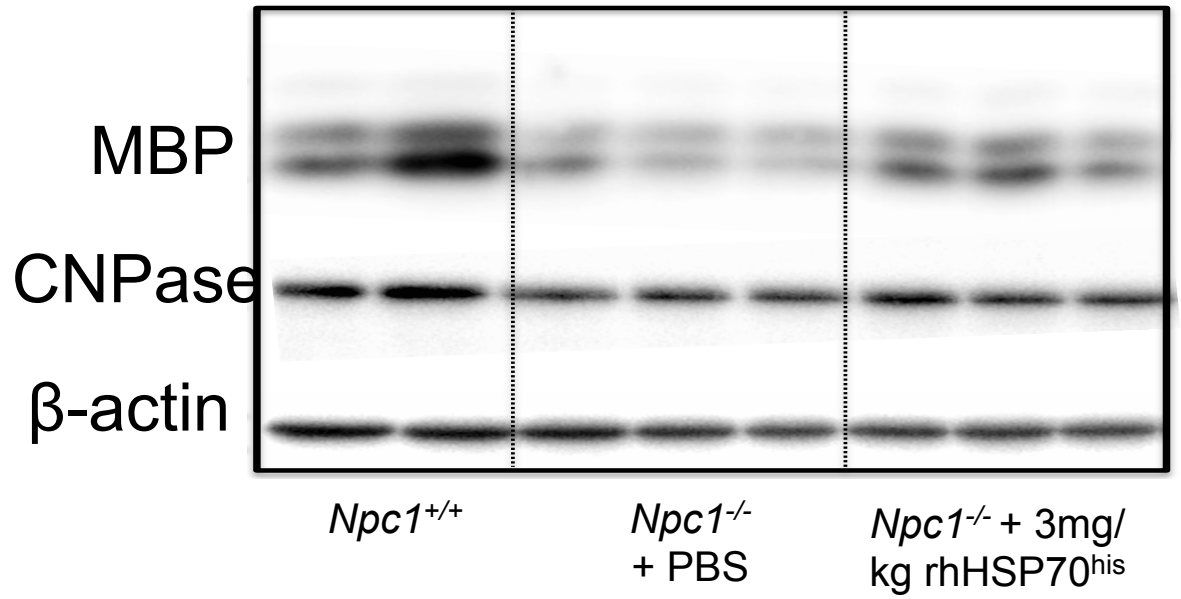


Figure 3.28: *Treatment of* Npc1$^{-/-}$ *mice with rhHSP70^{his} does affect neuroinflammation.* Representative images of microglia within lobule IV, stained with antibody against CD68 (green) and counterstained with filipin (blue) from a) untreated *Npc1$^{-/-}$* mice and b) 3mg/kg rhHSP70^{his} treated *Npc1$^{-/-}$* mice. Note that filipin colocalises with CD68^{+} cells. c) Comparisons of counts of CD68^{+} between untreated *Npc1$^{-/-}$* and *Npc1$^{-/-}$* mice treated with 3mg/kg rhHSP70^{his}. Treatment with 3mg/kg rhHSP70^{his} did not result in differences in infiltrating microglia when compared to untreated *Npc1$^{-/-}$* controls. *n*, untreated *Npc1$^{-/-}$* = 4, 3mg/kg rhHSP70^{his} treated *Npc1$^{-/-}$* = 4. 5 of each lobule from cerebellar midline sections were counted per animal. CD68^{+} cell numbers were normalised against lobule area. Data was analysed using multiple two-tailed students t-tests with Holm-Sidak corrections for multiple comparisons. Error bars are SEM.

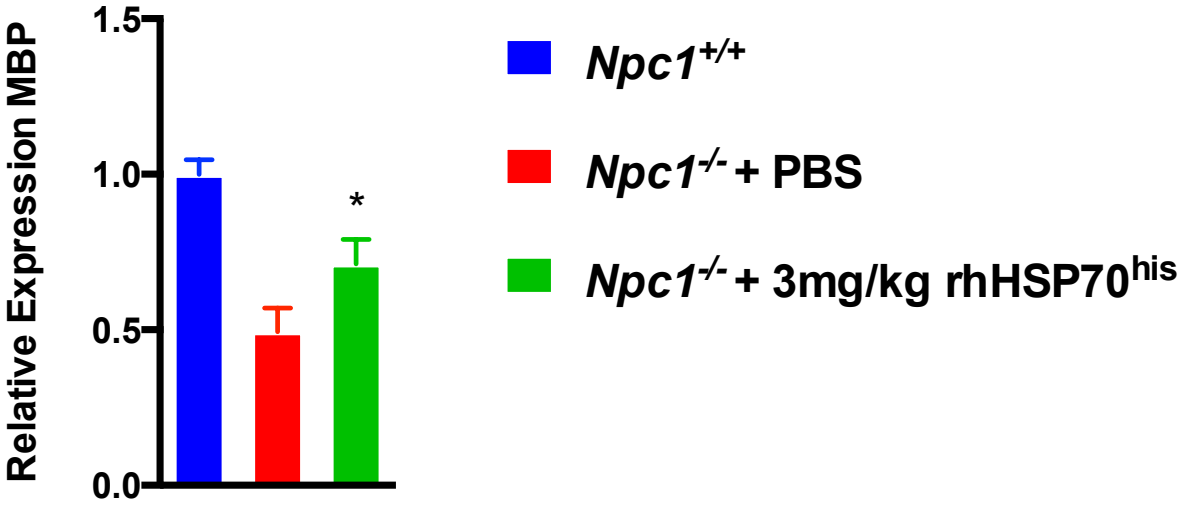


(a) (b)

Figure 3.29: *rhHSP70^{his} treatment shows increases in white matter area* Images showing a) Untreated and b) 3mg/kg rhHSP70^{his} treated *Npc1*$^{-/-}$ 7 week cerebellum stained with MBP (green) and calbindin (red). White matter area was determined by drawing around the white matter area (green) of the sections using ImageJ software. The area of the myelin was then normalised against the total lobular area. c) Treatment with rhHSP70^{his} showed a significant increase in the thinckness of the white matter. n= untreated, 3. 3mg/kg rhHSP70^{his} treated, 4. Significance was calculated using a two-tailed students t-test. *, $p<0.05$

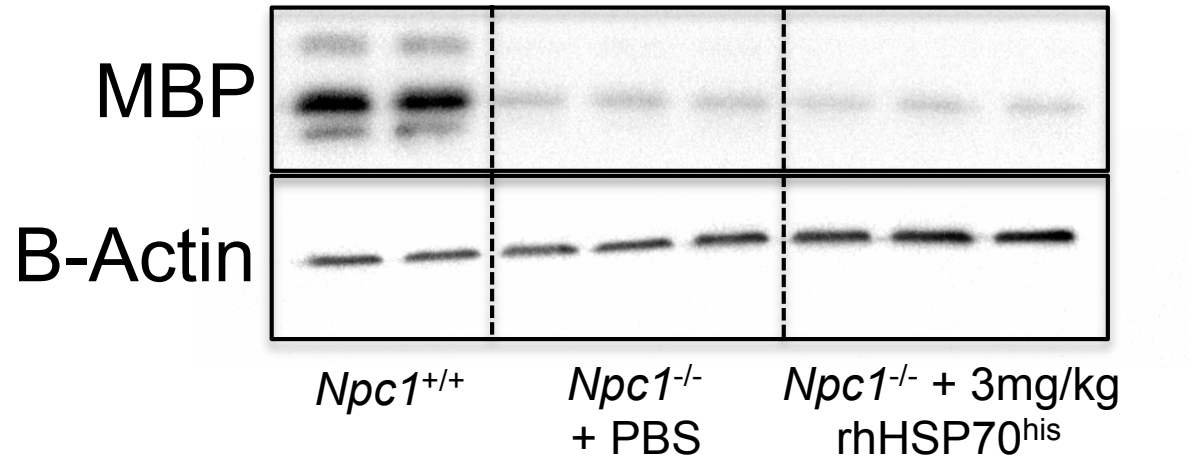


(a)

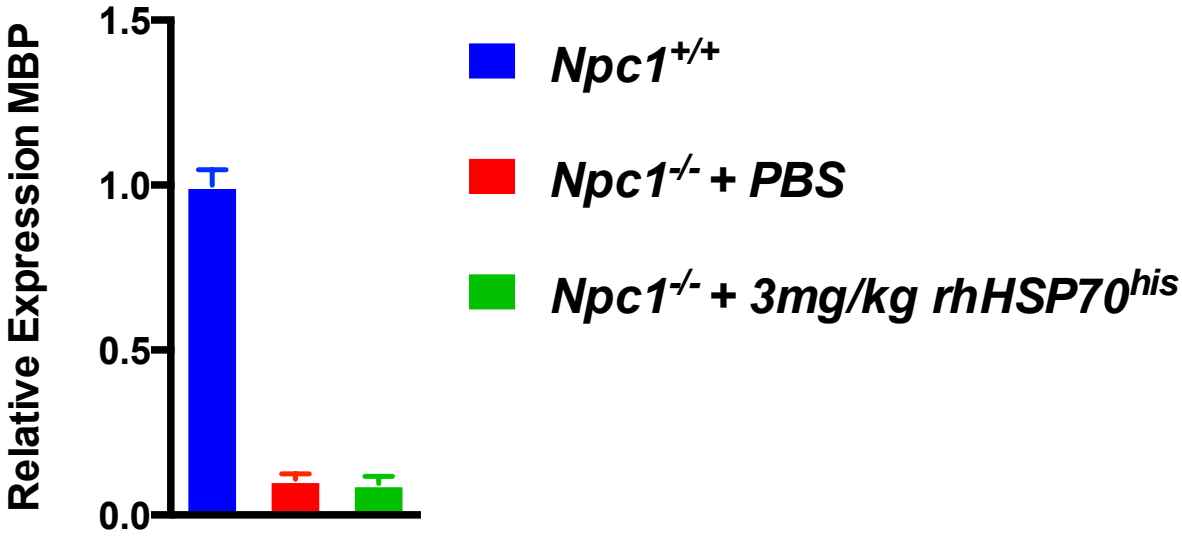


(b)

Figure 3.30: *rhHSP70^{his} treatment shows increases in cerebellar MBP, but not CNPase expression* a) Representative western blot of 7 week cerebellar homogenates from *Npc1*$^{+/+}$, untreated *Npc1*$^{-/-}$ and 3mg/kg rhHSP70^{his} treated *Npc1*$^{-/-}$ mice, probed with antibodies against MBP, CNPase and β-actin. b) Graph showing expression levels of MBP and CNPase, relative to *Npc1*$^{+/+}$ and normalised against β-actin expression. rhHSP70^{his} treated mice had significantly more cerebellar MBP expression than untreated controls. CNPase expression was unaffected. Data was the result of 3 seperate experiments.
n= *Npc1*$^{+/+}$, 4., untreated *Npc1*$^{-/-}$, 6., 3mg/kg rhHSP70^{his} treated *Npc1*$^{-/-}$, 6. Significance was calculated using a two-tailed students t-test. *, $p<0.05$



(a)



(b)

Figure 3.31: *rhHSP70^{his} treatment shows no increase in forebrain MBP expression.* a) Representative western blot of 7 week forebrain homogenates from wildtype, untreated *Npc1$^{-/-}$* and 3mg/kg rhHSP70^{his} treated *Npc1$^{-/-}$* mice, probed with antibodies against MBP and β-actin. b) Graph showing expression levels of MBP relative to wildtype and normalised against β-actin expression. rhHSP70^{his} treated mice showed no increase in global forebrain MBP expression compared to untreated controls. CNPase expression was unaffected. Data was the result of 2 seperate experiments.
n= *Npc1$^{+/+}$*, 4., untreated *Npc1$^{-/-}$*, 6., 3mg/kg rhHSP70^{his} treated *Npc1$^{-/-}$*, 6. Significance was calculated using a two-tailed students t-test.

3.4.11 Antibody Response

A pilot study previously performed had shown that both the behavioural and biochemical effects of rhHSP70^{his} were lost by 9 weeks of age. As such, we hypothesised that a neutralising antibody response against the protein may be causing diminishing effects over time. To assess whether treated animals mounted an antibody response, 3 week old *Npc1*$^{+/+}$ mice were treated with 0.3, 1 and 5mg/kg doses of rhHSP70^{his} i.p. **(Figure 3.32)**. Even at 1mg/kg, a significant response to the protein was detected within 1 week of treatment beginning and had reached a maximum by 2 weeks of treatment commencing. At the lower dose of 0.3mg/kg, a slower kinetic was observed, but had reached a maximum antibody response by 5 weeks of age.

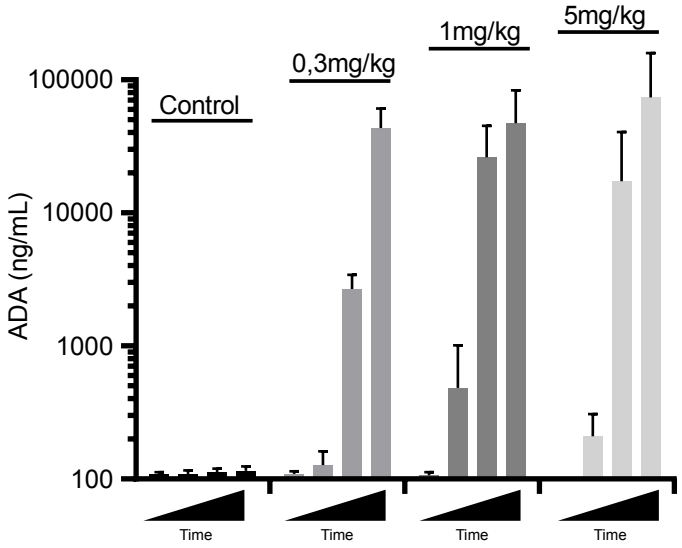


Figure 3.32: *rhHSP70^{his} invokes significant antibody response* 3 week old BALB/C mice given i.p. injections of rhHSP70^{his} show significant antibody response by 2 weeks following initial injection. Time points are as follows; t_1=pre-injection,t_2=1 week, t_3=2 weeks and t_4=5 weeks following first injection.n=x/group. *These experiments were carried out by A.Begley and are reproduced here with the permission of Orphazyme Aps.*

3.5 Discussion

NPC disease is a devastating neurological disorder for which there is only one therapy (miglustat) currently licensed for treatment within the EU. NPC is characterised by the accumulation and mislocalisation of intracellular lipids including GSLs, cholesterol, sphingosine, sphingomyelin

and BMP, within the LE/Ly system [148, 149, 151]. This is accompanied by symptoms of hepato-splenomegaly, and the progressive loss of neurological function and premature death [141]. Neurological pathology is typified by widespread neuroinflammation, axonal inclusions, hypomyelination and the progressive, patterned loss of cerebellar Purkinje cells [155, 156].

Miglustat, a GSL biosynthesis inhibitor, has shown efficacy in both pre-clinical trials on mice [159, 211] and cats [212], and in patients [212]. Miglustat reduces GSL accumulation within both the periphery and the CNS. In mice, miglustat treatment slows the degeneration of Purkinje cells along with the concurrent emergence of neuroinflammation and extends the lifespan of affected mice [211]. Whilst miglustat reduces GSL accumulation and Purkinje cell loss, it does not affect the accumulation of cholesterol [212, 211], which is also implicated in disease progression. Additionally, data (B. Boland, unpublished observation) from our laboratory shows that miglustat treatment does not improve the myelination status of *Npc1*$^{-/-}$ mice. As such, there is a need for therapies which address the other phenotypic aspects of NPC disease to provide better prognosis for sufferers of this disorder.

rhHSP70^{his} has previously shown the ability to correct both cholesterol and sphingomyelin storage in fibroblasts from sufferers of NPA [163], a lysosomal storage disorder caused by a deficiency in the activity of acid sphingomyelinase (ASM) [161]. rhHSP70^{his} was shown to facilitate the binding of mutated ASM to BMP, an anionic phospholipid located within the lysosomal luminal membrane. Improvement of this binding restored the activity of ASM, reducing sphingomyelin and cholesterol accumulation, and improved lysosomal stability [163].

As the main pathological burden in NPC disease is neurological, it is important that any treatment is able to cross the blood-brain barrier. Assessment of the bioavailability of rhHSP70^{his} showed that the protein efficiently crossed the blood-brain barrier **(Figure 3.1)**. Studies of the kinetics of rhHSP70^{his} suggested that the CNS uptake was probably receptor mediated, which is in keeping with the proposed function of LRP1 as a transcytotic receptor for HSP70 [316, 328]. HSP70 has been shown to be a target for endocytosis by the membrane protein LRP1 [316], which has been shown to be highly expressed in both hepatocytes and neurons, but is also expressed in some levels on most cell types, including on capillary epithelial cells, glia, oligodendrocytes and astrocytes of the CNS [317], where it has been proposed to play a role in the uptake of CNS

cholesterol through the uptake of ApoE [318].

Immunofluorescent labelling of rhHSP70^{his} with an anti-His tag antibody, showed widespread distribution of rhHSP70^{his} in the CNS 3.2). Three days following a single injection, the distribution was mainly nuclear, with some cytoplasmic distribution. However, the protein did not localise with all nuclei, and some regions showed very little localisation of the protein, such as the striatum, and cortex regions **(Figure 3.7)**. It is unclear whether this localisation pattern is due to different uptake of the protein due to differential LRP1 expression in the CNS, or whether certain cell types were degrading the protein more rapidly than others. Importantly, the protein seemed to be localised to the Purkinje cells of the cerebellum **(Figure 3.4)**, although further experiments need to be carried out to confirm it's differential uptake pattern. Also, further experiments to confirm colocalisation with an anti-HSP70 antibody will be needed to certify that this is true HSP70 staining.

Treatment of *Npc1*$^{-/-}$ mice with 3mg/kg rhHSP70^{his} resulted in significant improvements in rearing behaviour **(Figures 3.9–3.13)**, and improvements in the abnormal gait associated with NPC disease. These data are supported by observations of improved appearance of the mice, especially in the condition of the coats and the normal appearance of the eyes **(Figure 3.18)**. Although we also have data to suggest that rhHSP70^{his} treatment did not improve the development of tremor associated with disease progression, this data is difficult to interpret, as the tremor monitor was unable to detect a significant increase in tremor of untreated *Npc1*$^{-/-}$ mice **(Figure 3.14)**.

We observed several biochemical changes in mice treated with rhHSP70^{his}. In the periphery, reduced accumulation of GSLs in both the liver and kidney were observed **(Figure 3.19)**. The greatest reductions observed were in the abnormally accumulating GSLs, GM2-Gc and Gb3 respectively. GSL levels were also significantly reduced in the forebrains of treated mice, with largest reductions being observed in the major accumulating GSL species; GD1a, GM1a, GM1a-gc and GM1b **(Figure 3.4.8)**. A similar pattern was observed in the cerebellum, although these did not reach significance **(Figure 3.4.8)**. It is interesting to note that these species are the more complex of the gangliosides accumulating, and degradation of these species would yield less complex species downstream, which would need to be further degraded themselves. Our data

could indicate that either degradation of these lipids is preferentially increased following treatment, or that as the more complex lipids yield less complex species upon degradation, increased degradation of all species could result in a similar pattern. In accordance with this, lysosomal hydrolase binding data showed that HSP70 increased the binding capacity of several hydrolases to BMP, and this was attenuated (in three hydrolases tested) by the HSP70^{W90F} mutant **(Figure 3.24)**. This improved association with BMP could theoretically improve their activities *in vivo*, and it is likely this is a broad effect for multiple hydrolases, although significantly the β subunit of β-hexosaminidase did not display the same level of binding as the other hydrolases tested.

The precise reason why rhHSP70^{his} should have differing effects on GSLs in the forebrain and cerebellum is unclear. However, previous unpublished data from our laboratory shows that GSL levels in the cerebellum begin to decline as Purkinje cell death accelerates, suggesting that some of the accumulating lipids stored within dying cells are degraded. Whether this could be mediated through phagocytosis, or through apoptotic mechanisms is unclear. It may also be the case that the most altered GSLs species in the cerebellum contribute less to the overall GSL burden, than the same species in the forebrain.

Mice treated for 4 weeks with rhHSP70^{his} showed somewhat increased levels of sphingosine when compared to both untreated *Npc1*$^{-/-}$ and *Npc1*$^{+/+}$ controls **(Figure 3.23)**. This accumulation could be caused by several factors; firstly, an increased degradation of sphingolipids, through the improved activity of acid sphingomyelinase and/or other lysosomal hydrolases *without* improved lysosomal fusion events and clearance of stored contents could result in an increase of sphingosine within the lysosomal compartment. Secondly, if cell survival is improved, a clearance of stored lipids which may otherwise be degraded by cellular death mechanisms may not occur, although this does not appear to be the case, at least in the cerebellum.

Measurement of the lysosomal compartment volume using LysoTracker staining of circulating and splenic B cells has been shown to be a potential tool for the monitoring of NPC disease progression. Increased LysoTracker staining correlated with disease progression, and with the accumulation of oxysterols which have also shown potential as a biomarker [225]. Lysosomal volume in patients treated with miglustat is reduced [225]. As rhHSP70^{his} treatment also decreased

GSLs, we expected to find a corresponding reduction in lysosomal volume. Perhaps surprisingly, there was a slight increase in the compartment volume, although not signifcant. This is also in contrast to the effects on lysosomal volume following treatment with β-cyclodextrin, whereby patients showed approximately 2 fold increases in MEFL values following treatment, and a much increased GSL burden in isolated circulating B cells [225]. As sphingosine has been shown to inhibit lysosomal calcium store filling, which is sufficient to inhibit lysosomal fusion events [7], an accumulation of sphingosine would be expected to increase the lysosomal compartment volume. We observed modest increases in lysosomal compartment volume which did correspond to the increases in sphingosine, although these effects were not significant **(Figure 3.26)**.

Whilst CNS cholesterol does not increase in NPC disease until late into disease progression, peripheral storage of unesterified cholesterol increases throughout the life of the mouse [149]. Following treatment with 3mg/kg rhHSP70^{his}, we found significantly reduced levels of unesterified cholesterol in both the liver and kidney **(Figure 3.25)**.

The appearance and proliferation of activated microglial cells, and of GFAP^{+} astrocytes occurs as early as 2 weeks of age in the *Npc1*$^{-/-}$ mouse [155, 156]. Neuroinflammation has previously been implicated in exacerbating the course of NPC disease [159], although it is not responsible for loss of Purkinje cells[158], which has been shown to be a cell autonomous process [171]. It is probable that the early and widespread inflammation observed in the CNS of *Npc1*$^{-/-}$ mice is in response to the process of degeneration, and is not responsible for the neuronal loss. However, it appears that inflammation does contribute somewhat to the aggressive course of the disease, and alleviation of this phenotype could provide some therapeutic benefits[158, 159]. However, treatment with rhHSP70^{his} did not affect the numbers of CD68^{+} activated microglia in the cerebellum of treated mice **(Figure 3.28)**.

Surprisingly, given the improved behavioural data, and reductions in GSLs in the treated mice, we also observed reductions of Purkinje cell numbers within the cerebellum. Although this did not reach signifance for any lobule, it was a trend which affected every lobule **(Figure 3.27)**. This is unusual, given that no Purkinje cells are lost from lobule IX and X until very late in the disease course, and even then, the numbers are small. Given that the total number of Purkinje cells/unit length is decreased, it may arise as a consequence of increased brain area, although

no measurements were taken to support this. Conversely, the advancement of Purkinje cell loss could be a consequence of the accumulation of sphingosine, although this was not significant. However, this will need further work to exclude this as a possible side effect.

Optimised voxel-based morphometry data from NPC patients shows decreases in white matter thickness and quality [169], and post-mortem tissue from confirmed NPC cases shows decreased levels of galactosyl ceramide (GalCer), sulfatide and cholesterol, which are by far the most abundant lipids within myelin, accounting for 70% [333, 334] of total dry weight of myelin. *Npc1*$^{-/-}$ mice display a profound block in the development of myelin, particularly in the forebrain, but also in the cerebellum [170] and also display a reduced phosphorylation of Fyn kinase [172]. Fyn is a member of the src kinase family, and plays an important role in mediating the signalling of integrin and contactin between axons and developing myelin [335]. An important ligand of CNS integrin is laminin-2 expressed on developing axons, and integrin signalling through laminin-2 has been shown to be necessary for myelination of axons *in vitro* [336]. Laminin-2 deficient mice display a remarkably similar hypomyelination deficiency to *Npc1*$^{-/-}$ mice, a mechansim which is dependant on Fyn activation [337]. Whilst glial specific *Npc1* knockout mice did display delayed myelination, myelin largely recovered by P54 [172]. However, these mice did eventually exhibit tremor phenotype and significant Purkinje cell loss by 23 weeks of age, suggesting that whilst NPC1 function in oligodendrocytes is not essential for myelin formation, loss of oligodendrocyte NPC1 function is sufficient to exacerbate NPC disease course. Myelin basic protein (MBP) and proteolipid protein (PLP) account for 80% of myelin protein, and are abundantly expressed in the CNS [338]. PLP is synthesised in the ER and trafficked through the Golgi apparatus before being stored in LE/Ly of premyelinating oligodendrocytes. Upon the initiation of myelination, PLP is trafficked to the plasma membrane, following axonal signalling [338]. MBP was one of the earliest examples of localised translation of mRNA [339] by microtubule associated ribosomes [340, 341].

In mice treated with rhHSP70^{his}, we observed increases in both the white matter area, as measured by immunofluorescence **(Figure 3.29)**, and in the expression levels of MBP in the cerebellum **(Figure 3.30)**, though this benefit did not extend to the forebrain **(Figure 3.31)**. There exist several potential mechanisms by which rhHSP70^{his} may be affecting the myelina-

tion staus of the *Npc1*$^{-/-}$ mice. Improvements in the trafficking of lipids, such as GT1b and GD1a which are involved in myelin regulation [342] may allow the development of more stable myelin sheaths. Similarly, decreases in toxic metabolites such as GM1 by treatment may also improve the survival and competency of oligodendrocytes [343]. Another possibility is that signalling from axon to oligodendrocyte is improved following treatment, allowing increased pro-differentiation and survival signalling through Fyn kinase. Alternatively, the endocytosis of rhHSP70$^{\text{his}}$ by LRP1, and subsequent signalling of LRP1 may by-pass a deficient axon-oligodendrocyte signalling pathway. LRP1 has been implicated in several intracellular signalling events within neurons, having over 100 intracellular interacting proteins. Synthetic agonists of the LRP1 receptor have been shown to activate TrkA in a Src family kinase dependant manner [320], stimulating axonal growth *in vitro* and following CNS injury *in vivo* [321]. The cytoplasmic tail of LRP1 has a pair of NPXY microdomain motifs which have been shown to be phosphorylated upon binding of extracellular ligands. When prepared synthetically, and used to probe brain lysates, the distal NPXY^{4507} motif has been shown to have several binding partners including Fyn [322]. As oligodendrocytes also express LRP1, it may be a case that the effects of rhHSP70$^{\text{his}}$ on myelination may be independant of its effects on lysosomal catabolism.

Npc1$^{-/-}$ mice displayed an aggravated antibody response against the injected protein, which may be responsible for the loss of efficacy at later stages of disease progression **(Figure 3.32)**. The cause of the antibody response is unclear, however, LRP1 has been shown to be involved in the activation of CD4^{+} memory T-cells [344], which may also contribute to the enhanced antibody response seen following treatment of *Npc1*$^{-/-}$ mice with rhHSP70$^{\text{his}}$. It may also be a case that the antibody response is due to the use of a recombinant human protein, rather than the mouse protein. As such, the rhHSP70 protein may prove more efficacious in humans patients than it is in the *Npc1*$^{-/-}$ mouse, although antibody production against the protein would need to be closely monitored.

It is interesting to note that the majority of myelination of the CNS begins at P6 and is effectively finished in *Npc1*$^{+/+}$ mice by P54, with the earliest events on myelination observed in the brainstem and cerebellum, and optic nerve and olfactory tracts [345]. Given that myelin extension (excluding myelination of the optic nerve, and olfactory bulb) starts caudally, in the

brainstem and cerebellum, and extends towards the forebrain, the early 'window' (P21-P28) of optimum protein delivery may very well overlap with the natural timepoint for cerebellar myelination. The fact that effects on forebrain myelination were not observed could be due to the effects of high antibody titre during the later occuring forebrain myelination. Additionally, as Purkinje cell degeneration begins at 6 weeks of age, a neutralising antibody response to the protein makes it very difficult to draw solid conclusions regarding the effects on purkinje cell survival.

The evidence presented in this chapter indicates that rhHSP70^{his} offers a novel treatment for NPC disease, with effects both on the lysosomal storage burden of GSLs and the hypomyelination phenotype associated with this disease. However, the development of an antibody response against the protein, as well as a possible side effect of increased sphingosine accumulation suggest that this approach may be unsuitable as a long-term therapy for NPC disease.

4 In Vivo Use of Non-His Tagged rhHSP70

4.1 Introduction

Studies of His-tagged protein immunogenicity, have revealed mixed results, with several studies finding that His-tagged proteins increased the amplitude of antibody response to foreign protein[346, 347]. Other studies have suggested that His-tags can reduce immunogenicity to foreign proteins[348], possibly by limitiing access to the reactive epitope(s). To study this we used purified recombinant human HSP70 where the his-tag had been removed, to see if this improved the efficacy of the protein.

4.2 Hypothesis

Removal of the His-tag from rhHSP70 will reduce the antibody response against the protein and improve efficacy.

4.3 Materials & Methods

4.3.1 rhHSP70$^{\text{non-his}}$

Recombinant human HSP70 with the His-tag removed (rhHSP70$^{\text{non-his}}$) was a gift from Orphazyme ApS.

4.3.2 Treatment

3 week old *Npc1*$^{-/-}$ mice were treated with 3mg/kg rhHSP70$^{\text{non-his}}$ (n=6) of body weight or with PBS alone (n=6). Mice were injected 3 times per week i.p..Wildtype BALB/c mice (*Npc1*$^{+/+}$)

were used as baseline controls (n=6). Mice were killed at 54 days of age (7 week).

4.3.3 Anti-Drug Antibody Comparison

Npc1$^{-/-}$ mice (2 males, 3 females per group) were treated with 3mg/kg rhHSP70$^{\text{his}}$ or rhHSP70$^{\text{non-his}}$, or with PBS alone, as indicated 3x per week, i.p. for 4 weeks. Mice were termianlly anaesthetised with 600mg/kg bodyweight sodium pentobarbital. Blood was obtained by cardiac puncture, and collected in uncoated vials, incubated at RT for 2 hours and centrifuged (1000g, 10 min at RT) to obtain serum. The serum was frozen in three aliquots on dry ice and stored at -80°C until analysis.

All other methods were performed as described in **Chapter 2**.

4.4 Results

4.4.1 Growth Curves

Untreated *Npc1*$^{-/-}$ mice show a characteristically stunted growth curve compared to *Npc1*$^{+/+}$ control, whereby they gain weight more slowly than *Npc1*$^{+/+}$ mice and then begin to lose weight at around 7 weeks of age, culminating in their death around 10 weeks of age. Mice treated with 3mg/kg rhHSP70$^{\text{non-his}}$ showed no change in bodyweight kinetics compared to untreated *Npc1*$^{-/-}$ mice **(Figure 4.1)**.

4.4.2 Manual Rearing

In marked contrast to the improvements seen with the his-tagged protein **(Figure ??)**, treatment with 3mg/kg rhHSP70$^{\text{non-his}}$ showed no significant improvements in side rearing or centre rearing compared to untreated *Npc1*$^{-/-}$, when analysed either as 4 - 7 week averages **(Figure 4.2a & c)** or as weekly scores **(Figure 4.2b & d)** respectively.

4.4.3 SHIRPA Testing

As treatment with 3mg/kg rhHSP70$^{\text{his}}$ showed consistent improvements in several parameters assessed **(Figure 3.18)**, we assessed the same parameters following treatment with 3mg/kg

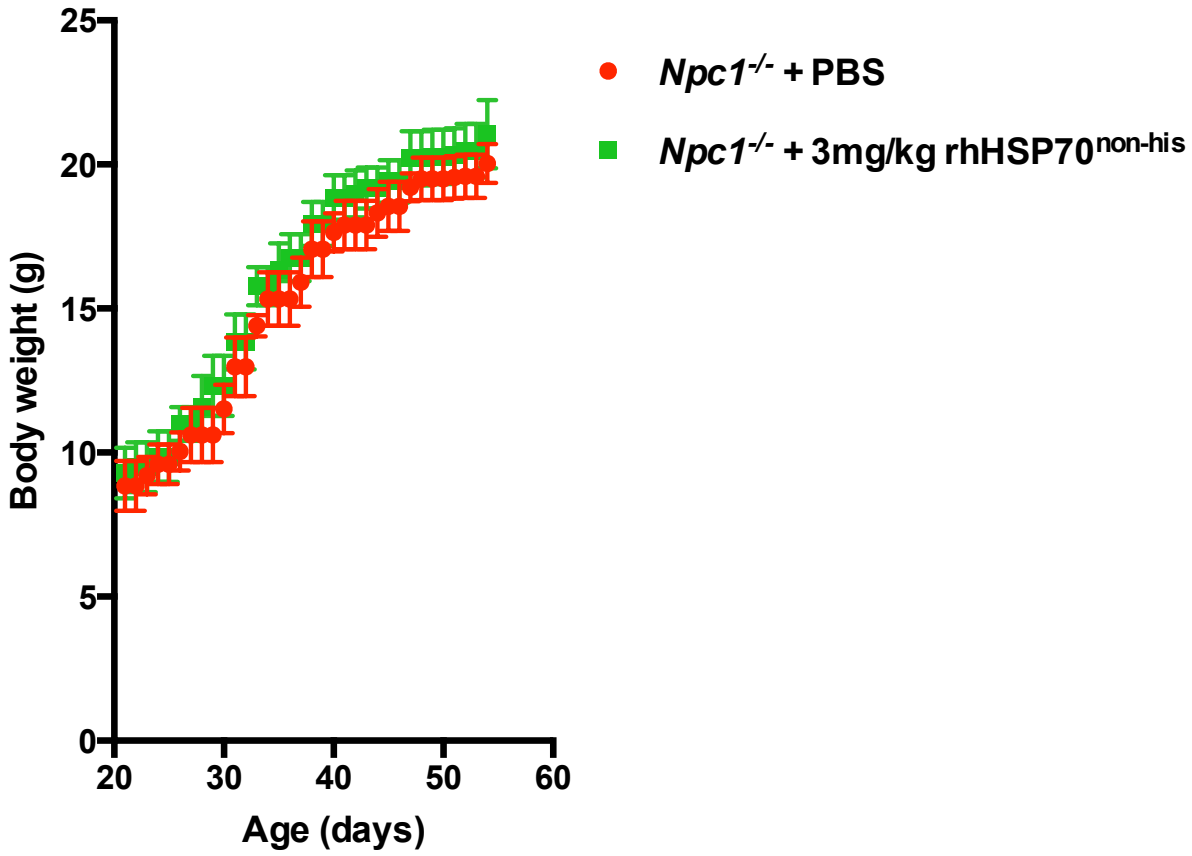


Figure 4.1: Growth curves showing absolute body weights. n= *Npc1*$^{-/-}$ + PBS, 6. *Npc1*$^{-/-}$ + 3mg/kg rhHSP70$^{\text{non-his}}$, 6. Mice were weighed 3x per week. Error bars show SEM.

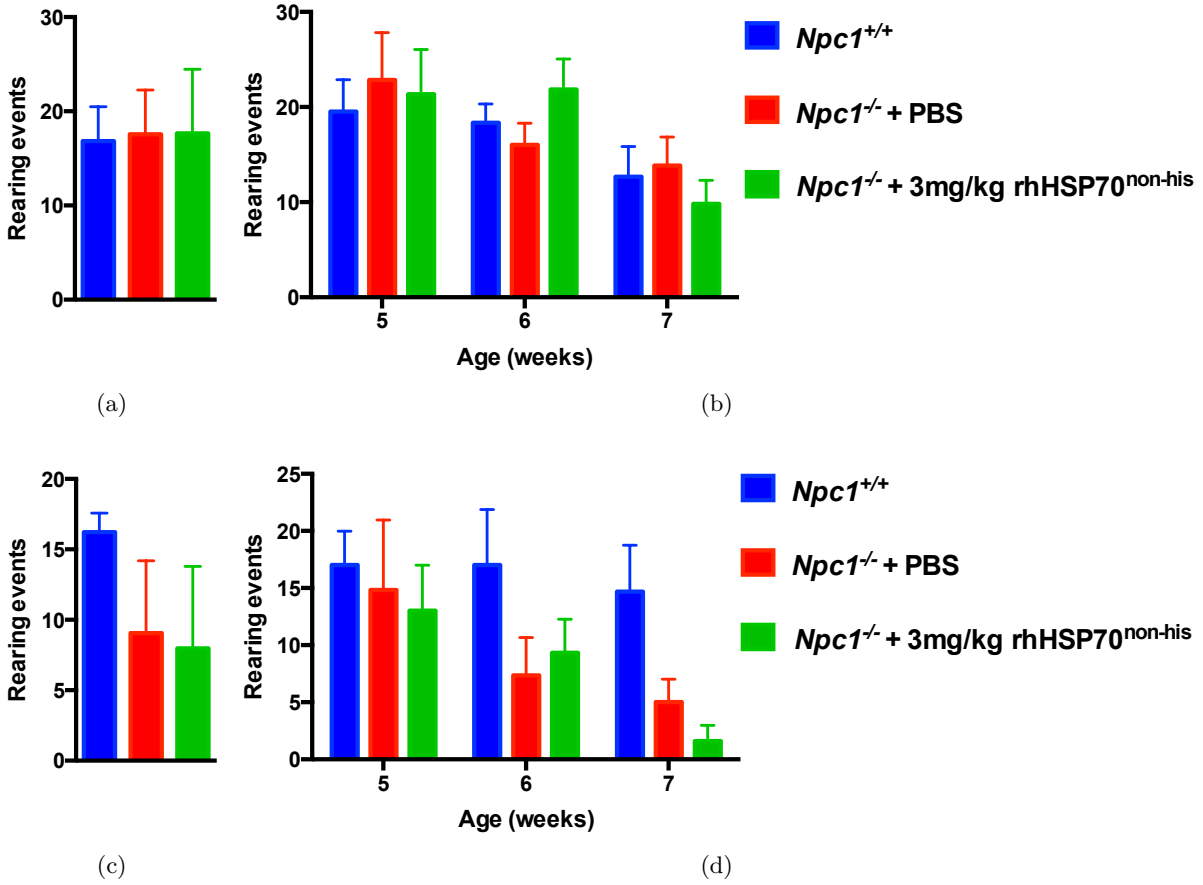


Figure 4.2: *Treatment with rhHSP70$^{non\text{-}his}$ shows no improvement in manual scores of side rearing and centre rearing.* a) Side rearing averages of 4-7 week rearing scores. b) weekly scores in side rearing. c) Centre rearing averages of weeks 4 - 7. d) weekly centre rearing scores.
Npc1$^{+/+}$, n= 6, 6, 6 *Npc1*$^{-/-}$ +PBS, n=6, 6, 6., 3mg/kg rhHSP70$^{non\text{-}his}$ treated *Npc1*$^{-/-}$ n= 6, 6, 6., for weeks 5, 6, and 7 respectively. Data was analysed using students two-tailed t-test (graphs a & c), and a two-way ANOVA with Dunnetts multiple comparison test (graphs b & d). Error bars are SEM.

rhHSP70$^{\text{non-his}}$. Whilst palpebral (eyelid) closure was improved following treatment, with all but one treated mice at 7 weeks showing no obvious eyelid phenotype, no change was observed in the other parameters **(Figure 4.3)**.

4.4.4 Glycosphingolipid Quantification

Glycosphingolipid accumulation was evaluated in forebrain following treatment with rhHSP70$^{\text{non-his}}$. In contrast to the changes seen following 3mg/kg rhHSP70$^{\text{his}}$ treatment, mice treated with 3mg/kg rhHSP70$^{\text{non-his}}$ showed no significant decrease in individual GSL species accumulation following treatment. Differences in GA2 (11%, p=0.965), GM3 (19%, p=0.726), GM2 (19%, p=0.690), GA1 (11% p=0.979), GM1b (30% p=0.631), GD1a (39% p=0.381) ,GD1b (37% p=0.800) GT1b (45% p=0.735) were detected, lower than seen with rhHSP70$^{\text{his}}$ treatment. The only species that showed a significant difference was Lac which showed an increase of 464% (p<0.0001) compared to untreated *Npc1*$^{-/-}$ controls **(Figure 4.4 a)**. Total GSL levels were also unchanged between untreated *Npc1*$^{-/-}$ and 3mg/kg rhHSP70$^{\text{non-his}}$ treated *Npc1*$^{-/-}$ mice **(Figure 4.4 b)**.

4.4.5 Sphingosine Quantification

To assess whether rhHSP70$^{\text{non-his}}$ was affecting the accumulation of sphingosine, we extracted sphingosine from forebrain homogenates using a method previously described [3], and modified as described in **section 2.8**. Sphingosine accumulation in both untreated *Npc1*$^{-/-}$ and 3mg/kg rhHSP70$^{\text{non-his}}$ treated *Npc1*$^{-/-}$ forebrains were raised when compared to *Npc1*$^{+/+}$ mice. Whilst rhHSP70$^{\text{non-his}}$ treated mice showed a greater accumulation when compared to untreated controls (20%, p=0.5625), this did not reach significance **(Figure 4.5)**.

4.4.6 Lysosomal Volume

Due to the profound endocytic block in NPC, patients and the *Npc1*$^{-/-}$ mouse model exhibit increased volume of the acidic compartment. To assess whether treatment of *Npc1*$^{-/-}$ with 3mg/kg rhHSP70$^{\text{non-his}}$ affected LysoTracker staining, we assessed acidic compartment volume of CD19^{+} splenic B-cells from 7 week old treated and untreated *Npc1*$^{-/-}$ mice, alongside *Npc1*$^{+/+}$ compara-

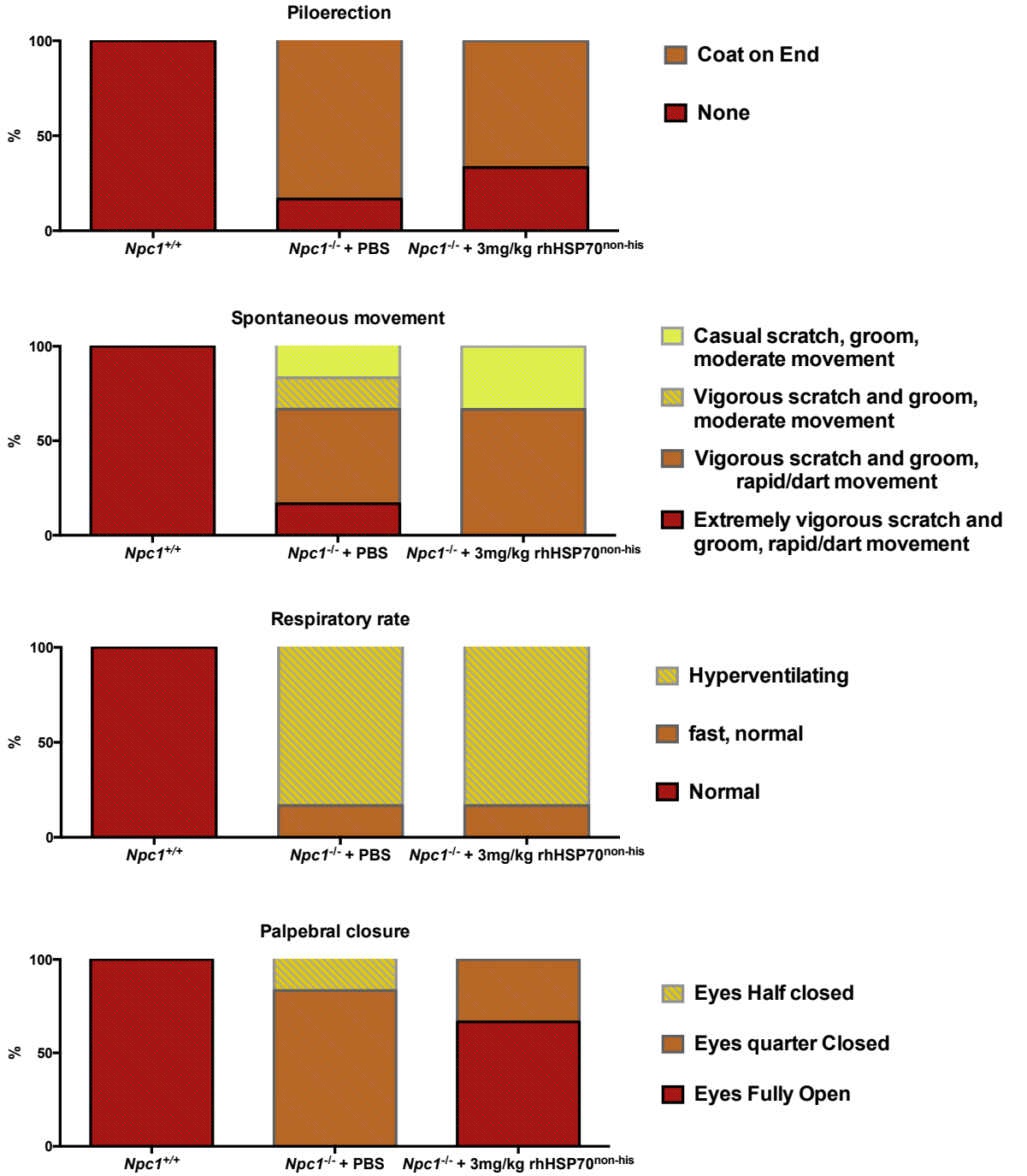
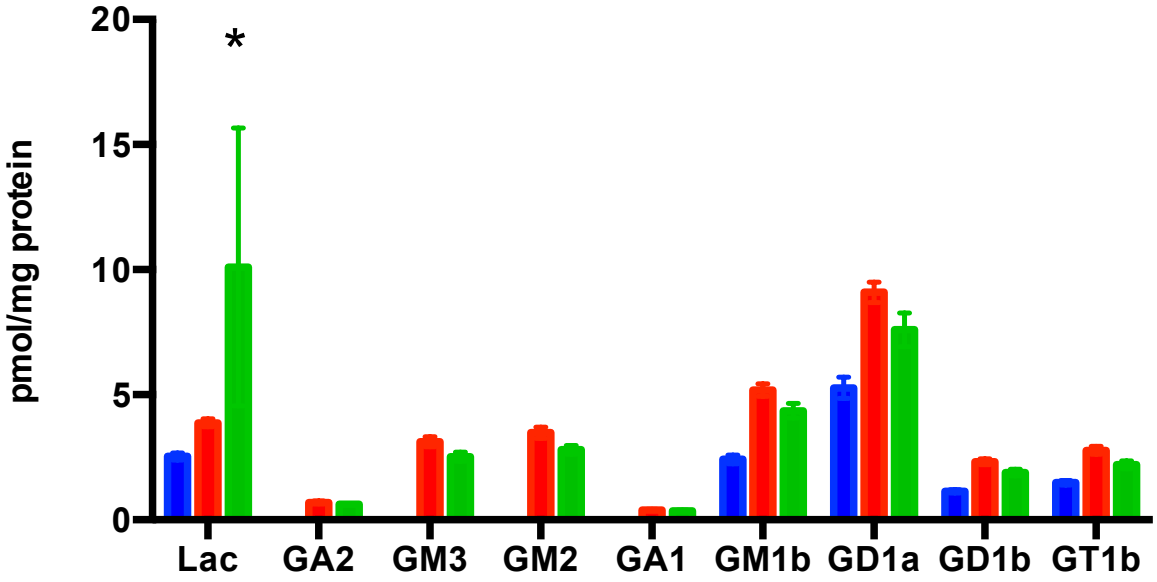
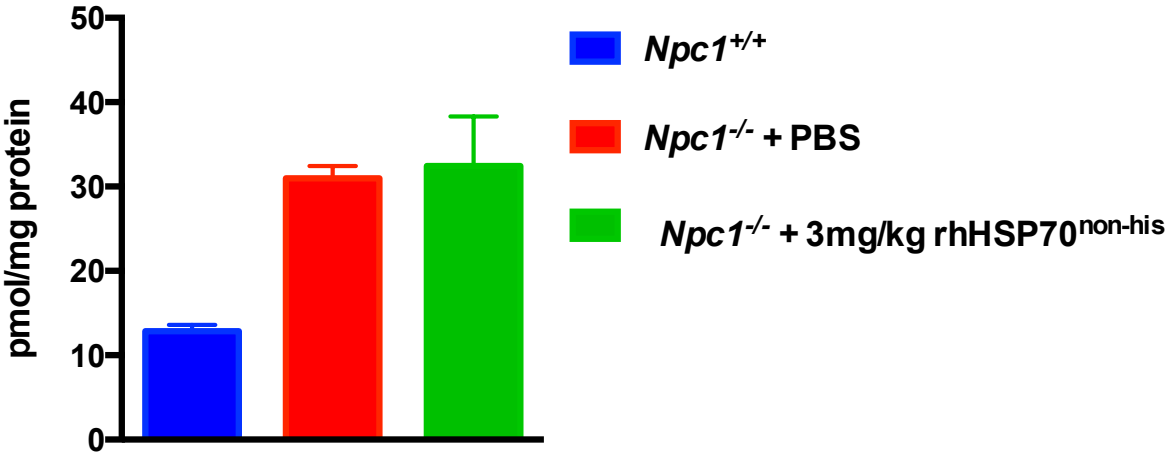


Figure 4.3: *rhHSP70$^{non\text{-}his}$ treatment did not improve disease phenotype when assessed by SHIRPA testing* SHIRPA testing was performed on 7 week old *Npc1*$^{+/+}$, untreated *Npc1*$^{-/-}$, and 3mg/kg rhHSP70$^{non\text{-}his}$ treated mice. Treated mice showed improvement in palpebral (eyelid) closure, but not in other phenotypic presentations. n=6/group

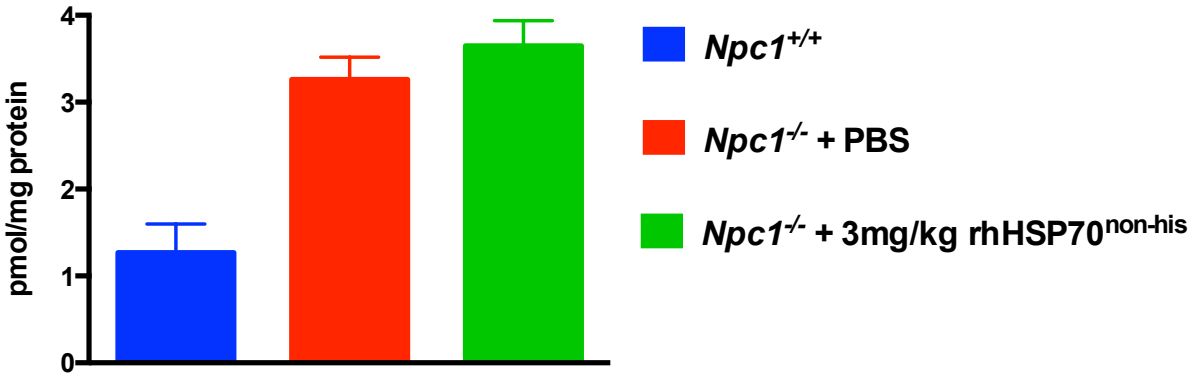


(a)



(b)

Figure 4.4: *Treatment of* Npc1$^{-/-}$ *mice with rhHSP70*$^{non\text{-}his}$ *shows no improvement in forebrain GSL accumulation.* a) Lac shows significant increase following treatment with rhHSP70$^{non\text{-}his}$, whilst other GSLs show small but non-significant changes. b) Total forebrain GSLs show no change following treatment with rhHSP70$^{non\text{-}his}$. *Npc1*$^{+/+}$, n= 6., *Npc1*$^{-/-}$ +PBS, n=6., 3mg/kg rhHSP70$^{non\text{-}his}$ treated *Npc1*$^{-/-}$ n= 5. Data was analysed using multiple t-tests with Holm-Sidak corrections for multiple comparisons, graph a), and individual two-tailed students t-tests, graph b).



(a)

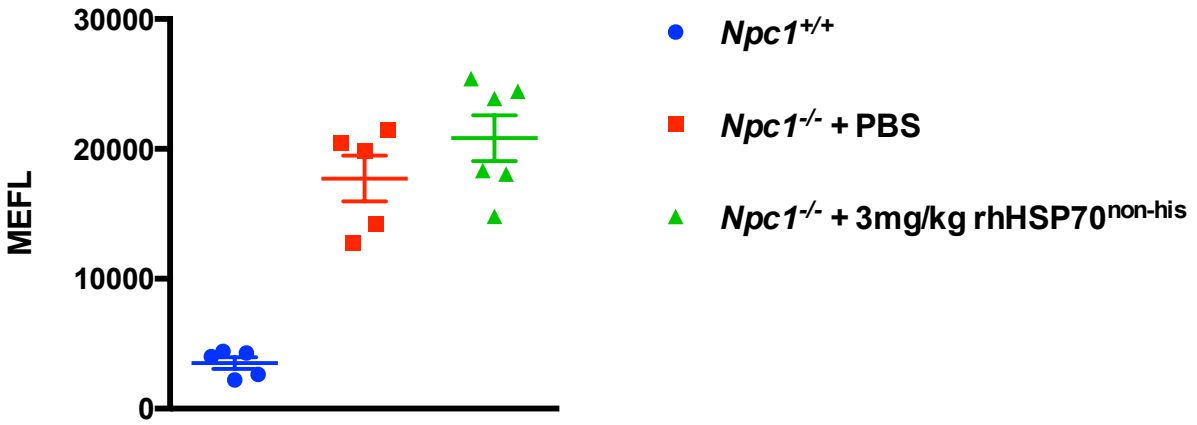
Figure 4.5: *Sphingosine accumulation dos not change following treatment with rhHSP70$^{non\text{-}his}$.* Treatment with rhHSP70$^{non\text{-}his}$ did not change the levels of sphingosine present in the forebrains of treated *Npc1*$^{-/-}$ mice when compared to untreated *Npc1*$^{-/-}$ controls. Both were significantly increased when compared to *Npc1*$^{+/+}$ mice.
n= *Npc1*$^{+/+}$ 4, untreated *Npc1*$^{-/-}$ 6, 3mg/kg rhHSP70$^{non\text{-}his}$ treated *Npc1*$^{-/-}$, 5. Error bars show SEM. Data was analysed using a two-tailed students t-test.

tors. Both were significantly raised when compared to *Npc1*$^{+/+}$ volumes, and a 20% increase in LysoTracker staining was observed between untreated *Npc1*$^{-/-}$ and 3mg/kg rhHSP70$^{non\text{-}his}$ treated mice although this was not significant (p=0.249) **(Figure 4.6)**.

4.4.7 Antibody response following rhHSP70$^{non\text{-}his}$ administration

We performed ELISA assays for anti-HSP70 antibodies, to assess whether the differences observed in behaviour and lipid accumulation between the his-tagged protein, and the non-his tagged protein, were due to a stronger antibody response. Similarly to the previous experiment, *Npc1*$^{-/-}$ mice treated with 3mg/kg rhHSP70^{his} developed a significant number of antibodies after 4 weeks treatment. Surprisingly, this was almost 10-fold higher than *Npc1*$^{+/+}$ mice treated with 3mg/kg rhHSP70^{his} protein (p=0.329) **(Figure 4.7)**.

Administration of rhHSP70$^{non\text{-}his}$ provoked a 6-fold stronger response than the rhHSP70^{his} protein in the *Npc1*$^{-/-}$ mice (p=0.0019), and in the *Npc1*$^{+/+}$ mice a15-fold greater response was observed between the two proteins (p=0.2928) **(Figure 4.7)**. If our hypothesis that antibodies against the protein are attenuating the effect is correct, this could account for the much reduced benefits of rhHSP70$^{non\text{-}his}$ compared to rhHSP70^{his} seen in *Npc1*$^{-/-}$ mice.



(a)

Figure 4.6: *Treatment with rhHSP70$^{non\text{-}his}$ does not significantly increase lysosomal compartment volume.* Gating strategy for measuring LysoTracker MEFL values of CD19+ cells. a) Panel showing representative gating of singlets according to FSC and SSC values b) panel showing representative gating of CD19+ cells c) representative histogram of MEFL values of CD19+ cells for individual *Npc1*$^{+/+}$, and untreated and 3mg/kg rhHSP70$^{non\text{-}his}$ treated *Npc1*$^{-/-}$ mice. d) Average MEFL values show small but non-significant differences between untreated *Npc1*$^{-/-}$ and *Npc1*$^{-/-}$ mice treated with 3mg/kg rhHSP70^{his}. Treatment with rhHSP70^{his} resulted in small but non-significant increases in MEFL values of LysoTracker stained CD19+ cells.
n= *Npc1*$^{+/+}$ 5, untreated *Npc1*$^{-/-}$ 5, 3mg/kg rhHSP70^{his} treated *Npc1*$^{-/-}$ 6. p= 0.2496 between untreated and 3mg/kg rhHSP70$^{non\text{-}his}$ treated mice.

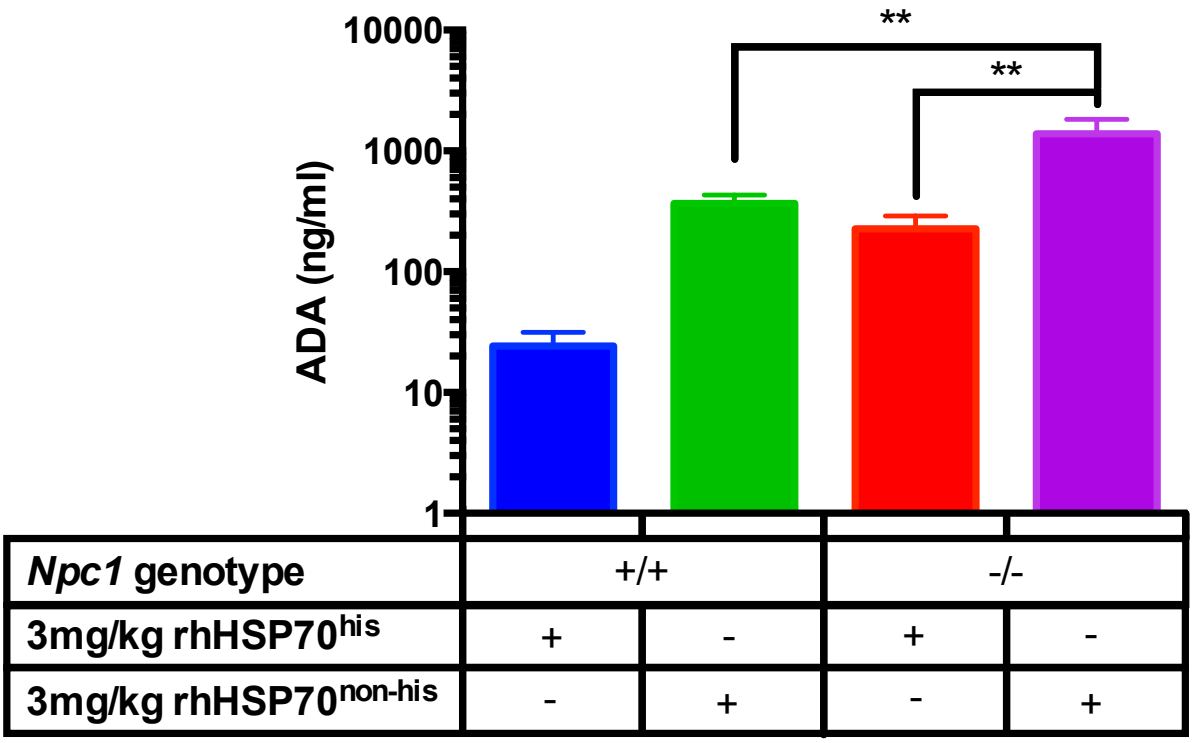


Figure 4.7: *rhHSP70$^{non\text{-}his}$ provokes a greater antibody response than rhHSP70^{his}*. Graph showing ADA response as assessed by ELISA. *Npc1*$^{-/-}$ mice treated with rhHSP70$^{non\text{-}his}$ show greater ADA response compared both to *Npc1*$^{+/+}$ mice treated with rhHSP70$^{non\text{-}his}$ and to *Npc1*$^{-/-}$ mice treated with rhHSP70^{his} protein after 4 weeks treatment.
n= 5/group. Error bars are SEM. Data was analysed using a one-way ANOVA with Dunnett's test for multiple comparisons, comparing all treatment groups. Experiment performed by QPS, Austria. Data provided courtesy of Orphazyme ApS. Data analysed by J. Gray

.

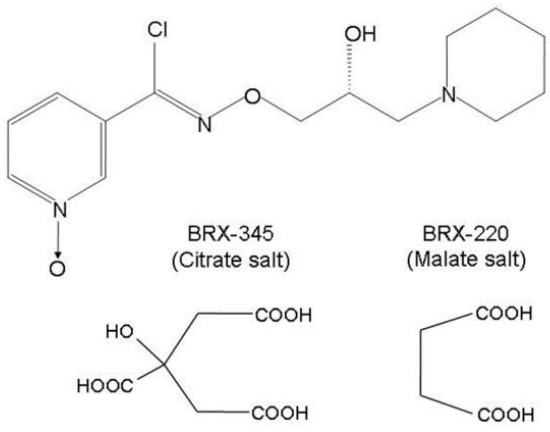
4.5 Discussion

Treatment of *Npc1*$^{-/-}$ mice with rhHSP70$^{\text{his}}$ protein showed significant behavioural and biochemical improvements of the NPC phenotype. This occured alongside small increases in sphingosine and lysosomal volume and a significant antibody response to the protein. We hypothesised that the antibody response may be in part due to the his tag on the recombinant protein. To test this we produced a protein without the his-tag (rhHSP70$^{\text{non-his}}$) and assessed the effects on a subset of behavioural and biochemical ouputs in the *Npc1*$^{-/-}$ mice. In contrast to the improvements seen in rearing and phenotypic behaviour following treatment with 3mg/kg rhHSP70$^{\text{his}}$, treatment with 3mg/kg rhHSP70$^{\text{non-his}}$ did not show any improvements in rearing ability **(Figure 4.2)**, and only slight improvement in the eye-closure phenotype of the mice **(Figure 4.3)**. Previous treatment with 3mg/kg rhHSP70$^{\text{his}}$ also showed significant decreases in forebrain GSL accumulation, both in terms of total burden, and in the major accumulating GSLs. However, treatment with the rhHSP70$^{\text{non-his}}$ had much less effect on forebrain GSL accumulation **(Figure 4.4)**. Additionally, very little difference was observed in the accumulation of forebrain sphingosine **(Figure 4.5)**, or in the lysosomal volume of splenic B-cells, as assessed by LysoTracker staining **(Figure 4.6)**. These differences in the efficacies between the proteins may, at least in part, be explained by a 6-fold increased antibody response to rhHSP70$^{\text{non-his}}$ when compared to the rhHSP70$^{\text{his}}$ protein **(Figure 4.7)**. This provides further evidence that the antibody response to the two recombinant proteins is neutralising and probably the cause of loss of efficacy seen at the later stages using the rhHSP70$^{\text{his}}$ protein.

5 Arimoclomol: Upregulator of the Heat-Shock Response as a Therapeutic for NPC Disease

5.1 Introduction

The use of rhHSP70^{his} to treat *Npc1*$^{-/-}$ mice has shown significant benefits in treating both the behavioural manifestations, and biochemcial storage associated with NPC disease progression up to 8 weeks of age. Treatment with 3mg/kg rhHSP70^{his} also significantly improved the myelination status of the mice at 8 weeks of age. However, upon treatment with both rhHSP70^{his} and a non-his tagged protein rhHSP70$^{non\text{-}his}$, a large neutralising antibody response was observed against the protein. As NPC disease is a chronic condition, this potentially poses problems for the use of rhHSP70 as a therapy. Additionally, infusions of a recombinant protein, are a significant burden on patients and their families as they require administration by medical practitioners. As such, orally available therapeutics would have significant advantages over a recombinant protein.



(a)

Figure 5.1: *Arimoclomol (BRX-345) and its maleate salt (BRX-220)* Figure adapted from[349]

Arimoclomol (BRX-345) is an analogue of bimoclomol and a citrate salt of a previous formulation analogue (BRX-220) **(Figure 5.1)**. Both arimoclomol and bimoclomol are small molecule upregulators of the endogenous HSR. Bimoclomol has been shown to induce HSP70 and HSP90 expression in the presence of cellular stress, but not in the absence of stress [350], and has been shown to act through prolonging the activity of trimerised HSF-1, driving the HSR further than in untreated cells [350]. Evidence has also been presented that bimoclomol specifically increases the fluidity of negatively charged membrane lipids, and signals a HSR through altered membrane dynamics [351]. This suggests that bimoclomol and its derivative arimoclomol may induce the HSR without the presence of unfolded proteins, although it is unclear whether this would be relevant under physiological conditions.

Bimoclomol, arimoclomol and BRX220 have shown positive effects in the treatment of a variety of disorders where an aberrant HSR is a prominent feature, including ALS [352], retinitis pigmentosa (RP) [353] and chemically induced diabetes [349, 354]. In these models, treatment with analogues of bimoclomol have shown pre-clinical efficacy in inducing the HSR, with the downstream effects of increasing the levels of the molecular chaperones HSP70 and HSP90. Furthermore, treatment increases the lifespan of ALS mice [352], and protects against diabetic retinopathy associated with hyperglycaemia [354]. In the RP model, arimoclomol treatment was shown to reduce the accumulation of cytotoxic aggregates of misfolded mutant rod opsin, and reduced the degeneration of photoreceptors [353]. Interestingly, these effects also appeard to be complemented by an increase in the unfolded protein response (UPR) [353]. Given recent evidence that both the HSR inducer, GGA, and HSP70 overexpression was able to rescue ERAD degradation of the $NPC1^{I1061T}$ mutated protein [305] along with the benefits seen following treatment with the $rhHSP70^{his}$ protein, treatment with arimoclomol may provide therapeutic benefits to the *Npc1*$^{-/-}$ mouse. Arimoclomol has been shown to be well tolerated in humans at doses up to 300mg/kg/day [355], and as such is an attractive target for treatment of lysosomal storage disorders.

5.2 Hypothesis

We hypothesise that treatment with arimoclomol may improve the behavioral and survival deficits seen in the *Npc1*$^{-/-}$ mouse, avoiding the attenuating antibody response observed with the HSP70 proteins.

5.3 Materials & Methods

5.3.1 Mice

Npc1 mice were bred and maintained as described previously in **Section 3.3.1**.

5.3.2 Taste Aversion Test

To ensure that mice did not avoid the arimoclomol when dissolved in drinking water, 8x 6-week old male *Npc1*$^{-/-}$ mice were housed in seperate cages, and half the mice offered bottles of normal water, and half offered water with 2g/L arimoclomol for 12 hours overnight. Following exposure to the first solution, the mice were then exposed to the second solution overnight for a further 12 hours. Bottles were weighed before and after each time period and the amount consumed was calculated from the difference in weights, assuming a specific density of 1g/ml.

5.3.3 Treatment

For the pilot study, 3 week old *Npc1*$^{-/-}$ mice (6 males, 4 females per group) were treated with 0.24g/L or 2.4g/L arimoclomol (4 males/4 females), corresponding to 30mg/kg/day or 300mg/kg/day arimoclomol respectively, dissolved in normal drinking water. Doses per day herein refered to as mg/kg. Normal drinking water alone was used as a control. The males were culled at 54 days, and the females were taken to survival with behaviourals every 2 weeks. Mice were culled when they reached a predetermined humane endpoint of >1g loss of body weight within 24 hours.

For the follow up study, 3 week old *Npc1*$^{-/-}$ mice (5 male, 5 females per group) were treated with either 0.08g/L, 0.24g/L, 0.8g/L and 2.4g/L arimoclomol (4 males/4 females) corresponding to 10, 30, 100 and 300mg/kg arimoclomol, respectively. Arimoclomol was dissolved in normal

drinking water, untreated mice were supplied with normal drinking water alone. Mice were culled at 54 days.

3 week old *Npc1*$^{+/+}$ mice were also maintained on a normal diet, and included as baseline controls.

5.4 Gait Analysis

Mice were run along the CatWalk weekly from 3 weeks of age, data was collected using camera settings of 0.44 intensity and 0.12 gain at a distance of 30 cm from the walkway. For analysis, CatWalk was set to include runs only which meet the following criteria; 8 steps minimum, 60% maximum variation and a speed range of 12-40cm/s. Runs were collected weekly from 5 weeks. Parameter values were averaged to generate front and hind separate values due to little variation between right and left paw data.

All other methods were performed as described in **Chapter 2**.

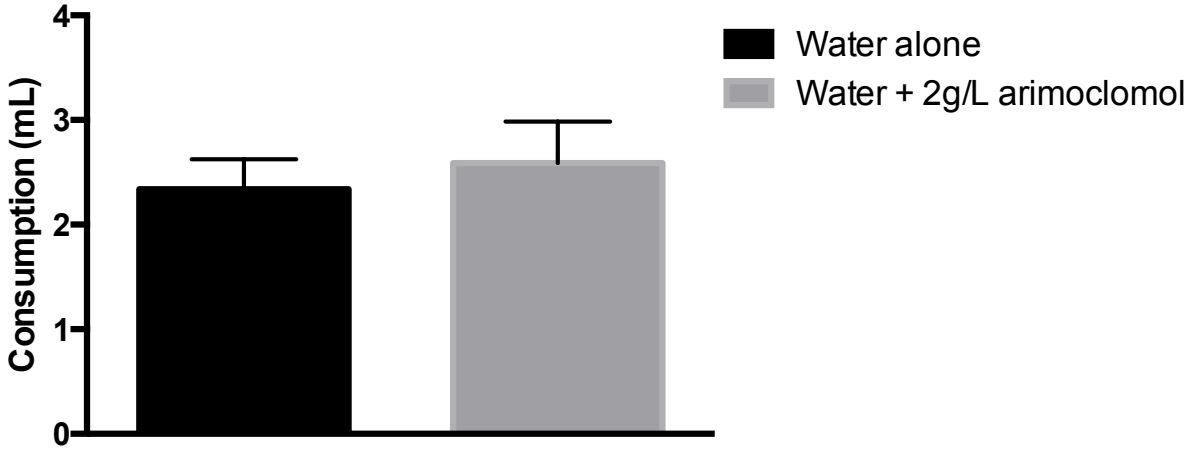
5.5 Results

5.5.1 Taste Aversion Test

Compounds dissolved in water may often taste bitter and mice may go to great lengths to avoid such substances. To ensure that the animals in this study were not avoiding consuming the drug we performed a taste aversion test. 6-week-old *Npc1*$^{-/-}$ mice were housed in seperate cages, and offered either water or 2g/L arimoclomol dissolved in water. Mice consumed slightly but not significantly more arimoclomol water, than normal water overnight indicating that these mice would not attempt to avoid the drug administration on the basis of taste **(Figure 5.2)**.

5.5.2 Weights

Treatment with arimoclomol did not affect the rate of weight gain of *Npc1*$^{-/-}$ when compared to untreated controls **(Figure 5.3 a, b)**. Althought the male 30mg/kg treatment group does have a lower maximum weight, compared to *Npc1*$^{-/-}$ controls, this is probably due to a lower average starting weight **(Figure 5.3 a)**. *Npc1*$^{-/-}$ mice display a charcteristic loss of weight from



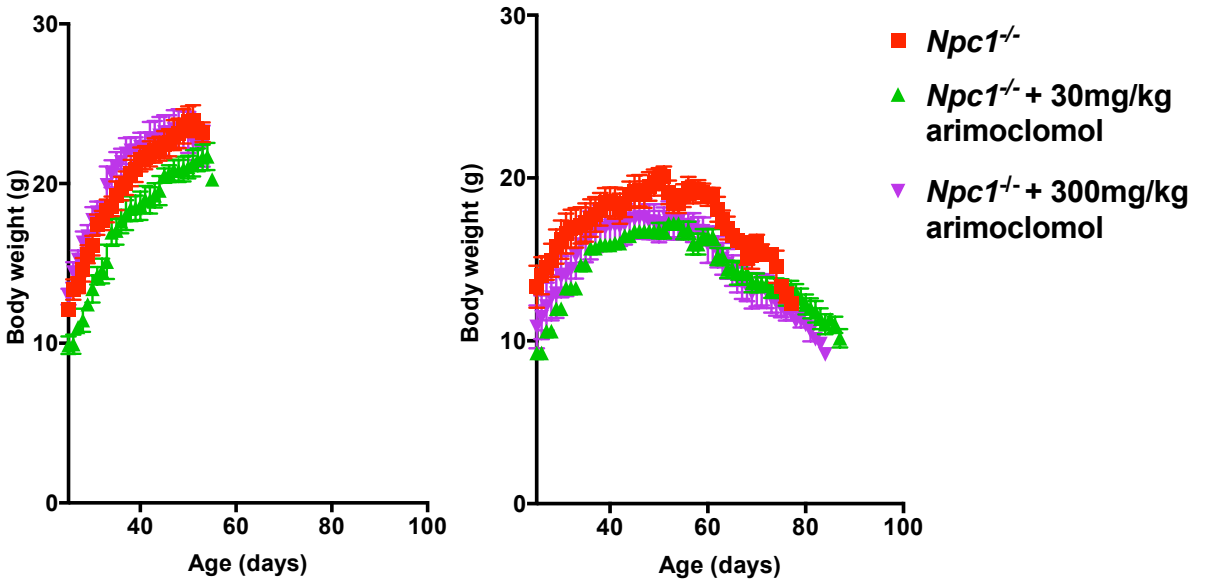
(a)

Figure 5.2: *Arimoclomol does not affect water consumption* Mice given either water alone or water with 2g/L arimoclomol showed no significant differences in the volume consumed overnight.
n=8/group. Data were analysed using a two-tailed Student's t-test.

approximately 7 weeks of age. Treatment with arimoclomol did not affect the point at which mice began to lose weight **(Figure 5.3 b)**, although it appears that the rate of weight loss was slightly slowed in the two treatment groups.

5.5.3 Survival

Npc1$^{-/-}$ mice have a lifespan of approximately 11 weeks. Death in these animals is usually preceded by significant loss of weight, presumably caused by loss of the ability to feed, which can be attributed to neuronal pathology as pan-neuronal specific knockouts (*Npc1*$^{flox/-}$;*Syn1*-Cre^{+}) [172] but not Purkinje cell specific knockouts (*Npc1*$^{flox/-}$;*Pcp2*-Cre^{+}) display reduced life expectancy [171]. The weight loss in *Npc1*$^{-/-}$ mice usually precedes death by a few days and as such the humane endpoint is determine as when a mouse loses >1 gram bodyweight in 24 hours. In this study, untreated *Npc1*$^{-/-}$ mice had a mean survival of 74 days. Mice treated with 30mg/kg and 300mg/kg arimoclomol had significantly increased mean life expectancies of 87 days (p=0.0067) and 82 days (p=0.0067) respectively. It is interesting to note that of the mice treated with 30mg/kg arimoclomol, 3 of the 4 mice did not lose 1g in 24 hours and were instead found dead, compared with 1 mouse from the untreated cohort, and 1 from the 300mg/kg cohort. This will likely account for some, but not all, of the difference in mean survival.



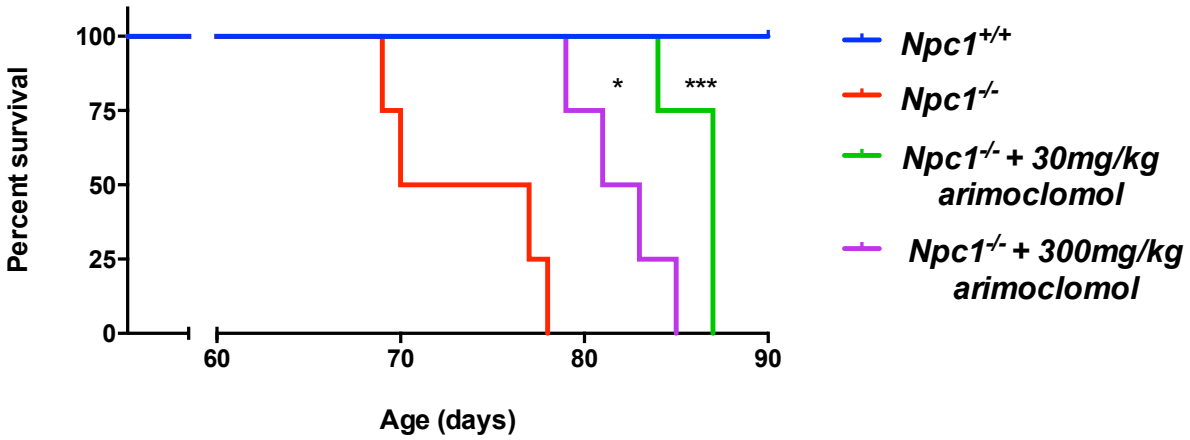
(a) (b)

Figure 5.3: *Treatment with arimoclomol does not affect the body weights of the animals.* a) No differences were observed in weight gain between untreated *Npc1*$^{-/-}$ male mice and arimoclomol treated *Npc1*$^{-/-}$ male mice. b) Untreated *Npc1*$^{-/-}$ mice display characteristic weight loss starting from 7 weeks of age. This weight loss is not significantly affected by arimoclomol treatment, although the 30mg/kg group does appear to have slightly slower rate of decline compared to untreated *Npc1*$^{-/-}$ mice. *Males* Untreated *Npc1*$^{-/-}$ mice, n= 6., *Npc1*$^{-/-}$ mice + 30mg/kg arimoclomol, n= 5., *Npc1*$^{-/-}$ mice + 300mg/kg arimoclomol mice, n = 5. *Females* Untreated *Npc1*$^{-/-}$ mice, n= 4., *Npc1*$^{-/-}$ mice + 30mg/kg arimoclomol, n= 4., *Npc1*$^{-/-}$ mice + 300mg/kg arimoclomol mice, n = 4.

5.5.4 Behavioural Data

Manual Rearing

Npc1$^{-/-}$ mice began to lose side rearing ability from 8 weeks, and this was completely lost by 10 weeks of age. Both 30mg/kg and 300mg/kg arimoclomol treated *Npc1*$^{-/-}$ mice performed significantly better than untreated *Npc1*$^{-/-}$ mice at both 8 and 10 weeks **(Figure 5.5a)** with 30mg/kg displaying side rearing ability comparable to *Npc1*$^{+/+}$ mice at 10 weeks of age. The centre rearing ability of *Npc1*$^{-/-}$ mice was completely lost by 8 weeks of age, and both 30mg/kg and 300mg/kg arimoclomol treated *Npc1*$^{-/-}$ mice displayed significantly improved centre rearing ability at 8 weeks, although this effect was lost by 10 weeks of age **(Figure 5.5b)**.



(a)

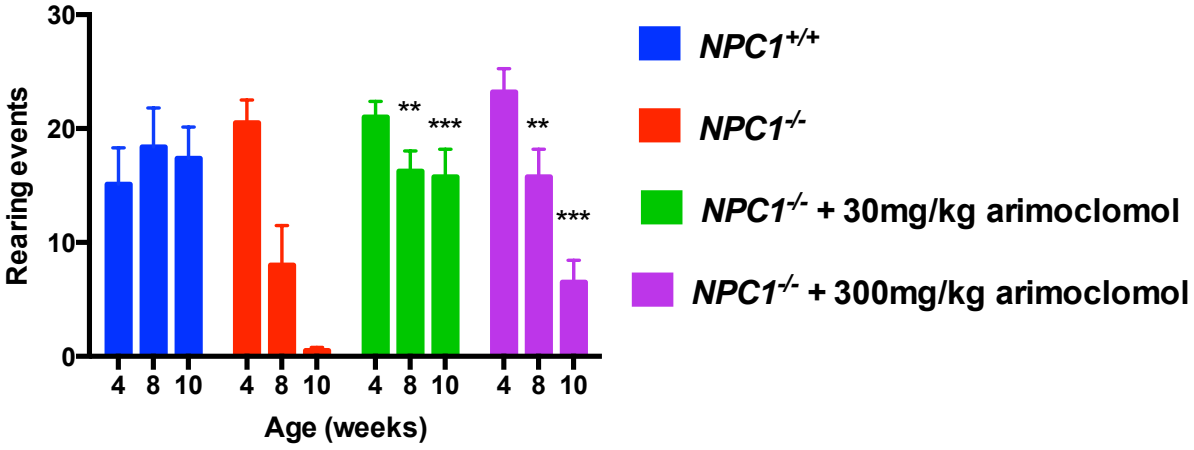
Figure 5.4: *Treatment of* Npc1$^{-/-}$ *mice with arimoclomol significantly improves survival.* Both 300mg/kg and 30mg/kg doses of arimoclomol showed significant improvements in the survival curves compared to *Npc1*$^{-/-}$ mice. Although every effort was made to monitor the mice, a certain number did not meet the humane endpoint criterion, and were found dead.
Untreated *Npc1*$^{-/-}$ mice, n= 4, (1 found dead)., *Npc1*$^{-/-}$ mice + 30mg/kg arimoclomol, n= 4 (3 found dead)., *Npc1*$^{-/-}$ mice + 300mg/kg arimoclomol mice, n = 4 (1 found dead). Data were analysed using multiple Mantle-Cox tests for survival, comparing untreated *Npc1*$^{-/-}$ to the two treatment groups. p= *, <0.05., ***, <0.001 The logrank test for trend gave a p value of <0.0001

Treatment	Timepoint					
	Week 6		Week 8		Week 10	
	n	p	n	p	n	p
Npc1$^{+/+}$	10	–	5	–	5	–
Npc1$^{-/-}$	10	–	4	–	3	–
Npc1$^{-/-}$ + 30mg/kg arimoclomol	9	0.8981	4	0.0042	4	<0.0001
Npc1$^{-/-}$ + 300mg/kg arimoclomol	9	0.6197	4	0.0063	4	<0.0001

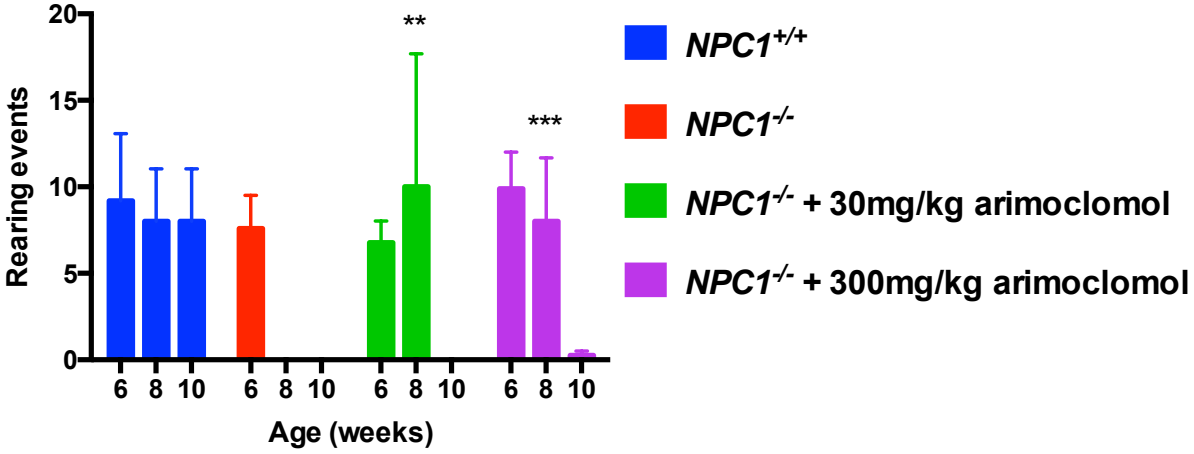
Table 5.1: Table showing n and p values for manual side rearing at each timepoint comparing treatments to untreated *Npc1*$^{-/-}$ mice.

Tremor

Untreated *Npc1*$^{-/-}$ mice display increased high frequency tremor from 8 weeks of age compared to *Npc1*$^{+/+}$ mice. Treatment with 30mg/kg arimoclomol resulted in a small but non-significant reduction in high frequency tremor at 10 weeks. 300mg/kg treatment however, showed a highly significant increase in high frequency tremor **(Figure 5.6)**.



(a)

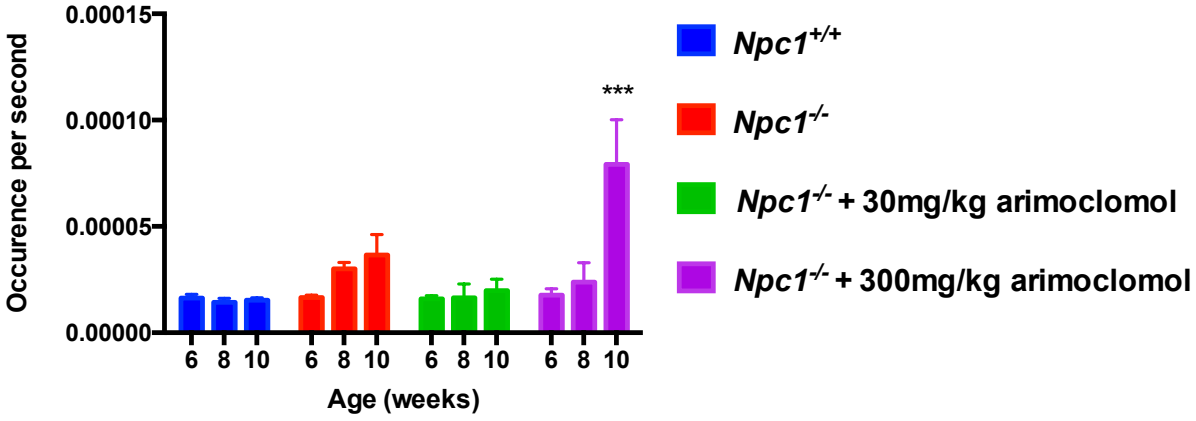


(b)

Figure 5.5: *Treatment with arimoclomol shows improvement in manual scores of side rearing and centre rearing.* a) Treatment with arimoclomol shows significant improvements in side rearing scores, at 8 and 10 weeks compared to untreated *Npc1*$^{-/-}$ mice. b) Centre rearing scores were also significantly improved at 8 weeks compared to untreated *Npc1*$^{-/-}$ mice following arimoclomol treatment.
n and p values for side and centre rearing graphs are given in **Tables 5.1 and 5.2**. Rearing data was transformed using Y=[LogY+1] to obtain a normal distribution. Data was analysed using a two-way ANOVA with Dunnetts multiple comparison test.

Treatment	Timepoint					
	Week 6		Week 8		Week 10	
	n	p	n	p	n	p
Npc1$^{+/+}$	10	–	5	–	5	–
Npc1$^{-/-}$	10	–	4	–	3	–
Npc1$^{-/-}$ + 30mg/kg arimoclomol	9	0.9909	4	0.0013	4	>0.999
Npc1$^{-/-}$ + 300mg/kg arimoclomol	9	0.5545	4	0.0005	4	0.9071

Table 5.2: Table showing n and p values for manual centre rearing at each time point comparing treatments to untreated *Npc1*$^{-/-}$ mice.



(a)

Figure 5.6: *Treatment with high doses of arimoclomol increases high frequency tremor.* Characteristic high frequency tremor develops in untreated *Npc1*$^{-/-}$ mice by 10 weeks of age. Treatment with 30mg/kg shows a small but non-significant reduction in high frequency tremor compared to untreated *Npc1*$^{-/-}$ mice. However, 300mg/kg arimoclomol treated *Npc1*$^{-/-}$ mice show a significant increase in high frequency tremor at 10 weeks of age compared to untreated *Npc1*$^{-/-}$ mice.
n and p values for side and centre rearing graphs are given in **Table 5.3** ***, $p<0.001$. Data was analysed using a two-way ANOVA with Dunnetts multiple comparison test.

Treatment	Timepoint					
	Week 6		Week 8		Week 10	
	n	p	n	p	n	p
Npc1$^{+/+}$	10	–	5	–	5	–
Npc1$^{-/-}$	10	–	4	–	3	–
Npc1$^{-/-}$ + 30mg/kg arimoclomol	9	0.9907	4	0.3073	4	0.2241
Npc1$^{-/-}$ + 300mg/kg arimoclomol	9	0.9766	4	0.7709	4	0.0007

Table 5.3: Table showing n and p values for manual centre rearing at each time point compared to untreated *Npc1*$^{-/-}$ mice.

5.5.5 Biochemistry Data

Cholesterol Quantification

Cholesterol storage in the liver of *Npc1*$^{-/-}$ mice was increased in comaprison to *Npc1*$^{+/+}$ mice. Treatment with 30mg/kg arimoclomol resulted in a small but non-significant reduction of cholesterol accumulation in the liver (p=0.0752) whereas 300mg/kg arimoclomol did not show any reduction (p=0.886) **(Figure 5.7)**.

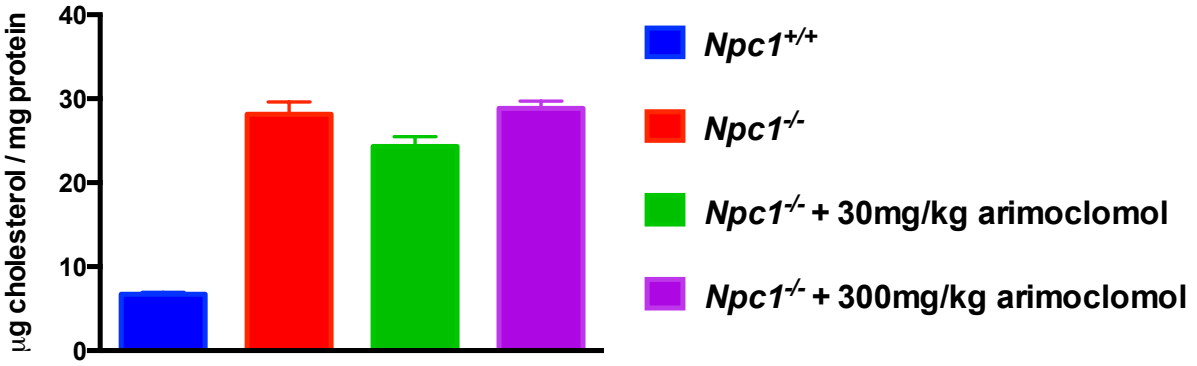


Figure 5.7: *Treatment with 30mg/kg arimoclomol may reduce peripheral cholesterol accumulation.* Treatment with 30mg/kg arimoclomol shows modest reduction in cholesterol storage in the liver of 7 week old *Npc1*$^{-/-}$ mice compared to untreated *Npc1*$^{-/-}$ mice. *Npc1*$^{+/+}$, n= 5., untreated *Npc1*$^{-/-}$, n= 5., 30mg/kg arimoclomol treated *Npc1*$^{-/-}$ n= 5., 300mg/kg arimoclomol treated *Npc1*$^{-/-}$ n= 5 . *, p<0.05. Data was analysed using a one-way ANOVA with Dunnett's multiple comparison test. Error bars are SEM. Data are the results of two seperate assays.

GSL Quantification

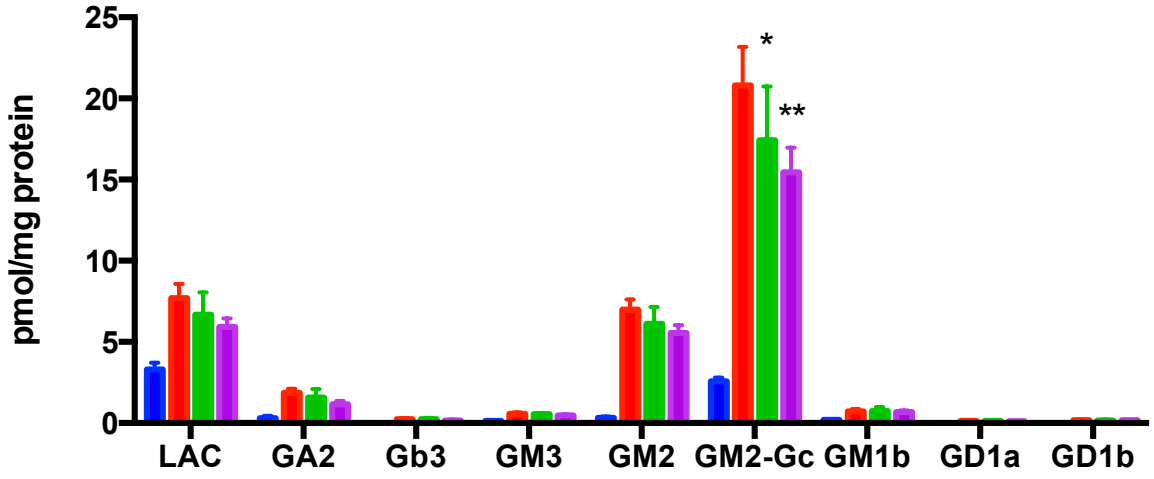
To assess the impact of arimoclomol on the accumulation of GSLs we measured the levels of GSL accumulation by HPLC. In livers of 7 week old untreated *Npc1*$^{-/-}$ mice, we observed typical accumulations of a variety of GSLs including lactosyl ceramide (lac), GM2, GM2-Gc, and to a lesser extent, GA2 and GM1b, compared to 7 week old *Npc1*$^{+/+}$ mice **(Figure 5.8a)**. Treatment of *Npc1*$^{-/-}$ mice with 300mg/kg arimoclomol resulted in reductions in GM2-Gc 29% (p=¡0.0001), and similar but non-significant reductions in the accumulations of lac (24%, p=0.0918), GA2 (37%, p=0.508), Gb3(29%, p=0.947), GM3(20%, p=0.911), GM2(20%, p=0.173), GM1b(22%, p=0.968) GD1a (65%, p=0.994) **(Figure 5.8a)**. Treatment with 30mg/kg arimoclomol saw sim-

ilar but less reduced GSL accumulations of lac (14%, p=0.505), GA2 (15%, p=0.853), GM3(5%, p=0.986), GM2(12%, p=0.569), GM2-Gc (16%, p=0.0311), GD1a (6%, p=0.999).

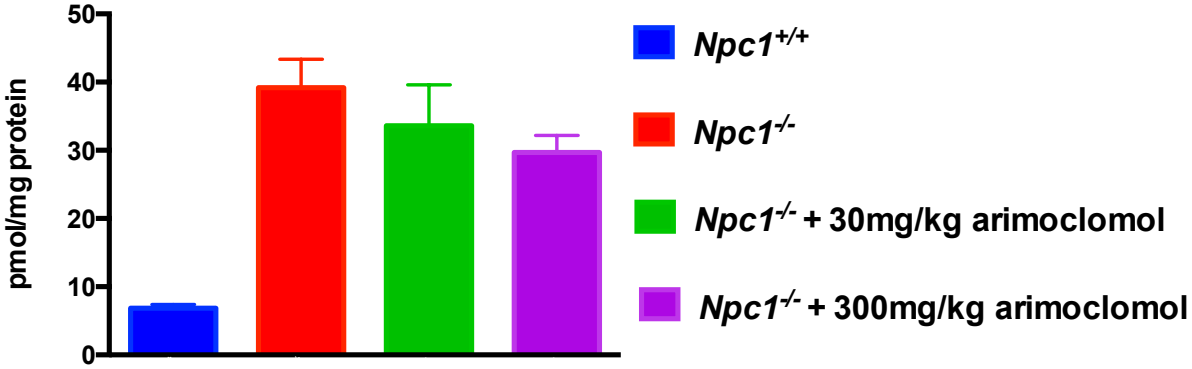
Total GSL levels did not display a significant reduction, however the pattern of reduction was the same with 30mg/kg displaying 17% (p=0.595) reduction and 300mg/kg a 29% (p=0.265) reduction **(Figure 5.8b)**.

As neuronal pathology correlates significantly with GSL accumulation, we analysed forebrain and cerebellar GSL accumulation to determine whether treatment with arimoclomol affects the accumulation of GSLs within these regions. In the cerebellum of *Npc1*$^{-/-}$ mice, we observed significant increases in both the major cerebellar GSLs GM1a, GD1a, GD1b and GT1b and other species not usually observed in *Npc1*$^{+/+}$ mice Lac, GM2, GA1, GA2, Gb3, GD3 **(Figure 5.9a)**. Treatment with 300mg/kg arimoclomol resulted in significant increases of the GSL species; GM2 (98%, p=0.00119), GM1a (258%, p=0.00395) and non-significant increases in Lac (121%, p=0.100), GM3 (113%, p=0.159), GA2 (129%, p=0.396) GA1 (173%, p=0.326), GD1a (73%, p=0.0763), GD1b (79%, p=0.176) and GT1b (72%, p=0.447). 30mg/kg arimoclomol treatment resulted in small decreases of most lipid species, but particularly the major GSL species, GM1a (67% p=0.258), GD1a (73% p=0.272), GD1b (82% p=0.220) and GT1b (78% p=0.223) where the levels were comparable to *Npc1*$^{+/+}$ **(Figure 5.9a)**. Total GSL accumulation displayed a similar pattern with 300mg/kg arimoclomol display a 118% increase of total GSL burden (p=0.0492) whereas 30mg/kg arimoclomol displayed a decrease of 43% (p=0.661) **(Figure 5.9b)**.

GSLs in the forebrains of the mice showed a similar pattern. Untreated *Npc1*$^{-/-}$ mice displayed increased storage of Lac , GM3 and GM2, although only minor increases in the major GSLs were observed **(Figure 5.10a)**. Treatment with 300mg/kg arimoclomol resulted in significant increases of the GSL species; Lac (100%, p<0.0001), GM3 (108%, p<0.0001), GM2 (98%, p<0.0001), GM1a (258%, p<0.0001) GD1a (467%, p<0.0001), and non-significant increases in GA2 (115%, p=0.145) GA1 (101%, p=0.320), GD1b (380%, p=0.077) and GT1b (960%, p=0.0794) **(Figure 5.10a)**. 30mg/kg arimoclomol resulted in no appreciable differences in GSL storage although Lac was significantly increased (92%, emphp=0.000169) **(Figure 5.10a)**. Total GSLs displayed a similar pattern, with 300mg/kg arimoclomol treated mice displaying a

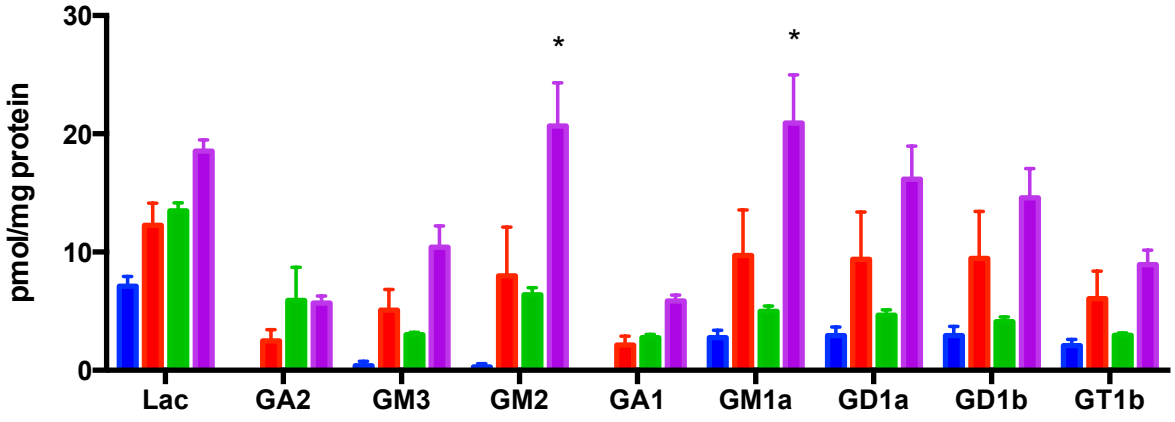


(a)

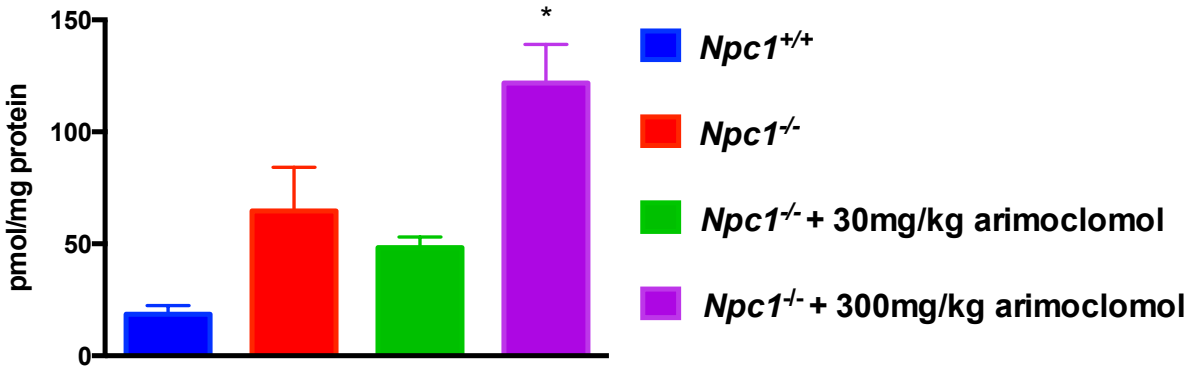


(b)

Figure 5.8: *Treatment with arimoclomol reduces liver GSL accumulation.* a) Treatment with both doses of arimoclomol shows reductions of individual GSL species in liver compared to untreated *Npc1*$^{-/-}$ mice b) Total GSLs show a similar pattern. *Npc1*$^{+/+}$, n= 5., untreated *Npc1*$^{-/-}$, n= 5., 30mg/kg arimoclomol treated *Npc1*$^{-/-}$ n= 5., 300mg/kg arimoclomol treated *Npc1*$^{-/-}$ n= 5 . *, p<0.05. **, p<0.01. Data was analysed using multiple t-tests with Holm-Sidak corrections for multiple comparison (graph a) and a one-way ANOVA with Dunnett's multiple comparison test (graph b). Error bars are SEM.



(a)



(b)

Figure 5.9: *Treatment with 300mg/kg arimoclomol increases cerebellar GSL accumulation.* a) Treatment with 300mg/kg arimoclomol causes increased storage of GSL species in the cerebellum, whereas 30mg/kg resulted in slight by non-significant reductions in GSL accumulation of individual GSL species compared to untreated *Npc1*$^{-/-}$ mice b) Total GSLs reflected this pattern compared to untreated *Npc1*$^{-/-}$ mice. *Npc1*$^{+/+}$, n= 5., untreated *Npc1*$^{-/-}$, n= 5., 30mg/kg arimoclomol treated *Npc1*$^{-/-}$ n= 5., 300mg/kg arimoclomol treated *Npc1*$^{-/-}$ n= 5 . *, p<0.05. Data was analysed using multiple t-tests with Holm-Sidak corrections for multiple comparisons (graph a) and a one-way ANOVA with Dunnett's multiple comparison test (graph b). Error bars are SEM.

63% increase (p=0.0923) and the 30mg/kg treated mice having a 5% increase (p=0.996) **(Figure 5.10b)**.

To examine the behavioural effects further, the following analyses were performed using a larger dose range of 10, 30, 100 and 300mg/kg arimoclomol

5.5.6 Dose Response : Manual Rearing

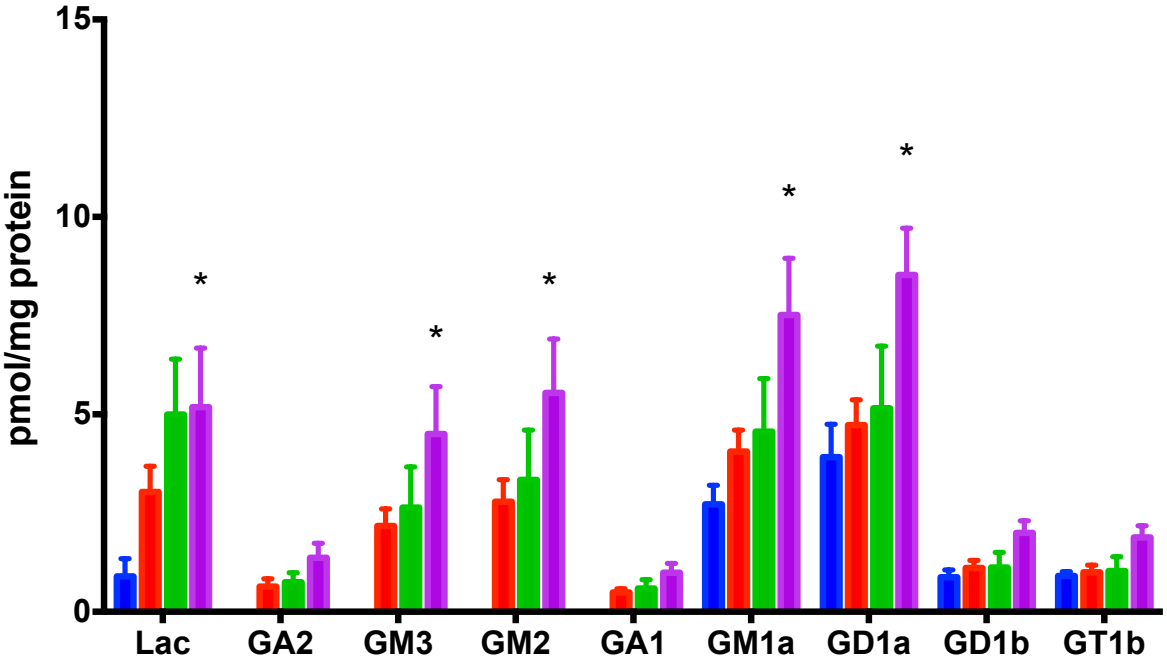
To examine the dosing effects, we treated mice with an expanded dose range of 10, 30, 100 and 300mg/kg arimoclomol and assessed the rearing behaviour at 7 weeks. *Npc1*$^{-/-}$ mice treated with 30 and 100mg/kg arimoclomol performed slightly better in side rearing (non-significant) than untreated *Npc1*$^{-/-}$ mice, whereas the 300mg/kg and 10mg/kg dose showed no difference in side rearing compared to untreated *Npc1*$^{-/-}$ mice **(Figure 5.11a)**. Centre rearing ability, which requires greater coordination from the mice was completely absent in untreated *Npc1*$^{-/-}$ mice at 7 weeks. Treatment of *Npc1*$^{-/-}$ mice with both 10 and 30mg/kg arimoclomol resulted in significantly improved centre rearing ability, whereas the higher doses showed no change **(Figure 5.11b)**.

Treatment	Side Rearing		Centre-Rearing	
	n	p	n	p
Npc1$^{+/+}$	10	–	10	–
Npc1$^{-/-}$	10	–	10	–
Npc1$^{-/-}$ + 10mg/kg arimoclomol	10	0.9695	10	0.0439
Npc1$^{-/-}$ + 30mg/kg arimoclomol	10	0.0575	10	0.0005
Npc1$^{-/-}$ + 100mg/kg arimoclomol	10	0.0911	10	>0.999
Npc1$^{-/-}$ + 300mg/kg arimoclomol	10	0.598	10	>0.999

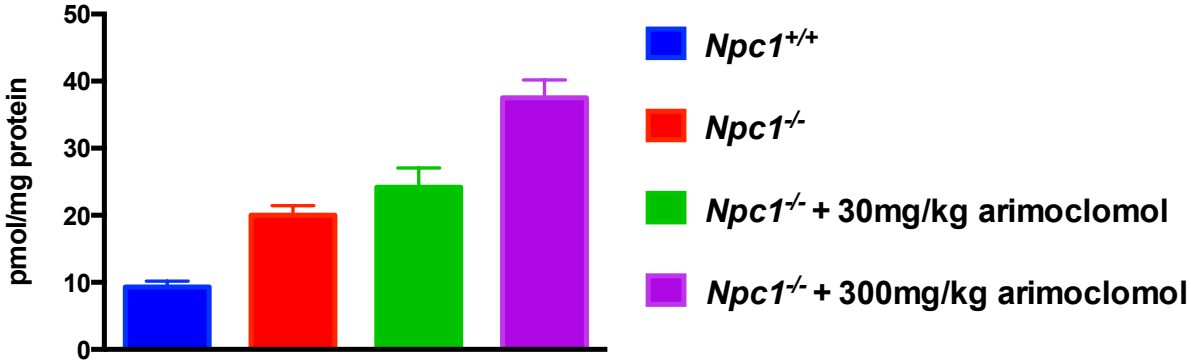
Table 5.4: Table showing n and p values for manual rearing events for each group at 7 weeks, compared to untreated *Npc1*$^{-/-}$ mice.

5.5.7 Dose Response : Gait Analysis

To assess the impact of arimoclomol on the gait of *Npc1*$^{-/-}$ mice, we used the CatWalk gait analysis system at 5 and 7 weeks of age to measure parameters associated with disease progression in *Npc1*$^{-/-}$ mice. As previously described, runs were only included when they met criterion of 8 or more uninterrupted steps, with a speed variation of 60% and a speed range between 12 and



(a)



(b)

Figure 5.10: *Treatment with 300mg/kg arimoclomol increases forebrain GSL accumulation.* a) Treatment with 300mg/kg arimoclomol causes increased storage of GSL species in the forebrain, whereas 30mg/kg resulted in slight by non-significant increases in GSL accumulation of individual GSL species compared to untreated *Npc1*$^{-/-}$ mice b) total GSLs changed in a similar, though non-significant manner compared to untreated *Npc1*$^{-/-}$ mice. *Npc1*$^{+/+}$, n= 5., untreated *Npc1*$^{-/-}$, n= 5., 30mg/kg arimoclomol treated *Npc1*$^{-/-}$ n= 5., 300mg/kg arimoclomol treated *Npc1*$^{-/-}$ n= 5 . *, p<0.05. Data was analysed using multiple t-tests with Holm-Sidak corrections for multiple comparisons (graph a) and a one-way ANOVA with Dunnett's multiple comparison test (graph b). Error bars are SEM. Data was the result of two seperate assays.

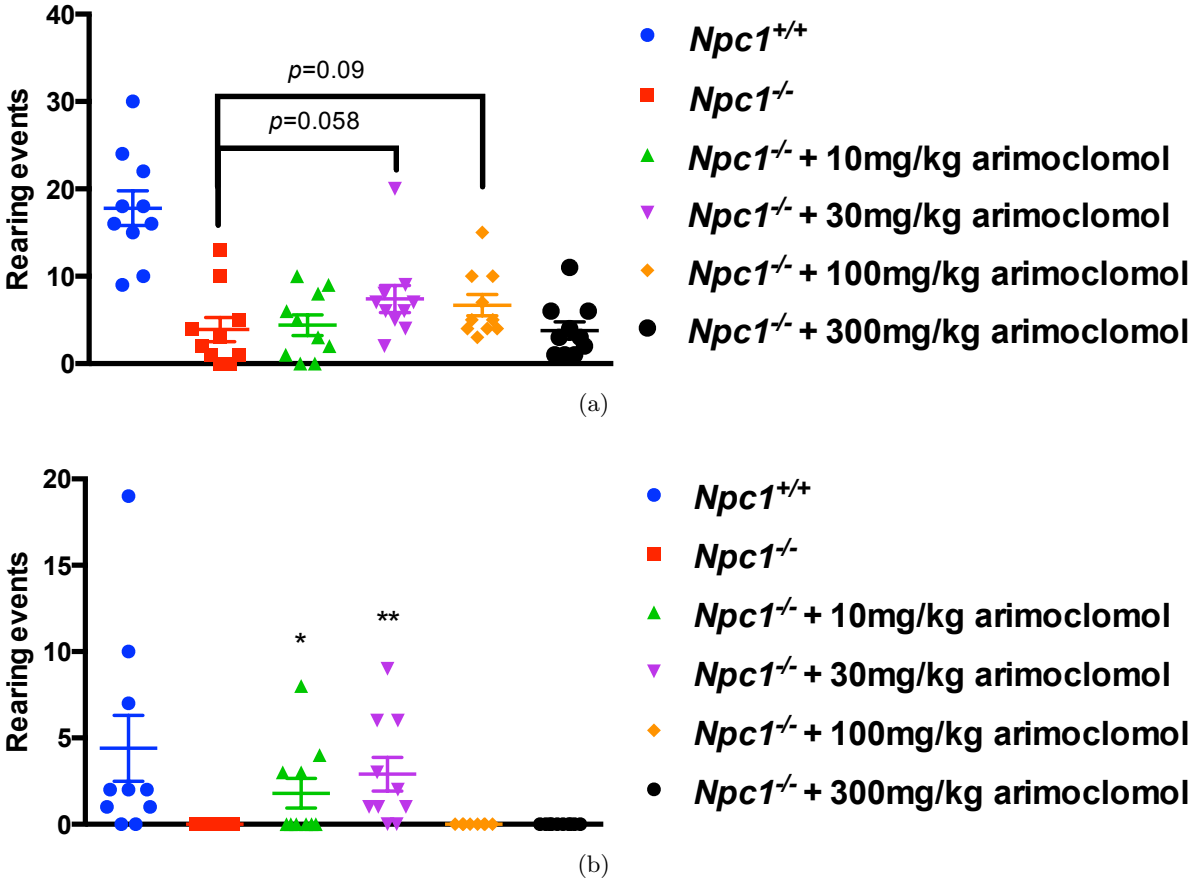


Figure 5.11: *Treatment with arimoclomol shows improvement in manual scores of side rearing and centre rearing at lower doses.* a) Side rearing scores of 7 week old mice show small, but non-significant increases at both 30 and 100mg/kg dose of arimoclomol compared to untreated *Npc1*$^{-/-}$ mice b) Centre rearing scores of 7 week old mice show significant improvements following 10 and 30mg/kg treatment with arimoclomol compared to untreated *Npc1*$^{-/-}$ mice.
n and p values are shown in **Table 5.4** *, $p<0.05$, **, $p<0.01$, ***, $p<0.001$. Rearing data was transformed using Y=[LogY+1] to obtain a normal distribution. Data was analysed using a two-way ANOVA with Dunnetts multiple comparison test.

45cm/s. The numbers of mice and numbers of runs included at each timepoint are shown in **Table 5.5**.

	Total Mice	Week 7	
		no. Mice	no. Runs
Npc1$^{+/+}$	10	10	29
Npc1$^{-/-}$	10	9	23
Npc1$^{-/-}$ + 10mg/kg arimoclomol	10	10	28
Npc1$^{-/-}$ + 30mg/kg arimoclomol	10	9	20
Npc1$^{-/-}$ + 100mg/kg arimoclomol	10	8	20
Npc1$^{-/-}$ + 300mg/kg arimoclomol	10	7	19

Table 5.5: Table showing numbers of mice and trials which met the inclusion criteria for gait analysis for each group at each time point.

Firstly, we assessed whether speed between untreated and arimoclomol treated was not significantly different as this can affect most parameters of the gait analysis [329]. Whilst all *Npc1*$^{-/-}$ groups were slower than *Npc1*$^{+/+}$ mice, there was no significant difference between the *Npc1*$^{-/-}$ groups **(Figure 5.12)**.

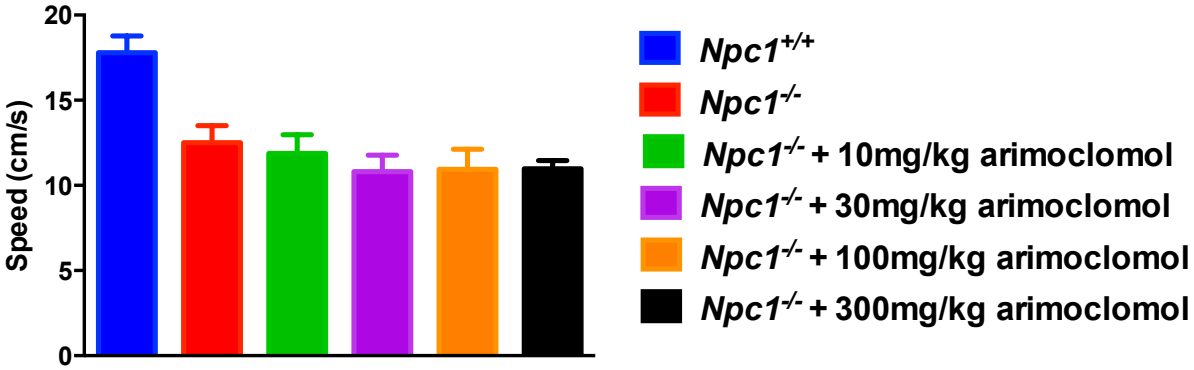


Figure 5.12: *Treatment with arimoclomol does not significantly affect the speeds of* Npc1$^{-/-}$ *mice.* Speed at 7 weeks stays relatively constant between *Npc1*$^{-/-}$ groups. *Npc1*$^{+/+}$, n= 10., *Npc1*$^{-/-}$, n= 9., *Npc1*$^{-/-}$ + 10mg/kg arimoclomol n= 10., *Npc1*$^{-/-}$ + 30mg/kg arimoclomol n= 9., *Npc1*$^{-/-}$ + 100mg/kg arimoclomol n= 8., *Npc1*$^{-/-}$ + 300mg/kg arimoclomol n= 7. Data was analysed using a one-way ANOVA with Dunnetts multiple comparison test.

Cadence is the number of steps per second and is a broad measure of the level of coordination of the mice. Cadence has previously been shown to decrease in response to striatal lesions in a rat model of stroke, and lesions in a chemically induced rat model of Parkinson's disease [356, 330]. Cadence also decreases in *Npc1*$^{-/-}$ mice, and we have previously seen a modest improvement in

cadence with rhHSP70^{his} treatment. As before, untreated *Npc1*$^{-/-}$ gradually lose cadence as by 7 weeks of age. Treatment of *Npc1*$^{-/-}$ mice with 10mg/kg arimoclomol significantly improved the cadence of the mice, although this improvement was lost as the dosage increased **(Figure 5.13)**.

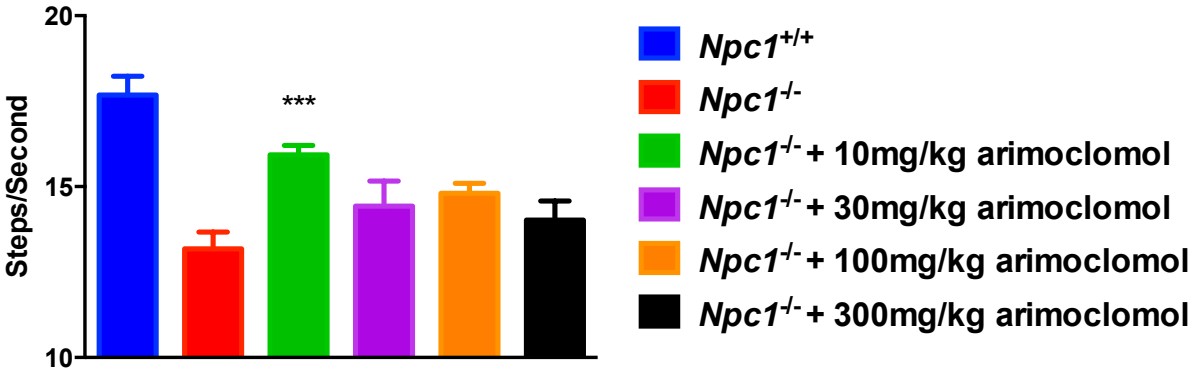


Figure 5.13: *Treatment with arimoclomol shows improvement in footstep cadence.* Cadence (number of steps per second) is significantly reduced in *Npc1*$^{-/-}$ compared to *Npc1*$^{+/+}$. Treatment with 10mg/kg arimoclomol significantly improves the cadence of the mice, compared to untreated *Npc1*$^{-/-}$ mice.
Npc1$^{+/+}$, n= 10., *Npc1*$^{-/-}$, n= 9., *Npc1*$^{-/-}$ + 10mg/kg arimoclomol n= 10., *Npc1*$^{-/-}$ + 30mg/kg arimoclomol n= 9., *Npc1*$^{-/-}$ + 100mg/kg arimoclomol n= 8., *Npc1*$^{-/-}$ + 300mg/kg arimoclomol n= 7. p=***<0.001. Data was analysed using a one-way ANOVA with Dunnetts multiple comparison test.

Stand time is the average amount of time the paws are in contact with the plate during each paw placement, indicating a slower and more unsteady footplacement [356]. Increases are observed between *Npc1*$^{-/-}$ mice and *Npc1*$^{+/+}$ in both front and hind paw stand time at 7 weeks **(Figure 5.14)**. Treatment with arimoclomol resulted in decreases at all doses, although only 10 and 100mg/kg arimoclomol reached statistical significance **(Figure 5.14)**.

Initial and terminal dual stance refer to the amount of time that both girdle (i.e. left and right front/hind paws) are both in contact with the plate, both for the initial and terminal step in a step-sequence, respectively. In a normal mouse, this time is very transient, as the placement of alternating diagonal paws means that there is very little overlap during normal motion. Both initial and terminal dual stance parameters have been shown to be a useful parameter in a PD model [356], and we have also found both initial **(Figure 5.15a)** and terminal **(Figure 5.15b)** to be consisitently changed between untreated *Npc1*$^{-/-}$ and *Npc1*$^{+/+}$ mice at 7 weeks

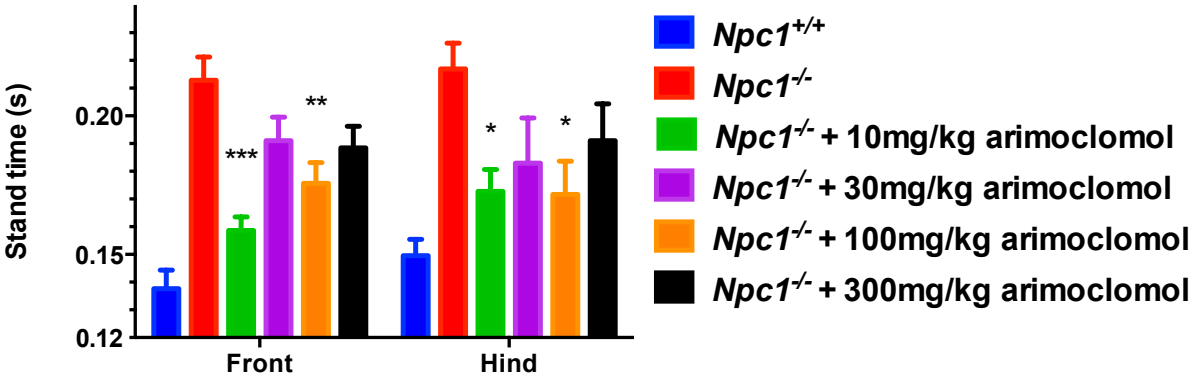
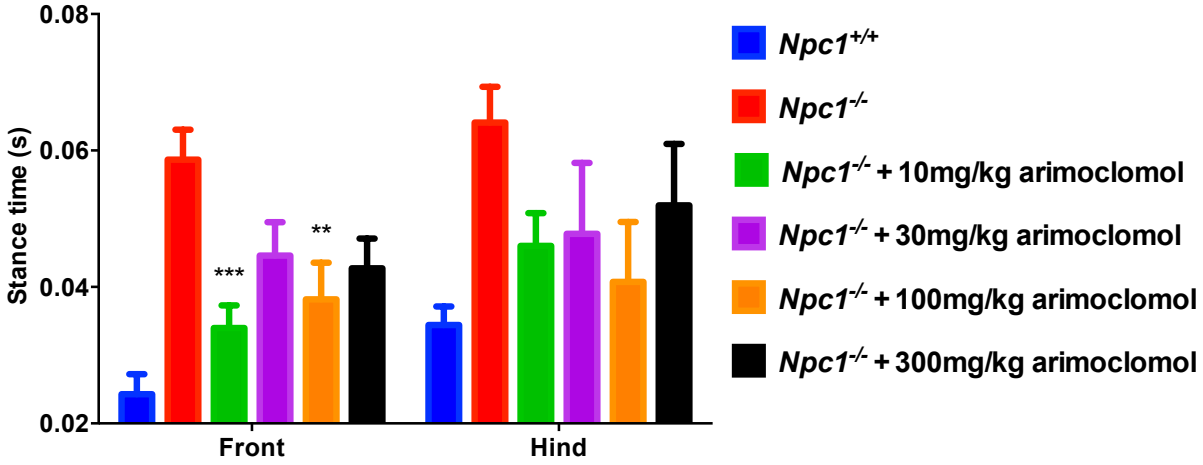


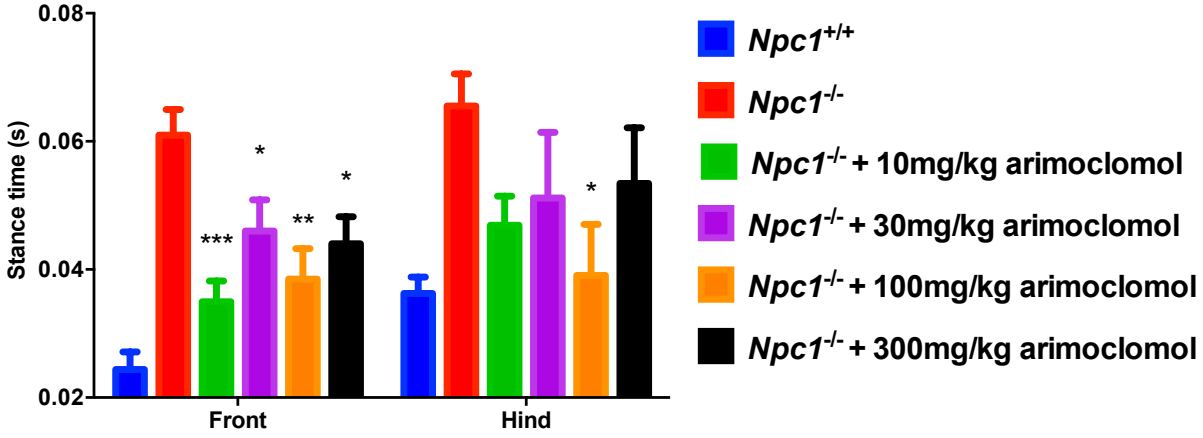
Figure 5.14: *Treatment with arimoclomol shows improvement in both front and hindpaw stand time* The stand time (time each paw is in contact with the plate per step) is significantly increased in *Npc1*$^{-/-}$ compared to *Npc1*$^{+/+}$. Treatment with arimoclomol improves the stand time of the mice, although only 10mg/kg and 100mg/kg arimoclomol reached significance compared to untreated *Npc1*$^{-/-}$ mice.
Npc1$^{+/+}$, n= 10., *Npc1*$^{-/-}$, n= 9., *Npc1*$^{-/-}$ + 10mg/kg arimoclomol n= 10., *Npc1*$^{-/-}$ + 30mg/kg arimoclomol n= 9., *Npc1*$^{-/-}$ + 100mg/kg arimoclomol n= 8., *Npc1*$^{-/-}$ + 300mg/kg arimoclomol n= 7. p= *<0.05, **<0.01, ***<0.001. Data was analysed using a one-way ANOVA with Dunnett's multiple comparison test.

of age, as would be expected as stand time also increases. Treatment with arimoclomol showed improvements in both initial **(Figure 5.15a)** and terminal **(Figure 5.15b)** dual stance, with the front paws showing the greatest response to treatment. Again, 10mg/kg appears to perform best, with the greatest reduction for the front paws, although 100mg/kg arimoclomol provides the greatest effects for the back paws.

Another parameter which is indicative of the abnormal gait is the step sequence and base of support of the animals. Step sequence in a normal mouse' walking pattern has been described in detail elsewhere [332], but typically consists almost solely of "alternate" patterns of moving both paws on one side of the body before switching to the other paws on the other side, (for example, LF → LH → RF → RH repeat), or moving diagonally placed paws (e.g. LF → RH → RF → LH repeat). The other walking pattern sometimes observed is a "cruciate" pattern of hopping forwards, using a repeating L → R, front then hind paw sequence (e.g. LF → RF → LH → RH repeat). This is typically seen in normal mice when stopping or initiating a walking sequence, and as such constitutes a small percentage of the walking pattern. An abnormal pattern which is rarely observed in normal mice is a "rotate" pattern whereby footfalls proceed



(a)



(b)

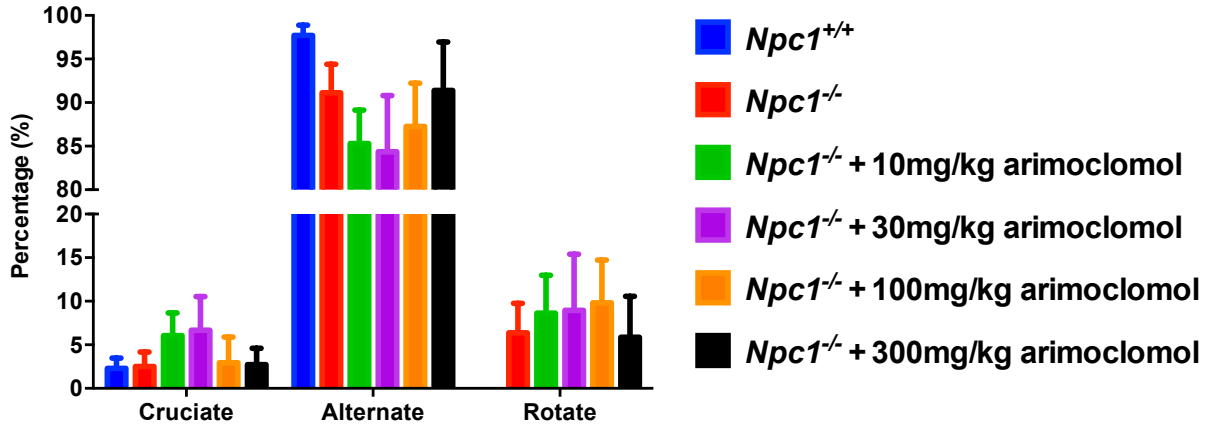
Figure 5.15: *Treatment with arimoclomol shows improvement in both initial and terminal dual stance times for both front and hind paws.* a) Initial and b) terminal dual stance times were significantly improved, particularly in the front paws, for both 10mg/kg and 100mg/kg arimoclomol treatment compared to untreated *Npc1*$^{-/-}$ mice, although 30 and 300mg/kg arimoclomol treatment also showed some improvements. *Npc1*$^{+/+}$, n= 10., *Npc1*$^{-/-}$, n= 9., *Npc1*$^{-/-}$ + 10mg/kg arimoclomol n= 10., *Npc1*$^{-/-}$ + 30mg/kg arimoclomol n= 9., *Npc1*$^{-/-}$ + 100mg/kg arimoclomol n= 8., *Npc1*$^{-/-}$ + 300mg/kg arimoclomol n= 7. p= *<0.05, **<0.01, ***<0.001. Data were analysed using one-way ANOVAs with Dunnett's multiple comparison test.

in a clockwise or anti-clockwise pattern (e.g. LF → RF → RH → LH repeat). At 7 weeks, both untreated *Npc1*$^{-/-}$ and *Npc1*$^{+/+}$ exhibited mainly alternate step patterns (98% and 91% respectively), and there was no significant change between untreated *Npc1*$^{-/-}$ and arimoclomol treated groups **(Figure 5.16a)**, although the percentage of alternate patterns did drop. There were no significant differences between any groups for either the cruciate or rotate patterns, although rotate patterns were not observed in any *Npc1*$^{+/+}$ mice **(Figure 5.16a)**. It may be the case that these patterns do not become fully apparent until later in the disease course.

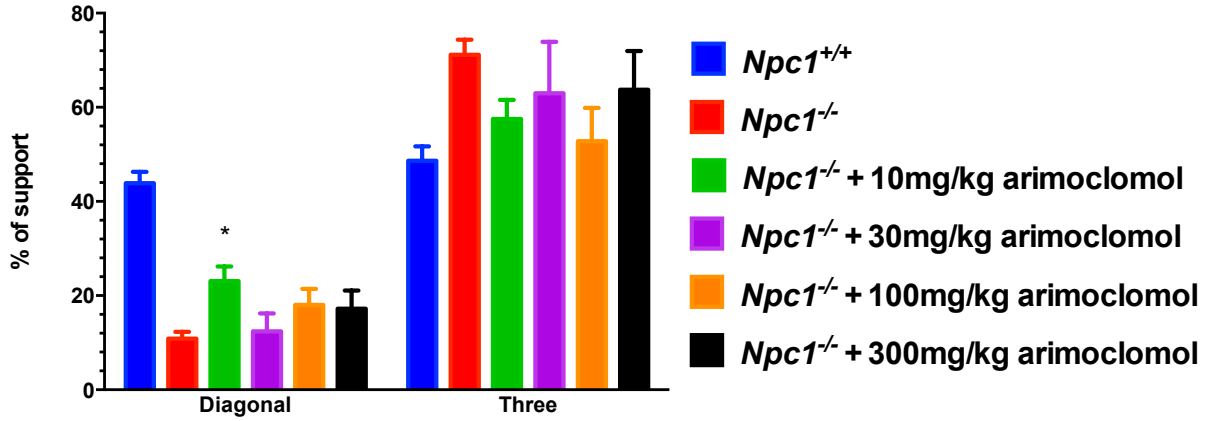
Support figures show the type of support the mice employ during each step cycle as a percentage. At 7 weeks *Npc1*$^{+/+}$ mice normal employ mainly diagonal and three paws in roughly equal proportion (49% and 44%) during each step cycle. In the untreated *Npc1*$^{-/-}$ groupd, the number of paw placements involving three paws increases to 70% and the diagonal paw placement decreases to 11% suggesting a requirement for greater support **(Figure 5.16b)**. Treatment of *Npc1*$^{-/-}$ mice with arimoclomol decreased the percentage of three paw support (non-significant) and increased the percentage of diagonal support, although this was only significant for the 10mg/kg arimoclomol treatment group **(Figure 5.16b)**.

5.6 Discussion

Arimoclomol (BRX-345) is an analogue of bimoclomol and a citrate salt of a previous formulation analogue (BRX-220). The parent compound bimoclomol has been shown to result in increased levels of HSP70 and HSP90 in the presence of cellular stress, but not eustress [350]. Bimoclomol and arimoclomol have displayed efficacy in several disease models including ALS [352], retinitis pigmentosa (RP) [353] and chemically induced diabetes [349, 354]. Bimoclomol has a halflife of 1 hour, whereas arimoclomol has a half-life of 4 hours [354]. Arimoclomol has been shown to delay disease progression in ALS mice [352] presumably by stabilisation of the trimerised active form of HSF-1, leading to increased levels of HSP70 and HSP90 in motor neurons of SOD-1 mice [352]. Treatment of *Npc1*$^{-/-}$ mice with arimoclomol, especially at the low doses of both 10mg/kg and 30mg/kg, provides significant improvement in both rearing behaviour and gait abnormalities associated with NPC disease progression. Mice treated with 30mg/kg arimoclomol performed significantly better than *Npc1*$^{-/-}$ in centre-rearing in both pilot **(Figure 5.5)** and follow-up



(a)



(b)

Figure 5.16: *Treatment with arimoclomol shows improvement in support stance, but not support style.* a) Support style did not show any improvement following treatment with arimoclomol compared to untreated *Npc1*$^{-/-}$ mice. b) Support stance was significantly improved, 10mg/kg arimoclomol treatment, although 30, 100 and 300mg/kg arimoclomol treatment also showed some improvements compared to untreated *Npc1*$^{-/-}$ mice.
Npc1$^{+/+}$, n= 10., *Npc1*$^{-/-}$, n= 9., *Npc1*$^{-/-}$ + 10mg/kg arimoclomol n= 10., *Npc1*$^{-/-}$ + 30mg/kg arimoclomol n= 9., *Npc1*$^{-/-}$ + 100mg/kg arimoclomol n= 8., *Npc1*$^{-/-}$ + 300mg/kg arimoclomol n= 7. p= *<0.05, **<0.01, ***<0.001. Data were analysed using multiple one-way ANOVAs with Dunnetts multiple comparison test.

study, as did the mice treated with 10mg/kg arimoclomol **(Figure 5.11)**. Whilst in the pilot study 300mg/kg arimoclomol also improved behavioural data **(Figure 5.5)**, particularly at the 8 week timepoint, this was not replicated in the follow-up study **(Figure 5.11)**. This may partly be explained by better scores seen in the untreated *Npc1*$^{-/-}$ mice in side rearing than the previous experiments.

In general, there appears to be a trend of decreasing efficacy in behavioural response to increasing dosage, as evidenced by gait analysis using the CatWalk system, whereby the lower doses generally performed better in all parameters measured **(Figures 5.13, 5.14, 5.15)**. This inverse dose-response may be partly explained by an interesting effect highlighted in the initial studies of the parent compound bimoclomol. Use of this compound *in vitro* also showed a similar dose-response [350]. Cells heat shocked at 42 ℃ displayed a prolonged trimerisation of HSF-1 at 90 minutes when pre-treated with 1µM bimoclomol. However, this effect on the HSR was diminished to a level comparable with untreated cells when the concentration was increased to 10µM [350]. The HSR is self-limiting under normal circumstances, due to the proposed mechansim by which the downstream HSPs inhibit the activity of HSF-1. HSP90 has been shown to maintain HSF-1 in the cytoplasm [251, 252, 253] as well as inhibiting the HSF1 coactivator Daxx[258]. HSP70 and HSP40 have also shown evidence of inhibition of HSF-1 [257]. It is thus a possibility that high doses of arimoclomol may be self-limiting in terms of inducing a heat-shock response. Indeed, studies of arimoclomol in ALS [352] and in chemically induced diabetes [354] have shown efficacy at doses below 30mg/kg.

Another interesting point is the significant increases in GSLs observed in both the forebrain and cerebellum following treatment with 300mg/kg arimoclomol but not 30mg/kg. In the forebrain **(Figure 5.10)** and cerebellum **(Figure 5.9)**, 300mg/kg arimoclomol displayed an approximately two-fold increase in GSL accumulation compared to controls, whereas 30mg/kg arimoclomol appeared to be tending towards reducing the accumulation. As the accumulation of GSLs in the CNS correlates with disease progression [168], this could explain the decreased efficacy of the higher dose, along with increased tremor **(Figure 5.6)**. It is not clear as to what causes the increase in GSLs in the CNS at the higher doses of arimoclomol but a possible explanation could be that high doses of arimoclomol may be driving the biosynthesis of GSLs

in the CNS, resulting in increased storage. An alternative mechanism could be through a decrease in degradation of lysosomal lipids. Interestingly, work showing that bimoclomol induces a heat-shock response through interaction with negatively charged membrane lipids in a manner which does not rescue unfolded proteins was performed with concentrations of 100µM bimoclomol [351] and it is unclear whether these effects also occur at lower doses. As such, high doses of arimoclomol may cause disruption of negatively charged lipids. The anionic phospholipid, BMP is integral to the functioning of lysosomal hydrolases and sphingolipid activator proteins [48], and is dependant on the negative charge of the lipid [49, 50]. Disruption of anionic lipid membranes within lysosomes could therefore result in decreased degradation of sphingolipid species, although it is unclear what the concentration of arimoclomol within the lysosome could be.

There was a different effect observed in the livers of *Npc1*$^{-/-}$ mice treated with arimoclomol, wherein both 30 and 300mg/kg doses resulted in modest decreases of GSL accumulation **(Figure 5.8)**. There are two possibilities which may explain this phenomenon. Firstly, a difference in the levels of stress experienced by the cells may mean that the liver may not be inducing as strong a HSR as cells in the CNS. In NPC, peripheral organs such as the liver, which although they store GSLs and lipids, do not have the same level of widespread cell death and inflammation, although by 56 days, TUNEL positive cells are detectable in the liver [357]. Inflammation is seen throughout the CNS by 2 weeks [155, 156] and neuronal death, axonal inclusions and widespread inflammation is observed by 4 weeks [156]. As the actions of arimoclomol are thought to be an augmentation of the endogenous HSR, rather than a simple induction, it may be that the differential GSL accumulation seen in the liver is simply a result of a reduced response to the arimoclomol treatment in this organ. Further experiments to assess the levels of the induction of HSPs in these organs would certainly help elucidate this as a possible mechanism.

Interestingly, a biphasic response to bimoclomol has been demonstrated in an *ex vivo* pharmacological assay on the its effects on the ryanodine receptor (RyR) in canine ventricular myocytes [358]. In isolated myocytes, action potentials were increased at low concentrations of 10nM, unaffected at 0.1-1µM and significantly decreased at concentrations above 10µM [358]. A similar effect was observed on isolated RyR incorporated into artificial bilayers, though the concentrations had shifted by an order of magnitude [358]. This biphasic effect was not due to the

effect on the SERCA pump, as concentrations of bimoclomol up to 1mM did not affect Ca^{2+} stimulated Ca^{2+} uptake. The rate of maximal response in these experiments was 5 minutes. As discussed in **Chapter 1**, NPC patient fibroblasts have been shown to have a sphingosine-dependant lysosomal calcium deficiency [7]. This is results in impaired lysosomal fusion events, and has been proposed as a mechanism by which NPC1 results in a broad range of storage lipids [7]. Treatment of both fibroblasts with curcumin, a modest naturally occuring SERCA inhibitor results in improvement of the lysosomal trafficking phenotype by increasing basal calcium levels, and *Npc1*$^{-/-}$ mice treated with curcumin display improvements in lifespan and rearing behaviour [7].

A biphasic effect on Ca^{2+} release from the sarcoplasmic reticulum via the RyR may be the cause of the biphasic effect in *Npc1*$^{-/-}$ mice in response to increasing levels of arimoclomol. An increase in calcium release from the SR, would in theory operate in a similar manner to curcumin, resulting in an improvement of lysosomal fusion events. Inhibition of the RyR with high doses of arimoclomol on the other hand may exacerbate the storage phenotype. The obvious question remains as to why a high dose of arimoclomol in the liver, which would, due to increased bioavailability induce an even more severe inhibition of the RyR displays a modest, yet significant decrease in storage. The RyR is expressed in 3 main splice variants. RyR1 is expressed in mainly in skeletal muscle, RyR2 predominantly in cardiac muscle, whilst RyR3 has been shown to be expressed widely on a variety of cell types [359, 360]. Interestingly, all 3 isoforms are expressed in the mammalian brain, of which the predominant isoform is RyR2 [360]. The liver expresses a truncated RyR1 which has been shown to lack direct calcium release properties in response to ryanodine, although it can induce calcium release in response to IP_3 [361]. These differences in RyR epression support the observed differences between liver and CNS accumulation of GSLs following high doses of arimoclomol.

Taken together, these data provide evidence that arimoclomol treatment at low doses provides therapeutic and survival benefits in the treatment of *Npc1*$^{-/-}$ mice. The improvements in behaviour were not replicated with treatment with the higher doses of arimoclomol, and this was accompanied by an increased accumulation of GSLs at 300mg/kg arimoclomol, suggesting that high doses of the drug may be inappropriate of NPC disease, due to inhibition of the RyR

at high doses of arimoclomol.

6 Arimoclomol & HSP70: Effects on Fabry and Sandhoff Disease

6.1 Sandhoff Disease

6.1.1 Introduction

Sandhoff and Tay-Sachs diseases are autosomal recessive metabolic disorders caused by differential isozyme mutations of the lysosomal hydrolase β-hexosaminidase. In humans, both Tay-Sachs and Sandhoff disease display severe neurological phenotypes such as cerebellar and motor neurone dysfunction, spasticity, muscle wasting and ataxia [362], the age of onset and severity of which are closely related to the residual activity of the mutated hydrolase. In addition to neurological symptoms, Sandhoff disease also presents with peripheral symptoms such as hepatosplenamegaly, and cardiac fibrosis. β-hexosaminidase is expressed as two isozymes, hexosaminidase A (Hex A) and B (Hex B), composed of either $\alpha\beta$ subunits, or $\beta\beta$ subunits respectively which are in turn encoded by the *Hexa* and *Hexb* genes. A and B isozymes share a similar capacity to degrade asialoGM2 (GA2) into LacCer, whereas only Hex A is able to degrade GM2 to GM3. The α subunit of Hex conveys specificity of the hydrolase for negatively charged substrates, whilst the β subunit hydrolyses uncharged substrates [43]. Whilst there is no current therapy licensed for Sandhoff disease, preclinical trials of both SRT, using miglustat [207], and bone marrow transplantation [183, 363] have show effects both individually and synergistically [184]. Similarly, gene therapy in a feline Sandhoff model has shown promising effects on reducing storage and increasing life expectancy [189].

In humans, Tay-Sachs disease and Sandhoff disease share a similarly severe neurological phenotype [364]due to a lack of activity of human sialidase on GM2, meaning that all GM2 must be

degraded by the Hex A isozyme, rendering α and β mutations phenotypically very similar [365]. In Tay-Sachs mice with *Hexa* mutations, the ability of the murine sialidase to convert GM2 to GA2, allows the still functioning Hex B isozyme to rescue the phenotype, and thus, whilst still showing abnormal GM2 accumulation, Tay-Sachs mice do not display neurological symptoms [365, 366]. Sandhoff mice ($HexB^{-/-}$) which are deficient in both isozymes display abnormal accumulation of both GA2 and GM2, severe neuronal and peripheral pathologies, which closely mimic the more severe infantile cases of Sandhoff and Tay-Sachs disease [365, 366].

$Hexb^{-/-}$ mice typically present with hindlimb weakness and gait abnormalities from 12 weeks of age, eventually resulting in near paralysis at around 16 weeks of age [362, 367]. These abnormalities closely follow the progression of storage of both GM2 and GA2 within the forebrain, cerebellum, dorsal root ganglion and spinal cord. Neurons in these regions display abnormal cellular anatomy such as meganeurite out growths, multivesicular bodies, and pleiomorphic cell bodies [362, 368]. Additionally, there is a degree of hypomyelination within the corpus callosum [368] and neural inflammation characterised by the infiltration of $CD68^{+}$ microglia [363].

Whilst the mechanism triggering neurodegeneration in Sandhoff disease is unclear, $Hexb^{-/-}$ mice display a calcium uptake deficiency mediated by the sarco/endoplasmic reticulum Ca^{2+}-ATPase (SERCA) [369]. Substrate reduction therapy using miglustat has shown significant benefits in a preclinical trial using the $Hexb^{-/-}$ mouse model. Treatment with miglustat reduces GM2 and GA2 accumulation in the CNS and periphery, as well as increasing life span by approximately 40% [207]. Improvements in the storage profiles of the CNS, were also apparent upon ultra-structural analysis of neurons, which displayed reduced storage burdens [207]. Treatment with miglustat also corrected the SERCA mediated calcium phenotype, and this appeared to be mediated via reductions in GM2 [369]. This appears to be specific for GM2 accumulation as GA2 does not appear to inhibit SERCA Ca^{2+} influx [370].

Having observed GSL reductions in the $NPC1^{-/-}$ mouse model, we hypothesised that treatment with Arimoclomol and rmHsp70 would result in improvements in behavioural phenotypes of $Hexb^{-/-}$ mice, alongside survival benefits and reductions in GSL accumulation.

6.1.2 Materials & Methods

Mice

The Sandhoff (*Hexb*$^{-/-}$) disease mouse model was provided by Dr Richard Proia (NIH). Mice were maintained by heterozygote brother/sister matings and recently fully backcrossed to C57B/6 background. The *Hexb*$^{-/-}$ mouse has a lifespan of approximately 14 weeks (the change in life span occurred post-backcross, resulting in a more severe phenotype) with neurological symptoms presenting at approximately 10 weeks of age. Mice were group housed in ventilated cages with irradiated food and bedding and autoclaved water available *ad libitum*. Control mice were *Hexb*$^{+/+}$generated from the same litters as the *Hexb*$^{-/-}$ mice. All animal studies were approved by the UK Home Office for the conduct of regulated procedures under license (Animal scientific Procedures Act, 1986).

Treatment

Three-week-old *Hexb*$^{-/-}$ mice were treated with 300mg/kg Arimoclomol (batch SAM-1111100001) in drinking water, protected from light or with injections of 3mg/kg rmHsp70 i.p. 3x weekly. 3-week-old *Hexb*$^{-/-}$ mice given normal drinking water and 3x weekly i.p. injections of PBS were used as control C57B/6 (*Hexb*$^{+/+}$) mice were used as baseline controls. Each group consisted of 10 mice (5M/5F). Mice were either sacrificed at 12 weeks of age for biochemistry (5 males from each group) or at the humane endpoint for survival (5 females from each group). Mice were weighed 3 times per week.

Horizontal Bar-Crossing

A horizontal barcrossing test was used to evaluate motor coordination and hind limb strength. Mice were trained from weaning age to acclimatise them to the barcrossing apparatus. Briefly, the mouse was held by its tail and allowed to grasp the centre of a suspended thin bar with only its forepaws, and after releasing the tail, the time to cross the bar from centre to one side post was determined. The maximum time given is 180 seconds, and mice start with a score of 180. Healthy mice take about 3-4 seconds to cross and are given a positive score of 180 minus crossing time (180 + 180 - crossing time = 360 -crossing time). As the disease progresses they

struggle to get their back legs onto the bar so the time increases, resulting in a decreasing score. When very sick they fall from the bar rather than cross it. Fall time (FT) is the time it takes to fall from when they are placed on the bar. This is results in a negative score (-180 + FT) being added to the starting score of 180. Therefore the closer the mouse scores to 360, the faster the mouse crossed the bar and the closer the score to 0, the faster the mouse fell from the bar.

Survival

Survival was measured in the female cohort of each group, a humane end point being applied when the mice became moribund and were no longer able to right themselves within 20 seconds of being laid on their side.

Tissue Processing for Biochemistry

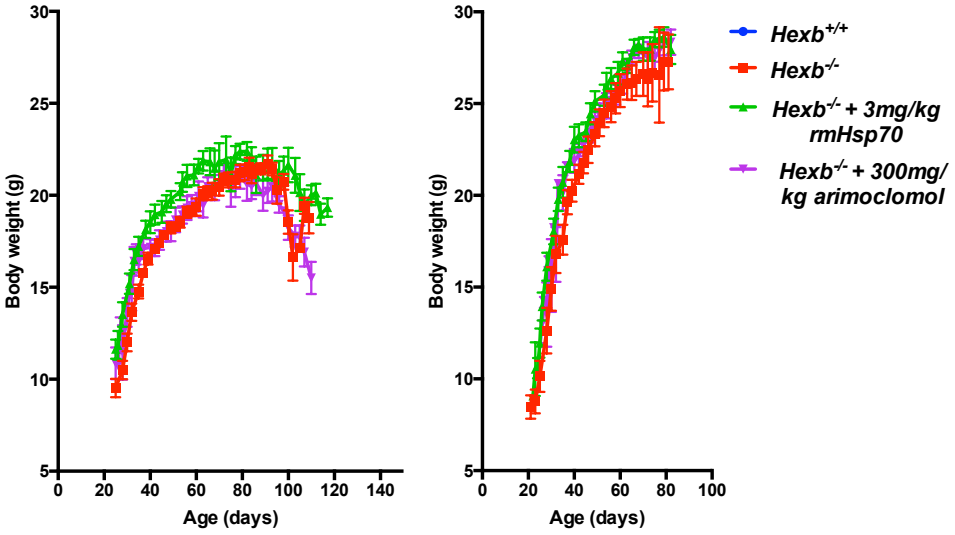
Mice were killed by asphyxiation in rising concentrations of CO_2 and perfused through the left cardiac ventricle with ice-cold phosphate-buffered saline (PBS). Brain, liver and spleens were removed and stored at -20 ℃ until needed. Brain and liver were homogenised with a glass Dounce homogeniser in ddH_2O at 10mg/ml wet weight.

All other methods were performed as described in **Chapter 2**.

6.1.3 Results

Weights

The body weights for female *Hexb*$^{-/-}$ mice showed no discerenable difference following treatment with 300mg/kg arimclomol **(Figure 6.1a)**. Although 3mg/kg treated *Hexb*$^{-/-}$ mice did put on more weight at their maximum, this could be due to a higher starting weight, however they did appear to lose weight more slowly than untreated control **(Figure 6.1a)**, although there are fluctuations in the weights due to the loss of mice reaching endstage. Male *Hexb*$^{-/-}$ mice treated with either compound showed no difference in their weights **(Figure 6.1b)**.



(a) (b)

Figure 6.1: *rmHsp70 and arimoclomol do not affect growth kinetics* Growth curves showing a) female absolute body weights and b) male absolute bodyweights. n= 5/group. Error bars are SEM. *Body weight data were provided by Dr K. Wallom. Analysis performed by J. Gray*

Survival

Untreated *Hexb*$^{-/-}$ develop hind-limb paralysis at the end stage of disease, which results in the mice not being able to feed, eventually leading to death. To preclude this, our humane end-point was set as the mice being unable to right themselves within 20 seconds of being laid on their side. Of the female mice taken to survival, the first untreated *Hexb*$^{-/-}$ mice started to reach endstage at 12 weeks and had a median survival of 15.1 weeks **(Figure 6.2)**. In comparison, *Hexb*$^{-/-}$ mice treated with 3mg/kg rmHsp70 and 300mg/kg arimoclomol began reaching end-stage at 16 weeks and had a median survival of 16.6 weeks and 16.4 weeks respectively (p=0.0018 for both curves) **(Figure 6.2)**. The significantly later onset of death in the treated mice indicates significant improvement of the disease phenotype.

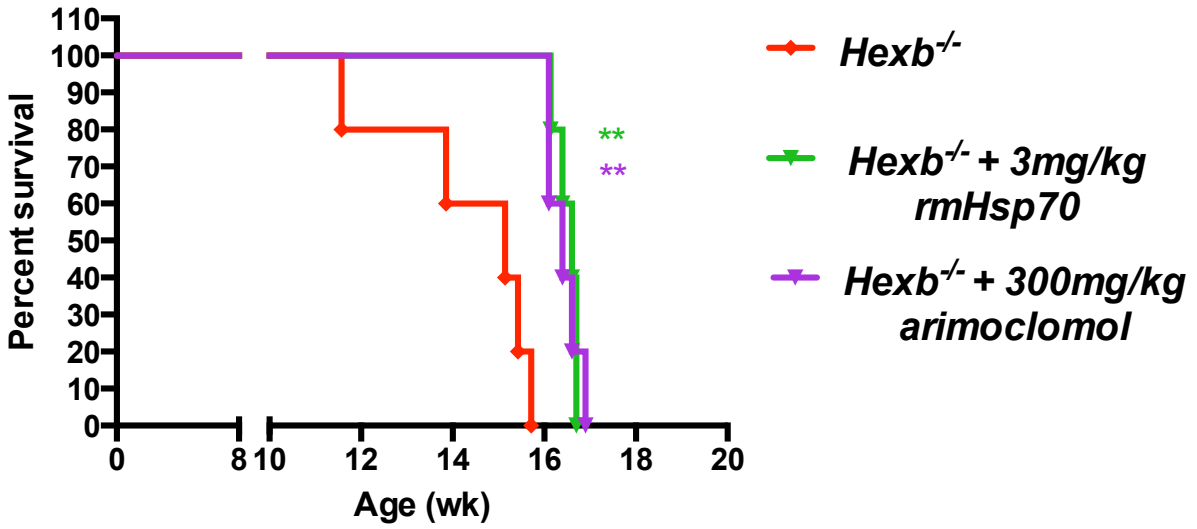


Figure 6.2: *Treatment with both 3mg/kg rmHsp70 and 300mg/kg arimoclomol significantly improves the survival of* Hexb$^{-/-}$ *mice* Kaplain-Meier plot of survival shows significant benefits of treatment with both rmHsp70 and arimoclomol. n=5/group. Data were analysed using Chi-squared comparison of curves. **,.$p<0.01$. *Survival data were provided by Dr K. Wallom. Analysis performed by J. Gray*

Rearing Behaviour

The loss of rearing ability is associated with disease progression in *Hexb*$^{-/-}$ mice, and treatment with miglustat has been shown to improve this phenotype [207]. Rearing was measured bi-weekly to assess whether there was any effect on the rearing behaviour following treatment with rmHsp70 or arimoclomol. Untreated *Hexb*$^{-/-}$ mice began to lose rearing ability compared to *Hexb*$^{+/+}$ controls from 8 weeks, although differences were observed as early as 6 weeks **(Figure 6.3)**. Treatment with either compound did not affect the rearing behaviour of *Hexb*$^{-/-}$ mice.

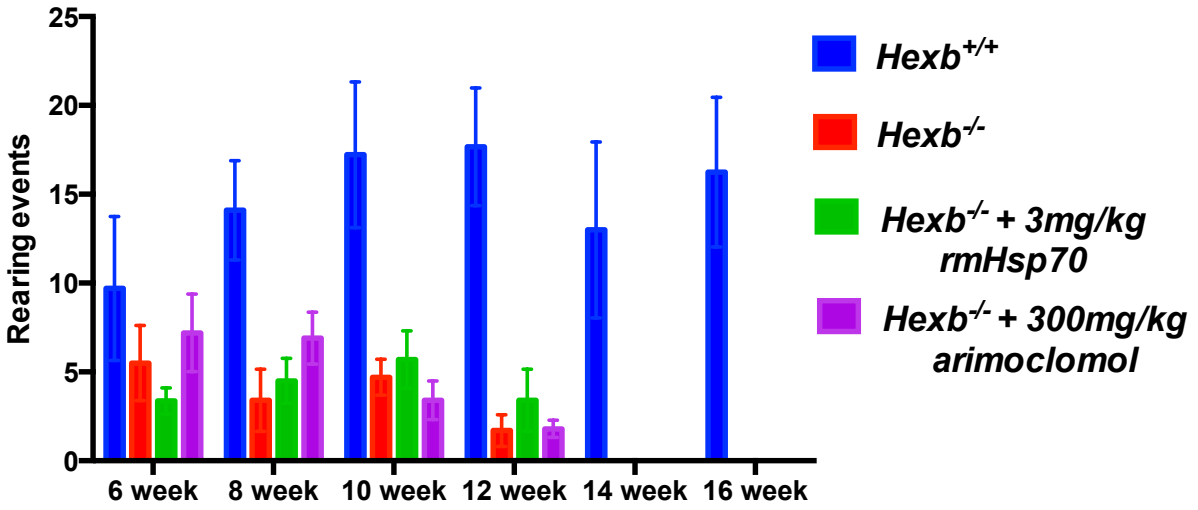


Figure 6.3: *Treatment with both 3mg/kg rmHsp70 and 300mg/kg arimoclomol does not improve centre-rearing ability of* Hexb$^{-/-}$ *mice* There were no observed differences in centre-rearing ability of either groups compared to untreated *Hexb*$^{-/-}$ mice. weeks 6-12, n= 10/group., week 14, n=5/group., week 16, *Hexb*$^{+/+}$ n= 5., *Hexb*$^{-/-}$ n= 2 *Hexb*$^{-/-}$ + 3mg/kg rmHsp70 n=4., *Hexb*$^{-/-}$ + 300mg/kg arimoclomol n= 5. This data was not normally distributed, and even following Log[Y+1] transformation, no normal distribution was attained. Error bars are SEM. *Rearing data were provided by Dr K. Wallom. Analysis performed by J. Gray*

Horizontal Bar-Crossing

Horizonal bar-crossing ability has been shown to be lost in *Hexb*$^{-/-}$ mice at approximately 100 days [207]. At this point untreated mice rapidly lose the ability to pull themselves onto the bar, and fall off, resulting in a rapid drop in score [207]. In this study *Hexb*$^{-/-}$ mice began to lose bar-crossing ability by 14 weeks, in accordance with previosuly published data [207] **(Figure 6.4)**. Treatment with either 3mg/kg rmHsp70 and 300mg/kg arimoclomol did not improve this. Although some 3mg/kg rmHsp70 mice did begin to fall off at 13 and 14 weeks, this was not statistically significant (p=0.601 & 0.757 respectively). Likewise the drop seen with 300mg/kg arimoclomol was not significant at 14 weeks (p=0.370) **(Figure 6.4)**.

GSL accumulation

The accumulation of the GSLs GM2 and GA2 are a hallmark of Sandhoff disease [111], and have been shown to accumulate significantly in both the CNS and liver [207]. Whilst CNS accumulation is reasonably thought to be the basis of neurological phenotypes [207], correction of

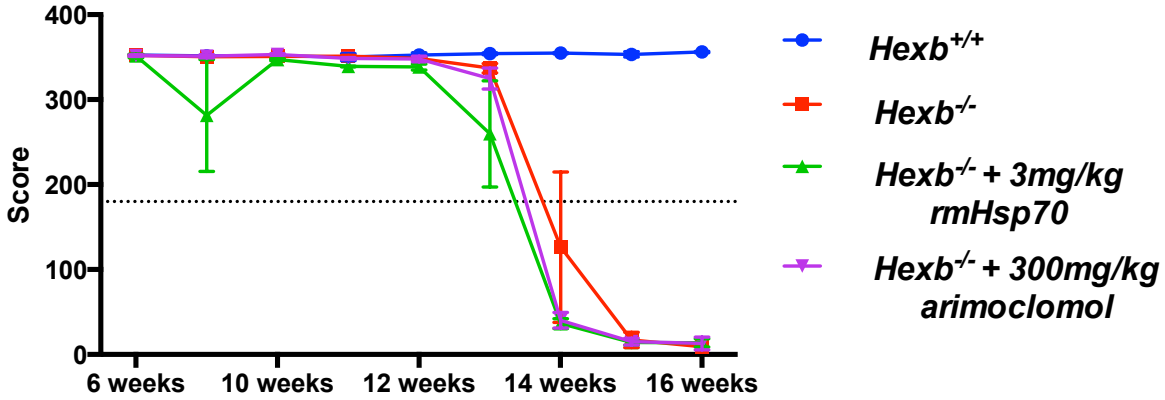
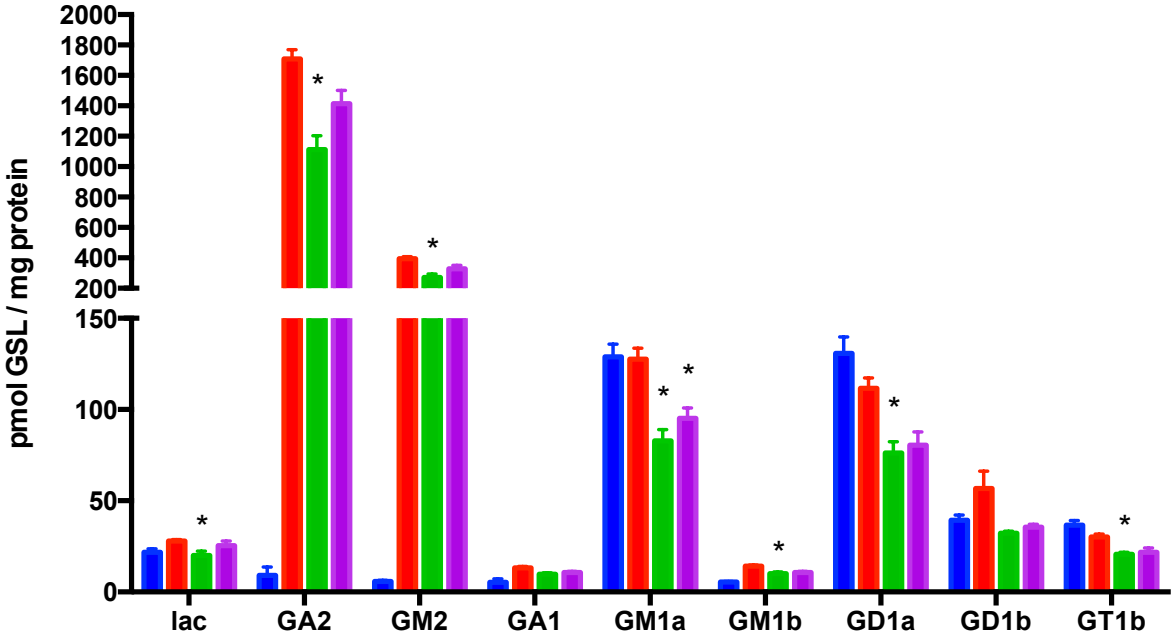


Figure 6.4: *Treatment with both 3mg/kg rmHsp70 and 300mg/kg arimoclomol does not improve centre-rearing ability of* Hexb$^{-/-}$ *mice* There were no observed differences in centre-rearing ability of either groups compared to untreated *Hexb*$^{-/-}$ mice. n= 10/group weeks 6-12, *Hexb*$^{-/-}$ n=5/group weeks 13-16., *Hexb*$^{-/-}$ n= 4 week 13., n= 3 week 14 & 15., n= 2 week 16. *Hexb*$^{-/-}$ +3mg/kg rmHsp70 n=5 weeks 13-15, n=3 week 16. *Hexb*$^{-/-}$ + 300mg/kg arimoclomol n=5 weeks 13-16. This data was transformed using Log[Y+1] transformation, to attain a normal distribution. Data was analysed using a two-way ANOVAs comparing untreated to each treatment group. Error bars are SEM. *Bar-crossing data were provided by Dr K. Wallom. Analysis performed by J. Gray*

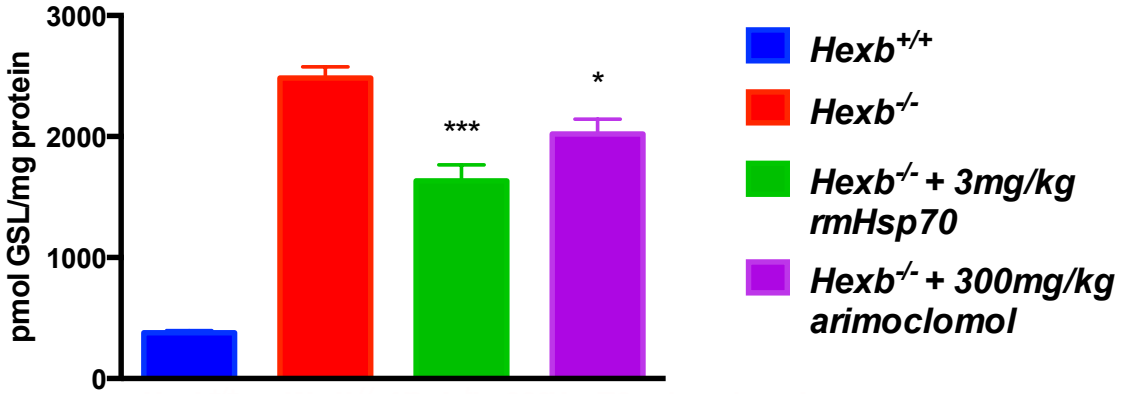
peripheral accumulation using bone-marrow transplantation in the *Hexb*$^{-/-}$ has shown significant benefits on survival without correcting CNS storage, although the prescence of bone-derived glial cells in the CNS may provide some cross-correction, or potential attenuated inflammation [183].

To assess whether treatment affected the CNS accumulation of both GA2 and GM2, we evaluated GSL accumulation in the male cohorts of mice treated with both 3mg/kg rmHsp70 and 300mg/kg. In the CNS we found significant reductions of GM2 (31%, p=0.0025) and GA2 (35%, p<0.001) GSL species in the brains of *Hexb*$^{-/-}$ mice treated with 3mg/kg rmHsp70. Surprisingly, we also observed significant reductions in all GSL species, including Lac (28%, p=0.013), GM1a (35%, p=0.00139), GM1b (35%, p=0.0071), GD1a (32%, p=0.00451) and GT1b (32%, p=0.00205), whilst reductions in GA1 (26%) and GD1b (43%) weren't significant (p= 0.025 and 0.058, respectively) **(Figure 6.5a)**. Treatment with 300mg/kg arimoclomol also displayed a similar pattern in GSL reduction. Although this only reached significance for GM1a (25%, p=0.00442), the following GSLs were also reduced; Lac (9%, p=0.374), GA2(17%, p=0.0245), GM2(17%, p=0.0454), GA1(19%, p=0.0487), GM1b(24%, p=0.00651), GD1a(29%, p=0.0104), GD1b(37%, p=0.0593) and GT1b(28%, p=0.0171) **(Figure 6.5a)**. Total brain

GSLs were significantly reduced for both treatments, with 3mg/kg rmHsp70 (34%, $p<0.001$) showing the greatest reduction of GSLs, whereas 300mg/kg arimoclomol reduced total GSLs by 19% ($p=0.0246$) **(Figure 6.5b)**.



(a)



(b)

Figure 6.5: *Treatment of* Hexb$^{-/-}$ *mice with both 3mg/kg rmHsp70 and 300mg/kg arimoclomol reduced CNS GSLs* a) Graph showing individual GSL species in the CNS. All individual GSL species were reduced following treatment, with rmHsp70 treatment showing the greatest effects. b) Total GSL burden in the CNS was also significantly reduced. Data were analysed using multiple Student's *t*-tests with Holm-Sidak corrections for multiple comparisons. Error bars are SEM. *, $p<0.05$., **$p<0.01$., ***, $p<0.001$. *GSL data was provided by Dr K. Wallom. Analysis performed by J. Gray*

In the liver, a different pattern of GSL accumulation was observed following treatment. Whilst treatment with 3mg/kg rmHsp70 resulted in a small, but non-significant reduction of GA2 (10% p=0.51), the levels of both Lac (150%) and Gb4 (134%) both increased significantly (p=<0.001 for both), whilst GM2 showed no change **(Figure 6.6a)**. Similar increases were also seen following arimoclomol treatment in both Lac (60%, p=0.065) and Gb4 (170% p=0.002), whilst no change in other GSLs were observed, although GA2 again showed a slight, non-significant decrease (10%, p=0.505) **(Figure 6.6a)**. In total, there was no change in total GSL accumulation in the livers of mice treated with either 3mg/kg rmHsp70 or 300mg/kg arimoclomol **(Figure 6.6b)** although there was a 5% drop in both treatment groups (p=0.768 and 0.680, respectively).

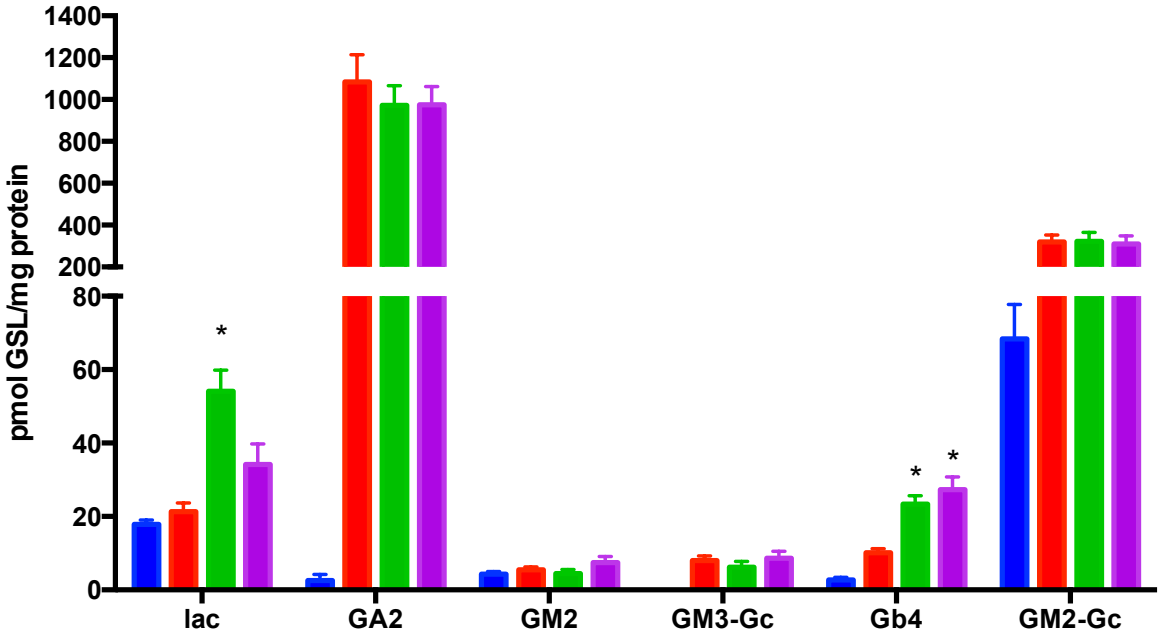
6.1.4 Lysosomal Volume Assay

To assess whether treatment with rmHsp70, or arimoclomol had any impact on lysosomal volume, we assessed LysoTracker staining of $CD19^+$ B cells using FACS. Treatment with 3mg/kg rmHsp70 resulted in a 20% reduction in LysoTracker staining (p=0.205) whereas treatment with 300mg/kg arimoclomol resulted in a 6% increase (p=0.754) **(Figure 6.7)**.

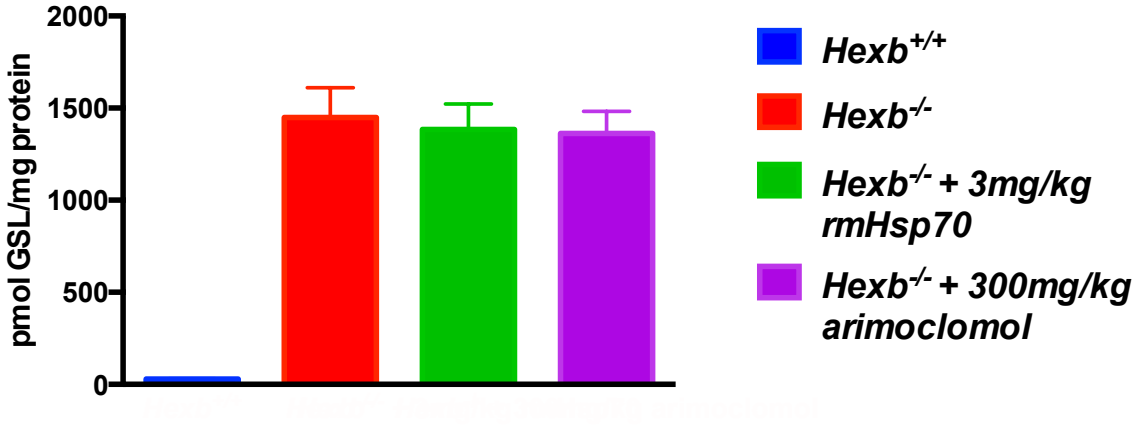
6.2 Discussion

Treatment with 300mg/kg arimcolomol showed a significant improvement in life expectancy of the *Hexb*$^{-/-}$ mouse **(Figure 6.2)**, which is in accordance with the arimoclomol data gathered for the *Npc1*$^{-/-}$ mouse. Treatment with rmHsp70 also resulted in an increase in life expectancy **(Figure 6.2)**. Although this was done with a murine, rather than a human, recombinant protein, this fits with the behavioural improvements seen in the *Npc1*$^{-/-}$ mouse following treatment with rhHSP70^{his} protein. Although neither treatment resulted in significant rearing **(Figure 6.3)** or bar crossing **(Figure 6.4)** behavioural benefits in the Sandhoff disease model, this could be clouded by the earlier deaths of untreated *Hexb*$^{-/-}$ mice, which presumably were more symptomatic, leaving the better performing, and thus surviving untreated animals in the study.

The increases in survival in both treatments correlate well with a reduction in CNS accumulation of GSLs **(Figure 6.5)**. Interestingly, not only were the accumulating species GM2 and GA2



(a)



(b)

Figure 6.6: *Treatment of* Hexb$^{-/-}$ *mice with either 3mg/kg rmHsp70 or 300mg/kg arimoclomol did not change liver GSLs* a) Graph showing individual GSL species in the liver. Only the GSL species GA2 showed a reduction with either treatment. All other species were unchanged or increased, such as lac and Gb4. b) Total GSL in the liver showed no overall change following treatment. Data were analysed using multiple Student's t tests with Holm-Sidak corrections for multiple comparisons. n= 5/group. Error bars are SEM. *, $p<0.05$. *GSL data was provided by Dr K. Wallom. Analysis performed by J. Gray*

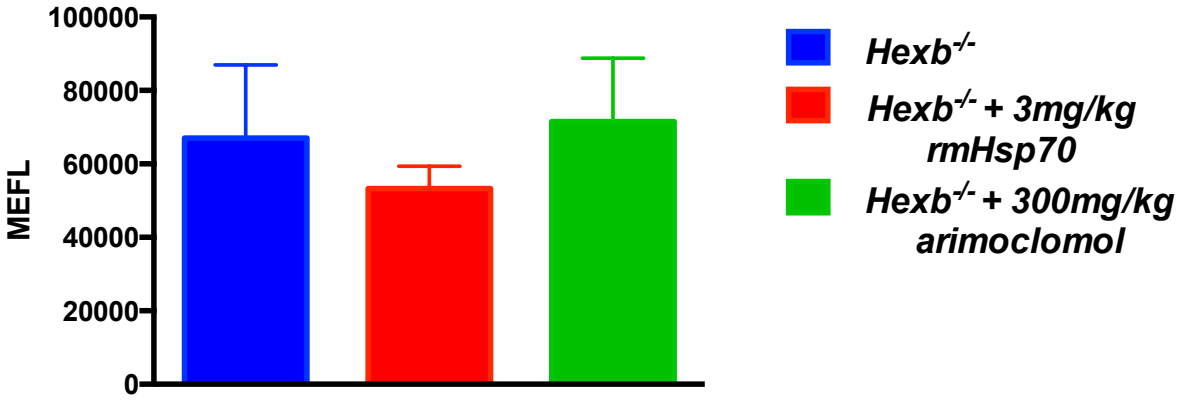


Figure 6.7: *Treatment of* Hexb$^{-/-}$ *mice with 3mg/kg rmHsp70 or 300mg/kg arimoclomol showed differing effects on lysosomal volume* Data were analysed using individual two-tailed Student's *t* tests comparing untreated *Hexb*$^{-/-}$ to each treatment. Untreated *Hexb*$^{-/-}$, n=3., *Hexb*$^{-/-}$ + 3mg/kg rmHsp70 n=5, *Hexb*$^{-/-}$ + 300mg/kg arimoclomol, n= 5. Error bars are SEM. *Lysotracker assay was performed and analysed by Dr K. Wallom.*

reduced (which were particularly significant in the 3mg/kg rmHsp70 treated group), but all GSL species within the CNS experienced similar reductions. Why this should be the case is unclear, but an increase in the activity of lysosomal hydrolases through increased interactions with the anionic phospholipid BMP would fit well with these data. Given that *Hexb*$^{-/-}$ mice are lacking in both HexA, ($\alpha\beta$) subunits, and HexB ($\beta\beta$ subunits), the question remains as to what hydrolase HSP70 may be affecting to reduce the accumulation of GM2 and GA2. A third isozyme of hexosaminidase exists, β-hexosaminidase S (HexS) ($\alpha\alpha$ subunits) [111]. Double knockouts of *Hexa* and *Hexb* displayed storage of glycosaminoglycans (GAGs) similar to an mucopolysaccharidosis phenotype in addition to the expected storage pattern of the GM2-gangliosidoses [365]. Further studies showed that HexS was able, in the prescence of BMP and GM2AP to remove 5'-GalNAc sulfated residues from lipids [371]. Additionally, *Hexb*$^{-/-}$ mice displayed residual enzyme activity of 2% for the synthetic substrate 4-methylbelliferyl-2-acetamido-2-deoxy-β-D-glucopyranoside (MU-GlcNAc) and also 4-methylbelliferyl-6-sulfo-2-acetamido-2-deoxy-β-D-glucopyranoside (MU-GlcNAc-6-SO_4) [365], in a preparation from *Hexb*$^{-/-}$ mouse liver. A later study showed that whilst the enzyme purified from mouse liver had 50 fold less activity for MU-GlcNAc, a recombinant HexS had an activity comparable to HexA for MU-GlcNAc, and a significantly higher activity than both HexA and HexB for MU-GlcNAc-6-SO_4. The differences between the activities of the purified and recombinant protein could be due to both the labile na-

ture of HexS [372] and the differences in activity (50 fold) of a mature and precursor form [371]. Physiologically, the role of HexS has been questioned, as it is expressed in much lower amounts than HexA and B in all tissues analysed. Additionally, the differences of activity between the mature and precursor proteins would further compound tissue specific differences. Whilst HexS could potentially reduce the levels of GM2 in the brain, the ability of HexS to reduce the storage of GA2 would be dependant of the activity of murine sialidase in the CNS. The Tay-Sachs mouse model, *Hexa*$^{-/-}$ displays no overt neurological symptoms, which is presumed to be due to the activity of murine sialidase activity within the CNS [365, 366]. Conversion of GM2 to GA2 by sialidase would potentially allow the activity of HexS to reduce the storage of both GM2 and GA2. In support of this, sialidase splice variants are expressed at moderate levels in the CNS [373]. This proposed mechanism would provide a route by which storage of GM2 could be degraded by the combined actions of sialidase and HexS, augmented by the increased binding of sialidase and the α-subunits of hexosaminidase to BMP as shown in **Chapter 3**. Certainly the increased binding to BMP by Neuraminidase 1 and β-hexosaminidase α subunit in the presence of HSP70 would support this as a possible mechanism.

In the liver, the major accumulating GSL was GA2, whilst GM2 accounted for less than 1% of the accumulating GSLs. There was only a very modest decrease (10%) in the levels of accumulating GA2 following treatment with 3mg/kg rmHsp70 **(Figure 6.6)**, which is perhaps surprising, given the increased penetration in the liver compared to the brain. We also observed significant increases in the levels of Lac and Gb4 in the liver following treatment with rmHsp70 whilst significant increases in Gb4 were observed following treatment with 300mg/kg arimoclomol. Whilst the increases in Lac and Gb4 are significant following rmHsp70 treatment, Gb4 is typically only detected on erythrocytes where, along with Gb3 and Lac, it is the main GSL [374]. Circulating erythrocytes are broken down by phagocytic cells such as Kuppfer cells in the liver, and the enzyme responsible for the degradation of Gb4 is hexosaminidase [34]. Whilst we see accumulation of Gb4 in the liver in untreated *Hexb*$^{-/-}$ mice presumably from lack of hexosaminidase activity, the cause of the further accumulation in mice treated with both arimoclomol and rmHsp70 is unclear as it could arise both from an increased uptake of erythrocytes in the liver, or from a reduced catabolism of Gb4 by hexosaminidase. As there is also a con-

current increase in Lac, this suggests that there may be an increase in the rate of erythrocyte degradation in treated mice. Previously published data has shown that the *Hexb*$^{-/-}$ mouse has macrocytotic red blood cells, indicated by increased mean corpuscular volume, red cell distribution width and haematocit, alongside a deficiency in iron homeostasis [375]. Further work to evaluate these parameters following treatment with HSP70 and arimoclomol could shed further light on whether we are affecting iron homeostasis in this disease.

The decreases observed in CNS GSL accumulation in *Hexb*$^{-/-}$ mice treated with the high dose of arimoclomol contrast sharply with the increases observed with this dose in the *Npc1*$^{-/-}$ mouse. As explained in the previous chapter, the inhibition of RyR by high doses of arimoclomol may partially explain this effect. As *Hexb*$^{-/-}$ mice display an increase in cellular calcium due to the inhibition of SERCA by GM2, an inhibition of the RyR receptor by high doses of arimoclomol may serve to attenuate this phenotype. Whether this would result in a decrease in CNS accumulation of GSLs is unclear as, of yet there is no evidence either way to suggest that the calcium dysregualtion in Sandhoff disease contributes to the storage of GSLs. Similarly to what was described in the previous chapter, the lack of a typical functioning RyR in the liver, may also explain the difference between the CNS and liver effects observed, and why they are similar between *Npc1*$^{-/-}$ mice and *Hexb*$^{-/-}$ mice at the high dose of arimoclomol.

6.3 Arimoclomol & HSP70: Effects on Fabry Disease

6.3.1 Introduction

Fabry disease is caused by a deficiency of the lysosomal hydrolase α-galactosidase-A (GalA) encoded by the *GALA* gene, located at Xq22 [127]. Whilst the classical form of Fabry disease in the general population is rare (1:117,000) [133], it is estimated that the true incidence could be much higher, due to heterogenous presentation of non-classical forms, resulting in misdiagnosis [134, 135]. Loss of function of this enzyme results in the accumulation of lipids containing terminal α-galactosyl sugar moieties within the LE/Ly system. A model of Fabry disease, using a GalA mutant mouse shows extensive storage in the epithelium and vasculature smooth muscle cells. However whilst male mice show early renal complications, they display only very mild

cardiac phenotype and suffer no survival or behavioural detriment [323, 376]. GalA mutant mice also accumulate Gb3 within the dorsal-root ganglia, and this is thought to correlate with the development of neuropathic pain in humans.

Current therapies for Fabry disease include enzyme replacement therapy (ERT) of the GalA enzyme, for which two current treatments are available, comprising agalsidase alpha (Replagal) and agalsidase beta (Fabrazyme), which have both been shown to have beneficial effects on disease course [177, 178]. However, many patients still experience long-term complications despite therapy [377], and the high cost of this therapy remains prohibitive. SRT using miglustat has also been tested in the Fabry disease mouse model, but the effects were limited to a modest correction of Gb3 in vascular endothelial cells [378].

6.3.2 Materials & Methods

Mice

The Fabry mouse model (kindly provided to us by Asok Kulkarni, NIH) was generated by targeted disruption of the emphGALA gene in C57BL/6 mice[323]. Hemizygous α-Gal A males ($Gala^{-/0}$) were bred with homozygouse females ($Gala^{-/-}$). The $Gala^{-/0}$ males had no/negligible α-Gal A activity in all tissues analysed, compared to normal measurable levels in wild-type C57/B6 mice. β-hexosaminidase activity in tissues was unchanged [323]. From this point, $Gala^{-/0}$ and $Gala^{-/-}$ mice will both be referred to as $Gala^{-/-}$ mice.

Treatment

Three-week-old male and female $Gala^{-/-}$ mice (4 males/4 females) were treated with 300mg/kg Arimoclomol (batch SAM-1111100001) in drinking water, protected from light or with injections of 3mg/kg rmHsp70 i.p. 3x weekly (4 males/4 females). 3-week-old $Gala^{-/-}$ mice given normal drinking water and 3x weekly i.p. injections of PBS were used as control (3 males/2 females).

Tissue Processing for Biochemistry

Mice were killed at 18 weeks by asphyxiation in rising concentrations of CO_2 and perfused through the left cardiac ventricle with ice-cold phosphate-buffered saline (PBS). Kidney, heart

and dorsal root ganglia were removed and stored at -20 ℃ until needed. Tissues were homogenised with a glass Dounce homogeniser in ddH_2O at 10mg/ml wet weight.

All other methods were performed as described in **Chapter 2**.

6.3.3 Results

GSL accumulation

Untreated *Gala*$^{-/-}$ mice show marked evelation of Gb3 at 18 weeks of age in kidney, heart and DRG tissue **(Figure 6.8)**. Treatment with 3mg/kg rmHsp70 showed a significant reduction in Gb3 accumulation, in kidney, heart and DRG **(Figure 6.8)**. The greatest decreases were observed in DRG (39%, p=0.0378) and kidney (31%, p=0.0447), which displayed the most marked storage, whilst the reduction in heart was 18% (p=0.0055).

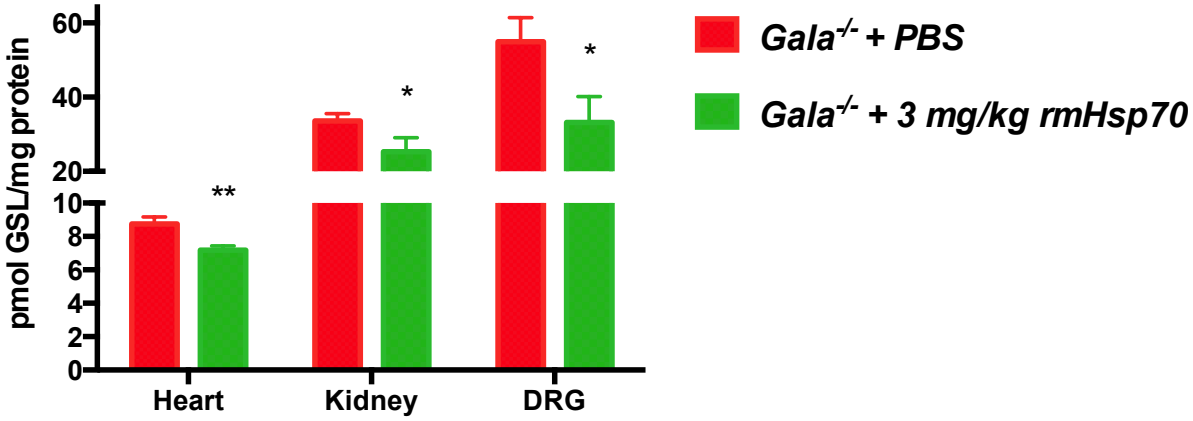


Figure 6.8: *Treatment of* Gala$^{-/-}$ *mice with 3mg/kg rmHsp70 significantly reduced Gb3 accumulation in all tissues analysed* Graphs showing absolute molar quantities of Gb3 in heart, kidney, and DRG. Gb3 accumulation was significantly decreased following treatment relative to untreated *Gala*$^{-/-}$ mice. n= 8/group. Data were analysed using unpaired two-tailed Student's t tests. Error bars are SEM. *, p<0.05., **, p<0.01. *Gb3 data was provided by Dr D.A. Priestman. Analysis performed by J. Gray*

Treatment with 300mg/kg arimoclomol shows a different effect on the storage of Gb3. The kidney showed a significant increase in the accumulation of Gb3 following treatment with 300mg/kg arimoclomol, corresponding to a 60% increase in this organ (p=0.0126) **(Figure 6.9)**. In the heart, there was no change (p=0.998) in the levels of accumulating Gb3 following treatment with arimoclomol **(Figure 6.9)**.

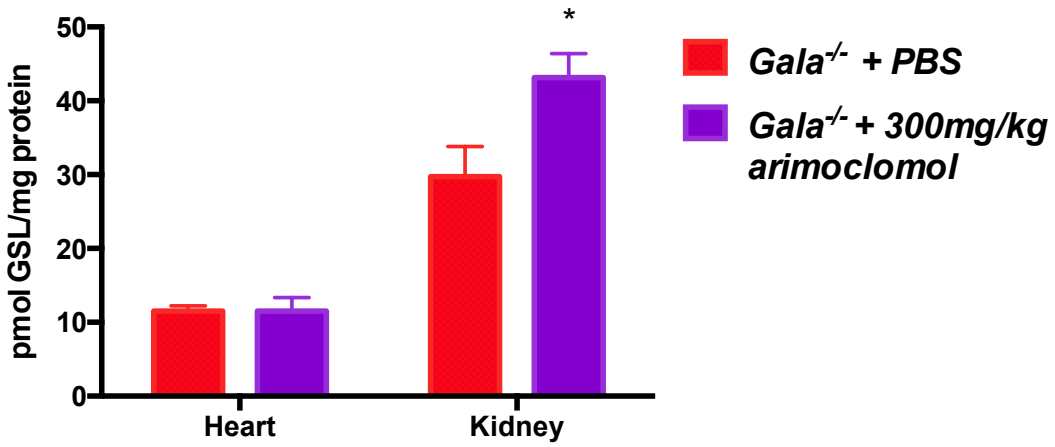


Figure 6.9: *Treatment of* Gala$^{-/-}$ *mice with 300mg/kg arimoclomol significantly increased Gb3 accumulation in kidney, whilst levels in the heart were unchanged* Graph showing absolute molar quantities of Gb3 in heart and kidney. Kidney of arimoclomol treated *Gala*$^{-/-}$ mice show a 60% increase in Gb3 accumulation upon treatment whereas heart Gb3 values are unchanged. n= 8/group. Data were analysed using unpaired two-tailed Student's t tests. Error bars are SEM. *$p<0.05$. *Gb3 data was provided by Dr D.A. Priestman. Analysis performed by J. Gray*

6.4 Discussion

Fabry disease is an X-linked inherited metabolic disorder arising from deficiencies in the lysosomal hydrolase GalA [137]. The prevalence of kidney and cardiac complications, along with a debilitating peipheral pain neuropathy associated with this disease result in significant disease burdens and early death [128]. Recent studies suggest that the incidence of Fabry disease maybe as high as 1:4000 in the general population [134, 135]. Despite the availability of two ERT treatments currently licensed for this treatment (fabrazyme and replagal), there still remains an urgent need for efficacious treatment of this disease, and its associated pathologies.

Deficiencies of GalA lead to the accumulation of Gb3 in a variety of tissues [136, 137], and although the mechanistic cause of the disease is unclear, it is presumed that accumulation of these lipids within tissues is the primary cause of cellular dysfunction, eventually leading to the complications arising in the affected organs [137]. The *Gala*$^{-/-}$ mouse displays accumulations of Gb3 comparable in distribution and magnitude to the hemizygous human form of Fabry disease [136, 137]. However, despite the accumulation of Gb3 closely mimicing the classical form of Fabry disease, *Gala*$^{-/-}$ mice remain remarkably asymptomatic, with the kidney being

the only organ affected, displaying only minor dysfunction [323, 376]. As such there are no useful behavioural and symptomatic tests in live *Gala*$^{-/-}$ mice. The treatment of *Gala*$^{-/-}$ mice with rmHsp70 lead to significant reductions in the levels of Gb3 in the kidney, liver ad DRG **(Figure 6.8a, b and c, respectively)**, and the greatest decreases in storage occurred in the kidney and DRG **(Figure 6.8d)**. Quite why the reduction observed in the heart was less, is unclear. However, storage of Gb3 in the *Gala*$^{-/-}$ mouse heart plateaus after 40 weeks (unpublished observations for our laboratory), and it has been suggested that an alternate galactosidase, *N*-actetylgalactosaminidase (NAGA) may be up regulated in this organ, partialy compensating for the loss of GalA [379]. These data corresponds to the reductions observed in the CNS and liver following rhHSP70$^{\text{his}}$ treatment in the *Npc1*$^{-/-}$ mouse model, and also to the reductions observed in the CNS in the *Hexb*$^{-/-}$ mouse.

In general, these data would support the role of HSP70 in facilitating the binding of lysosomal hydrolases to the anionic phospholipid BMP, as shown in NPA fibroblasts [163], although it is unclear whether the activity of GalA, or the putative activity of NAGA would be responsible. Whether the reduction of Gb3 results in the stabilisation of lysosomes in a similar manner is unclear, as this has not been a demonstrated phenotype in Fabry disease cells.

The use of arimoclomol showed altogether different effects on the accumulation of Gb3. In the kidneys of *Gala*$^{-/-}$ mice treated with 300mg/kg arimoclomol, an increase in Gb3 of 60% was observed, whereas the heart was unaffected **(Figure 6.9)**. As mentioned in previous chapters, a possible explaination of this effect could be that arimoclomol only augments rather than induces a HSR [350]. Therefore differential levels of stress experienced by storing cells may result in arimoclomol having no effect on cells which aren't actively inducing a HSR. As the kidney in the *Gala*$^{-/-}$ mouse displays some, albeit mild pathology whereas the heart is largely unaffected [323, 376], this could explain why the heart has no response. As to why arimoclomol causes an *increase* in the kidney, is unclear. It is also unclear as to whether this effect is due to upregulation of HSP70, or if there may some other contributing effect. As discussed previously in this chapter, and in **Chapter 4**, the biphasic effect of arimoclomol on the RyR may play a role in the increases observed following high doses of arimoclomol treatment, although there is no conclusive evidence of calcium dysfunction in Fabry disease. However, it remains to been

seen if reducing the dosage of arimoclomol may result in decreases in GSL storage in the $Gala^{-/-}$ mouse kidney. Additionally, given the role of arimoclomol as a HSR upregulator, a Fabry model which recapitulates the human clinical presentation may be required to see a true representation of arimoclomols effects. Unfortunately, such a model is currently unavailable.

In summary, HSP70 provides clear evidence of effects in reductions of GSL storage in the Fabry disease mouse model. Given the positive behavioural benefits observed in NPC disease, and survival effects observed in Sandhoff, and the generalised reductions of GSLs accompanying them, it seems that HSP70 provides a wide-acting mechanism for reducing GSL storage in these diseases. Arimoclomol, despite the increases in GSLs seen in Fabry disease, still holds promise as a therapeutic, given the benefits seen in models of NPC and Sandhoff disease, although further work needs to be carried out to acheive the optimal dosing strategy.

7 Discussion

7.1 Lysosomal Storage Disorders

Lysosomal storage disorders (LSDs) comprise a broad family of metabolic disorders, arising from the dysfunction of proteins integral to lysosomal function. The different LSDs present with a wide variety of symptoms, many of which have a severe neurological component. Due to the difficulties in delivering treatment to the CNS, treatment in most cases is limited to management of symptoms or slowing the disease progression.

Direct replacement of missing enzyme function by either ERT or BMT has worked particularly well at correcting the peripheral storage (non-neuronopathic Gaucher disease (type-I) is one success story for ERT), but difficulty of delivery to the CNS is poor, meaning that the neurological disease component goes almost completely untreated. While viral induced expression of recombinant proteins is an attractive therapeutic target, the issues of reliable gene expression, immunogenicity, and delivery to the brain without direct intrathecal injection, remain problematic for the development of successful gene therapy [194]. Additionally, ERT, BMT and GT are only appropriate therapies for soluble protein deficiencies, as there is no mechanism to implant membrane bound proteins through endocytosis of exogenous proteins, or via cross-correction.

SRT using the glucosyltransferase inhibitor *N*B-DNJ (miglustat), has shown significant clinical benefits in treatment of both type-I Gaucher disease [209] and NPC disease [210]. However, whilst this strategy provides some protection against the deleterious effects of substrate accumulation, without concurrent restoration of enzyme function, SRT only delays the onset of pathological events. When combined with therapies which also restore enzyme function, SRT and ERT operate synergistically [184, 380, 381].

Full restoration of the function of defective enzymes with the treatments currently in devel-

opment is unlikely to occur in the near future, particularly so within the CNS. It is likely that combinations of treatments to partially restore enzymatic function alongside SRT will provide the greatest benefits for patients.

7.2 Heat-Shock Therapies

The molecular machinery governing cellular proteostasis includes not only the molecular chaperones HSP70, HSP90, HSP60 and Hsc70, but also a wide range of co-chaperones and co-factors which assist in the folding and degradation of newly-synthesised and denatured proteins [231]. These proteins operate in a coordinated fashion to both determine and effect the fate of proteins within the cell.

Aberrant proteostasis has been implicated in a wide range of pathological disease states, including Parkinson's disease [382], amyloid lateral sclerosis [352], cystic fibrosis [306], and several lysosomal storage disorders [108, 304, 305, 383, 384]. Modulation of the heat-shock machinery in these states has provided proof-of-principle of the potential therapeutic benefit that modulation of the HSR, termed heat-shock therapy (HST) may play.

Missense mutation of $NPC1^{I1061T}$ results in the mutated protein being degraded through the actions of Hsp70 and CHIP [305] and treatment of fibroblasts carrying missense mutations for *NPC1* with the proteasome inhibitor prevented NPC1 ERAD and restored NPC1 function [304]. Furthermore, overexpression of HSP70 in $NPC1^{I1061T}$ mutant fibroblasts attenuated ERAD [305].

Further to the effects of HSP70 on ERAD, exogenous addition of HSP70 stabilises lysosomes and provides protection against LMP [311, 312]. A recent study showed that addition of HSP70 could protect the lysosome from increased susceptibility to LMP in NPA patient fibroblasts by increasing the binding of acid-sphingomyelinase to BMP, resulting in restoration of ASM activity [163]. As LMP has been shown to occur in a variety of LSDs, including NPC [315] both systemically administered HSP70 and the small molecule upregulator of the HSR, arimoclomol, were assessed for their potential in the treatment of NPC, Sandhoff disease and Fabry disease.

7.3 Heat-Shock Therapies: Effects of HSP70

We hypothesised that HSP70 treatment would be beneficial both in terms of phenotype and substrate accumulation in mouse models of NPC, Sandhoff and Fabry disease. The results of the findings are summarised in **Table 7.1**.

Due to the CNS pathology observed in many LSDs, including NPC and SD, for a treatment to be effective in these diseases, it needs access to the CNS and must cross the blood-brain barrier. In **Chapter 3** we first demonstrated that rhHSP70^{his} was able to penetrate the CNS and delivered to cell types in a pattern consistent with the previously observed distribution of the proposed HSP70 receptor, LRP1 [317]. HSP70 treatment was able to reduce the levels of accumulating GSLs in both NPC, Sandhoff and Fabry disease mice. The proposed mechanism by which HSP70 mediates GSL reduction is via increased GSL degradation through enhancing the activity of lysosomal hydrolases. HSP70, but not the HSP70^{W90F} mutant, increased the interactions of lysosomal hydrolases with BMP, as shown by studies on the binding of these enzymes in the presence of HSP70. Since the BMP-hydrolase interaction has been shown to be necessary for the activity of most lysosomal hydrolases, this greatly increases the potential impact of this treatment, and could be applicable to *all* hydrolase deficiencies. Given that the *Hexb* and *Gala* mice are completely deficient in their relevant enzymes, if the effects of HSP70 were mediated through its lysosomal hydrolase binding properties, HSP70 must be allowing alternative lysosomal hydrolases to compensate for these missing enzymes. It is thus likely then, that in cases where the patient has a reduced activity of the relevant hydrolase, HSP70 would have further beneficial effects, both by allowing degradation of substrate by alternative hydrolases, but also by potentially increasing the activity of the mutant hydrolase.

The improvement of myelination in the *Npc1*$^{-/-}$ cerebellum following treatment sets it apart from SRT as a therapy, and is an important consequence of treatment. The hypomyelination phenotype seen in NPC mice likely contributes toward the neuronal pathology observed in NPC, and as such may explain why without any apparent benefits to Purkinje cell survival, behavioural benefits are observed following rhHSP70^{his} treatment. Myelination is a tightly controlled process requiring axon-oligodendrocyte signalling. This pathway has been shown to be perturbed in *Npc1*$^{-/-}$ mice, and may occur as a result of decreased phosphorylation of the

Src-kinase family member, Fyn [172]. Fyn is required to mediate the axonal signalling through the β-integrin pathway [335]. Interestingly, activation of LRP1 by a variety of ligands has also been shown to result in intracellular signalling in a Src-family kinase dependant manner [320]. As the intracellular domain of LRP1 has been shown to bind Fyn [322] it is possible that binding of HSP70 to the LRP1 receptor induces a signalling cascade activating Fyn in oligodendrocytes. Exploration of this as a possible mechanism, could shed light on the potential roles that LRP1 signalling plays in myelination, and may open doors for HSP70 therapy in demyelinating disorders.

The frankly remarkable level of penetrance in the brain we observed with HSP70, the reductions in GSLs, as well as the hydrolase binding data obtained, suggests that possibly its best use would be in combination with ERT for therapies where an enzyme deficiency is the primary dysfunction. Tagging the replacement hydrolases with rhHSP70, could facilitate enhanced CNS delivery of the hydrolases, in conjunction with an enhancement of BMP binding and function. As seen in the hydrolase binding assay, the effects of rhHSP70 treatment are not universal, as out of the 6 proteins tested, hexosaminidase β subunit did not show a significant response. Full characterisation of the effects of HSP70 on the BMP binding of hydrolases, should be carried out to select the most promising candidate(s), once this has been selected, further *in vitro* work to establish this as a therapeutic concept should precede work in relevant *in vivo* disease models, for example in mice expressing common missense mutations.

However, there are significant drawbacks associated with the use of this protein as a long term therapy. Firstly, the development of significant antibody levels against both a his-tagged, and non-his tagged recombinant human HSP70 protein in the *Npc1*$^{-/-}$ mouse. Further experiments will need to be performed to discover if the antibody response is neutralising, whether this occurs with the recombinant mouse protein and, whether this is an effect specific to NPC disease, or LSDs in general. Obviously, chronic treatment of a patient producing a neutralising antibody response will not be efficacious, and may lead to other immune complications. An exacerbated loss of cerebellar Purkinje cells in *Npc1*$^{-/-}$ mice, as a consequence of treatment is a further worry. Although this didn't reach significance, any deleterious effects need fully investigating. If an increase of cerebellar volume is skewing the results, through either increased

Disease Model	Protein	Dosage	Behavioural Improvement	Survival Improvement	Peripheral GSL Accumulation	CNS GSL Accumulation	ADA
NPC1	rhHSP70$^{\text{his}}$	0.3mg/kg	$+$	*n/a*	*n/a*	*n/a*	$+$
		1.5mg/kg	$++$	*n/a*	*n/a*	*n/a*	$++$
		3mg/kg	$+++$	*n/a*	$\downarrow^*$	$\downarrow^*$	$+++$
	rhHSP70$^{\text{non-his}}$	3mg/kg	–	–	*n/a*	*Lac:* $\uparrow^*$ *others:* $\downarrow$	$++++$
Sandhoff	rmHsp70	3mg/kg	–	*2 weeks**	*Lac, Gb4:* $\uparrow^*$ *others :* –	$\downarrow^*$	*n/a*
Fabry			*n/a*	*n/a*	*kidney :* $\downarrow^*$ *heart :* $\downarrow^*$ *DRG :* $\downarrow^*$	*n/a*	*n/a*

Table 7.1: Table showing a summary of our experiences with arimoclomol in the different disease models. $\uparrow$ *indicates increase,* $\downarrow$ *indicates decrease,* – *indicates no change, n/a indicates that no such measurement was taken, * indicates that at least one outcome showed significance, increasing +'s mean increasing effect.*

mitosis in development or improved myelination, future studies may need to use complete counts of cerebellar Purkinje cells to try to control for any differences in cerebellar volume. In addition to the medical factors, the potential cost of a chronic therapy of protein infusions may be very high, especially if used in conjunction with existing ERT methods. A further issue is patient compliance, and feasibility of treatment; if a patient needs multiple monthly/weekly infusions at a medical centre, this places a high burden on patients and their families.

7.4 Heat-Shock Therapies: Effects of Arimoclomol

As discussed in **chapter 4**, the activation of the HSR by the small molecule arimoclomol presents an attractive prospect as a potential therapy for LSDs. It is well tolerated and has passed Phase-I safety trials in humans, and gives a high distribution to the CNS [355]. Arimoclomol and its analogue bimoclomol are proposed to work by increasing the trimerisation of the transcription factor, HSF1 driving an increased HSR under conditions of stress [350]. The induction of HSPs through the actions of arimoclomol could provide benefits to the treatment of LSDs by the driving the production of HSPs, potentially helping rescue mutated enzymes from ERAD, and through the BMP-binding activity of HSP70 within lysosomes.

Disease Model	Dosage	Behavioural Improvement	Survival Improvement	Peripheral GSL Accumulation	CNS GSL Accumulation
NPC1	30mg/kg	*yes**	*+2 weeks**	*liver:* ↓	*cereb:* ↓ *forebrain:* –
	300mg/kg	*yes**	*+2 weeks**	*liver:* ↓*	*cereb:* ↑* *forebrain:* ↑*
Sandhoff	300mg/kg	*no*	*+2 weeks**	–	↓*
Fabry	300mg/kg	*n/a*	*n/a*	*heart:* – *kidney:* ↑*	*n/a*

Table 7.2: Table showing a summary of our experiences with arimoclomol in the different disease models. ↑ *indicates increase,* ↓ *indicates decrease,* – *indicates no change, n/a indicates that no such measurement was taken, * indicates that at least one outcome showed significance.*

In **chapter 4** we tested the effects of various doses of arimoclomol on *Npc1*$^{-/-}$, *Hexb*$^{-/-}$, and *Gala*$^{-/0}$/$^{-/-}$ mice The findings of these studies are summarised in **table 7.2**. We found a significant increase in survival of *Npc1*$^{-/-}$ mice treated with arimoclomol, which was replicated

with our studies in the *Hexb*$^{-/-}$ mouse in **chapter 5**.

Npc1$^{-/-}$ mice displayed significant benefits in rearing behaviour at the low doses of arimoclomol compared to the high dose, correlating with reductions seen in CNS GSL accumulation at the 30mg/kg dose, and large increases seen at the 300mg/kg dose. However, a different pattern of GSL accumulation was observed in the livers of treated *Npc1*$^{-/-}$ mice. We hypothesised that this could be due to one, or a combination of factors;

1. Differential levels of organ stress, between liver, forebrain and cerebellum, may result in a varying HSR up-regulation.

2. Off-target effects of high doses of arimoclomol: increasing GSL biosynthesis, or interfering with anionic lipid membranes important for degradation, may increase the storage of accumulating lipids.

3. The inhibitory effects of high doses of bimoclomol on the sarcoplasmic reticulum calcium channel, the ryanodine receptor.

A further clue as to the potential mechanism behind arimoclomol's differing effects, came from our studies in the *Hexb*$^{-/-}$ mouse. In contrast to the *Npc1*$^{-/-}$ mouse, 300mg/kg arimoclomol treatment of *Hexb*$^{-/-}$ mice resulted in significant decreases in brain GLS accumulation, but again, little change in the liver accumulation was observed. If indeed higher stress levels were behind the increase in CNS GSLs in the *Npc1*$^{-/-}$ mouse, one might expect similar levels of stress to be experienced in the *Hexb*$^{-/-}$ CNS as they share a similarly severe neurodegenerative phenotype. Similarly, if off-target effects of GSL biosynthesis, or a disruption of anionic degradative membranes were the cause, a similar effect would likely be observed in both disease models.

Given that the two models have essentially the opposite calcium phenotype, if would seem that the 3rd mechanism fits our data best. In NPC disease, endocytic transport is blocked by a depleted intra-lysosomal calcium store, inhibiting LE/Ly fusion events. In this model, low doses of arimoclomol in NPC disease would stimulate the RyR, and raise intracellular calcium, partially compensating for reduced lysosomal calcium. Inhibition with high doses of arimoclomol would inhibit SR calcium release, and exacerbate the NPC phenotype. Conversely, in Sandhoff disease, where there is an inhibition of the SERCA pump, and constitutively raised intracellular

calcium, inhibition of the RyR could lower the cytosolic calcium levels, potentially correcting this phenotype.

Correspondingly with the data in the CNS, are the differential expression of the RyRs. In the brain, multiple types are expressed. In the liver however, no true RyR is detected, potentially explaining why the dose causes such variable results between the liver and the CNS. Similar increases seen in kidney, and DRG in Fabry disease, may indicate the prescence of an as yet unidentifed calcium deficiency in this disorder.

In summary, arimoclomol therapy has shown efficacy at treating both NPC disease, and Sandhoff disease mice, although the differences in dose response remain to be elucidated. Given the high tolerability of this compound, and its current stage of clinical development, it certainly warrants further development, although the mechanism behind the differing dose-responses should be thoroughly explored. Initial studies of the effects of arimoclomol doses on calcium release in LSD should be undertaken to assertain, at least in principle that arimoclomol can affect this *in vitro*, and how best to characterise this response. Further studies on animal models with respect to the most efficacious dosing strategies would then be needed.

7.5 Current Therapies

Whilst there is only one currently licensed treatment available for NPC (miglustat), clinical trials are currently underway using intra-thecal injections of cyclodextrin, having shown great efficacy in both cat and mouse models of the disease.

In comparison to these therapies, both HSP70 and arimoclomol have relatively modest effects on behaviour and survival in *Npc1*$^{-/-}$ mice, as well as comparitively small effects on GSL and cholesterol accumulation. Cyclodextrin and miglustat both provide significant protection against Purkinje cell loss, and are able to improve behaviour and survival to a much greater extent than arimoclomol and HSP70. One advantage of HSP70 over miglustat is its effects on myelination. However, whilst miglustat does not affect myelination [212, 213], cyclodextrin does improve myelination in *Npc1*$^{-/-}$ mice [217, 218] with greater efficacy than that observed with HSP70. It is unclear, given the high doses of cyclodextrin and invasive procedures required for this effect, whether this will be well tolerated in humans over the course of the treatment.

Whilst it appears that HSP70 itself is able to improve lysosomal hydrolase function in NPC disease, this correction, at least at the levels observed, is not sufficient to protect against the pathological events associated with disease progression. As the causative pathological event in NPC disease is still unclear, it may be that the accumulation of GSLs, whilst probably toxic at some level, does not play a major and defining role in the pathology of NPC, indeed GM2/GD2 (*Galgt1*$^{-/-}$) and GM3 (*Sial9*$^{-/-}$) synthase null mutants backcrossed with *Npc1*$^{-/-}$ mice (*Npc1*$^{-/-}$/ *Galgt1*$^{-/-}$ and *Npc1*$^{-/-}$/ *Sial9*$^{-/-}$, respectively) showed only minor changes in behavioural defecits, despite full reductions in storage of gangliosides [385]. This is not to say that corrections of GSL accumulation will not be of benefit, as *Npc1*$^{-/-}$/ *Sial9*$^{-/-}$ mice displayed a significantly reduced life expectancy. However, without correction of the causative dysfunction, it appears any relief of secondary accumulations may only provide limited benefits. In the primary lipidoses, there may be greater opportunity for correction, given that most of these disorders do have residual levels of enzyme function. Particularly important is the greatly enhanced CNS availability of HSP70 when delivered peripherally, when compared to peripherally delivered ERT.

7.6 Future Directions

Treatment with HSP70 has shown partial efficacy in reducing the accumulation of lysosomal substrates in three LSDs, but it remains to be proved that these are indeed the effects of increased binding of lysosmal hydrolases to BMP. If this were the case, further investigation of these proteins in combination with existing therapies would be warranted. It is likely that a synergistic effect between HSP70 and SRT would occur, as if the model of a toxic storage 'threshold' were to hold true, these two therapies should complement each other well. Additionally, the use of HSP70 to augment the activity of replacement enzymes could also show a distinct improvement in the activity of these replacement enzymes. Given the capacity for HSP70 to bind LRP1 and be delivered to the brain with frankly, remarkable efficacy, a potential role of HSP70 tethered to lysosomal hydrolases, could improve both the delivery and functional capacity of ERT.

Arimoclomol has also shown surprising effects, and the dose range of this treatment needs to be properly characterised in each model, with particular focus on the induction of HSPs, and how this is contributing to the different effects. If indeed arimoclomol also modulates calcium

release through the RyR, this may provide benefits to LSDs with calcium dysregulation as a central pathological event. Conversely, any secondary effect to the induction of the HSR, may mean result in problems acheiving an effective therapeutic dosage.

Bibliography

[1] AH. Merrill, E. Wang, RE. Mullins, WC. Jamison, S. Nimkar, and DC. Liotta. Quantitation of free sphingosine in liver by high-performance liquid chromatography. *Analytical biochemistry*, 171(2):373–381, 1988.

[2] H. Fyrst, DR. Herr, GL. Harris, and JD. Saba. Characterization of free endogenous c14 and c16 sphingoid bases from drosophila melanogaster. *Journal of lipid research*, 45(1):54–62, 2004.

[3] X. He, Y. Huang, B. Li, C. Gong, and EH. Schuchman. Deregulation of sphingolipid metabolism in alzheimer's disease. *Neurobiology of aging*, 31(3):398–408, 2010.

[4] C. De Duve and R. Wattiaux. Functions of lysosomes. *Annual review of physiology*, 28:435–492, 1966.

[5] P. Saftig and J. Klumperman. Lysosome biogenesis and lysosomal membrane proteins: trafficking meets function. *Nature reviews molecular cell biology*, 10(9):623–635, 2009.

[6] C. Settembre and A. Ballabio. Lysosomal adaptation: how the lysosome responds to external cues. *Perspectives in biology*, 6(6):1–15, 2014.

[7] E. Lloyd-Evans, AJ. Morgan, X. He, DA. Smith, E. Elliot-Smith, DJ. Sillence, GC. Churchill, EH. Schuchman, A. Galione, and FM. Platt. Niemann-pick disease type c1 is a sphingosine storage disease that causes deregulation of lysosomal calcium. *Nature medicine*, 14(11):1247–1255, 2008.

[8] FR. Maxfield and TE. McGraw. Endocytic recycling. *Nature reviews. molecular cell biology*, 5(2):121–132, 2004.

[9] P. Ghosh, NM. Dahms, and S. Kornfeld. Mannose 6-phosphate receptors: new twists in the tale. *Nature reviews. molecular cell biology*, 4(3):202–212, 2003.

[10] JS. Bonifacino and J. Lippincott-Schwartz. Coat proteins: shaping membrane transport. *Nature reviews. molecular cell biology*, 4(5):409–414, 2003.

[11] T. Braulke and JS. Bonifacino. Sorting of lysosomal proteins. *Biochimica et biophysica acta*, 1793(4):605–614, 2009.

[12] JP. Luzio, V. Poupon, MR. Lindsay, BM. Mullock, RC. Piper, and PR. Pryor. Membrane dynamics and the biogenesis of lysosomes. *Molecular membrane biology*, 20(2):141–154, 2003.

[13] T. Shintani and DJ. Klionsky. Autophagy in health and disease: a double-edged sword. *Science*, 306(5698):990–995, 2004.

[14] NM. Dahms and MK. Hancock. P-type lectins. *Biochimica et biophysica acta*, 1572(2-3):317–340, 2002.

[15] E. van Meel and J. Klumperman. Imaging and imagination: understanding the endo-lysosomal system. *Histochemistry and cell biology*, 129(3):253–266, 2008.

[16] G. Sun-Wada, Y. Wada, and M. Futai. Lysosome and lysosome-related organelles responsible for specialized functions in higher organisms, with special emphasis on vacuolar-type proton atpase. *Cell structure and function*, 28(5):455–463, 2003.

[17] RF. Murphy. Maturation models for endosome and lysosome biogenesis. *Trends in cell biology*, 1(4):77–82, 1991.

[18] RC. Piper and JP. Luzio. Late endosomes: sorting and partitioning in multivesicular bodies. *Traffic*, 2(9):612–621, 2001.

[19] JP. Luzio, SR. Gray, and NA. Bright. Endosome-lysosome fusion. *Biochemical society transactions*, 38(6):1413–1416, 2010.

[20] NA. Bright, MJ. Gratian, and PJ. Luzio. Endocytic delivery to lysosomes mediated by concurrent fusion and kissing events in living cells. *Current biology*, 15(4):360–365, 2005.

[21] GF. van der Goot and J. Gruenberg. Intra-endosomal membrane traffic. *Trends in cell biology*, 16(10):514–521, 2006.

[22] JH. Hurley and SD. Emr. The escrt complexes: structure and mechanism of a membrane-trafficking network. *Annual review of biophysics and biomolecular structure*, 35:277–298, 2006.

[23] W. Mabius, A. van Donselaar, Y. Ohno-Iwashita, T. Shimada, HFG. Heijnen, JW. Slot, and HJ. Geuze. Recycling compartments and the internal vesicles of multivesicular bodies harbor most of the cholesterol found in the endocytic pathway. *Traffic*, 4(4):222–231, 2003.

[24] R. Zoncu, L. Bar-Peled, A. Efeyan, S. Wang, Y. Sancak, and DM. Sabatini. mtorc1 senses lysosomal amino acids through an inside-out mechanism that requires the vacuolar h(+)-atpase. *Science*, 334(6056):678–683, 2011.

[25] L. Bar-Peled and DM. Sabatini. Regulation of mtorc1 by amino acids. *Trends in cell biology*, 24(7):400–406, 2014.

[26] Y. Sancak, L. Bar-Peled, R. Zoncu, AL. Markhard, S. Nada, and DM. Sabatini. Ragulator-rag complex targets mtorc1 to the lysosomal surface and is necessary for its activation by amino acids. *Cell*, 141(2):290–303, 2010.

[27] C. Settembre, A. Fraldi, DL. Medina, and A. Ballabio. Signals from the lysosome: a control centre for cellular clearance and energy metabolism. *Nature reviews molecular cell biology*, 14(5):283–296, 2013.

[28] JA. Martina and R. Puertollano. Rag gtpases mediate amino acid-dependent recruitment of tfeb and mitf to lysosomes. *The Journal of cell biology*, 200(4):475–491, 2013.

[29] Carmine Settembre, Chiara Di Malta, Vinicia Assunta Polito, Moises Garcia Arencibia, Francesco Vetrini, Serkan Erdin, Serpil Uckac Erdin, Tuong Huynh, Diego Medina, Pasqualina Colella, Marco Sardiello, David C. Rubinsztein, and Andrea Ballabio. Tfeb links autophagy to lysosomal biogenesis. *Science*, 332(6036):1429–1433, 2011.

[30] JA. Martina, Y. Chen, M. Gucek, and R. Puertollano. Mtorc1 functions as a transcriptional regulator of autophagy by preventing nuclear transport of tfeb. *Autophagy*, 8(6):903–914, 2012.

[31] A. Roczniak-Ferguson, CS. Petit, F. Froehlich, S. Qian, J. Ky, B. Angarola, TC. Walther, and SM. Ferguson. The transcription factor tfeb links mtorc1 signaling to transcriptional control of lysosome homeostasis. *Science signaling*, 5(228):ra42, 2012.

[32] C. Settembre, R. Zoncu, DL. Medina, F. Vetrini, S. Erdin, S. Erdin, T. Huynh, M. Ferron, G. Karsenty, MC. Vellard, V. Facchinetti, DM. Sabatini, and A. Ballabio. A lysosome-to-nucleus signalling mechanism senses and regulates the lysosome via mtor and tfeb. *The EMBO journal*, 31(5):1095–1108, 2012.

[33] M. Sardiello, M. Palmieri, A. di Ronza, DL. Medina, M. Valenza, VA. Gennarino, C. Di Malta, F. Donaudy, V. Embrione, RS. Polishchuk, S. Banfi, G. Parenti, E. Cattaneo, and A. Ballabio. A gene network regulating lysosomal biogenesis and function. *Science*, 325(5939):473–477, 2009.

[34] H. Schulze and K. Sandhoff. Sphingolipids and lysosomal pathologies. *Biochimica et biophysica acta*, 1841(5):799–810, 2014.

[35] RL. Stevens, AL. Fluharty, H. Kihara, MM. Kaback, LJ. Shapiro, B. Marsh, K. Sandhoff, and G. Fischer. Cerebroside sulfatase activator deficiency induced metachromatic leukodystrophy. *American journal of human genetics*, 33(6):900–906, 1981.

[36] S. Locatelli-Hoops, N. Remmel, R. Klingenstein, B. Breiden, M. Rossocha, M. Schoeniger, C. Koenigs, W. Saenger, and K. Sandhoff. Saposin a mobilizes lipids from low cholesterol and high bis(monoacylglycerol)phosphate-containing membranes: patient variant saposin a lacks lipid extraction capacity. *The Journal of biological chemistry*, 281(43):32451–32460, 2006.

[37] KA. Kretz, GS. Carson, S. Morimoto, Y. Kishimoto, AL. Fluharty, and JS. O'Brien. Characterization of a mutation in a family with saposin b deficiency: a glycosylation site defect. *Proceedings of the national academy of sciences*, 87(7):2541–2544, 1990.

[38] H. Christomanou, A. Aignesberger, and RP. Linke. Immunochemical characterization of two activator proteins stimulating enzymic sphingomyelin degradation in vitro. absence of one of them in a human gaucher disease variant. *Biological chemistry*, 367(9):879–890, 1986.

[39] M. Hiraiwa, BM. Martin, Y. Kishimoto, GE. Conner, S. Tsuji, and JS. O'Brien. Lysosomal proteolysis of prosaposin, the precursor of saposins (sphingolipid activator proteins): its mechanism and inhibition by ganglioside. *Archives of biochemistry and biophysics*, 341(1):17–24, 1997.

[40] E. Eskelinen, Y. Tanaka, and P. Saftig. At the acidic edge: emerging functions for lysosomal membrane proteins. *Trends in cell biology*, 13(3):137–145, 2003.

[41] M. Schwake, B. Schröder, and P. Saftig. Lysosomal membrane proteins and their central role in physiology. *Traffic*, 14(7):739–748, 2013.

[42] T. Wollert and JH. Hurley. Molecular mechanism of multivesicular body biogenesis by escrt complexes. *Nature*, 464(7290):864–869, 2010.

[43] T. Kolter and K. Sandhoff. Principles of lysosomal membrane digestion: stimulation of sphingolipid degradation by sphingolipid activator proteins and anionic lysosomal lipids. *Annual review of cell and developmental biology*, 21:81–103, 2005.

[44] JK. Burkhardt, S. Hüttler, A. Klein, W. Möbius, A. Habermann, G. Griffiths, and K. Sandhoff. Accumulation of sphingolipids in sap-precursor (prosaposin)-deficient fibroblasts occurs as intralysosomal membrane structures and can be completely reversed by treatment with human sap-precursor. *European journal of cell biology*, 73(1):10–18, 1997.

[45] W. Mabius, V. Herzog, K. Sandhoff, and G. Schwarzmann. Intracellular distribution of a biotin-labeled ganglioside, gm1, by immunoelectron microscopy after endocytosis in fibroblasts. *Journal of histochemistry & cytochemistry*, 47(8):1005–1014, 1999.

[46] T. Kobayashi, E. Stang, KS. Fang, P. de Moerloose, RG. Parton, and J. Gruenberg. A lipid associated with the antiphospholipid syndrome regulates endosome structure and function. *Nature*, 392(6672):193–197, 1998.

[47] DR. Body and GM. Gray. The isolation and characterisation of phosphatidylglycerol and a structural isomer from pig lung. *Chemistry and physics of lipids*, 1(3):254—263, 1967.

[48] T. Kolter and K. Sandhoff. Principles of lysosomal membrane digestion: stimulation of sphingolipid degradation by sphingolipid activator proteins and anionic lysosomal lipids. *Annual review of cell and developmental biology*, 21:81–103, 2005.

[49] A. Giehl, T. Lemm, O. Bartelsen, K. Sandhoff, and A. Blume. Interaction of the gm2-activator protein with phospholipid–ganglioside bilayer membranes and with monolayers at the air–water interface. *European journal of biochemistry*, 261(3):650–658, 1999.

[50] G. Wilkening, T. Linke, G. Uhlhorn-Dierks, and K. Sandhoff. Degradation of membrane-bound ganglioside gm1 stimulation by bis (monoacylglycero) phosphate and the activator proteins sap-b and gm2-ap. *Journal of biological chemistry*, 275(46):35814–35819, 2000.

[51] ML. Wang, M. Motamed, RE. Infante, L. Abi-Mosleh, HJ. Kwon, MS. Brown, and JL. Goldstein. Identification of surface residues on niemann-pick c2 essential for hydrophobic handoff of cholesterol to npc1 in lysosomes. *Cell metabolism*, 12(2):166–173, 2010.

[52] N. Friedland, H. Liou, P. Lobel, and AM. Stock. Structure of a cholesterol-binding protein deficient in niemann–pick type c2 disease. *Proceedings of the national academy of sciences*, 100(5):2512–2517, 2003.

[53] S. Xu, B. Benoff, H. Liou, P. Lobel, and AM. Stock. Structural basis of sterol binding by npc2, a lysosomal protein deficient in niemann-pick type c2 disease. *Journal of biological chemistry*, 282(32):23525–23531, 2007.

[54] RE. Infante, ML. Wang, A. Radhakrishnan, HJ. Kwon, MS. Brown, and JL. Goldstein. Npc2 facilitates bidirectional transfer of cholesterol between npc1 and lipid bilayers, a step in cholesterol egress from lysosomes. *Proceedings of the national academy of sciences*, 105(40):15287–15292, 2008.

[55] HJ. Kwon, L. Abi-Mosleh, ML. Wang, J. Deisenhofer, JL. Goldstein, MS. Brown, and RE. Infante. Structure of n-terminal domain of npc1 reveals distinct subdomains for binding and transfer of cholesterol. *Cell*, 137(7):1213–1224, 2009.

[56] HD. Gallala and K. Sandhoff. Biological function of the cellular lipid bmp – bmp as a key activator for cholesterol sorting and membrane digestion. *Neurochemical research*, 36(9):1594–1600, 2011.

[57] RA. Zager, KM. Burkhart, and A. Johnson. Sphingomyelinase and membrane sphingomyelin content determinants of proximal tubule cell susceptibility to injury. *Journal of the american society of nephrology*, 11(5):894–902, 2000.

[58] MS. Brown, PT. Kovanen, and JL. Goldstein. Regulation of plasma cholesterol by lipoprotein receptors. *Science*, 212(4495):628–635, 1981.

[59] AA. Spector, SN. Mathur, and TL. Kaduce. Role of acylcoenzyme a: cholesterol o-acyltransferase in cholesterol metabolism. *Progress in lipid research*, 18(1):93–96, 1979.

[60] U. Panzenboeck, Z. Balazs, A. Sovic, A. Hrzenjak, S. Levak-Frank, A. Wintersperger, E. Malle, and W. Sattler. Abca1 and scavenger receptor class b, type i, are modulators of reverse sterol transport at an in vitro blood-brain barrier constituted of porcine brain capillary endothelial cells. *Journal of biological chemistry*, 277(45):42781–42789, 2002.

[61] I. Björkhem and S. Meaney. Brain cholesterol: long secret life behind a barrier. *Arteriosclerosis, thrombosis, and vascular biology*, 24(5):806–815, 2004.

[62] JW. Koper, EC. Zeinstra, M. Lopes-Cardozo, and LM. van Golde. Acetoacetate and glucose as substrates for lipid synthesis by rat brain oligodendrocytes and astrocytes in serum-free culture. *Biochimica et biophysica acta*, 796(1):20–26, 1984.

[63] J. Shanmugaratnam, E. Berg, L. Kimerer, RJ. Johnson, A. Amaratunga, BM. Schreiber, and RE. Fine. Retinal muller glia secrete apolipoproteins e and j which are efficiently assembled into lipoprotein particles. *Brain research. molecular brain research*, 50(12):113–120, 1997.

[64] DK. Strickland, SL. Gonias, and SW. Argraves. Diverse roles for the ldl receptor family. *Trends in endocrinology and metabolism*, 13(2):66–74, 2002.

[65] SL. Hofmann, DW. Russell, JL. Goldstein, and MS. Brown. mrna for low density lipoprotein receptor in brain and spinal cord of immature and mature rabbits. *Proceedings of the national academy of sciences*, 84(17):6312–6316, 1987.

[66] LW. Swanson, DM. Simmons, SL. Hofmann, JL. Goldstein, and MS. Brown. Localization of mrna for low density lipoprotein receptor and a cholesterol synthetic enzyme in rabbit nervous system by in situ hybridization. *Proceedings of the national academy of sciences*, 85(24):9821–9825, 1988.

[67] M. Ishiguro, Y. Imai, and S. Kohsaka. Expression and distribution of low density lipoprotein receptor-related protein mrna in the rat central nervous system. *Brain research. molecular brain research*, 33(1):37–46, 1995.

[68] I Björkhem, D. Lütjohann, U. Diczfalusy, L. Ståhle, G. Ahlborg, and J. Wahren. Cholesterol homeostasis in human brain: turnover of 24s-hydroxycholesterol and evidence for a cerebral origin of most of this oxysterol in the circulation. *Journal of lipid research*, 39(8):1594–1600, 1998.

[69] KY. Hostetler and PJ. Yazaki. The subcellular localization of neutral sphingomyelinase in rat liver. *Journal of lipid research*, 20(4):456–463, 1979.

[70] S. Gatt. Enzymic hydrolysis and synthesis of ceramides. *Journal of biological chemistry*, 238(9):3131–3133, 1963.

[71] JO. Babalola, M. Wendeler, B. Breiden, C. Arenz, G. Schwarzmann, S. Locatelli-Hoops, and K. Sandhoff. Development of an assay for the intermembrane transfer of cholesterol by niemann-pick c2 protein. *Biological chemistry*, 388(6):617–626, 2007.

[72] M. Abdul-Hammed, B. Breiden, MA. Adebayo, JO. Babalola, G. Schwarzmann, and K. Sandhoff. Role of endosomal membrane lipids and npc2 in cholesterol transfer and membrane fusion. *Journal of lipid research*, 51(7):1747–1760, 2010.

[73] J. Xu, CH. Yeh, S. Chen, L. He, SL. Sensi, LM. Canzoniero, DW. Choi, and CY. Hsu. Involvement of de novo ceramide biosynthesis in tumor necrosis factor-alpha/cycloheximide-

induced cerebral endothelial cell death. *The Journal of biological chemistry*, 273(26):16521–16526, 1998.

[74] JT. Nickels and JR. Broach. A ceramide-activated protein phosphatase mediates ceramide-induced g1 arrest of saccharomyces cerevisiae. *Genes and development*, 10(4):382–394, 1996.

[75] GS. Dbaibo, MY. Pushkareva, S. Jayadev, JK. Schwarz, JM. Horowitz, LM. Obeid, and YA. Hannun. Retinoblastoma gene product as a downstream target for a ceramide-dependent pathway of growth arrest. *Proceedings of the national academy of sciences*, 92(5):1347–1351, 1995.

[76] M. Abdul-Hammed, B. Breiden, MA. Adebayo, JO. Babalola, G. Schwarzmann, and K. Sandhoff. Role of endosomal membrane lipids and npc2 in cholesterol transfer and membrane fusion. *Journal of lipid research*, 51(7):1747–1760, 2010.

[77] A. Klein, M. Henseler, C. Klein, K. Suzuki, K. Harzer, and K. Sandhoff. Sphingolipid activator protein d (sap-d) stimulates the lysosomal degradation of ceramide in vivo. *Biochemical and biophysical research communications*, 200(3):1440–1448, 1994.

[78] N. Okino, X. He, S. Gatt, K. Sandhoff, M. Ito, and EH. Schuchman. The reverse activity of human acid ceramidase. *The Journal of biological chemistry*, 278(32):29948–29953, 2003.

[79] S. Spiegel and S. Milstien. Functions of the multifaceted family of sphingosine kinases and some close relatives. *The Journal of biological chemistry*, 282(4):2125–2129, 2007.

[80] G Tettamanti, R Bassi, P Viani, and L Riboni. Salvage pathways in glycosphingolipid metabolism. *Biochimie*, 85(3):423–437, 2003.

[81] JG. Cyster and SR. Schwab. Sphingosine-1-phosphate and lymphocyte egress from lymphoid organs. *Annual review of immunology*, 30:69–94, 2012.

[82] R. Pappu, SR. Schwab, I. Cornelissen, JP. Pereira, JB. Regard, Y. Xu, E. Camerer, Y. Zheng, Y. Huang, JG. Cyster, and SR. Coughlin. Promotion of lymphocyte egress into

blood and lymph by distinct sources of sphingosine-1-phosphate. *Science*, 316(5822):295–298, 2007.

[83] S. Chae, RL. Proia, and T. Hla. Constitutive expression of the s1p1 receptor in adult tissues. *Prostaglandins and other lipid mediators*, 73(1-2):141–150, 2004.

[84] K. Mizugishi, T. Yamashita, A. Olivera, GF. Miller, S. Spiegel, and RL. Proia. Essential role for sphingosine kinases in neural and vascular development. *Molecular and cellular biology*, 25(24):11113–11121, 2005.

[85] MA. Kingsbury, SK. Rehen, JJA. Contos, CM. Higgins, and J. Chun. Non-proliferative effects of lysophosphatidic acid enhance cortical growth and folding. *Nature neuroscience*, 6(12):1292–1299, 2003.

[86] S. Chae, J. Paik, ML. Allende, RL. Proia, and T. Hla. Regulation of limb development by the sphingosine 1-phosphate receptor s1p1/edg-1 occurs via the hypoxia/vegf axis. *Developmental biology*, 268(2):441–447, 2004.

[87] J. Edsbagge, JK. Johansson, F. Esni, Y. Luo, GL. Radice, and H. Semb. Vascular function and sphingosine-1-phosphate regulate development of the dorsal pancreatic mesenchyme. *Development*, 132(5):1085–1092, 2005.

[88] R. Bottega, RM. Epand, and EH. Ball. Inhibition of protein kinase c by sphingosine correlates with the presence of positive charge. *Biochemical and biophysical research communications*, 164(1):102–107, 1989.

[89] C. Rodriguez-Lafrasse, R. Rousson, S. Valla, P. Antignac, P. Louisot, and MT. Vanier. Modulation of protein kinase c by endogenous sphingosine: inhibition of phorbol dibutyrate binding in niemann-pick c fibroblasts. *The biochemical journal*, 325(3):787–791, 1997.

[90] YH. Zeidan and YA. Hannun. Activation of acid sphingomyelinase by protein kinase c delta-mediated phosphorylation. *The Journal of biological chemistry*, 282(15):11549–11561, 2007.

[91] R. Betto, A. Teresi, G. Fachechi-Cassano, G. Salviati, and RA. Sabbadini. Sphingosine inhibits calcium release from sarcoplasmic reticulum membranes. *Advances in experimental medicine and biology*, 311:403–404, 1992.

[92] K Kagedal, Ming Zhao, Irene Svensson, and Ulf Brunk. Sphingosine-induced apoptosis is dependent on lysosomal proteases. *Biochemical Journal*, 359(2):335–343, 2001.

[93] E. Lloyd-Evans and FM. Platt. Lipids on trial: the search for the offending metabolite in niemann-pick type c disease. *Traffic*, 11(4):419–428, 2010.

[94] C. Scott and YA. Ioannou. The npc1 protein: structure implies function. *Biochimica et biophysica acta - molecular and cell biology of lipids*, 1685(1):8–13, 2004.

[95] V. Turk, B. Turk, and D. Turk. Lysosomal cysteine proteases: facts and opportunities. *The EMBO journal*, 20(17):4629–4633, 2001.

[96] U. Repnik, M. Hafner Eesen, and B. Turk. Lysosomal membrane permeabilization in cell death: Concepts and challenges. *Mitochondrion*, 19(A):49–57, 2014.

[97] M. Jäättelä. Programmed cell death: many ways for cells to die decently. *Annals of medicine*, 34(6):480–488, 2002.

[98] M. Leist and M. Jäättelä. Triggering of apoptosis by cathepsins. *Cell death and differentiation*, 8(4):324–326, 2001.

[99] DE. Johnson. Noncaspase proteases in apoptosis. *Leukemia*, 14(9):1695–1703, 2000.

[100] LP. Deiss, H. Galinka, H. Berissi, O. Cohen, and A. Kimchi. Cathepsin d protease mediates programmed cell death induced by interferon-gamma, fas/apo-1 and tnf-alpha. *The EMBO journal*, 15(15):3861–3870, 1996.

[101] F. Antunes, E. Cadenas, and U. Brunk. Apoptosis induced by exposure to a low steady-state concentration of h2o2 is a consequence of lysosomal rupture. *Journal of biochemistry*, 356:549—555, 2001.

[102] T. Cirman, K. Oresić, GD. Mazovec, V Turk, JC. Reed, RM. Myers, GS Salvesen, and B. Turk. Selective disruption of lysosomes in hela cells triggers apoptosis mediated by

cleavage of bid by multiple papain-like lysosomal cathepsins. *Journal of biological chemistry*, 279(5):3578–3587, 2004.

[103] P. Boya, K. Andreau, D. Poncet, N. Zamzami, J. Perfettini, D. Metivier, DM. Ojcius, M. Jäättelä, and G. Kroemer. Lysosomal membrane permeabilization induces cell death in a mitochondrion-dependent fashion. *The Journal of experimental medicine*, 197(10):1323–1334, 2003.

[104] J. Nylandsted, M. Gyrd-Hansen, A. Danielewicz, N. Fehrenbacher, U. Lademann, M. Høyer-Hansen, E. Weber, G. Multhoff, M. Rohde, and M. Jäättelä. Heat shock protein 70 promotes cell survival by inhibiting lysosomal membrane permeabilization. *The Journal of experimental medicine*, 200(4):425–435, 2004.

[105] P. Leinekugel, S. Michel, and E. Conzelmann. Quantitative correlation between the residual activity of b-hexosaminidase a and arylsulfatase a and the severity of the resulting lysosomal storage disease. *Human genetics*, 88(5):513–523, 1992.

[106] J. Fan. A counterintuitive approach to treat enzyme deficiencies: use of enzyme inhibitors for restoring mutant enzyme activity. *Biological chemistry*, 389(1):1–11, 2008.

[107] UH. Schueler, T. Kolter, CR Kaneski, GC Zirzow, K Sandhoff, and RO Brady. Correlation between enzyme activity and substrate storage in a cell culture model system for gaucher disease. *Journal of inherited metabolic disease*, 27(5):649–658, 2004.

[108] I. Ron and M. Horowitz. Er retention and degradation as the molecular basis underlying gaucher disease heterogeneity. *Human molecular genetics*, 14(16):2387–2398, 2005.

[109] K. Suzuki and GC. Chen. Brain ceramide hexosides in tay-sachs disease and generalized gangliosidosis (gm1-gangliosidosis). *Journal of lipid research*, 8(2):105–113, 1967.

[110] EF. Neufeld. Lysosomal storage diseases. *Annual review of biochemistry*, 60(1):257–280, 1991.

[111] HW. Moser, KD. Smith, PA. Watkins, J. Powers, AB. Moser, CR. Scriver, AL. Beaudet, WS. Sly, and D. Vallwe. *The metabolic and molecular bases of inherited disease*. McGraw-Hill, New York, 2001.

[112] L. Svennerholm. The chemical structure of normal human brain and tay-sachs gangliosides. *Biochemical and biophysical research communications*, 9(5):436–441, 1962.

[113] R. Ledeen and K. Salsman. Structure of the tay-sachs' ganglioside. i. *Biochemistry*, 4(10):2225—2233, 1965.

[114] K. Sandhoff, U. Andreae, and H. Jatzkewitz. Deficient hexosaminidase activity in an exceptional case of tay-sachs disease with additional storage of kidney globoside in visceral organs. *Life sciences*, 7(6):283—288, 1968.

[115] SK. Srivastava and E. Beutler. Studies on human β-dn-acetylhexosaminidases iii. biochemical genetics of tay-sachs and sandhoff's diseases. *Journal of biological chemistry*, 249(7):2054–2057, 1974.

[116] M Carroll and D Robinson. Immunological properties of N-acetyl-β-d-glucosaminidase of normal human liver and of gm2- gangliosidosis liver. *The biochemical journal*, 131(1):113—118, 1973.

[117] K. Suzuki, K. Suzuki, I. Rapin, Y. Suzuki, and N. Ishii. Juvenile gm2-gangliosidosis clinical variant of tay-sachs disease or a new disease. *Neurology*, 20(2):190–204, 1970.

[118] B. Rosengren, J. Månsson, and L. Svennerholm. Composition of gangliosides and neutral glycosphingolipids of brain in classical tay-sachs and sandhoff disease: More lyso-gm2 in sandhoff disease? *Journal of neurochemistry*, 49(3):834–840, 1987.

[119] CJ. Tifft and RL. Proia. The β-hexosaminidase deficiency disorders: Development of a clinical paradigm in the mouse. *Annals of medicine*, 29(6):557–561, 1997.

[120] K. Sandhoff, K. Harzer, W. Wässle, and H. Jatzkewitz. Enzyme alterations and lipid storage in three variants of tay-sachs disease. *Journal of neurochemistry*, 18(12):2469–2489, 1971.

[121] CL. Dolman, E. Chang, and RJ. Duke. Pathologic findings in sandhoff disease. *Archives of pathology*, 96(4):272–275, 1973.

[122] M. Iwamori and Y. Nagai. Ganglioside composition of brain in tay-sachs disease: increased amounts of gd2 and n-acetyl-β-d-galactosaminyl gd1a ganglioside. *Journal of neurochemistry*, 32(3):767–777, 1979.

[123] M. Iwamori and Y. Nagai. Isolation and characterization of a novel ganglioside, monosialosyl pentahexaosyl ceramide from human brain. *Journal of biochemistry*, 84(6):1601–1608, 1978.

[124] E. Conzelmann and K. Sandhoff. Ab variant of infantile gm2 gangliosidosis: deficiency of a factor necessary for stimulation of hexosaminidase a-catalyzed degradation of ganglioside gm2 and glycolipid ga2. *Proceedings of the national academy of sciences*, 75(8):3979–3983, 1978.

[125] GM. Hadfield, P. Mamunes, and RB. David. The pathology of sandhoff's disease. *The Journal of pathology*, 123(3):137–144, 1977.

[126] RJ Desnick, KY Allen, SJ Desnick, MK Raman, RW Bernlohr, and W Krivit. Fabry's disease: enzymatic diagnosis of hemizygotes and heterozygotes. alpha-galactosidase activities in plasma, serum, urine, and leukocytes. *The Journal of laboratory and clinical medicine*, 81(2):157–171, 1973.

[127] CM. Eng, LA. Resnick-Silverman, DJ. Niehaus, KH. Astrin, and RJ. Desnick. Nature and frequency of mutations in the alpha-galactosidase a gene that cause fabry disease. *American journal of human genetics*, 53(6):1186–1197, 1993.

[128] C. Whybra, CHR. Kampmann, I. Willers, J. Davies, B. Winchester, J. Kriegsmann, K. Brühl, A. Gal, S. Bunge, and M. Beck. Anderson–fabry disease: clinical manifestations of disease in female heterozygotes. *Journal of inherited metabolic disease*, 24(7):715–724, 2001.

[129] G. Von Gemmingen, RR. Kierland, and JM. Opitz. Angiokeratoma corporis diffusum (fabry's disease). *Archives of dermatology*, 91(3):206–218, 1965.

[130] A. Sodi, AS. Ioannidis, A. Mehta, C. Davey, M. Beck, and S. Pitz. Ocular manifestations

of fabrys disease: data from the fabry outcome survey. *British journal of ophthalmology*, 91(2):210—214, 2007.

[131] MJ. Ferraz, WW. Kallemeijn, M. Mirzaian, D. Herrera Moro, A. Marques, P. Wisse, RG. Boot, LI. Willems, HS. Overkleeft, and JM. Aerts. Gaucher disease and fabry disease: New markers and insights in pathophysiology for two distinct glycosphingolipidoses. *Biochimica et biophysica acta - molecular and cell biology of lipids*, 1841(5):811–825, 2014.

[132] R. Dobrovolny, L. Dvorakova, J. Ledvinova, S. Magage, J. Bultas, JC. Lubanda, M. Elleder, D. Karetova, M. Pavlikova, and M. Hrebicek. Relationship between x-inactivation and clinical involvement in fabry heterozygotes. eleven novel mutations in the α-galactosidase a gene in the czech and slovak population. *Journal of molecular medicine*, 83(8):647–654, 2005.

[133] PJ. Meikle, JJ. Hopwood, AE. Clague, and WF. Carey. Prevalence of lysosomal storage disorders. *Jama*, 281(3):249–254, 1999.

[134] TP. Mechtler, S. Stary, TF. Metz, VR. De Jesús, S. Greber-Platzer, A. Pollak, KR. Herkner, B. Streubel, and DC. Kasper. Neonatal screening for lysosomal storage disorders: feasibility and incidence from a nationwide study in austria. *The lancet*, 379(9813):335–341, 2012.

[135] M. Spada, S. Pagliardini, M. Yasuda, T. Tukel, G. Thiagarajan, H. Sakuraba, A. Ponzone, and RJ. Desnick. High incidence of later-onset fabry disease revealed by newborn screening. *The american journal of human genetics*, 79(1):31–40, 2006.

[136] HW. Moser, KD. Smith, PA. Watkins, J. Powers, AB. Moser, CR. Scriver, AL. Beaudet, WS. Sly, and D. Vallwe. *The metabolic and molecular bases of inherited disease*. McGraw-Hill, New York, 2001.

[137] JH. Sung. Autonomic neurons affected by lipid storage in the spinal cord in fabry's disease: distribution of autonomic neurons in the sacral cord. *Journal of neuropathology and experimental neurology*, 38(2):87–98, 1979.

[138] GA. de Veber, GA. Schwarting, EH. Kolodny, and NW. Kowall. Fabry disease: immunocytochemical characterization of neuronal involvement. *Annals of neurology*, 31(4):409–415, 1992.

[139] ED. Carstea, JA. Morris, KG. Coleman, SK. Loftus, D. Zhang, C. Cummings, J. Gu, MA. Rosenfeld, WJ. Pavan, DB. Krizman, et al. Niemann-pick c1 disease gene: homology to mediators of cholesterol homeostasis. *Science*, 277(5323):228–231, 1997.

[140] S Naureckiene, DE Sleat, H Lackland, A Fensom, MT Vanier, R Wattiaux, M Jadot, and P Lobel. Identification of he1 as the second gene of niemann-pick c disease. *Science*, 290(5500):2298–2301, 2000.

[141] YS. Hsu, WL. Hwu, SF. Huang, MY. Lu, RL. Chen, DT. Lin, SSF. Peng, and KH. Lin. Niemann–pick disease type c (a cellular cholesterol lipidosis) treated by bone marrow transplantation. *Bone marrow transplantation*, 24(1):103–107, 1999.

[142] SJ. Steinberg, CP. Ward, and AH. Fensom. Complementation studies in niemann-pick disease type c indicate the existence of a second group. *Journal of medical genetics*, 31(4):317—320, 1994.

[143] SJ. Steinberg, D. Mondal, and AH. Fensom. Co-cultivation of niemann-pick disease type c fibroblasts belonging to complementation groups α and β stimulates ldl-derived cholesterol esterification. *Journal of inherited metabolic disease*, 19(6):769–774, 1996.

[144] MT. Vanier, S. Duthel, C Rodriguez-Lafrasse, P. Pentchev, and ED. Carstea. Genetic heterogeneity in niemann-pick c disease: a study using somatic cell hybridization and linkage analysis. *American journal of human genetics*, 58(1):481–489, 1996.

[145] MT. Vanier and G. Millat. Niemann–pick disease type c. *Clinical genetics*, 64(4):1750–1768, 2003.

[146] ME Gelsthorpe, N Baumann, E Millard, SE Gale, JS Langmade, JE Schaffer, and DS. Ory. Niemann-pick type c1 i1061t mutant encodes a functional protein that is selected for endoplasmic reticulum-associated degradation due to protein misfolding. *Journal of Biological Chemistry*, 283(13):8229–8236, 2008.

[147] PG. Pentchev, AD. Boothe, HS. Kruth, H. Weintroub, J. Stivers, and RO. Brady. A genetic storage disorder in balb/c mice with a metabolic block in esterification of exogenous cholesterol. *Journal of biological chemistry*, 259(9):5784–5791, 1984.

[148] MT. Vanier. Lipid changes in niemann-pick disease type c brain: personal experience and review of the literature. *Neurochemical research*, 24(4):481–489, 1999.

[149] JD. Butler, MT. Vanier, and PG. Pentchev. Niemann-pick c disease: cystine and lipids accumulate in the murine model of this lysosomal cholesterol lipidosis. *Biochemical and biophysical research communications*, 196(1):154–159, 1993.

[150] FW. Chen, RE. Gordon, and YA. Ioannou. Npc1 late endosomes contain elevated levels of non-esterified ('free') fatty acids and an abnormally glycosylated form of the npc2 protein. *The biochemical journal*, 390:549–561, 2005.

[151] D. te Vruchte, E. Lloyd-Evans, RJ. Veldman, DCA. Neville, RA Dwek, FM. Platt, WJ. van Blitterswijk, and DJ. Sillence. Accumulation of glycosphingolipids in niemann-pick c disease disrupts endosomal transport. *Journal of biological chemistry*, 279(25):26167–26175, 2004.

[152] JR. Sarna, M. Larouche, H. Marzban, RV. Sillitoe, DE. Rancourt, and R. Hawkes. Patterned purkinje cell degeneration in mouse models of niemann-pick type c disease. *Journal of comparative neurology*, 456(3):279–291, 2003.

[153] JP. Welsh, G. Yuen, DG. Placantonakis, TQ. Vu, F. Haiss, E. O'Hearn, ME. Molliver, and SA. Aicher. Why do purkinje cells die so easily after global brain ischemia? aldolase c, eaat4, and the cerebellar contribution to posthypoxic myoclonus. *Advances in neurology*, 89:331–359, 2001.

[154] J. Sarna, SRP. Miranda, EH. Schuchman, and R. Hawkes. Patterned cerebellar purkinje cell death in a transgenic mouse model of niemann pick type a/b disease. *European journal of neuroscience*, 13(10):1873–1880, 2001.

[155] M. Baudry, Y. Yao, D. Simmons, J. Liu, and X. Bi. Postnatal development of inflammation

in a murine model of niemann-pick type c disease: immunohistochemical observations of microglia and astroglia. *Experimental neurology*, 184(2):887–903, 2003.

[156] SNR. Pressey, DA. Smith, AMS. Wong, FM. Platt, and JD. Cooper. Early glial activation, synaptic changes and axonal pathology in the thalamocortical system of niemann-pick type c1 mice. *Neurobiology of disease*, 45(3):1086–1100, 2012.

[157] ME. Lopez, AD. Klein, UJ. Dimbil, and MP. Scott. Anatomically defined neuron-based rescue of neurodegenerative niemann-pick type c disorder. *The Journal of neuroscience*, 31(12):4367–4378, 2011.

[158] T. Yu, VG. Shakkottai, C. Chung, and AP. Lieberman. Temporal and cell-specific deletion establishes that neuronal npc1 deficiency is sufficient to mediate neurodegeneration. *Human molecular genetics*, 20(22):4440–4451, 2011.

[159] IM. Williams, KL. Wallom, DA. Smith, N. Al Eisa, C. Smith, and FM. Platt. Improved neuroprotection using miglustat, curcumin and ibuprofen as a triple combination therapy in niemann-pick disease type c1 mice. *Neurobiology of disease*, 67:9–17, 2014.

[160] M. Zhang, D. Strnatka, C. Donohue, JL. Hallows, I. Vincent, and RP. Erickson. Astrocyte-only npc1 reduces neuronal cholesterol and triples life span of npc1-/- mice. *Journal of neuroscience research*, 86(13):2848–2856, 2008.

[161] RO. Brady, JN. Kanfer, MB. Mock, and DS. Fredrickson. The metabolism of sphingomyelin. ii. evidence of an enzymatic deficiency in niemann-pick disease. *Proceedings of the national academy of sciences*, 55(2):366–369, 1966.

[162] JN. Kanfer, OM. Young, D. Shapiro, and RO. Brady. The metabolism of sphingomyelin i. purification and properties of a sphingomyelin-cleaving enzyme from rat liver tissue. *Journal of biological chemistry*, 241(5):1081–1084, 1966.

[163] T. Kirkegaard, AG. Roth, NHT. Petersen, AK. Mahalka, OD. Olsen, I. Moilanen, A. Zylicz, J. Knudsen, K. Sandhoff, C. Arenz, et al. Hsp70 stabilizes lysosomes and reverts niemann–pick disease-associated lysosomal pathology. *Nature*, 463(7280):549–553, 2010.

[164] PG. Pentchev, AE. Gal, AD Booth, F Omodeo-Sale, J Fours, BA Neumeyer, JM Quirk, G Dawson, and RO Brady. A lysosomal storage disorder in mice characterized by a dual deficiency of sphingomyelinase and glucocerebrosidase. *Biochimica et biophysica acta - lipids and lipid metabolism*, 619(3):669–679, 1980.

[165] JW. Reagan, ML. Hubbert, and GS. Shelness. Posttranslational regulation of acid sphingomyelinase in niemann-pick type c1 fibroblasts and free cholesterol-enriched chinese hamster ovary cells. *Journal of biological chemistry*, 275(48):38104–38110, 2000.

[166] H. Tamura, T. Takahashi, N. Ban, H. Torisu, H. Ninomiya, G. Takada, and N. Inagaki. Niemann–pick type c disease: Novel npc1 mutations and characterization of the concomitant acid sphingomyelinase deficiency. *Molecular genetics and metabolism*, 87(2):113–121, 2006.

[167] C. Devlin, NH. Pipalia, X. Liao, EH. Schuchman, FR. Maxfield, and I. Tabas. Improvement in lipid and protein trafficking in niemann-pick c1 cells by correction of a secondary enzyme defect. *Traffic*, 11(5):601–615, 2010.

[168] MT. Vanier. Lipid changes in niemann-pick disease type c brain: personal experience and review of the literature. *Neurochemical research*, 24(4):481–489, 1999.

[169] M. Walterfang, M. Fahey, P. Desmond, A. Wood, ML. Seal, C. Steward, C. Adamson, C. Kokkinos, M. Fietz, and D. Velakoulis. White and gray matter alterations in adults with niemann-pick disease type c: a cross-sectional study. *Neurology*, 75(1):49–56, 2010.

[170] S. Takikita, T. Fukuda, I. Mohri, T. Yagi, and K. Suzuki. Perturbed myelination process of premyelinating oligodendrocyte in niemann-picktype c mouse. *Journal of neuropathology and experimental neurology*, 63(6):660–673, 2004.

[171] MJ Elrick, CD. Pacheco, T. Yu, N. Dadgar, VG. Shakkottai, C. Ware, HL. Paulson, and AP. Lieberman. Conditional niemann-pick c mice demonstrate cell autonomous purkinje cell neurodegeneration. *Human molecular genetics*, 19(5):837–847, 2010.

[172] T. Yu and AP. Lieberman. Npc1 acting in neurons and glia is essential for the formation and maintenance of cns myelin. *PLoS genetics*, 9(4):e1003462, 2013.

[173] JE Wraith, FM Platt, and SU Walkley. *Lysosomal disorders of the brain*. Oxford University Press Oxford, 2004.

[174] NW. Barton, FS. Furbish, GJ. Murray, M Garfield, and RO. Brady. Therapeutic response to intravenous infusions of glucocerebrosidase in a patient with gaucher disease. *Proceedings of the national academy of sciences*, 87(5):1913–1916, 1990.

[175] GA. Grabowski, NW. Barton, G. Pastores, JM Dambrosia, TK Banerjee, MA. McKee, C. Parker, R. Schiffmann, SC. Hill, and RO. Brady. Enzyme therapy in type 1 gaucher disease: comparative efficacy of mannose-terminated glucocerebrosidase from natural and recombinant sources. *Annals of Internal Medicine*, 122(1):33–39, 1995.

[176] GA. Grabowski, N. Leslie, and R. Wenstrup. Enzyme therapy for gaucher disease: the first 5 years. *Blood reviews*, 12(2):115–133, 1998.

[177] R. Schiffmann, M. Ries, M. Timmons, JT. Flaherty, and RO. Brady. Long-term therapy with agalsidase alfa for fabry disease: safety and effects on renal function in a home infusion setting. *Nephrology dialysis transplantation*, 21(2):345–154, 2006.

[178] JE. Wraith, A. Tylki-Szymanska, N. Guffon, HY. Lien, M. Tsimaratos, A. Vellodi, and DP. Germain. Safety and efficacy of enzyme replacement therapy with agalsidase beta: an international, open-label study in pediatric patients with fabry disease. *The Journal of pediatrics*, 152(4):563–570, 2008.

[179] H. Van den Hout, AJJ. Reuser, AG. Vulto, M Christa B Loonen, A. Cromme-Dijkhuis, and AT. Van der Ploeg. Recombinant human α-glucosidase from rabbit milk in pompe patients. *The lancet*, 356(9227):397–398, 2000.

[180] A. Amalfitano, AR. Bengur, RP. Morse, JM. Majure, LE. Case, DL. Veerling, J. Mackey, P. Kishnani, W. Smith, A. McVie-Wylie, et al. Recombinant human acid alpha-glucosidase enzyme therapy for infantile glycogen storage disease type ii: Results of a phase i/ii clinical trial. *Genetics in Medicine*, 3(2):132–138, 2001.

[181] C. Vogler, B. Levy, NJ. Galvin, C. Thorpe, MS. Sands, JE. Barker, J. Baty, EH. Birkenmeier, and WS. Sly. Enzyme replacement in murine mucopolysaccharidosis type vii: neu-

ronal and glial response to β-glucuronidase requires early initiation of enzyme replacement therapy. *Pediatric research*, 45(6):838–844, 1999.

[182] RM. Shull, ED. Kakkis, MF. McEntee, SA. Kania, AJ. Jonas, and EF. Neufeld. Enzyme replacement in a canine model of hurler syndrome. *Proceedings of the national academy of sciences*, 91(26):12937—12941, 1994.

[183] F. Norflus, CJ. Tifft, MP. McDonald, G. Goldstein, JN. Crawley, A. Hoffmann, K. Sandhoff, K. Suzuki, and RL. Proia. Bone marrow transplantation prolongs life span and ameliorates neurologic manifestations in sandhoff disease mice. *Journal of clinical investigation*, 101(9):1881–1888, 1998.

[184] M. Jeyakumar, F. Norflus, CJ. Tifft, M. Cortina-Borja, TD. Butters, RL. Proia, HV. Perry, RA. Dwek, and FM. Platt. Enhanced survival in sandhoff disease mice receiving a combination of substrate deprivation therapy and bone marrow transplantation. *Blood*, 97(1):327–329, 2001.

[185] AS. O'Marcaigh and MJ. Cowan. Bone marrow transplantation for inherited diseases. *Current opinion in oncology*, 9(2):126–130, 1997.

[186] MS. Sands and BL. Davidson. Gene therapy for lysosomal storage diseases. *Molecular therapy*, 13(5):839—849, 2006.

[187] JE Wraith, FM Platt, and SU Walkley. *Lysosomal disorders of the brain.* In [173], 2004.

[188] EF Neufeld and JC Fratantoni. Inborn errors of mucopolysaccharide metabolism. *Science*, 169:141–146, 1970.

[189] AM. Bradbury, NJ Cochran, VJ. McCurdy, AK. Johnson, BL. Brunson, H. Gray-Edwards, SG. Leroy, M. Hwang, AN. Randle, LS. Jackson, et al. Therapeutic response in feline sandhoff disease despite immunity to intracranial gene therapy. *Molecular Therapy*, 21(7):1306–1315, 2013.

[190] TM. Daly, C. Vogler, B. Levy, ME. Haskins, and MS. Sands. Neonatal gene transfer leads to widespread correction of pathology in a murine model of lysosomal storage disease. *Proceedings of the national academy of sciences*, 96(5):2296–2300, 1999.

[191] AW. Frisella, LH. O'Connor, CA. Vogler, M. Roberts, S. Walkley, B. Levy, TM. Daly, and MS. Sands. Intracranial injection of recombinant adeno-associated virus improves cognitive function in a murine model of mucopolysaccharidosis type vii. *Molecular Therapy*, 3(3):351–358, 2001.

[192] MA. Rosenfeld, K. Yoshimura, BC. Trapnell, K. Yoneyama, ER. Rosenthal, W. Dalemans, M. Fukayama, J. Bargon, LE. Stier, L. Stratford-Perricaudet, et al. In vivo transfer of the human cystic fibrosis transmembrane conductance regulator gene to the airway epithelium. *Cell*, 68(1):143–155, 1992.

[193] C. Vogler, MS. Sands, B. Levy, N. Galvin, EH. Birkenmeier, and WS. Sly. Enzyme replacement with recombinant β-glucuronidase in murine mucopolysaccharidosis type vii: Impact of therapy during the first six weeks of life on subsequent lysosomal storage, growth, and survival. *Pediatric research*, 39(6):1050–1054, 1996.

[194] S. Seregin and A. Amalfitano. Gene therapy for lysosomal storage diseases: progress, challenges and future prospects. *Current pharmaceutical design*, 17(24):2558–2574, 2011.

[195] R. Shull, X. Lu, I. Dube, C. Lutzko, S. Kruth, A. Abrams-Ogg, HP. Kiem, S. Goehle, F. Schuening, C. Millan, et al. Humoral immune response limits gene therapy in canine mps i. *Blood*, 88(1):377–379, 1996.

[196] T. Ohashi, K. Watabe, K. Uehara, WS. Sly, C. Vogler, and Y. Eto. Adenovirus-mediated gene transfer and expression of human β-glucuronidase gene in the liver, spleen, and central nervous system in mucopolysaccharidosis type vii mice. *Proceedings of the national academy of sciences*, 94(4):1287—1292, 1997.

[197] Y. Suzuki, S. Ogawa, and Y. Sakakibara. Chaperone therapy for neuronopathic lysosomal diseases: competitive inhibitors as chemical chaperones for enhancement of mutant enzyme activities. *Perspectives in medicinal chemistry*, 3(7):9821–9825, 2009.

[198] S. Ishii, H. Sakuraba, and Y. Suzuki. Point mutations in the upstream region of the α-galactosidase a gene exon 6 in an atypical variant of fabry disease. *Human genetics*, 89(1):29–32, 1992.

[199] T. Okumiya, S. Ishii, T. Takenaka, R. Kase, S. Kamei, H. Sakuraba, and Y. Suzuki. Galactose stabilizes various missense mutants of α-galactosidase in fabry disease. *Biochemical and biophysical research communications*, 214(3):1219–1224, 1995.

[200] L. Tominaga, Y. Ogawa, M. Taniguchi, K. Ohno, J. Matsuda, A. Oshima, Y. Suzuki, and E. Nanba. Galactonojirimycin derivatives restore mutant human β-galactosidase activities expressed in fibroblasts from enzyme-deficient knockout mouse. *Brain and development*, 23(5):284–287, 2001.

[201] J. Fan, S. Ishii, N. Asano, and Y. Suzuki. Accelerated transport and maturation of lysosomal α–galactosidase a in fabry lymphoblasts by an enzyme inhibitor. *Nature medicine*, 5(1):112–115, 1999.

[202] R. Khanna, ER. Benjamin, L. Pellegrino, A. Schilling, BA. Rigat, R. Soska, H. Nafar, BE. Ranes, J. Feng, Y. Lun, et al. The pharmacological chaperone isofagomine increases the activity of the gaucher disease l444p mutant form of β-glucosidase. *FEBS Journal*, 277(7):1618–1638, 2010.

[203] Y. Sun, H. Ran, B. Liou, B. Quinn, M. Zamzow, W. Zhang, J. Bielawski, K. Kitatani, KDR. Setchell, YA. Hannun, et al. Isofagomine in vivo effects in a neuronopathic gaucher disease mouse. *PLoS one*, 6(4):e19037, 2011.

[204] S. Ishii, H. Chang, H. Yoshioka, T. Shimada, K. Mannen, Y. Higuchi, A. Taguchi, and J. Fan. Preclinical efficacy and safety of 1-deoxygalactonojirimycin in mice for fabry disease. *Journal of pharmacology and experimental therapeutics*, 328(3):723–731, 2009.

[205] FM. Platt and TD. Butters. *Inhibition of substrate synthesis: a pharmacological approach for glycosphingolipid storage disease therapy.* Oxford scholarship, 2004.

[206] FM. Platt, GR. Neises, RA. Dwek, and TD. Butters. N-butyldeoxynojirimycin is a novel inhibitor of glycolipid biosynthesis. *Journal of biological chemistry*, 269(11):8362–8365, 1994.

[207] M. Jeyakumar, TD. Butters, M. Cortina-Borja, V. Hunnam, RL. Proia, HV. Perry, RA. Dwek, and FM. Platt. Delayed symptom onset and increased life expectancy in sandhoff

disease mice treated with n-butyldeoxynojirimycin. *Proceedings of the national academy of sciences*, 96(11):6388–6393, 1999.

[208] FM. Platt, GR. Neises, G. Reinkensmeier, MJ. Townsend, HV. Perry, RL. Proia, B. Winchester, RA. Dwek, and TD. Butters. Prevention of lysosomal storage in tay-sachs mice treated with n-butyldeoxynojirimycin. *Science*, 276(5311):428–431, 1997.

[209] C. Moyses. Substrate reduction therapy: clinical evaluation in type 1 gaucher disease. *Philosophical transactions of the royal society of london. series b: biological sciences*, 358(1433):955–960, 2003.

[210] MC. Patterson, D. Vecchio, H. Prady, L. Abel, and JE. Wraith. Miglustat for treatment of niemann-pick c disease: a randomised controlled study. *The lancet. neurology*, 6(9):765–772, 2007.

[211] JB. Nietupski, JJ. Pacheco, W. Chuang, K. Maratea, L. Li, J. Foley, KM. Ashe, CGF. Cooper, JMFG. Aerts, DP. Copeland, RK. Scheule, SH. Cheng, and J. Marshall. Iminosugar-based inhibitors of glucosylceramide synthase prolong survival but paradoxically increase brain glucosylceramide levels in niemann-pick c mice. *Molecular genetics and metabolism*, 105(4):621–628, 2012.

[212] VM. Stein, A. Crooks, W. Ding, M. Prociuk, P. O'Donnell, C. Bryan, T. Sikora, J. Dingemanse, MT. Vanier, SU. Walkley, and CH. Vite. Miglustat improves purkinje cell survival and alters microglial phenotype in feline niemann-pick disease type c. *Journal of neuropathology and experimental neurology*, 71(5):434–448, 2012.

[213] D. Galanaud, A. Tourbah, S. Lehéricy, N. Leveque, B. Heron, T. Billette de Villemeur, N. Guffon, F. Feillet, N. Baumann, MT Vanier, et al. 24 month-treatment with miglustat of three patients with niemann-pick disease type c: follow up using brain spectroscopy. *Molecular genetics and metabolism*, 96(2):55–58, 2009.

[214] SH. Mellon, W. Gong, and MD. Schonemann. Endogenous and synthetic neurosteroids in treatment of niemann-pick type c disease. *Brain research reviews*, 57(2):410–420, 2008.

[215] B. Liu, H. Li, JJ. Repa, SD. Turley, and JM. Dietschy. Genetic variations and treatments that affect the lifespan of the npc1 mouse. *Journal of lipid research*, 49(3):663–669, 2008.

[216] B. Liu, SD. Turley, DK. Burns, AM. Miller, JJ. Repa, and JM. Dietschy. Reversal of defective lysosomal transport in npc disease ameliorates liver dysfunction and neurodegeneration in the npc1-/- mouse. *Proceedings of the national academy of sciences*, 106(7):2377–2382, 2009.

[217] CD. Davidson, NF. Ali, MC. Micsenyi, G. Stephney, S. Renault, K. Dobrenis, DS. Ory, MT. Vanier, and SU. Walkley. Chronic cyclodextrin treatment of murine niemann-pick c disease ameliorates neuronal cholesterol and glycosphingolipid storage and disease progression. *PloS one*, 4(9):e6951, 2009.

[218] CM. Ramirez, B. Liu, AM. Taylor, JJ. Repa, DK. Burns, AG. Weinberg, SD. Turley, and JM. Dietschy. Weekly cyclodextrin administration normalizes cholesterol metabolism in nearly every organ of the niemann-pick type c1 mouse and markedly prolongs life. *Pediatric research*, 68(4):309–315, 2010.

[219] L. Abi-Mosleh, RE. Infante, A. Radhakrishnan, JL. Goldstein, and MS. Brown. Cyclodextrin overcomes deficient lysosome-to-endoplasmic reticulum transport of cholesterol in niemann-pick type c cells. *Proceedings of the national academy of sciences*, 106(46):19316–19321, 2009.

[220] CC. Pontikis, CD. Davidson, SU. Walkley, FM. Platt, and DJ. Begley. Cyclodextrin alleviates neuronal storage of cholesterol in niemann-pick c disease without evidence of detectable blood–brain barrier permeability. *Journal of inherited metabolic disease*, 36(3):491–498, 2013.

[221] M. Saito, EP. Benson, and A. Rosenberg. Metabolism of cholesterol and triacylglycerol in cultured chick neuronal cells, glial cells, and fibroblasts: accumulation of esterified cholesterol in serum-free culture. *Journal of neuroscience research*, 18(2):319–325, 1987.

[222] S. Suzuki, K. Kiyosue, S. Hazama, A. Ogura, M. Kashihara, T. Hara, H. Koshimizu,

and M. Kojima. Brain-derived neurotrophic factor regulates cholesterol metabolism for synapse development. *The Journal of neuroscience*, 27(24):6417–6427, 2007.

[223] U. Funfschilling, S. Gesine, L. Xiao, W. Mobius, and K. Nave. Survival of adult neurons lacking cholesterol synthesis in vivo. *BMC Neuroscience*, 8(1):1471–1480, 2007.

[224] FW. Chen, C. Li, and YA. Ioannou. Cyclodextrin induces calcium-dependent lysosomal exocytosis. *PloS one*, 5(11):e15054, 2010.

[225] D. te Vruchte, AO. Speak, KL. Wallom, N Al Eisa, DA. Smith, CJ. Hendriksz, L. Simmons, RH. Lachmann, A. Cousins, R. Hartung, E. Mengel, H. Runz, M. Beck, Y. Amraoui, J. Imrie, E. Jacklin, K. Riddick, FD. Porter, M. Cortina-Borja, FM. Platt, et al. Relative acidic compartment volume as a lysosomal storage disorder-associated biomarker. *The Journal of clinical investigation*, 124(3):1320–1328, 2014.

[226] MD. Shahbazian and M. Grunstein. Functions of site-specific histone acetylation and deacetylation. *Annual review of biochemistry*, 76(75):75–100, 2007.

[227] AB. Munkacsi, FW. Chen, MA. Brinkman, K. Higaki, GD. Gutiérrez, J. Chaudhari, JV. Layer, A. Tong, M. Bard, C. Boone, YA. Ioannou, and SL. Sturley. An "exacerbate-reverse" strategy in yeast identifies histone deacetylase inhibition as a correction for cholesterol and sphingolipid transport defects in human niemann-pick type c disease. *The Journal of biological chemistry*, 286(27):23842–23851, 2011.

[228] NH. Pipalia, CC. Cosner, A. Huang, A. Chatterjee, P. Bourbon, N. Farley, P. Helquist, O. Wiest, and FR. Maxfield. Histone deacetylase inhibitor treatment dramatically reduces cholesterol accumulation in niemann-pick type c1 mutant human fibroblasts. *Proceedings of the national academy of sciences*, 108(14):5620–5625, 2011.

[229] ME. Gelsthorpe, N. Baumann, E. Millard, SE. Gale, JS. Langmade, JE. Schaffer, and DS. Ory. Niemann-pick type c1 i1061t mutant encodes a functional protein that is selected for endoplasmic reticulum-associated degradation due to protein misfolding. *The Journal of biological chemistry*, 283(13):8229–8236, 2008.

[230] EAA. Nollen and RI. Morimoto. Chaperoning signaling pathways: molecular chaperones as stress-sensing 'heat shock' proteins. *Journal of cell science*, 115(14):2809–2816, 2002.

[231] UF. Hartl, A. Bracher, and M. Hayer-Hartl. Molecular chaperones in protein folding and proteostasis. *Nature*, 475(7356):324–332, 2011.

[232] M Jäättelä. Heat shock proteins as cellular lifeguards. *Annals of medicine*, 31(4):261–271, 1999.

[233] RI. Morimoto. Proteotoxic stress and inducible chaperone networks in neurodegenerative disease and aging. *Genes and development*, 22(11):1427–1438, 2008.

[234] RI Morimoto. Regulation of the heat shock transcriptional response: cross talk between a family of heat shock factors, molecular chaperones, and negative regulators. *Genes and development*, 12(24):3788–3796, 1998.

[235] J. Amin, J. Ananthan, and R. Voellmy. Key features of heat shock regulatory elements. *Molecular and cellular biology*, 8(9):3761—3769, 1988.

[236] X. Xiao, X. Zuo, AA. Davis, DR. McMillan, BB. Curry, JA. Richardson, and IJ. Benjamin. Hsf1 is required for extra-embryonic development, postnatal growth and protection during inflammatory responses in mice. *The EMBO journal*, 18(21):5943–5952, 1999.

[237] DR. McMillan, X. Xiao, L. Shao, K. Graves, and IJ. Benjamin. Targeted disruption of heat shock transcription factor 1 abolishes thermotolerance and protection against heat-inducible apoptosis. *Journal of biological chemistry*, 273(13):7523–7528, 1998.

[238] P. Ostling, JK. Bjork, P. Roos-Mattjus, V. Mezger, and L. Sistonen. Heat shock factor 2 (hsf2) contributes to inducible expression of hsp genes through interplay with hsf1. *Journal of biological chemistry*, 282(10):7077–7086, 2007.

[239] M. Fujimoto, N. Hayashida, T. Katoh, K. Oshima, T. Shinkawa, R. Prakasam, K. Tan, S. Inouye, R. Takii, and A. Nakai. A novel mouse hsf3 has the potential to activate nonclassical heat-shock genes during heat shock. *Molecular biology of the cell*, 21(1):106–116, 2010.

[240] M. Fujimoto, H. Izu, K. Seki, K. Fukuda, T. Nishida, S. Yamada, K. Kato, S. Yonemura, S. Inouye, and A. Nakai. Hsf4 is required for normal cell growth and differentiation during mouse lens development. *The EMBO journal*, 23(21):4297–4306, 2004.

[241] AJ Morrison, SJ Rush, and IR Brown. Heat shock transcription factors and the hsp70 induction response in brain and kidney of the hyperthermic rat during postnatal development. *Journal of neurochemistry*, 75(1):363–372, 2000.

[242] MT. Fiorenza, T. Farkas, M. Dissing, D. Kolding, and V. Zimarino. Complex expression of murine heat shock transcription factors. *Nucleic acids research*, 23(3):467—474, 1995.

[243] KD. Sarge, SP. Murphy, and RI. Morimoto. Activation of heat shock gene transcription by heat shock factor 1 involves oligomerization, acquisition of dna-binding activity, and nuclear localization and can occur in the absence of stress. *Molecular and cellular biology*, 13(3):1392–1407, 1993.

[244] J. Cotto, S. Fox, and RI. Morimoto. Hsf1 granules: a novel stress-induced nuclear compartment of human cells. *Journal of cell science*, 110(23):2925–2934, 1997.

[245] C. Jolly, R. Morimoto, M. Robert-Nicoud, and C. Vourc'h. Hsf1 transcription factor concentrates in nuclear foci during heat shock: relationship with transcription sites. *Journal of cell science*, 110(23):2935–2941, 1997.

[246] PA. Mercier, NA. Winegarden, and JT. Westwood. Human heat shock factor 1 is predominantly a nuclear protein before and after heat stress. *Journal of cell science*, 112(16):2765–2774, 1999.

[247] M. Vujanac, A. Fenaroli, and V. Zimarino. Constitutive nuclear import and stress-regulated nucleocytoplasmic shuttling of mammalian heat-shock factor 1. *Traffic*, 6(3):214–229, 2005.

[248] J. Anckar and L. Sistonen. Heat shock factor 1 as a coordinator of stress and developmental pathways. *Advances in experimental medicine and biology*, 594:78–88, 2007.

[249] H. Xiao, O. Perisic, and JT. Lis. Cooperative binding of drosophila heat shock factor to arrays of a conserved 5 bp unit. *Cell*, 64(3):585–593, 1991.

[250] RI. Morimoto. Regulation of the heat shock transcriptional response: cross talk between a family of heat shock factors, molecular chaperones, and negative regulators. *Genes and development*, 12(24):3788–3796, 1998.

[251] J. Zou, Y. Guo, T. Guettouche, DF. Smith, and R. Voellmy. Repression of heat shock transcription factor hsf1 activation by hsp90 (hsp90 complex) that forms a stress-sensitive complex with hsf1. *Cell*, 94(4):471–480, 1998.

[252] Y. Guo, T. Guettouche, M. Fenna, F. Boellmann, WB. Pratt, DO. Toft, DF. Smith, and R. Voellmy. Evidence for a mechanism of repression of heat shock factor 1 transcriptional activity by a multichaperone complex. *The Journal of biological chemistry*, 276(49):45791–45799, 2001.

[253] C. Boyault, Y. Zhang, S. Fritah, C. Caron, B. Gilquin, SH. Kwon, C. Garrido, TP. Yao, C. Vourc'h, P. Matthias, and S. Khochbin. Hdac6 controls major cell response pathways to cytotoxic accumulation of protein aggregates. *Genes and development*, 21(17):2172–2181, 2007.

[254] A. Ali, S. Bharadwaj, R. OCarroll, and N. Ovsenek. Hsp90 interacts with and regulates the activity of heat shock factor 1 in xenopus oocytes. *Molecular and cellular biology*, 18(9):4949–4960, 1998.

[255] J. Zou, Y. Guo, T. Guettouche, DF. Smith, and R. Voellmy. Repression of heat shock transcription factor hsf1 activation by hsp90 (hsp90 complex) that forms a stress-sensitive complex with hsf1. *Cell*, 94(4):471–480, 1998.

[256] J. Lee, J. Gao, PA. Kosinski, SJ. Elliman, TE. Hughes, J. Gromada, and DM. Kemp. Heat shock protein 90 (hsp90) inhibitors activate the heat shock factor 1 (hsf1) stress response pathway and improve glucose regulation in diabetic mice. *Biochemical and biophysical research communications*, 430(3):1109–1113, 2013.

[257] Y. Shi, DD. Mosser, and RI. Morimoto. Molecular chaperones as hsf1-specific transcriptional repressors. *Genes and development*, 12(5):654–666, 1998.

[258] F. Boellmann, T. Guettouche, Y. Guo, M. Fenna, L. Mnayer, and R. Voellmy. Daxx interacts with heat shock factor 1 during stress activation and enhances its transcriptional activity. *Proceedings of the national academy of sciences*, 101(12):4100–4105, 2004.

[259] AK. Boehm, A. Saunders, J. Werner, and JT. Lis. Transcription factor and polymerase recruitment, modification, and movement on dhsp70 in vivo in the minutes following heat shock. *Molecular and cellular biology*, 23(21):7628–7637, 2003.

[260] I. Shamovsky, M. Ivannikov, ES. Kandel, D. Gershon, and E. Nudler. Rna-mediated response to heat shock in mammalian cells. *Nature*, 440(7083):556–560, 2006.

[261] JF. Kugel and JA. Goodrich. Beating the heat: A translation factor and an rna mobilize the heat shock transcription factor hsf1. *Molecular cell*, 22(2):135–154, 2006.

[262] L. Vigh, B. Maresca, and JL. Harwood. Does the membrane's physical state control the expression of heat shock and other genes? *Trends in biochemical sciences*, 23(10):369–374, 1998.

[263] L. Carratù, S. Franceschelli, CL. Pardini, GS. Kobayashi, I. Horvath, L. Vigh, and B. Maresca. Membrane lipid perturbation modifies the set point of the temperature of heat shock response in yeast. *Proceedings of the national academy of sciences*, 93(9):3870–3875, 1996.

[264] H. Wada, Z. Combos, and N. Murata. Enhancement of chilling tolerance of a cyanobacterium by genetic manipulation of fatty acid desaturation. *Nature*, 347(6289):200–203, 1990.

[265] L. Vigh, DA. Los, I. Horvath, and N. Murata. The primary signal in the biological perception of temperature: Pd-catalyzed hydrogenation of membrane lipids stimulated the expression of the desa gene in synechocystis pcc6803. *Proceedings of the national academy of sciences*, 90(19):9090—9094, 1993.

[266] S. Kunimoto, W. Murofushi, H. Kai, Y. Ishida, A. Uchiyama, T. Kobayashi, S. Kobayashi, H. Murofushi, and K. Murakami-Murofushi. Steryl glucoside is a lipid mediator in stress-responsive signal transduction. *Cell structure and function*, 27(3):157–162, 2002.

[267] O. Kozawa, K. Tanabe, H. Ito, H. Matsuno, M. Niwa, K. Kato, and T. Uematsu. Sphingosine 1-phosphate regulates heat shock protein 27 induction by a p38 map kinase-dependent mechanism in aortic smooth muscle cells. *Experimental cell research*, 250(2):376–380, 1999.

[268] S. Takai, H. Tokuda, R. Matsushima-Nishiwaki, Y. Hanai, K. Kato, and O. Kozawa. Phosphatidylinositol 3-kinase/akt plays a role in sphingosine 1-phosphate-stimulated hsp27 induction in osteoblasts. *Journal of cellular biochemistry*, 98(5):1249–1256, 2006.

[269] E. Nagy, Z. Balogi, I. Gombos, M. Åkerfelt, A. Björkbom, G. Balogh, Z. Török, A. Maslyanko, A. Fiszer-Kierzkowska, K. Lisowska, et al. Hyperfluidization-coupled membrane microdomain reorganization is linked to activation of the heat shock response in a murine melanoma cell line. *Proceedings of the national academy of sciences*, 104(19):7945–7950, 2007.

[270] Z. Török, T. Crul, B. Maresca, GJ. Schütz, F. Viana, L. Dindia, S. Piotto, M. Brameshuber, G. Balogh, M. Péter, et al. Plasma membranes as heat stress sensors: from lipid-controlled molecular switches to therapeutic applications. *Biochimica et biophysica acta - biomembranes*, 1838(6):1594–1618, 2014.

[271] DA. Jurivich, L. Sistonen, RA. Kroes, and RI. Morimoto. Effect of sodium salicylate on the human heat shock response. *Science*, 255(5049):1243–1245, 1992.

[272] JJ. Cotto, M. Kline, and RI. Morimoto. Activation of heat shock factor 1 dna binding precedes stress-induced serine phosphorylation. evidence for a multistep pathway of regulation. *The Journal of biological chemistry*, 271(7):3355–3358, 1996.

[273] DA. Jurivich, C. Pachetti, L. Qiu, and JF. Welk. Salicylate triggers heat shock factor differently than heat. *The Journal of biological chemistry*, 270(41):24489–24495, 1995.

[274] T. Guettouche, F. Boellmann, WS. Lane, and R. Voellmy. Analysis of phosphorylation of human heat shock factor 1 in cells experiencing a stress. *BMC biochemistry*, 6(4):1471–1475, 2005.

[275] F. Soncin, X. Zhang, B. Chu, X. Wang, A. Asea, M. Ann Stevenson, DB. Sacks, and SK. Calderwood. Transcriptional activity and dna binding of heat shock factor-1 involve

phosphorylation on threonine 142 by ck2. *Biochemical and biophysical research communications*, 303(2):700–706, 2003.

[276] Y. Lee, E. Kim, JS. Lee, D. Jeoung, S. Bae, SH. Kwon, and Y. Lee. Hsf1 as a mitotic regulator: phosphorylation of hsf1 by plk1 is essential for mitotic progression. *Cancer research*, 68(18):7550–7560, 2008.

[277] V. Mayya, DH. Lundgren, S. Hwang, K. Rezaul, L. Wu, JK. Eng, V. Rodionov, and DK. Han. Quantitative phosphoproteomic analysis of t cell receptor signaling reveals system-wide modulation of protein-protein interactions. *Science signaling*, 2(84):ra46, 2009.

[278] JV. Olsen, M. Vermeulen, A. Santamaria, C. Kumar, ML. Miller, LJ. Jensen, F. Gnad, J. Cox, TS. Jensen, EA. Nigg, S. Brunak, and M. Mann. Quantitative phosphoproteomics reveals widespread full phosphorylation site occupancy during mitosis. *Science signaling*, 3(104):ra3, 2010.

[279] M. Green, TJ. Schuetz, EK. Sullivan, and RE. Kingston. A heat shock-responsive domain of human hsf1 that regulates transcription activation domain function. *Molecular and cellular biology*, 15(6):3354–3362, 1995.

[280] CI. Holmberg, V. Hietakangas, A. Mikhailov, JO. Rantanen, M. Kallio, A. Meinander, J. Hellman, N. Morrice, C. MacKintosh, RI. Morimoto, JE. Eriksson, and L. Sistonen. Phosphorylation of serine 230 promotes inducible transcriptional activity of heat shock factor 1. *The EMBO journal*, 20(14):3800–3810, 2001.

[281] KA. Dunker, I. Silman, VN. Uversky, and JL. Sussman. Function and structure of inherently disordered proteins. *Current opinion in structural biology*, 18(6):756–764, 2008.

[282] UF. Hartl, A. Bracher, and M. Hayer-Hartl. Molecular chaperones in protein folding and proteostasis. *Nature*, 475(7356):324–332, 2011.

[283] DJ. Brockwell and SE. Radford. Intermediates: ubiquitous species on folding energy landscapes? *Current opinion in structural biology*, 17(1):30—37, 2007.

[284] B. Bolognesi, JR. Kumita, TP. Barros, EK. Esbjorner, LM. Luheshi, DC. Crowther, MR. Wilson, CM. Dobson, G. Favrin, and JJ. Yerbury. Ans binding reveals common features of cytotoxic amyloid species. *ACS chemical biology*, 5(8):735—740, 2010.

[285] MP. Mayer. Gymnastics of molecular chaperones. *Molecular cell*, 39(3):321–331, 2010.

[286] HH. Kampinga and EA. Craig. The hsp70 chaperone machinery: J proteins as drivers of functional specificity. *Nature reviews. molecular cell biology*, 11(8):579–592, 2010.

[287] D. Bimston, J. Song, D. Winchester, S. Takayama, JC. Reed, and RI. Morimoto. Bag-1, a negative regulator of hsp70 chaperone activity, uncouples nucleotide hydrolysis from substrate release. *The EMBO journal*, 17(23):6871–6878, 1998.

[288] EA. Nollen, AE. Kabakov, JF. Brunsting, B. Kanon, J. Höhfeld, and HH. Kampinga. Modulation of in vivo hsp70 chaperone activity by hip and bag-1. *The Journal of biological chemistry*, 276(7):4677–4682, 2001.

[289] MJ. Kerner, DJ. Naylor, Y. Ishihama, T. Maier, H. Chang, AP. Stines, C. Georgopoulos, D. Frishman, M. Hayer-Hartl, M. Mann, et al. Proteome-wide analysis of chaperonin-dependent protein folding in escherichia coli. *Cell*, 122(2):209–220, 2005.

[290] A. Brinker, G. Pfeifer, MJ. Kerner, DJ. Naylor, FU. Hartl, and M. Hayer-Hartl. Dual function of protein confinement in chaperonin-assisted protein folding. *Cell*, 107(2):223–233, 2001.

[291] Y. Tang, H. Chang, A. Roeben, D. Wischnewski, N. Wischnewski, MJ. Kerner, UF. Hartl, and M. Hayer-Hartl. Structural features of the groel-groes nano-cage required for rapid folding of encapsulated protein. *Cell*, 125(5):903–914, 2006.

[292] K. Chakraborty, M. Chatila, J. Sinha, Q. Shi, BC. Poschner, M. Sikor, G. Jiang, DC. Lamb, UF. Hartl, and M. Hayer-Hartl. Chaperonin-catalyzed rescue of kinetically trapped states in protein folding. *Cell*, 142(1):112–122, 2010.

[293] T. Langer, C. Lu, H. Echols, J. Flanagan, M. K Hayer, and UF. Hartl. Successive action of dnak, dnaj and groel along the pathway of chaperone-mediated protein folding. *Nature*, 356(6371):683–689, 1992.

[294] J. Frydman, E. Nimmesgern, K. Ohtsuka, and UF. Hartl. Folding of nascent polypeptide chains in a high molecular mass assembly with molecular chaperones. *Nature*, 14(6485):111–117, 1994.

[295] BD. Johnson, RJ. Schumacher, ED. Ross, and DO. Toft. Hop modulates hsp70/hsp90 interactions in protein folding. *The Journal of biological chemistry*, 273(6):3679–3686, 1998.

[296] C. Scheufler, A. Brinker, G. Bourenkov, S. Pegoraro, L. Moroder, H. Bartunik, FU. Hartl, and I. Moarefi. Structure of tpr domain-peptide complexes: critical elements in the assembly of the hsp70-hsp90 multichaperone machine. *Cell*, 101(2):199–210, 2000.

[297] G. Siligardi, B. Hu, B. Panaretou, PW. Piper, LH. Pearl, and C. Prodromou. Co-chaperone regulation of conformational switching in the hsp90 atpase cycle. *Journal of biological chemistry*, 279(50):51989–51998, 2004.

[298] MU. Ali, SM. Roe, CK. Vaughan, P. Meyer, B. Panaretou, PW. Piper, C. Prodromou, and LH. Pearl. Crystal structure of an hsp90-nucleotide-p23/sba1 closed chaperone complex. *Nature*, 440(7087):1013–1017, 2006.

[299] AK. Shiau, SF. Harris, DR. Southworth, and DA. Agard. Structural analysis of e. coli hsp90 reveals dramatic nucleotide-dependent conformational rearrangements. *Cell*, 127(2):329–340, 2006.

[300] V. Arndt, C. Rogon, and J. Höhfeld. To be, or not to be. molecular chaperones in protein degradation. *Cellular and molecular life sciences*, 64(19-20):2525–2541, 2007.

[301] RR. Kopito. Aggresomes, inclusion bodies and protein aggregation. *Trends in cell biology*, 10(12):524–530, 2000.

[302] LT. Hunt and MO. Dayhoff. Amino-terminal sequence identity of ubiquitin and the nonhistone component of nuclear protein a24. *Biochemical and biophysical research communications*, 74(2):650–655, 1977.

[303] SA. Wagner, P. Beli, BT. Weinert, ML. Nielsen, J. Cox, M. Mann, and C. Choudhary. A proteome-wide, quantitative survey of in vivo ubiquitylation sites reveals widespread regulatory roles. *Molecular and Cellular Proteomics*, 10(10):1–13, 2011.

[304] S. Zampieri, B. Bembi, N. Rosso, M. Filocamo, and A. Dardis. Treatment of human fibroblasts carrying npc1 missense mutations with mg132 leads to an improvement of intracellular cholesterol trafficking. In *JIMD reports- case and research reports, 2011/2*, pages 59–69. Springer, 2012.

[305] N. Nakasone, YS. Nakamura, K. Higaki, N. Oumi, K. Ohno, and H. Ninomiya. Endoplasmic reticulum-associated degradation of niemann-pick c1: Evidence for the role of heat shock proteins and identification of lysine residues that accept ubiquitin. *Journal of biological chemistry*, 289(28):19714–19725, 2014.

[306] GC. Meacham, C. Patterson, W. Zhang, MJ. Younger, and DM. Cyr. The hsc70 co-chaperone chip targets immature cftr for proteasomal degradation. *Nature cell biology*, 3(1):100–105, 2000.

[307] Z. Batulan, GA. Shinder, S. Minotti, BP He, MM. Doroudchi, J Nalbantoglu, MJ. Strong, and HD. Durham. High threshold for induction of the stress response in motor neurons is associated with failure to activate hsf1. *The Journal of neuroscience*, 23(13):5789–5798, 2003.

[308] GK. Sprang and IR. Brown. Selective induction of a heat shock gene in fibre tracts and cerebellar neurons of the rabbit brain detected by in situ hybridization. *Brain research*, 427(1):89–93, 1987.

[309] I. Guzhova, K. Kislyakova, O. Moskaliova, I. Fridlanskaya, M. Tytell, M. Cheetham, and B. Margulis. In vitro studies show that hsp70 can be released by glia and that exogenous hsp70 can enhance neuronal stress tolerance. *Brain research*, 914(1-2):66–73, 2001.

[310] J. Nylandsted, M. Gyrd-Hansen, A. Danielewicz, N. Fehrenbacher, U. Lademann, M. Høyer-Hansen, E. Weber, G. Multhoff, M. Rohde, and M. Jäättelä. Heat shock protein

70 promotes cell survival by inhibiting lysosomal membrane permeabilization. *The Journal of experimental medicine*, 200(4):425–435, 2004.

[311] M. Gyrd-Hansen, T. Farkas, N. Fehrenbacher, L. Bastholm, M. Høyer-Hansen, F. Elling, D. Wallach, R. Flavell, G. Kroemer, J. Nylandsted, and M. Jäättelä. Apoptosome-independent activation of the lysosomal cell death pathway by caspase-9. *Molecular and cellular biology*, 26(21):7880–7891, 2006.

[312] C. Bivik, I. Rosdahl, and K. Ollinger. Hsp70 protects against uvb induced apoptosis by preventing release of cathepsins and cytochrome c in human melanocytes. *Carcinogenesis*, 28(3):537–544, 2007.

[313] VG. Pereira, ML. Gazarini, LC. Rodrigues, FH. da Silva, SW. Han, AM. Martins, ILS. Tersariol, and V. D'Almeida. Evidence of lysosomal membrane permeabilization in mucopolysaccharidosis type i: rupture of calcium and proton homeostasis. *Journal of cellular physiology*, 223(2):335–342, 2010.

[314] MC. Micsenyi, J. Sikora, G. Stephney, K. Dobrenis, and SU. Walkley. Lysosomal membrane permeability stimulates protein aggregate formation in neurons of a lysosomal disease. *The Journal of neuroscience*, 33(26):10815–10827, 2013.

[315] A. Amritraj, K. Peake, A. Kodam, C. Salio, A. Merighi, JE. Vance, and S. Kar. Increased activity and altered subcellular distribution of lysosomal enzymes determine neuronal vulnerability in niemann-pick type c1-deficient mice. *The american journal of pathology*, 175(6):2540–2556, 2009.

[316] S. Basu, RJ. Binder, T. Ramalingam, and PK. Srivastava. Cd91 is a common receptor for heat shock proteins gp96, hsp90, hsp70, and calreticulin. *Immunity*, 14(3):303–313, 2001.

[317] A Gaultier, X Wu, N Le Moan, S Takimoto, G Mukandala, K Akassoglou, WM Campana, and SL. Gonias. Low-density lipoprotein receptor-related protein 1 is an essential receptor for myelin phagocytosis. *Journal of cell science*, 122(8):1155–1162, 2009.

[318] G Bu. Apolipoprotein e and its receptors in alzheimer's disease: pathways, pathogenesis and therapy. *Nature reviews. neuroscience*, 10(5):333–344, 2009.

[319] Y. Li, W. Lu, MP. Marzolo, and G. Bu. Differential functions of members of the low density lipoprotein receptor family suggested by their distinct endocytosis rates. *The Journal of biological chemistry*, 276(21):18000–18006, 2001.

[320] Y. Shi, E. Mantuano, G. Inoue, WM. Campana, and SL. Gonias. Ligand binding to lrp1 transactivates trk receptors by a src family kinase-dependent pathway. *Science signaling*, 2(68):ra18, 2009.

[321] C. Yoon, EA. Van Niekerk, K. Henry, T. Ishikawa, S. Orita, MH. Tuszynski, and MW. Campana. Low-density lipoprotein receptor-related protein 1 (lrp1)-dependent cell signaling promotes axonal regeneration. *The Journal of biological chemistry*, 288(37):26557–26568, 2013.

[322] M. Guttman, GN. Betts, H. Barnes, M. Ghassemian, P. van der Geer, and EA. Komives. Interactions of the npxy microdomains of the low density lipoprotein receptor-related protein 1. *Proteomics*, 9(22):5016–5028, 2009.

[323] T. Ohshima, GJ. Murray, WD. Swaim, G. Longenecker, JM. Quirk, CO. Cardarelli, Y. Sugimoto, I. Pastan, MM. Gottesman, RO. Brady, et al. α-galactosidase a deficient mice: a model of fabry disease. *Proceedings of the national academy of sciences*, 94(6):2540–2544, 1997.

[324] PK. Smith, RI. Krohn, GT. Hermanson, AK. Mallia, FH. Gartner, MD. Provenzano, EK. Fujimoto, NM. Goeke, BJ. Olson, and DC. Klenk. Measurement of protein using bicinchoninic acid. *Analytical biochemistry*, 150(1):76–85, 1985.

[325] D. te Vruchte, E. Lloyd-Evans, RJ. Veldman, DCA Neville, RA. Dwek, FM. Platt, WJ. van Blitterswijk, and DJ. Sillence. Accumulation of glycosphingolipids in niemann-pick c disease disrupts endosomal transport. *The Journal of biological chemistry*, 279(25):26167–26175, 2004.

[326] A. Reis, A. Rudnitskaya, GJ. Blackburn, NM. Fauzi, AR. Pitt, and CM. Spickett. A comparison of five lipid extraction solvent systems for lipidomic studies of human ldl. *Journal of lipid research*, 54(7):1812–1824, 2013.

[327] DC. Rogers, EM. Fisher, SD. Brown, J. Peters, AJ. Hunter, and JE. Martin. Behavioral and functional analysis of mouse phenotype: Shirpa, a proposed protocol for comprehensive phenotype assessment. *Mammalian genome*, 8(10):711–713, 1997.

[328] S. Takemoto, M. Nishikawa, and Y. Takakura. Pharmacokinetic and tissue distribution mechanism of mouse recombinant heat shock protein 70 in mice. *Pharmaceutical research*, 22(3):419–426, 2005.

[329] RJ. Batka, TJ. Brown, KP. Mcmillan, RM. Meadows, KJ. Jones, and MM. Haulcomb. The need for speed in rodent locomotion analyses. *Anatomical record*, 297(10):1839—1864, 2014.

[330] Y. Liu, LJ. Ao, G. Lu, E. Leong, Q. Liu, XH. Wang, XL. Zhu, DTF. Sun, Z. Fei, T. Jiu, X. Hu, and WS. Poon. Quantitative gait analysis of long-term locomotion deficits in classical unilateral striatal intracerebral hemorrhage rat model. *Behavioural brain research*, 257:166–177, 2013.

[331] JE. Westin, MLF. Janssen, TN. Sager, and Y. Temel. Automated gait analysis in bilateral parkinsonian rats and the role of l-dopa therapy. *Behavioural brain research*, 226(2):519–528, 2012.

[332] FPT. Hamers, GC. Koopmans, and EAJ. Joosten. Catwalk-assisted gait analysis in the assessment of spinal cord injury. *Journal of neurotrauma*, 23(3-4):537–548, 2006.

[333] WT. Norton and W. Cammer. Isolation and characterization of myelin. In P. Morell, editor, *Myelin*, pages 147–195. Springer US, 1984.

[334] H. Jurevics and P. Morell. Cholesterol for synthesis of myelin is made locally, not imported into brain. *Journal of neurochemistry*, 64(2):895–901, 1995.

[335] LS. Laursen, CW. Chan, and C. French-Constant. An integrin-contactin complex regulates cns myelination by differential fyn phosphorylation. *The Journal of neuroscience*, 29(29):9174–9185, 2009.

[336] EE. Frost, PC. Buttery, R. Milner, and C. French-Constant. Integrins mediate a neuronal survival signal for oligodendrocytes. *Current biology*, 9(21):1251–1254, 1999.

[337] J. Relucio, ID. Tzvetanova, W. Ao, S. Lindquist, and H. Colognato. Laminin alters fyn regulatory mechanisms and promotes oligodendrocyte development. *The Journal of neuroscience*, 29(38):11794–11806, 2009.

[338] T. Boiko and B. Winckler. Myelin under construction – teamwork required. *The Journal of cell biology*, 172(6):799–801, 2006.

[339] DR. Colman, G. Kreibich, AB. Frey, and DD. Sabatini. Synthesis and incorporation of myelin polypeptides into cns myelin. *The Journal of cell biology*, 95(2):598–608, 1982.

[340] C. Brumwell, C. Antolik, JH. Carson, and E. Barbarese. Intracellular trafficking of hnrnp a2 in oligodendrocytes. *Experimental cell research*, 279(2):310–320, 2002.

[341] LD. Kosturko, MJ. Maggipinto, C. D'Sa, JH. Carson, and E. Barbarese. The microtubule-associated protein tumor overexpressed gene binds to the rna trafficking protein heterogeneous nuclear ribonucleoprotein a2. *Molecular biology of the cell*, 16(4):1938–1947, 2005.

[342] RL. Schnaar. Brain gangliosides in axon-myelin stability and axon regeneration. *FEBS letters*, 584(9):1741–1747, 2010.

[343] A. Tessitore, M. del P Martin, R. Sano, Y. Ma, L. Mann, A. Ingrassia, ED. Laywell, DA. Steindler, LM. Hendershot, and A. d'Azzo. Gm1-ganglioside-mediated activation of the unfolded protein response causes neuronal death in a neurodegenerative gangliosidosis. *Molecular cell*, 15(5):753–766, 2004.

[344] N. Fischer, M. Haug, WW. Kwok, H. Kalbacher, D. Wernet, GE. Dannecker, and U. Holzer. Involvement of cd91 and scavenger receptors in hsp70-facilitated activation of human antigen-specific cd4+ memory t cells. *European journal of immunology*, 40(4):986–997, 2010.

[345] DR. Foran and AC. Peterson. Myelin acquisition in the central nervous system of the mouse revealed by an mbp-lac z transgene. *The Journal of neuroscience*, 12(12):4890–4897, 1992.

[346] F. Khan, PM. Legler, RM. Mease, EH. Duncan, ES. Bergmann-Leitner, and E. Angov. Histidine affinity tags affect msp1(42) structural stability and immunodominance in mice. *Biotechnology journal*, 7(1):133–147, 2012.

[347] BU. von Specht, J. Gabelsberger, B. Knapp, E. Hundt, H. Schmidt-Pilger, S. Bauernsachs, U. Lenz, and H. Domdey. Immunogenic efficacy of differently produced recombinant vaccines candidates against pseudomonas aeruginosa infections. *Journal of biotechnology*, 83(1-2):3–12, 2000.

[348] A. Mayer, SK. Sharma, B. Tolner, NP. Minton, D. Purdy, P. Amlot, G. Tharakan, RHJ. Begent, and KA. Chester. Modifying an immunogenic epitope on a therapeutic protein: a step towards an improved system for antibody-directed enzyme prodrug therapy (adept). *British journal of cancer*, 90(12):2402–2410, 2004.

[349] KK Bíró, A Jednákovits, T Kukorelli, L Korányi, et al. Bimoclomol (brlp-42) ameliorates peripheral neuropathy in streptozotocin-induced diabetic rats. *Brain research bulletin*, 44(3):259–263, 1997.

[350] J. Hargitai, H. Lewis, I. Boros, T. Rácz, A. Fiser, I. Kurucz, I. Benjamin, L. Vigh, Z. Pénzes, P. Csermely, et al. Bimoclomol, a heat shock protein co-inducer, acts by the prolonged activation of heat shock factor-1. *Biochemical and biophysical research communications*, 307(3):689–695, 2003.

[351] Z. Török, NM. Tsvetkova, G. Balogh, I. Horváth, E. Nagy, Z. Pénzes, J. Hargitai, O. Bensaude, P. Csermely, JH. Crowe, et al. Heat shock protein coinducers with no effect on protein denaturation specifically modulate the membrane lipid phase. *Proceedings of the national academy of sciences*, 100(6):3131–3136, 2003.

[352] D. Kieran, B. Kalmar, JRT. Dick, J. Riddoch-Contreras, G. Burnstock, and L. Greensmith. Treatment with arimoclomol, a coinducer of heat shock proteins, delays disease progression in als mice. *Nature medicine*, 10(4):402–405, 2004.

[353] DA. Parfitt, M. Aguila, CH. McCulley, D. Bevilacqua, HF. Mendes, D. Athanasiou, SS. Novoselov, N. Kanuga, PM. Munro, PJ. Coffey, et al. The heat-shock response co-inducer

arimoclomol protects against retinal degeneration in rhodopsin retinitis pigmentosa. *Cell death and disease*, 5:e1236, 2013.

[354] M. Kürthy, T. Mogyorósi, K. Nagy, T. Kukorelli, A. Jednákovits, L. Tálosi, and K. Bíró. Effect of brx-220 against peripheral neuropathy and insulin resistance in diabetic rat models. *Annals of the new york academy of sciences*, 967(1):482–489, 2002.

[355] ME. Cudkowicz, JM. Shefner, E. Simpson, D. Grasso, H. Yu, H. Zhang, A. Shui, D. Schoenfeld, RH. Brown, S. Wieland, et al. Arimoclomol at dosages up to 300 mg/day is well tolerated and safe in amyotrophic lateral sclerosis. *Muscle and nerve*, 38(1):837–844, 2008.

[356] XH. Wang, G. Lu, X. Hu, KS. Tsang, WH. Kwong, FX. Wu, HW. Meng, S. Jiang, SW. Liu, HK. Ng, et al. Quantitative assessment of gait and neurochemical correlation in a classical murine model of parkinsons disease. *BMC neuroscience*, 13(1):142–155, 2012.

[357] EP. Beltroy, JA. Richardson, JD. Horton, SD. Turley, and JM. Dietschy. Cholesterol accumulation and liver cell death in mice with niemann-pick type c disease. *Hepatology*, 42(4):886–893, 2005.

[358] PP Nánási, S. Sárközi, G Szigeti, I Jóna, C Szegedi, A Szabó, T Bányász, J Magyar, P Szigligeti, A Körtvély, et al. Biphasic effect of bimoclomol on calcium handling in mammalian ventricular myocardium. *British journal of pharmacology*, 129(7):1405–1412, 2000.

[359] MW. Ledbetter, JK. Preiner, CF. Louis, and JR. Mickelson. Tissue distribution of ryanodine receptor isoforms and alleles determined by reverse transcription polymerase chain reaction. *Journal of biological chemistry*, 269(50):31544–31551, 1994.

[360] R. Zucchi and S. Ronca-Testoni. The sarcoplasmic reticulum ca2+ channel/ryanodine receptor: modulation by endogenous effectors, drugs and disease states. *Pharmacological Reviews*, 49(1):1–51, 1997.

[361] N. Pierobon, DC. Renard-Rooney, LD. Gaspers, and AP. Thomas. Ryanodine receptors in liver. *Journal of biological chemistry*, 281(45):34086–34095, 2006.

[362] J. Huang, JM. Trasler, S. Igdoura, J. Michaud, N. Hanai, and RA. Gravel. Apoptotic cell death in mouse models of gm2 gangliosidosis and observations on human tay-sachs and sandhoff diseases. *Human molecular genetics*, 6(11):1879–1885, 1997.

[363] R. Wada, CJ. Tifft, and RL. Proia. Microglial activation precedes acute neurodegeneration in sandhoff disease and is suppressed by bone marrow transplantation. *Proceedings of the national academy of sciences*, 97(20):10954–10959, 2000.

[364] T. Kolter and K. Sandhoff. Sphingolipid metabolism diseases. *Biochimica et biophysica acta - biomembranes*, 1758(12):2057—2079, 2006.

[365] K Sango, S. Yamanaka, A. Hoffmann, Y. Okuda, A. Grinberg, H. Westphal, MP. McDonald, JN. Crawley, K. Sandhoff, K. Suzuki, et al. Mouse models of tay–sachs and sandhoff diseases differ in neurologic phenotype and ganglioside metabolism. *Nature genetics*, 11(2):170–176, 1995.

[366] D. Phaneuf, N. Wakamatsu, J. Huang, A. Borowski, AC. Peterson, SR. Fortunato, G. Ritter, SA. Igdoura, CR Morales, G. Benoit, et al. Dramatically different phenotypes in mouse models of human tay-sachs and sandhoff diseases. *Human molecular genetics*, 5(1):1–14, 1996.

[367] CA. Denny, JL. Kasperzyk, KN. Gorham, RT. Bronson, and TN. Seyfried. Influence of caloric restriction on motor behavior, longevity, and brain lipid composition in sandhoff disease mice. *Journal of neuroscience research*, 83(6):1028–1038, 2006.

[368] K. Suzuki, K. Sango, RL. Prola, and C. Langaman. Mice deficient in all forms of lysosomal beta-hexosaminidase show mucopolysaccharidosis-like pathology. *Journal of neuropathology and experimental neurology*, 56(6):693–703, 1997.

[369] D. Pelled, E. Lloyd-Evans, C. Riebeling, M. Jeyakumar, FM. Platt, and AH. Futerman. Inhibition of calcium uptake via the sarco/endoplasmic reticulum ca2+-atpase in a mouse model of sandhoff disease and prevention by treatment with n-butyldeoxynojirimycin. *Journal of biological chemistry*, 278(32):29496–29501, 2003.

[370] L. Ginzburg, S. Li, Y. Li, and AH. Futerman. An exposed carboxyl group on sialic acid is essential for gangliosides to inhibit calcium uptake via the sarco/endoplasmic reticulum ca2+-atpase: relevance to gangliosidoses. *Journal of neurochemistry*, 104(1):140–146, 2008.

[371] ST. Hepbildikler, R. Sandhoff, M. Kolzer, RL. Proia, and K. Sandhoff. Physiological substrates for human lysosomal beta–hexosaminidase s. *The Journal of biological chemistry*, 277(4):2562–2572, 2002.

[372] JU. Ikonne, MC. Rattazzi, and RJ. Desnick. Characterization of hex s, the major residual beta hexosaminidase activity in type o gm2 gangliosidosis (sandhoff-jatzkewitz disease). *American journal of human genetics*, 27(5):628–638, 1975.

[373] SA. Igdoura, C. Gafuik, C. Mertineit, F. Saberi, AV. Pshezhetsky, M. Potier, JM. Trasler, and RA. Gravel. Cloning of the cdna and gene encoding mouse lysosomal sialidase and correction of sialidase deficiency in human sialidosis and mouse sm/j fibroblasts. *Human molecular genetics*, 7(1):115–121, 1998.

[374] DM. Marcus, M. Naiki, and SK. Kundu. Abnormalities in the glycosphingolipid content of human pk and p erythrocytes. *Proceedings of the national academy of sciences*, 73(9):3263–3267, 1976.

[375] M. Jeyakumar, IM. Williams, DA. Smith, TM. Cox, and FM. Platt. Critical role of iron in the pathogenesis of the murine gangliosidoses. *Neurobiology of disease*, 34(3):406–416, 2009.

[376] YA. Ioannou, KM. Zeidner, RE. Gordon, and RJ. Desnick. Fabry disease: preclinical studies demonstrate the effectiveness of α-galactosidase a replacement in enzyme-deficient mice. *The american journal of human genetics*, 68(1):14–25, 2001.

[377] AC. Vedder, GE. Linthorst, G. Houge, JEM. Groener, EE. Ormel, BJ. Bouma, JMFG. Aerts, A. Hirth, and CEM. Hollak. Treatment of fabry disease: outcome of a comparative trial with agalsidase alfa or beta at a dose of 0.2 mg/kg. *PloS one*, 2(7):e598, 2007.

[378] T. Heare, NJ. Alp, DA. Priestman, AB. Kulkarni, P. Qasba, TD. Butters, RA. Dwek, K. Clarke, KM. Channon, and FM. Platt. Severe endothelial dysfunction in the aorta of a mouse model of fabry disease; partial prevention by n-butyldeoxynojirimycin treatment. *Journal of inherited metabolic disease*, 30(1):79–87, 2007.

[379] G. Altarescu, D. Elstein, and M. Beck. *Fabry Disease*. Springer, 2010.

[380] J. Lee, M. Jeyakumar, R. Gonzalez, H. Takahashi, P. Lee, RC. Baek, D. Clark, H. Rose, G. Fu, J. Clarke, et al. Stem cells act through multiple mechanisms to benefit mice with neurodegenerative metabolic disease. *Nature medicine*, 13(4):439–447, 2007.

[381] R. Schiffmann, EJ. FitzGibbon, C. Harris, C. DeVile, EH. Davies, L. Abel, IN. Van Schaik, WS. Benko, M. Timmons, M. Ries, et al. Randomized, controlled trial of miglustat in gaucher's disease type 3. *Annals of neurology*, 64(5):514–522, 2008.

[382] PK. Auluck and NM. Bonini. Pharmacological prevention of parkinson disease in drosophila. *Nature medicine*, 8(11):1185–1196, 2002.

[383] C. Yang, S. Rahimpour, J. Lu, K. Pacak, B. Ikejiri, RO. Brady, and Z. Zhuang. Histone deacetylase inhibitors increase glucocerebrosidase activity in gaucher disease by modulation of molecular chaperones. *Proceedings of the national academy of sciences*, 110(3):966–971, 2013.

[384] EM. O'Leary and SA. Igdoura. The therapeutic potential of pharmacological chaperones and proteosomal inhibitors, celastrol and mg132 in the treatment of sialidosis. *Molecular genetics and metabolism*, 107(1):173–185, 2012.

[385] Hao Li, Stephen D Turley, Benny Liu, Joyce J Repa, and John M Dietschy. Gm2/gd2 and gm3 gangliosides have no effect on cellular cholesterol pools or turnover in normal or npc1 mice. *Journal of lipid research*, 49(8):1816–1828, 2008.